DOE/MC/29248 -- 5659
(DE97002293)

Kinetic Inhibition of Natural Gas Hydrates in Offshore Drilling, Production and Processing

Annual Report
January 1 - December 31, 1993

Work Performed Under Contract No.: DE-FG21-92MC29248

For
U.S. Department of Energy
Office of Fossil Energy
Federal Energy Technology Center
Morgantown Site
P.O. Box 880
Morgantown, West Virginia 26507-0880

By
Center for Hydrate Research
Colorado School of Mines
Golden, Colorado 80401

Disclaimer

I. Executive Summary

Natural gas hydrates are a potential problem in offshore drilling, production, and processing. Substantial expense is incurred using thermodynamic inhibitors (such as methanol or glycol) for hydrate prevention at severe pressure and temperature conditions in winter or ocean operations.

This study proposed a new, kinetic means of hydrate prevention with the object of economical inhibition. We proposed:
1. to define the best kinetic hydrate inhibitors,
2. to measure the rate of hydrate formation,
3. to define a kinetic mechanism of hydrate formation, and
4. to develop a model for the new inhibition scheme(s).

In the period from January 1 - December 31, 1993 we had the following 7 major accomplishments:
1. We found vastly better kinetic inhibitors (PVCAP, VC-713 and copolymers/blends of 5- and 7-member lactam ring polymers, including HE300, an electrolyte) relative to the best previous kinetic inhibitor (PVP) for which field success was reported in 1992.
2. We measured the performance limits of inhibitors at more stringent conditions (such as at the temperature of the ocean floor) with respect to pressure, inhibitor concentration, and salt concentration.
3. We determined that kinetic inhibitors (in 1) were effective in preventing hydrates in condensates and drilling muds systems.
4. We determined common characteristics of the best inhibitors, and constructed the first molecular model of kinetic inhibitor performance with support from Raman and UV-Visible spectroscopy, as well as from molecular modelling.
5. We constructed a high pressure sapphire visual cell to determine the location and morphology of hydrate formation as a function of inhibitors such as PVP and VC-713. A videotape is provided.
6. We began to synthesize new chemicals for hydrate inhibition.
7. We began collaborative efforts on a temperature-controlled, pilot plant flow loop at the Exxon Production Research facility. In addition four member companies reported field success with the kinetic inhibitors in existing natural gas pipelines.

During 1994 we propose to do the following:
1. Define a rational approach for inhibitor design.
2. Improve performance of inhibitors.
3. Test inhibitors on CSM apparatus and the Exxon flow loop.
4. Act as a forum for sharing of field and pilot plant results.

During 1993, 13 member companies (Amoco, ARCO, Chevron, Conoco, DoE (U.S.), Exxon, Marathon, Mobil, Oryx, Petrobras, Phillips, Shell and Texaco) participated in the consortium, yielding a substantial leverage for each company's investment.

II. Table of Contents

Section/Topic Page

I. Executive Summary....1
II. Table of Contents....2
III. Introduction....4
A. Statement of the Problem....4
B. Goals, Objectives, and History of the Project....4
C. A Physical Picture of Hydrate Formation/Inhibition....5
1. Molecular Picture of Hydrate Formation....6
a. Consequences of Formation Hypothesis....8
2. Molecular Picture of Hydrate Kinetic Inhibition...8
a. Growth Inhibition by Viscous Blocking....9
b. Growth Inhibition by Steric Stabilization....10
1. Inhibitor Structure & Aqueous Solubility...10
2. Mechanism for Steric Stabilization....11
a. Effect of Salt on Performance....12
b. Effect of Inhibitor Concentration....12
IV. What Was Accomplished in 1993....13
A. A Synopsis of New Findings....13
1. Vastly Improved Inhibitors & Performance Limits..14
2. Evidence to Support an Inhibition Mechanism....15
3. Support of Field Implementation....16
B. Progress in Specific Areas....17
1. Screening Apparatus....17
a. Experiment....17
b. Chemicals Tested....19
1. Unsuccessful Chemicals....19
a. The Urea Family....19
b. Other Ring Polymers....20
c. Polyelectrolytes....20
2. Successful Chemical Characteristics....20
a. Polymer Blending Studies....21
b. Influence of Methanol on Efficiency....22
c. Supporting Evidence....23
1. Viscosity Studies of PVCAP....23
2. UV-Visible Studies of PVCAP....24
c. Future Chemicals/Experiments....26
2. High Pressure Experiments....27
a. Apparatus and Operating Procedure....27
b. Thermodynamic Experiments and Results....30
c. Kinetic Experiments and Results....31
1. Performance of New Inhibitors....32
a. Copolymers of PVP....32
b. VC-713....32
c. PVCAP....34
d. Co-polymers of PVP and PVCAP....36
e. PVCAP and Methanol....37
f. HE300 and Blends of PVP with PVCAP....38
d. Extended Time Inhibition Tests of Chemicals...39
e. Viscosity Effects on Kinetic Inhibition....40

II. Table of Contents (continued)

f. Inhibition of Both sI and sII by PVP.....42
g. Mixing and Material Effects.....42
h. Inhibition of Systems with Liquid Condensates.43
i. Inhibition of Drilling Mud.....45
3. New Sapphire Cell for Visual Observation.....46
a. Apparatus and Operating Procedure.....46
b. Visual Observations of Hydrate Formation.....47
1. Natural Gas and Deionized Water.....48
2. Natural Gas and Sodium Dodecyl Sulfate.....49
3. Natural Gas and Sea Water.....52
4. Natural Gas, Amorphous Silica & Sea Water..53
5. Natural Gas, n-Decane and Deionized Water..53
6. Natural Gas, 0.5wt% VC-713, and Seawater...54
7. Natural Gas, 0.5wt% PVP, and Seawater.....54
8. CO_2 in Deionized Water.....54
4. Collaborative Effort with Exxon.....55
a. CSM Experiments on Systems proposed for Loop..55
5. Raman Spectroscopic Studies.....57
a. Experimental Procedure.....57
b. Experimental Results.....58
1. VC-713+Water+THF System.....58
a. Possible Interpretation.....59
2. PVP+Water+THF System.....60
3. PVCAP+Water+THF System.....61
c. Conclusions from Raman Studies.....61
6. Computer Simulation.....62
a. Docking Studies of Polymers on Hydrate & Ice..62
b. Kinetic Inhibitor Interaction with Water.....64
c. Interfacial Studies of Hydrate and Water.....66
1. Crystal Growth Studies.....67
d. Hydrophobic Interaction.....68
V. What is Proposed for 1994.....69
A. Objectives for 1994.....69
1. Define a Rational Approach for Inhibitor Design..69
2. Improve Inhibitor Performance.....69
3. Test Inhibitors on CSM and Exxon Apparatuses.....69
4. Act as a Forum for Sharing Field & Pilot Results.69
B. Personnel Changes to Accomplish Objectives.....70

Appendices
A. Company Representatives
B. Expenses for 1992 and 1993
C. Conceptual Design of Polymer Recovery

III. Introduction

III.A. Statement of Problem

Natural gas hydrates are solid crystalline compounds which form when small organic molecules contact molecules of water at elevated pressures and reduced temperatures, both above and below the ice point. Because these crystalline compounds plug flow channels, their presence is undesirable, so that every attempt is made to prevent hydrates from forming large masses.

In the history of hydrates four classical means have been used to prevent their formation:
1. Removal of water, typically through contacting the hydrocarbon with ethylene/diethylene/triethylene glycol or molecular sieve desiccant,
2. Increasing the system temperature above the hydrate formation point through heat exchange,
3. Reduction of the system pressure below the hydrate formation point, through pressure depletion or flaring, and
4. Injection of inhibitors such as methanol or ethylene glycol to shift the hydrate equilibrium, so that the system operates in the vapor-liquid region.

In deep sea operations, the ambient operating conditions (low temperature and high pressure) are very conducive to hydrate formation. In such cases, the above traditional approaches can be ineffective due to either extreme conditions or high cost. In this project we proposed the alternate approach to controlling hydrate formation by preventing hydrate growth to a sizeable mass which could block a flow channel.

III.B. Goals, Objectives, and History of the Project

The goal of the project was to provide industry with more economical hydrate inhibitors. This goal was to be accomplished by a program involving the following four steps:

1. First, provide rapid screening of a large number (ca. 1000/year) of potential hydrate inhibition chemicals.
2. Second, test the best of the chemicals from Step 1, in high pressure hydrate formation apparatuses, with simulated pipeline compositions, temperatures, and pressures.
3. Third, those chemicals which passed inhibition tests in Step 2 would be tested in a temperature-controlled, pilot-plant flow loop, made available at Exxon Production and Research in Houston, and
4. Finally, consortium member companies would field test the chemicals and the project would provide a forum for the sharing of hydrate inhibition field results.

During the first 15 months of the project (9/90 -12/91) we

developed a rapid screening apparatus and tested about 50 inhibitors. We also modified two high pressure apparatuses, determined their principal operating variables and established a baseline for comparison of future experiments. Finally, using a computer, we simulated the first stages of hydrate formation as water clusters around apolar molecules.

During 1992, the second year, we tested about 700 inhibitor candidates using the screening apparatus and determined transferability of screening results to the high pressure apparatuses. We applied for a chemical use patent on the two best inhibitors (polyvinylpyrrolidone (PVP) and hydroxyethyl cellulose (HEC)), with the contractual agreement that consortium members would have royalty-free license. With the aid of computer simulation and Raman spectroscopic studies, we began to formulate a kinetic inhibition mechanism. In mid-1992 field testing began on PVP; success in varying degrees was reported for PVP performance, notably on a multiple-pipeline field test by Amoco, but also on smaller tests by Oryx, Shell and Texaco.

In 1993 we proposed four objectives:
1. continue both screening and high pressure experiments to determine optimum inhibitors,
2. investigate molecular mechanisms of hydrate formation/ inhibition, through microscopic and macroscopic experiments,
3. begin controlled tests on the Exxon pilot plant loop at their Houston facility, and
4. continue to act as a forum for the sharing of field test results.

The second of the above 1993 objectives, a microscopic picture of hydrate inhibition, provides a vehicle to comprehend the other sections of this report; the mechanism of formation/ inhibition, while somewhat premature and incomplete, is included in the following section.

III.C. Physical Hypothesis for Hydrate Formation/Inhibition

A physical picture of hydrate formation and inhibition is needed to unify the following report which contains many different parts, some of which may appear disjointed to a reader with limited time. The purpose of this section is to tie together evidence presented in the following sections to present an underlying hypothesis of hydrate formation/inhibition.

There is a risk of being in substantial error by proposing such a picture, and both readers and formulators should be mindful of that potential risk. What we are attempting here is to connect the dots provided by experimental evidence to compose a somewhat incomplete, outlined picture which unifies these observations.

While there is the danger that, if there are not enough dots of evidence, the outline will be entirely erroneous, perhaps the outline itself can aid in determining the need of missing (future) experiments to provide a better picture. We are following Francis Bacon's maxim that unifying concepts (even if erroneous) are better than confused stupor.

It is worth emphasizing that a second danger (of proposing a mechanism when the data are incomplete) is that one tends to fix upon the hypothesis as fact and may miss or misinterpret conflicting data.

In this section we propose a microscopic "picture" of a hydrate formation/inhibition mechanism. However the picture is based principally on macroscopic observations, such as hydrate formation/inhibition at various temperatures, pressures, visual observations, solution viscosities, etc. The danger of the hypothesis is that there may be several entirely different microscopic paths which can provide the same macroscopic observations. However, the microscopic evidence (Raman spectroscopy, UV-Visible spectroscopy, and molecular dynamics computer simulation), while somewhat preliminary and limited, does seem to be consistent with the hypothesis proposed.

In order to postulate a mechanism for hydrate kinetic inhibition, it helps to first have a picture of hydrate formation. The following two subsections present hypotheses: (III.C.1.) for hydrate formation, and (III.C.2.) for hydrate inhibition on a molecular level.

III.C.1. Molecular Picture of Hydrate Formation

A simplified, molecular-scale picture of hydrate crystal structure II (which forms with minor exceptions in this report) shows it to be constructed of two types of water cavities: (1) 5^{12} with 12 pentagonal faces and (2) $5^{12}6^4$ with 12 pentagonal and 4 hexagonal faces. Each cavity can contain at most one guest hydrocarbon molecule. In the repeating unit crystal of structure II there are 16 of the 5^{12} cavities and 8 of the $5^{12}6^4$ cavities. One may construct the entire unit cell from either cavity in the absence of the other (e.g. the spaces between the large $5^{12}6^4$ cavities form the 5^{12} cavities, and vice versa.) With this simplified molecular picture of the time-independent crystal structures, we proceed to the kinetic formation hypothesis. Readers interested in further details of crystal structure are referred to the monograph by Sloan (Clathrate Hydrates of Natural Gases, Marcel Dekker, New York, 1990).

Hydrate formation may be considered as a process similar to

that depicted in Figure 1, as summarized by Christiansen and Sloan, (Proceedings New York Academy of Sciences International Hydrate Conference, June 1993). The figure shows the progression (left to right) of water and gas phases, as they combine to form substantial amounts of hydrate crystals.

Leftmost in Figure 1, water is depicted as a network of hydrogen-bonded ring species, with predominantly five and six-member rings as determined by the simulations of Rahman and Stillinger (J. Amer. Chem. Soc., **95**, 7943, 1973). Note that these five- and six-member ring structures are also the ingredients of the pentagonal and hexagonal faces of the cavities in hydrate unit crystals.

Second from the left in Figure 1, clusters are formed by the dissolution of gas in water. As shown by the computer simulations of Long and Sloan (Molecular Simulation, **11**, 145 (1993)), when gas dissolves in water, the hydrophobic nature of the gas molecule creates a cavity in the liquid and causes water to cluster around it, to maximize the tetrahedral "hydrogen-bonding" nature of water molecules. Evidence for such clustering is substantial, most recently in the NMR study of Fleyfel and Kobayashi (Proceedings New York Academy of Sciences International Hydrate Conference, June, 1993).

While these labile clusters should not be considered as solid-like, the residence time of a water molecule in the cluster is much greater than that in pure water. The number of the water molecules in such clusters is quantized in units of four (approximately 20, 24, 28, etc.) as a function of the size of the dissolved gas molecule. These numbers are identical with the numbers of water molecules in hydrate cavities, which are the building blocks for hydrate unit crystals.

In the third picture from the left in Figure 1, clusters have progressed to group together, via a hydrophobic bonding phenomena summarized in the monograph of Ben-Naim (Hydrophobic Interaction, Plenum Press, New York, 1980). In an attempt to maximize entropy, nature causes a gathering of the clusters, increasing the system disorder as a result of ejection of water molecules at adjoining cluster faces.

At some point in time aggregates of clusters become more solid-like than their previous liquid-like nature. When solid-like, hydrate clusters join together; it appears that joining the hexagonal faces may provide a key to hydrate growth. Recall that only the large hydrate cavities have hexagonal faces, while the smaller, more numerous cavities are composed solely of pentagonal faces. Thus hexagonal cavity faces can only be combined to hexagonal faces of other large cavities. In other words, blocking crystal growth at a hexagonal face would prevent juncture with a neighboring large cavity.

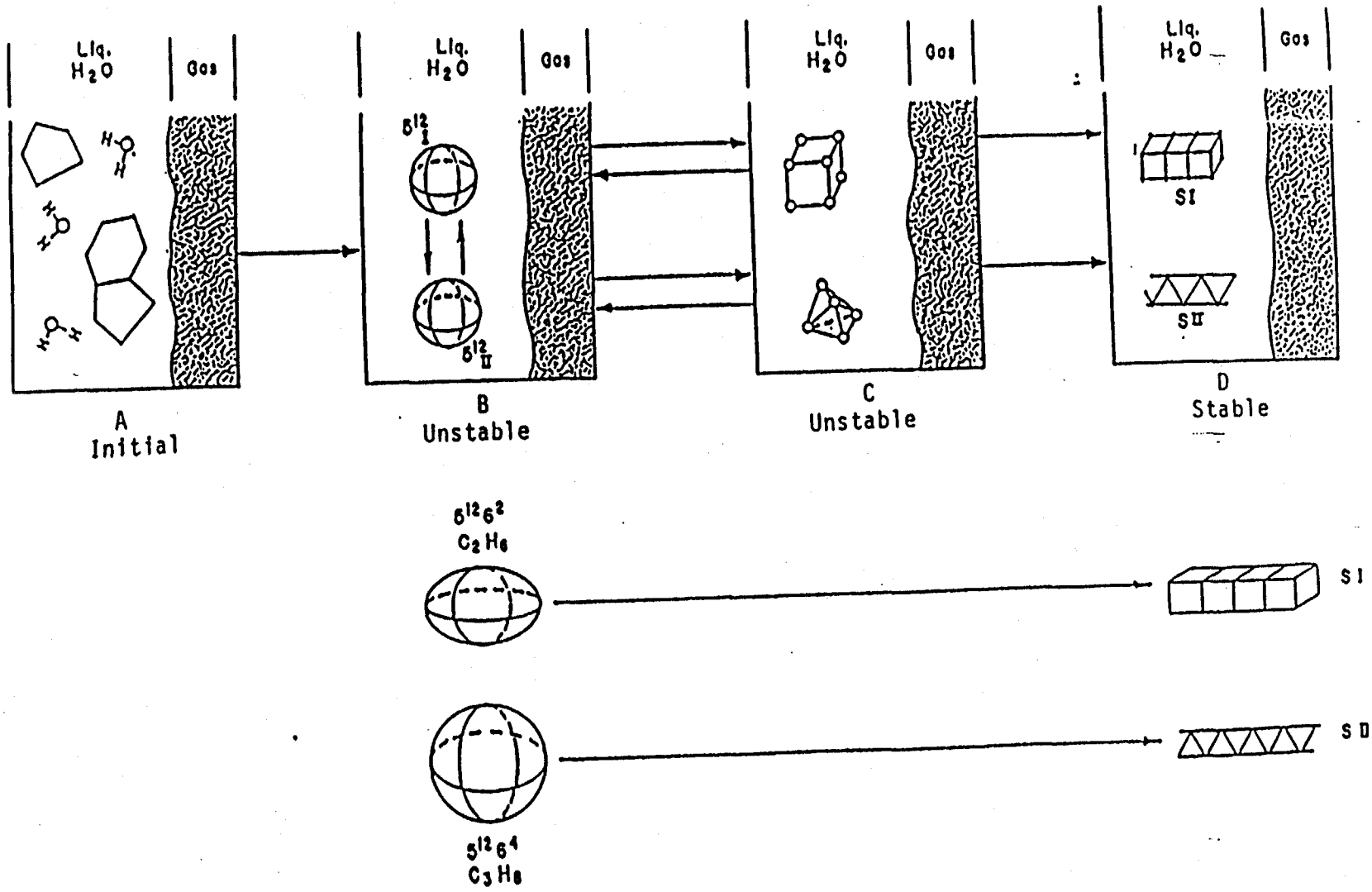

Figure 1. Physics of a mechanism of hydrate formation from water.

Before the crystal mass achieves a critical size, it may either grow or shrink. This phenomenon has been related (Sloan, op. cit., 1990) to metastability, for which hydrates are infamous. In the rightmost picture of Figure 1, the unit crystal has grown beyond the critical size, so that continued hydrate growth is very rapid, sometimes described as catastrophic growth.

In summary of molecular hypothesis then, the hydrate formation shown in Figure 1 may be considered as a physical reaction which progresses from left to right. The water molecules in the proposed reaction are connected by weaker hydrogen bonds, than the normal bonds in a chemical reaction. The reaction is suggested to be autocatalytic in nature, using previously formed species as seeds for further growth.

The reaction is reversible at formation conditions but the species which comprise the clusters and crystal masses are fairly hardy on a molecular scale and may require a substantial time to disperse. The reaction process in Figure 1 may be quantitatively described in selective cases (Sloan and Fleyfel, AIChE J., 37, 1281, 1991) for which a template for hydrate formation (e.g. ice or other hydrate) is available.

III.C.1.a. Macroscopic Consequences of Formation Hypothesis

On a macroscopic scale, the above microscopic picture is reflected in the fact that homogeneous hydrate nucleation (the initiation of hydrate formation in an uncontaminated fluid system) is a statistically random, stochastic process. At some point in time, a collection of molecules become more solid-like than liquid-like, due to minor fluctuations in molecular behavior, which are beyond the control of macroscopic experiments. Thus hydrate initiation, in terms of homogeneous nucleation, is not normally reproducible in time. In addition note that, while homogeneous nucleation strictly refers to a single phase, a minimum of two phases are required for all hydrate formation; thus it is doubtful that anyone has observed homogeneous nucleation in hydrates.

For large scale reproducibility in hydrate formation, we must observe the hydrate growth domain, in which the initial hydrate nuclei are formed at a heterogeneous surface such as a wall, a gas+liquid interface, or an amorphous silica crystal. Hydrate formation occurs at an interface unless it is disrupted, or unless other, more preferred surfaces are in the system. Evidence for the initial growth hypothesis is provided in the sapphire cell studies of this report, which is accompanied by a videotape of hydrate formation processes.

III.C.2. Molecular Picture of Hydrate Kinetic Inhibition

The kinetic inhibition of hydrates is achieved principally via the prevention of crystal growth. In almost all cases tested over a three year period, hydrate crystals were readily initiated in our high pressure cell. Thus while the initial nucleation of the crystal may be difficult to prevent, it is very feasible to inhibit crystal growth, so hydrates stay suspended in a liquid as small particles, without agglomeration to larger masses.

The inhibition of hydrate crystal growth occurs by preventing the components of a crystal mass from coming together. By maintaining small fragments of hydrate crystals, the system is kept in a fluid-like flow regime. While eventually hydrate fragments may accumulate, the system may be kept fluid-like for a time which greatly can exceed, for example, the normal residence time of the fluid in a pipeline.

To date we have found two methods which are effective in an inhibition scheme such as the one described above. The first method is to increase the water viscosity to decrease the collision frequency of hydrates fragments in the water. The second method is to sterically interfere with interactions between the small crystal fragments. While each inhibition mechanism is discussed separately in the following subsections, some combination of the two mechanisms is probably acting.

III.C.2.a. Growth Inhibition by Viscous Blocking

One means to inhibit hydrate growth is to increase the viscosity of the water using a water-soluble polymer. The evidence in the viscosity portion (Section IV.B.2.e.) of this report indicates that the chemical structure of the water-soluble polymer is not too important, so long as it provides a high liquid viscosity.

On a molecular level, a viscosity increase is interpreted as a decrease in the mean free path between molecules, preventing molecules from flowing easily past each other. Thus a polymer molecule which increases water viscosity may be thought of as blocking the path between hydrate crystal fragments in the water, hindering mass transfer of agglomeration to larger fragments.

One disadvantage of such an inhibition mechanism, is that any polymer which significantly increases the viscosity of the fluid makes the fluid more sluggish, increasing its residence time in a flow channel. An increase in flow channel residence time results in an undesirable increase in the period available for hydrate aggregation and blockage.

A second disadvantage of highly viscous fluids is that they

are difficult to handle in the field, e.g. for pumping from storage into a pipeline. A possible counter to this second disadvantage is the use of a non-Newtonian fluid which could have a low viscosity in the low shear of storage, but a greater viscosity in the high shear of a pipeline.

While the above disadvantages might be mitigated by other means, we have elected to follow a second path to hydrate growth inhibition, that of steric stabilization.

III.C.2.b. Growth Inhibition by Steric Stabilization

As an aid to understanding this molecular scale inhibition process, a look at the structures of the best inhibitors (Section III.C.2.b.1) might be of value before discussing the mechanism of these kinetic inhibitors in Section III.C.2.b.2.

III.C.2.b.1. Inhibitor Structure and Aqueous Solubility

The best hydrate growth inhibitors found to date are polymers containing a lactam ring attached to a carbon polymer backbone. The lactam structures, shown in Figure 2, are non-planar, non-aromatic rings which have two hydrogen bonding species, a nitrogen (N) immediately adjacent to the carbon backbone, and a carbonyl (C=O) group on the ring itself.

We have had success with 5- and 7-member lactam ring polymers, but it is difficult to obtain both higher and lower (odd) ring numbers of lactam compounds. It appears that lactam rings with even numbers of members cannot be fabricated, for thermodynamic reasons.

One key to inhibitor performance appears to be aqueous solubility. The 5-member lactam ring found in polyvinyl-pyrrolidone (PVP) promotes aqueous solubility; PVP has no cloud point in the temperature range of interest. The 7-member lactam ring in polyvinylcaprolactam (PVCAP) has much lower solubility, with a cloud point of 27°C. Co-polymers of 5- and 7-member rings have intermediate solubilities (e.g. VC-713 has cloud point of 37°C). Table 1 shows a strong correlation between solubility (as indicated by cloud point) and fraction of 5- or 7-member rings in the copolymer.

When the polymers dissolve in water they change the hydrogen bonding nature of the water itself, as indicated by the studies summarized in the report sections dealing with Raman spectroscopy (Section IV.B.5.) and the thermodynamic studies of inhibitors (Section IV.B.2.b.). In a salt solution, while the 5-member lactam ring (e.g. in PVP) does not change the hydrogen bonding nature appreciably, the 7-member ring increases both the strength

Figure 2. The most effective kinetic gas - hydrate inhibitors known to date

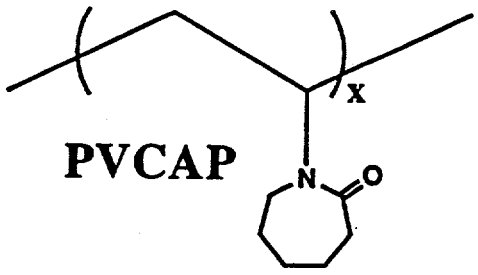

Poly(N-vinylcaprolactam)

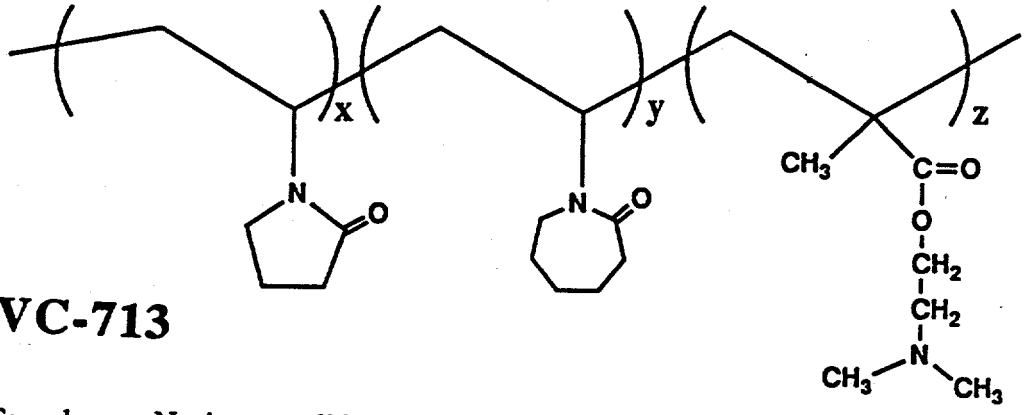

Terpolymer N-vinypyrrolidone/N-vinylcaprolactam/N,N-dimethylaminoethyl methacrylate

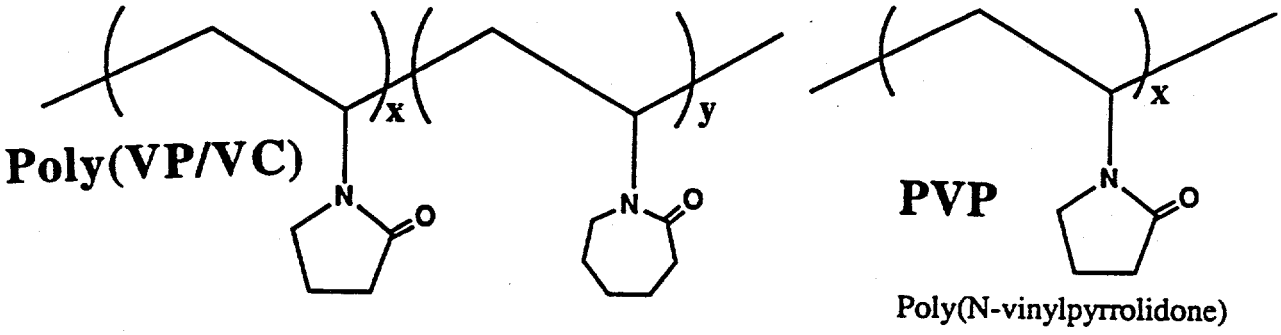

Poly(N-vinylpyrrolidone)

Poly(N-vinylpyrrolidone-co-N-vinylcaprolactam) (VP/VC)

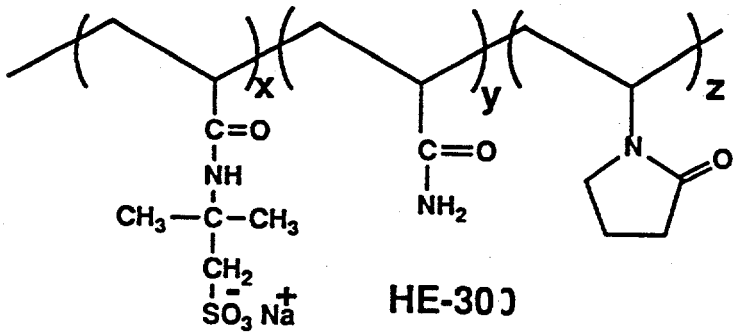

*Require blending with poly(VP/VC)

and the population of hydrogen bonds in water.

Table 1. Cloud Point as a Function of Polymer Composition

Polymer Ring Ratio (5-member ring:7-member ring)	Upper Cloud Point °C
100:0	none
75:25	60
50:50	34
0:100	27

At first glance, since hydrates themselves are composed of hydrogen bonds, it is counter-intuitive to think that a hydrate inhibitor might increase water hydrogen bonding. However, if the hydrogen bonds are shifted, for example from a normal predominance of 5- and 6-member rings in water, to 7-member rings (or other abnormal distributions) with the polymer, then hydrates might not be formed as easily with 5- or 6-member faces of hydrogen bonds.

Alternatively, one might think of a sequential, two-step hydrate formation process: (1) breaking the hydrogen bonds in water, and (2) reforming hydrogen bonds in hydrate. The 7-member lactam polymer makes the first step more difficult, and therefore decreases the combined rate of hydrate formation by its interaction with water.

Beyond the interaction with water however, the inhibiting polymer also interacts with the growing hydrate crystal itself as discussed in the next section.

III.C.2.b.2. Mechanism for Steric Stabilization

Our hypothesis for steric stabilization suggests that, when the hydrate crystal begins to grow the inhibitor "docks" or adsorbs on a preferred growth site such as a pentagonal face, or better, a hexagonal face of the crystal. Mr. Ben Bloys of ARCO showed using molecular models that the 5-member lactam ring is an approximate fit to the pentagonal hydrate face, and the 7-member ring approximately fits the hexagonal hydrate face.

The hypothesis also suggests that docking or adsorbing of an inhibitor on a hydrate face is enabled by the fact that two hydrogen bonding sites (N and C=O) are on the inhibitor ring. Perhaps the docking of the 7-member ring species on a hexagonal hydrate face provides more efficient inhibition than the docking of a 5-member species to a pentagonal hydrate face, since large cavity growth occurs via 6-membered faces. The non-ring (carbon

polymer) portions of the inhibitor molecule act to repel and disperse other crystal fragments, which have similarly bonded inhibitors.

One way to interpret the docking phenomena is to consider the aqueous inhibitor solutions as a supersaturated or metastable fluid with respect to adsorbing from solution. Just as a low vapor pressure indicates the ready adsorption (of a vapor) on a solid, a low, (upper) cloud point indicates the ready adsorption (of a polymer) from solution. An upper cloud point indicates that temperature above which the polymer forms a separate phase.

When hydrates nucleate and begin to grow, they provide a precipitation/adsorption site for the inhibitor polymer to leave its metastable state in solution. The metastable polymer molecules leave the aqueous solution to dock their rings on growing hydrate crystal faces, sterically stabilizing the active growth site.

When components in liquids either precipitate or adsorb from solution they generally seek an interface. In the present case the active growth sites on a hydrate crystal fragment provide a convenient landing or docking site for the polymer coming from solution. If a polymer (e.g. a 7-member lactam such as PVCAP) has lower solubility, it's higher metastability will encourage substantial adsorption to block more hydrate sites. At the same concentration if a polymer has increased solubility (brought about by the presence of 5-member lactam rings) it will have more difficulty precipitating or adsorbing on the growing hydrate nucleus.

III.C.2.b.2.a. Effect of Salt on Inhibitor Performance. A salt effect may also be considered to be another factor of the above solubility concept. When salt is added to a polymer solution, UV-Vis spectroscopy (Section IV.B.1.b.2.c.2.) indicates that the lactam rings are compressed. This may be caused by the fact that the salt ions tie up water molecules which would normally be used in polymer hydration.

For the case in which the polymer precipitation is already borderline, the addition of salt causes polymer precipitation before hydrates form, making the inhibitor less effective. However, for a polymer with some solubility (perhaps caused by the presence of the 5-member ring) the addition of salt ions tie up water molecules and thus decreases the polymer solubility to cause it to approach the solubility limit. When a polymer becomes more metastable, it will be more likely to precipitate when a growing hydrate crystal appears.

III.C.2.b.2.b. Effect of Concentration on Inhibitor Performance. An extension of the same concept can be used to explain polymer concentration effects. The ideal inhibitor

system may be one that has a substantial amount of metastability, so that the polymer will readily adsorb at the site of a growing hydrate mass. However when the polymer concentration is too high, it becomes too supersaturated in solution, and polymer precipitation will occur.

When polymer precipitation occurs from a supersaturated, metastable solution, the polymer concentration in the remaining solution will decrease to the equilibrium concentration. After polymer precipitation the remaining polymer in solution will be less likely to adsorb on hydrate than the previous, (higher and more metastable) polymer concentration.

The analogous situation may be considered in ice nucleation from a subcooled solution of liquid water. Subcooled water may be maintained at -5°C for an extended period of time; yet when the temperature is decreased slightly ice can precipitate and the solution temperature will rise to 0°C. The analogy to polymer precipitation is realized by considering decreased temperature as the independent variable for ice precipitation, in place of increased concentration for polymer precipitation.

III.C.2.b.2.c. Steric Stabilization Hypothesis Summary. The above physical hypothesis suggests that the inhibitor polymer acts to inhibit hydrates (1) by changing the hydrogen bond pattern of liquid water to a more unfavorable distribution and (2) by adsorption of polymers whose rings hydrogen bond to preferred growth site(s) of the hydrate face. In the latter case, the non-ring portions of the polymer additionally act to shield the hydrate fragment from other crystal fragments.

The hypothesis is preliminary in nature, and is by no means flawless or without exception. However, the physical picture provided by the hypothesis may be used to unify the phenomena included in this report. An extension of this picture suggests regions for verification and investigation during the 1994 effort (Section V.).

IV. What Was Accomplished in 1993

IV.A. A Synopsis of New Findings

In 1993 we found several chemicals (VC-713, PVCAP, VP/VCP copolymers and blends, and blends with HE-300) which performed substantially better than PVP, the best chemical found in the previous two years. New chemical performance was evaluated in terms of time required for rapid hydrate growth from natural gas and seawater at 39.2°F, within limits of minimum inhibitor concentration, maximum pressure, and salt concentration. These

chemicals are also effective in terms of inhibiting hydrate formation from gas-condensate mixtures and from drilling muds. A synopsis of the improved performance (and performance limitations) of new chemicals is in Section IV.A.1.

A second major result in 1993 work was the discovery of evidence supporting the mechanism for inhibitor performance, which is summarized in the previous section (III.C.). This mechanism will aid in the design of better hydrate inhibition candidates in the future. Section IV.A.2 contains a listing of the evidence for the mechanism. Using the new sapphire cell apparatus, we generated a video tape (provided with this report) as a visual record of inhibitor effect on hydrate formation and morphology.

Finally, we began work (Section IV.A.3) which will support implementation of hydrate inhibitors in the field. While we do not yet report the field tests results here, a graduate student began experiments at the Exxon pilot flow loop in Houston, and the Chemical Engineering Senior Design class performed a conceptual evaluation of polymer recovery pipeline processes.

IV.A.1. Vastly Improved Inhibitors and Their Performance Limits

In 1993 we found much better inhibitors than PVP (the best previous chemical for which field tests began in 1992). Polymers containing a lactam ring with five members (vinyl pyrrolidone [VP]) or seven members (vinyl caprolactam [VCP]) were particularly effective. Of the chemicals found, VC-713, PVCAP, and copolymers and blends of VP and VCP were particularly efficient in delaying the onset time of hydrate growth (the dependent variable) as a function of independent variables (temperature, pressure, inhibitor concentration, and salt concentration.)

Because the above chemicals were extremely efficient we worked to find limits to their performance. In mid-year we lowered the temperature of the high pressures tests from 54.5°F to 39.2°F, a much more stringent temperature typical of seafloor conditions. The mid-year test pressure was also changed from 1125 psig to a nominal 1000 psig.

At 39.2°F and 1000 psig, the following inhibitor and salt concentrations were determined as near optimum:

Inhibitor	Near-Optimum Inhibitor Conc. wt%	Near-Optimum Sea Salt Conc. wt%
VC-713	0.5	3.5
PVCAP	0.5	3.5

PVCAP 1.0 w/o salt

In the above results 1.0 wt% PVCAP without sea salt performed better than 0.5wt% PVCAP with 3.5 wt% sea salt. Yet a system of 1 wt% PVCAP without seasalt performed much better than 1 wt% PVCAP with 3.5wt% salt. In addition small concentrations (2.5wt%) of methanol decreased PVCAP inhibition performance, while larger methanol concentrations increased inhibition. These surprising results may be interpreted through the "metastability/ adsorption" hypothesis of Section III.C.2.b.2.a.

For copolymers of the 5- and 7-member lactam rings, inhibitor performance was proportional to the fraction of the 7-member ring present. Above 75% caprolactam (7-member) ring, no difference was observed. Blends of PVP and PVCP showed almost the same efficiency as copolymers with the same ring ratios. A new electrolyte inhibitor (HE300) appeared to be very efficient when combined with a 25/75 copolymer of VP/VCP.

Lengthy (>24hrs) duration tests of VC-713 and PVCAP were made with a second (ARCO) gas and n-decane. In these tests 0.75 wt% PVCAP without salt produced the longest inhibition time (45 hours), while 0.5wt% VC-713 (with 500 ppm salt) formed hydrates very rapidly at pressures of 1000 psig and above. Solutions of PVCAP (0.5 wt% with 3.5% salt) were very sensitive to pressures and their performance was limited to 1000 psig.

With n-decane in the normal (Green Canyon) gas system, PVP appeared to provide only a slight increase in inhibition, while VC-713 appeared to significantly inhibit hydrate formation; PVCAP was not tested with this system. With drilling muds, VC-713 also appeared to inhibit hydrate formation; again due to time constraints PVCAP was not tested with drilling muds.

IV.A.2. Evidence to Support an Inhibition Mechanism

As a result of the work done during 1993 we can cite evidence in support of our hydrate formation mechanism, (detailed in Section III.C.):

1. The best inhibitors are polymers with lactam ring appendages of either 5-members (e.g. PVP), 7-members (e.g. PVCAP), or combinations of the 5- and 7-member rings. It appears that two hydrogen bonding sites are needed on each ring.

2. The best inhibitors have borderline solubility. In a polymer with different ratios of ring structures, the 5-member ring encourages solubility, while the 7-member ring is much less soluble. Therefore a polymer with the 7-member ring (PVCAP) is the best inhibitor found to date.

3. The 5- and 7-member lactam rings change the strength and population of hydrogen bonds in the liquid water itself, as determined by Raman and UV-Visible spectroscopy. While at 0°C neither PVCAP nor VC-713 changes the hydrogen bonding of the solution without salt appreciably, the addition of VC-713 with salt increases both the hydrogen bond strength and population. In contrast at 0°C, PVP with salt causes no change in the hydrogen bonds, but PVP without salt increases both the hydrogen bond strength and population.

4. In a deionized water system, the addition of 0.5% PVCAP and VC-713 increased the equilibrium temperature of hydrate formation (by up to 6°C), while the addition of 0.5% PVP did not change the hydrate formation temperature appreciably.

5. Inhibitor effectiveness was found to be proportional to solution viscosity, a macroscopic property related to hydrodynamic volume. A very viscous solution will inhibit hydrate growth without strong dependence on the chemical nature of the viscosifier; however the inhibition performance of low viscosity solutions is significantly enhanced by the presence of 7- and 5-member rings.

6. In a quiescent system, hydrates normally grow at the gas-liquid interface. Hydrates can be caused to grow in either bulk phase by making the interface less attractive, by coating the interface with a surfactant, or by providing a high energy surface in the bulk with amorphous silica.

The evidence cited above has helped us formulate a more complete picture of how kinetic inhibitors might work, and this will help us design better hydrate kinetic inhibitors in the future.

IV.A.3. Support of Field Implementation

A significant new area of effort in 1993 was the direct support of field testing the chemicals. At our consortium meetings in March and August, success in field testing PVP was reported in 9 pipelines in Wyoming by Amoco, and varying degrees of success in individual pipeline tests reported by Oryx, Shell, and Texaco. While some preliminary tests (without quantitative results) were reported with VC-713, no company field tested PVCAP in 1993.

In an effort to perform better controlled tests, Exxon Production Research afforded us the opportunity to run pilot plant tests on their temperature controlled flow loop in Houston. In September and October 1993, we ran tests in our laboratory on similar systems to be tested on the flow loop. In late October

1993 Mr. Joe Lederhos, a senior graduate student began work on Exxon's flow loop in Houston. Exxon has graciously agreed that all results from the work of Mr. Lederhos will be available to the consortium. At year's end, Mr. Lederhos had established a baseline of operation of the loop, but no inhibitor results are yet reported. The Exxon flow loop results will be reported at the 1994 March consortium meeting, and in the 1994 Annual Report.

In 1993 we filed for patent protection on hydrate kinetic inhibitors containing a lactam ring. This filing was in the U.S.A. Patent Office by CSM's patent attorneys, and in a European/South American filing through an "in kind" contribution of Marathon's attorneys.

In a project initiated by Amoco, the CSM Senior Design Class performed a conceptual design of the recovery of kinetic inhibition polymers from a North Sea pipeline. The conceptual design was independently done by 7 groups (three persons each) for recovery of PVP and VC-713. The almost unanimous choice for recovery was an ultrafiltration membrane system, and a sample design report is included in the appendix of this report.

IV.B. Progress in Specific Areas

IV.B.1. Screening Apparatus

IV.B.1.a. Experiment and Results

The purpose of the screening apparatus was to test as many as 1000 potential hydrate inhibitors in one year. Rapid screening was made possible by the use of tetrahydrofuran (THF) a miscible hydrate former, rather than an immiscible former, such as natural gas, which can cause delays due to mass transfer and surface renewal difficulties. THF is the saturated four carbon member of the furan family. With THF, hydrate formation occurred at 4°C from a solution that is 20 weight% THF in water. At that concentration and temperature without inhibitor, all of an inhibited solution will become hydrate, and the THF molecule will occupy only the large cage of sII hydrate.

The screening apparatus shown in Figure 3, consists of a motor driven rack that rotates at 15rpm. The rack held a maximum of 12 test tubes. Each test tube was charged with 6 ml of inhibitor test solution and 2 ml of THF. This provided about 20wt% THF in the solution, fulfilling the criteria of a molar ratio of 17:1 (water:THF) for hydrate formation. Mixing was achieved using a 3/8 inch 440 stainless steel ball. This type of ball also provided the best material for hydrate initiation as was found in a series of experiments reported in the 1991 annual report.

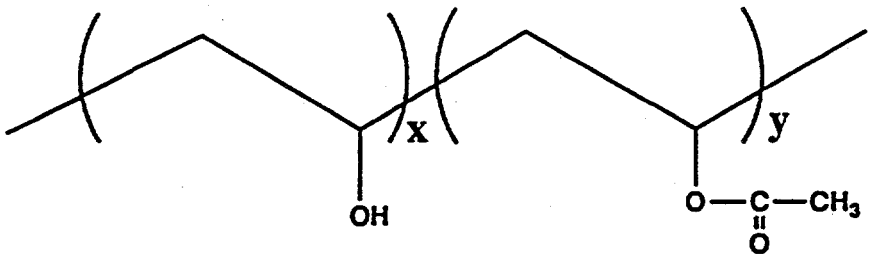

Poly(vinyl alcohol-co-vinyl acetate)

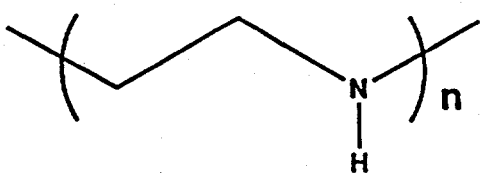

Poly(ethyleneimine)

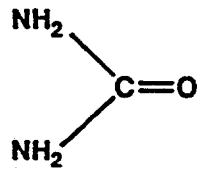

Urea

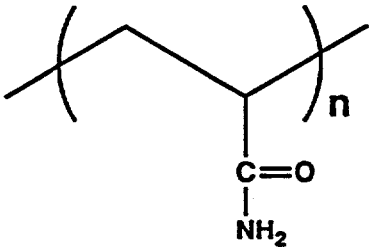

Poly(acrylamide)

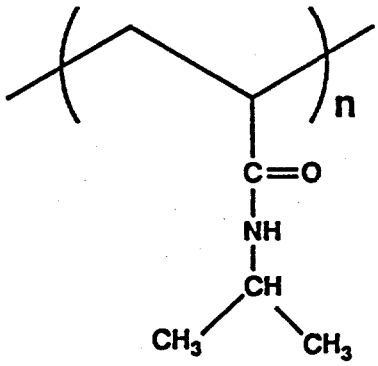

Poly(N-isopropylacrylamide)

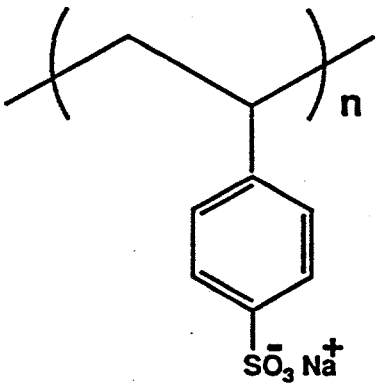

Poly(styrene sulfonate)

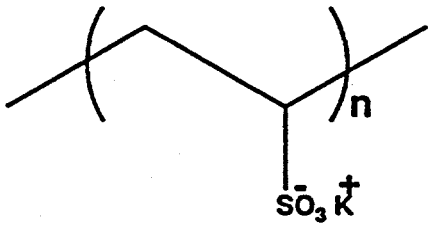

Poly(potassium-vinylsulfonate)

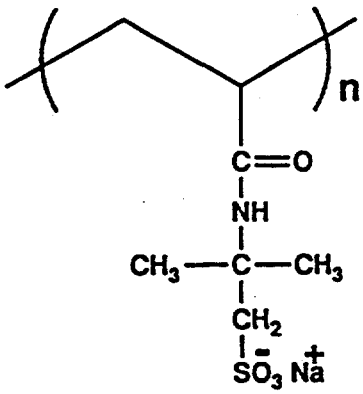

Poly(sodium-2-acrylamido-2-methylpropane sulfonate)

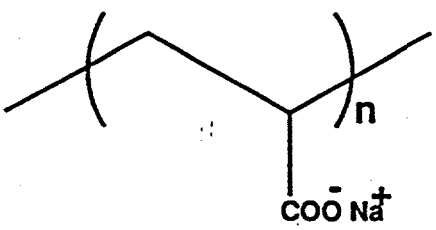

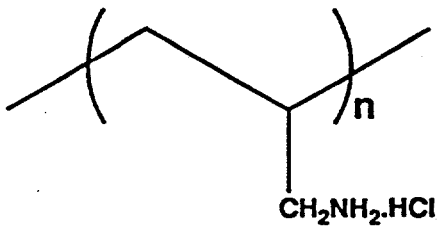

Poly(potassium-vinylsulfonate)

Figure 3a. Screened water soluble polymers

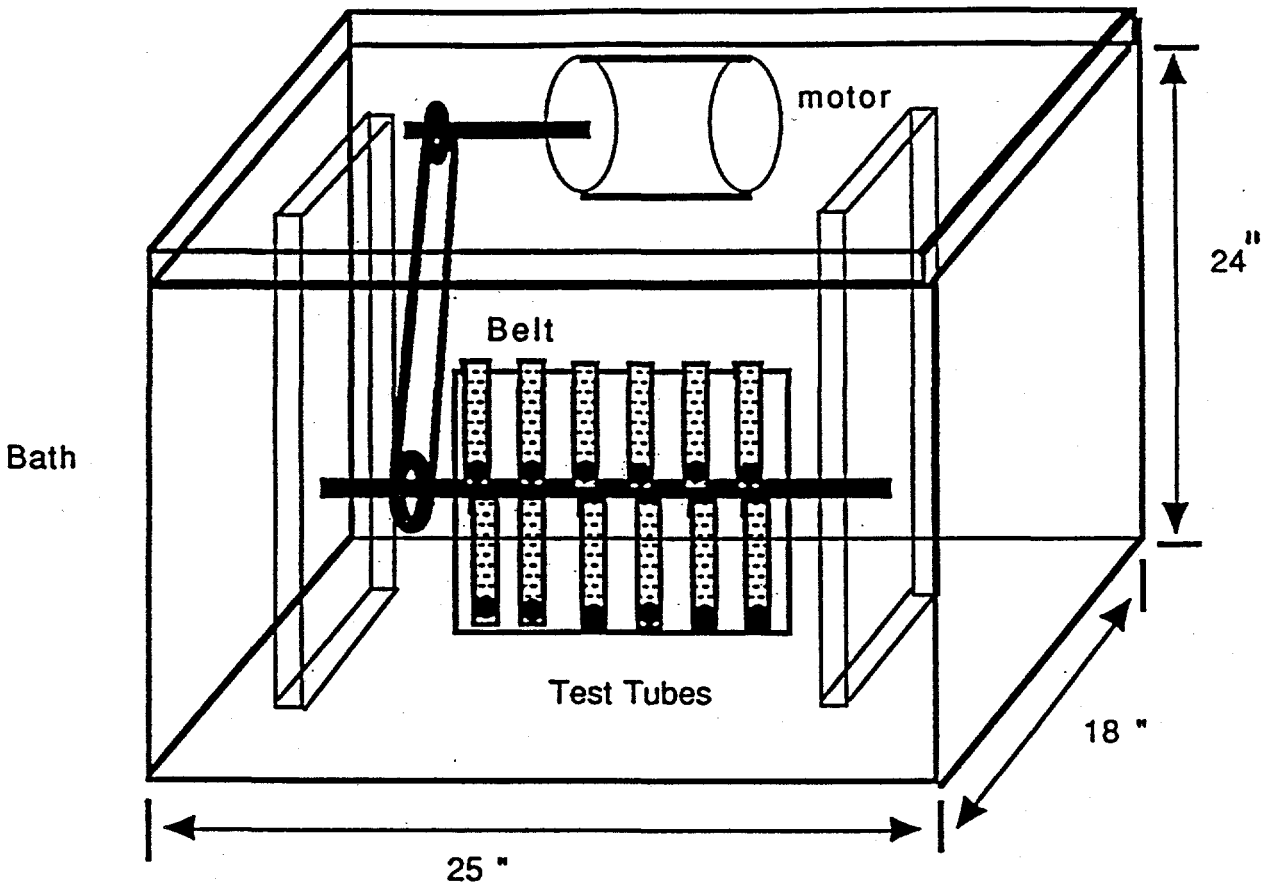

Figure 3. Schematic diagram of the THF hydrate multiple screening reactor.

At the start of an experiment, the test tube rack was submersed in an insulated water bath that was maintained at a constant experimental temperature of 0°C. Two time-dependent measurements were made from the experiment. The start of both measurements began at the placement of the test tube rack in the constant temperature bath and the start of rotation.

The induction time is defined as the time when hydrate crystals were first visually observed on the wall of the test tube. The ball stop time is defined as the time from the start of the experiment to the time when the ball either could no longer move through the test solution, could only move through a few centimeters in the test solution or through a small empty pocket where there was no longer any solution.

Test solutions were made from a combination of chemical inhibitor solution and a sea salt solution. First, 200 grams of concentrated solution of inhibitor was made at 5wt% inhibitor in deionized water. Sea salt solution was also made at 5wt% concentration from ASTM synthetic sea salt and deionized water. The sea salt solution was mixed for approximately 4 hours then filtered through a 0.45 micron filter. Standard inhibitor concentrations were 0.5wt% inhibitor with 3.5wt% sea salt. Planned deviations from this standard ranged from 0.1wt% to 1.0wt% for inhibitor and from 0 to 3.5wt% for sea salt.

An inhibitor was labeled "poor" if the ball stop time was less than 1 hour after the start of the test. Some inhibitors had short induction times - less than 30 minutes - yet had ball stop times greater than 4-5 hours. Good inhibitors had ball stop times greater than 5 hours. In most cases, the experiment was terminated after 5 or 6 hours.

Figure 2 lists the successful chemicals tested including their structures. Results from 1993 showed that inhibitors with 5- or 7-member lactam rings attached to a polymer chain performed well.

One polymer and a series of copolymers have proven to outperform the good inhibitor polyvinylpyrrolidone (PVP) found 1 year ago as seen in Figures 4, 5 and 6. The polymer, polyvinylcaprolactam, (PVCAP) has a seven-member ring attached to the polymer chain. In the initial tests, PVCAP did not show hydrate formation for greater than 13 hours at 0.5wt% with 3.5wt% sea salt.

PVCAP was also tested at 0.25wt% with 3.5wt% sea salt. Hydrate crystals appeared (at the induction time) 45 minutes after the start of the experiment; there was no ball stop time. At 0.1wt% PVCAP with 3.5wt% sea salt, the induction and ball stop times were 27 and 31 minutes, respectively.

Screening Apparatus Results

0.5%wt chemical, 3.5%wt seasalt, 0°C

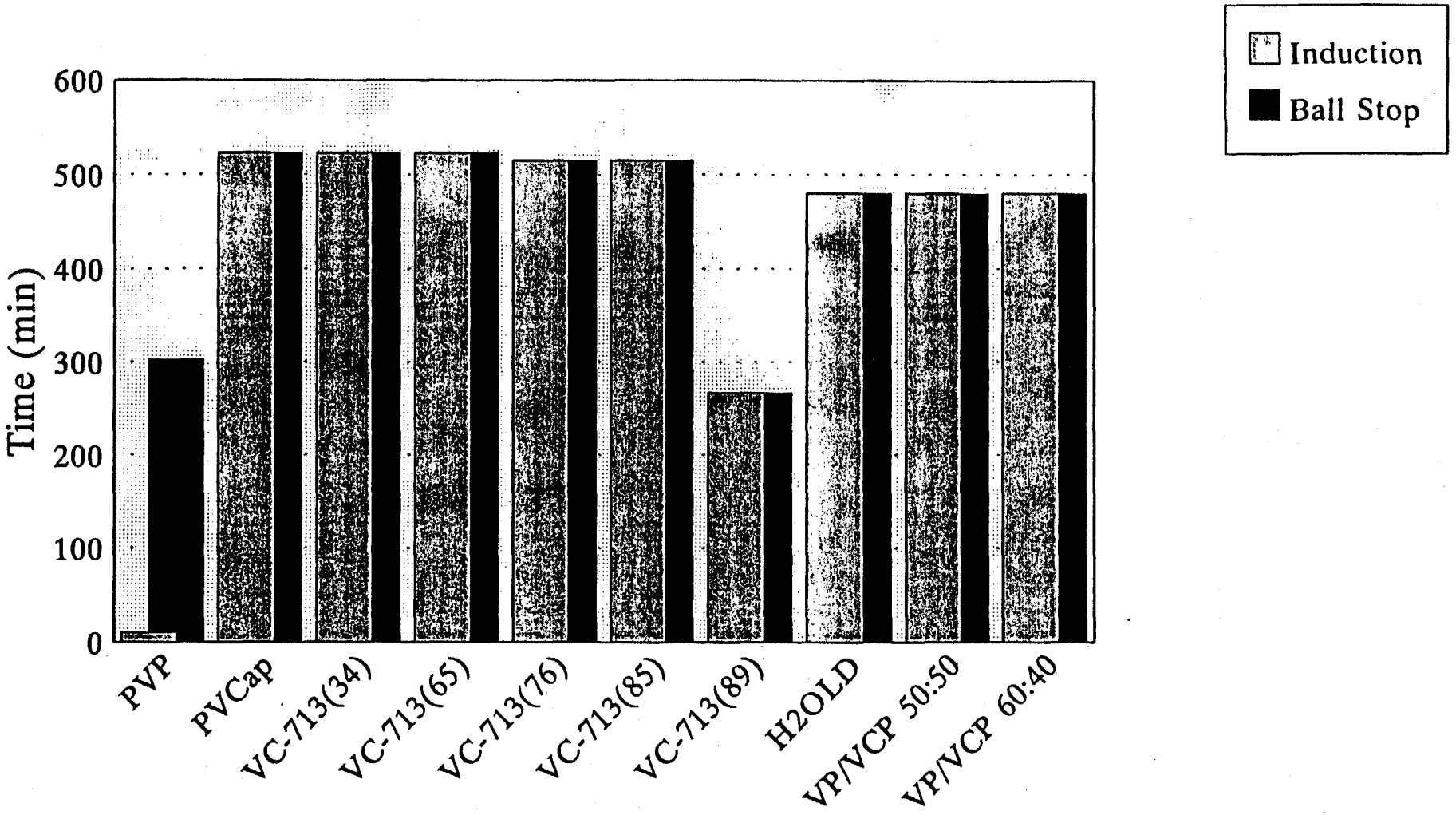

Only PVP had an induction time.
None showed a ball stop time.

Figure 4. Results from the Screening Apparatus

Screening Apparatus Results

0.25%wt chemical, 3.5%wt seasalt, 0°C

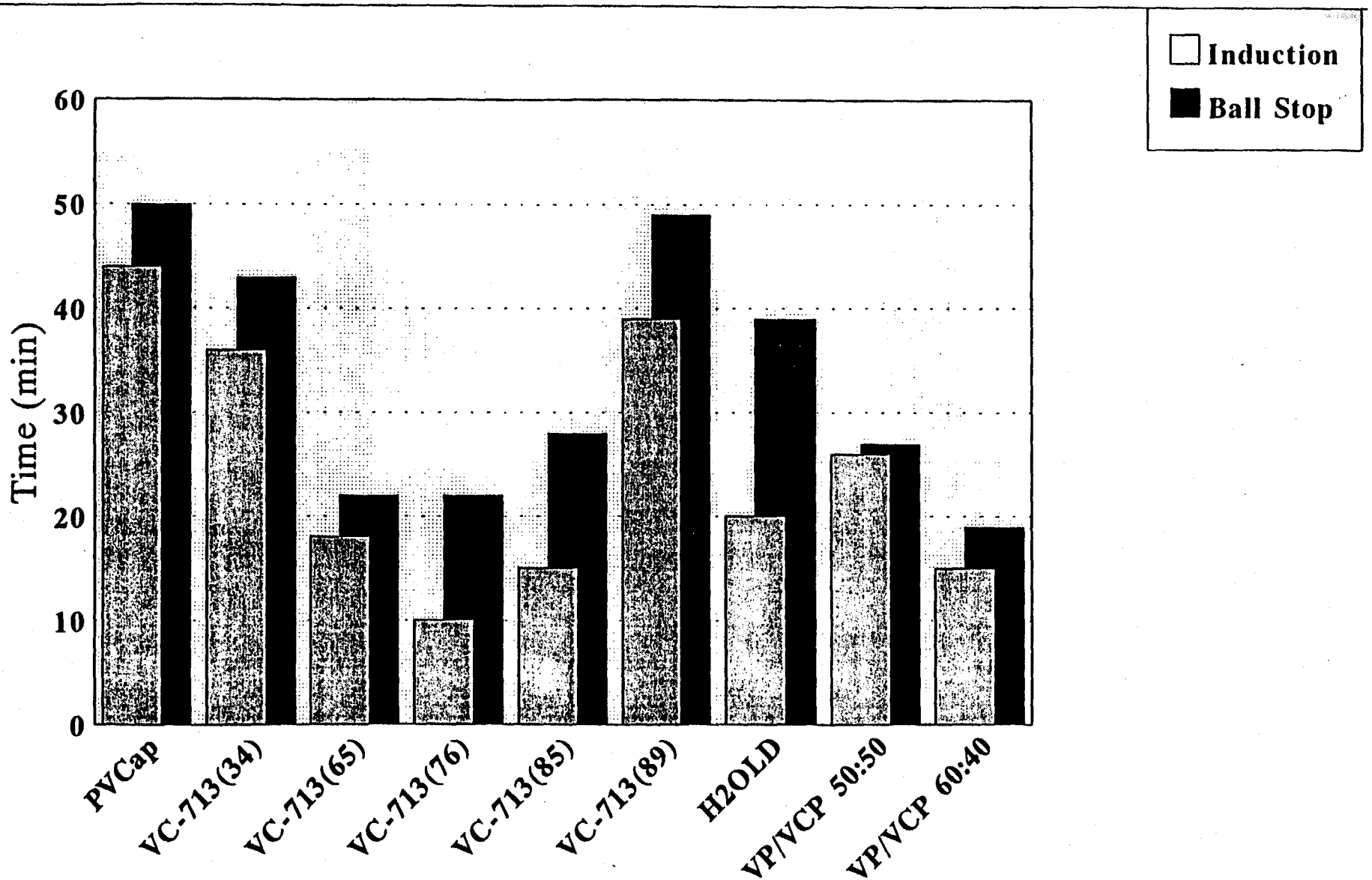

At lower concentrations, the chemicals perform poorly.

Figure 5. Results from the Screening Apparatus

Screening Apparatus Results

0.1%wt chemical, 3.5%wt seawater. 0°C

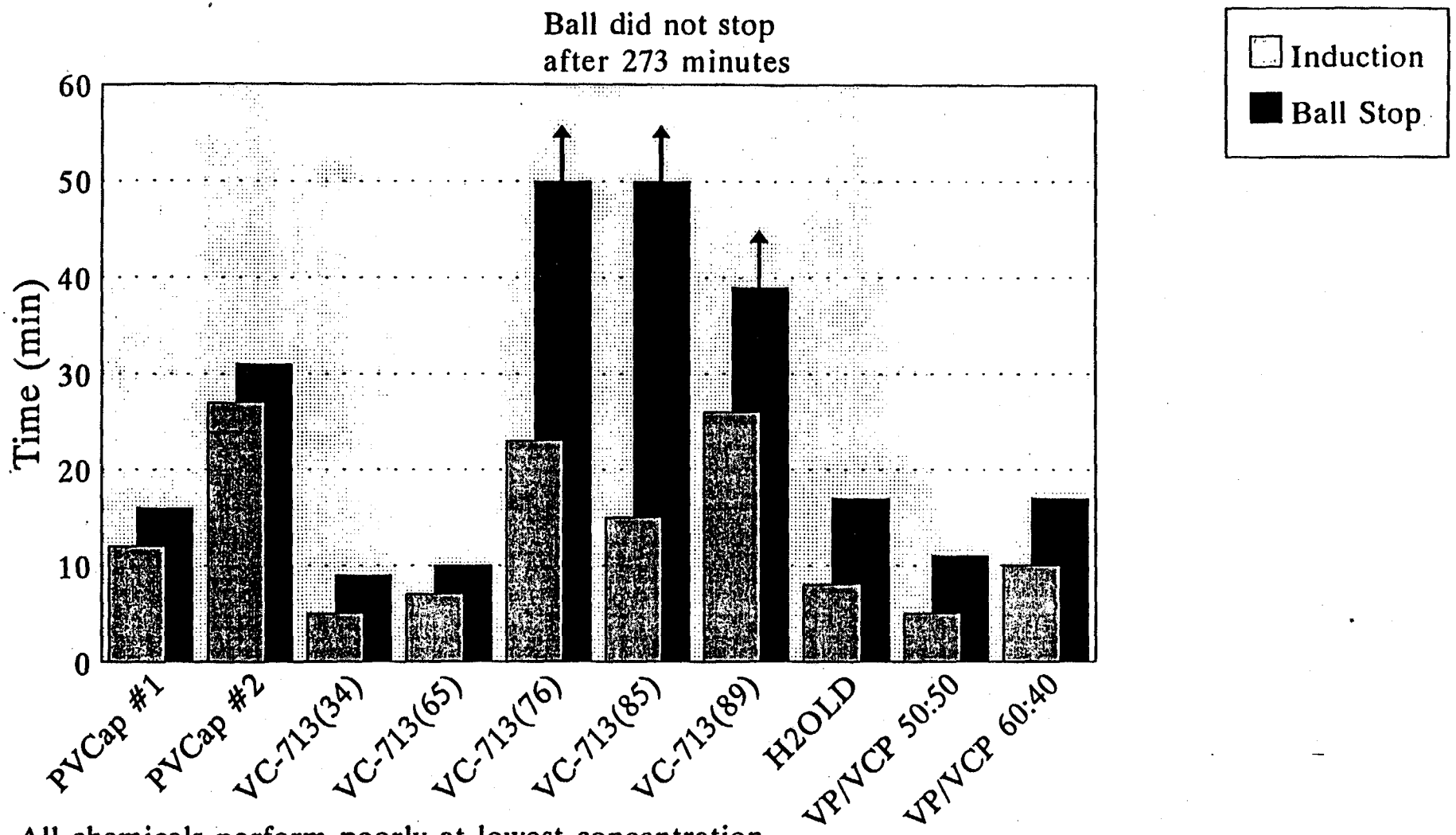

All chemicals perform poorly at lowest concentration.

Lots 76 and 85 of VC-713 have an unexplained ball stop time.

Figure 6. Results from the Screening Apparatus

A series of copolymers, consisting of a 5- and a 7-member ring in varying ratios, tested well. Copolymer ratios tested were 0:100, 25:75, 50:50, 60:40, and 75:25 (vinylpyrrolidone: vinylcaprolactam). Figure 4 shows that at 0.5wt%, every ratio performed well, with no hydrate formation in 8 hours. Figures 5 and 6 show that at 0.25wt% and 0.1wt% hydrate inhibition was less effective, and was directly proportional to the amount of caprolactam in the inhibitor.

Another inhibitor which has provided good performance is a copolymer with the trade name of VC-713, consisting of a 5-member ring, a 7-member ring, and an amine group. Five batches of VC-713 (34, 65, 76, 85 and 89) have been tested. Figure 4 shows that at 0.5wt% inhibitor and 3.5wt% sea salt, all of the batches performed well with none forming hydrates in 8 hours, except when the experiment was prematurely stopped for VC-713 batch 89. Figure 5 shows that both induction and ball stop times were less than one hour at 0.25wt% inhibitor. Figure 6 indicates that both times were less than 40 minutes for 0.1wt% inhibitor - 3.5wt% sea salt for all VC-713 batches except 76 and 85.

Another series of screening tests determined the effect of sea salt concentration on inhibitor performance. Figures 7 and 8 show the performance of PVCAP and VC-713 at variations from the standard 3.5wt% sea salt to 2wt%, 1wt%, and 0wt% sea salt. There was a marked difference in the inhibitor performance at the lower sea salt concentrations, with a decrease in induction times with salt concentration, from a matter of hours to minutes. Note that the salt effect for PVCAP was different than that found in the high pressure apparatus (Section IV.B.2.c.1.c.), perhaps due to the presence of THF.

IV.B.1.b. Chemicals Tested in 1993

The polymers which were tested in the screening apparatus in 1993 are shown in Figures 2 and 9. The most promising polymers are shown in Figure 2. Other polymers and chemicals which were tested in 1993 are shown in Figures 9a, 9b, and 9c, but they all showed poor inhibition (ball stop times less than 30 minutes.)

IV.B.1.b.1. Characteristics of Unsuccessful Chemicals

IV.B.1.b.1.a.The Urea Family of Compounds In the literature urea is reported as a hydrogen bond breaker. It was suggested that if urea could break hydrogen bonds in water, perhaps it might inhibit hydrate formation. However, urea was found to be ineffective. Urea's polymeric analogue, polyacrylamide (PAM) was also found to be ineffective. Another member of the PAM family, poly(N-isopropylacrylamide) (PNIPAM, Figure 9a) has been reported to form an ice-like structure along

Screening Apparatus Results

0.5%wt PVCap, varied salinity, 0°C

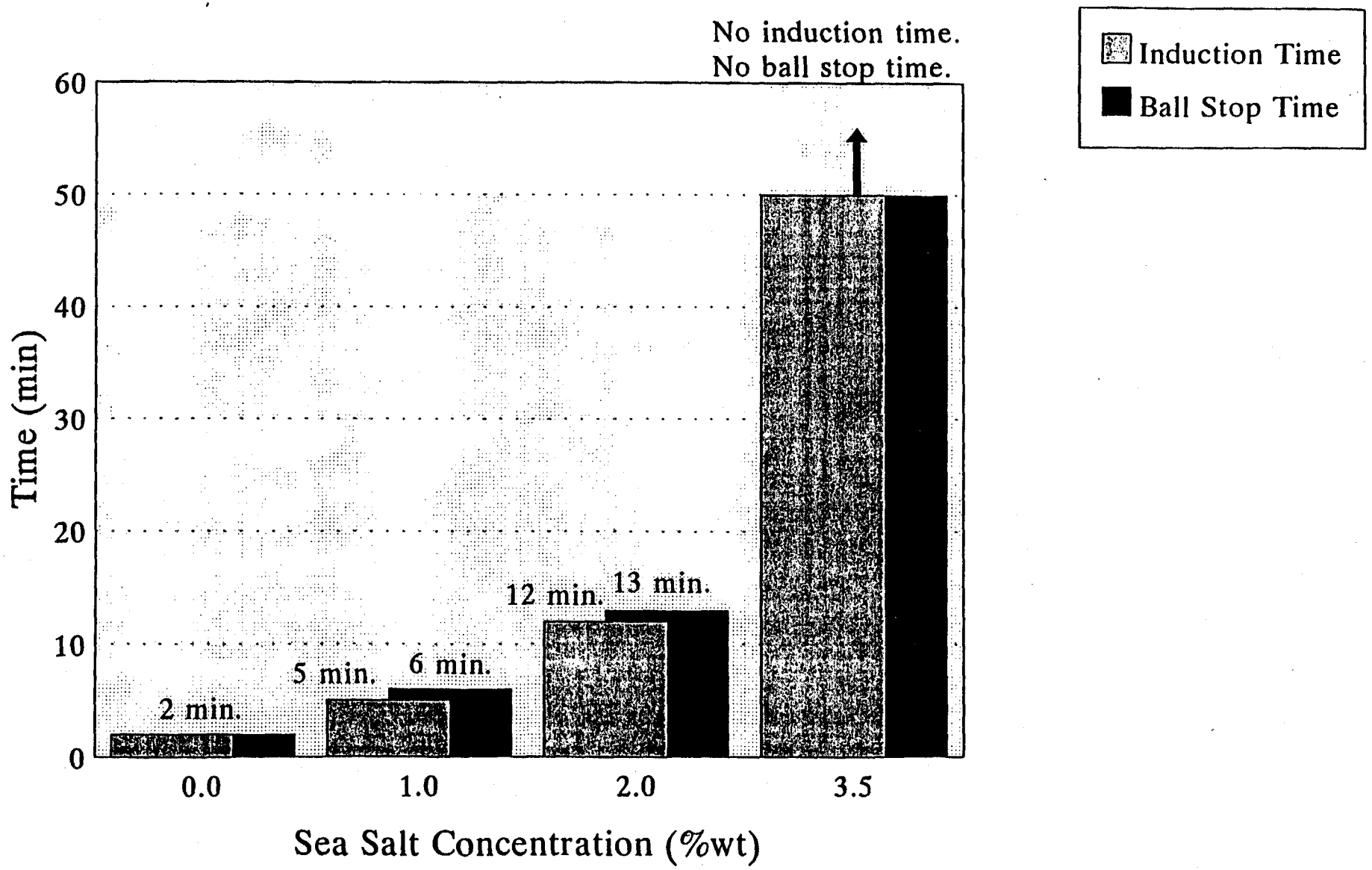

Figure 7. Results from the Screening Apparatus

Screening Apparatus Results

0.5%wt VC-713(65), varied salinity, 0°C

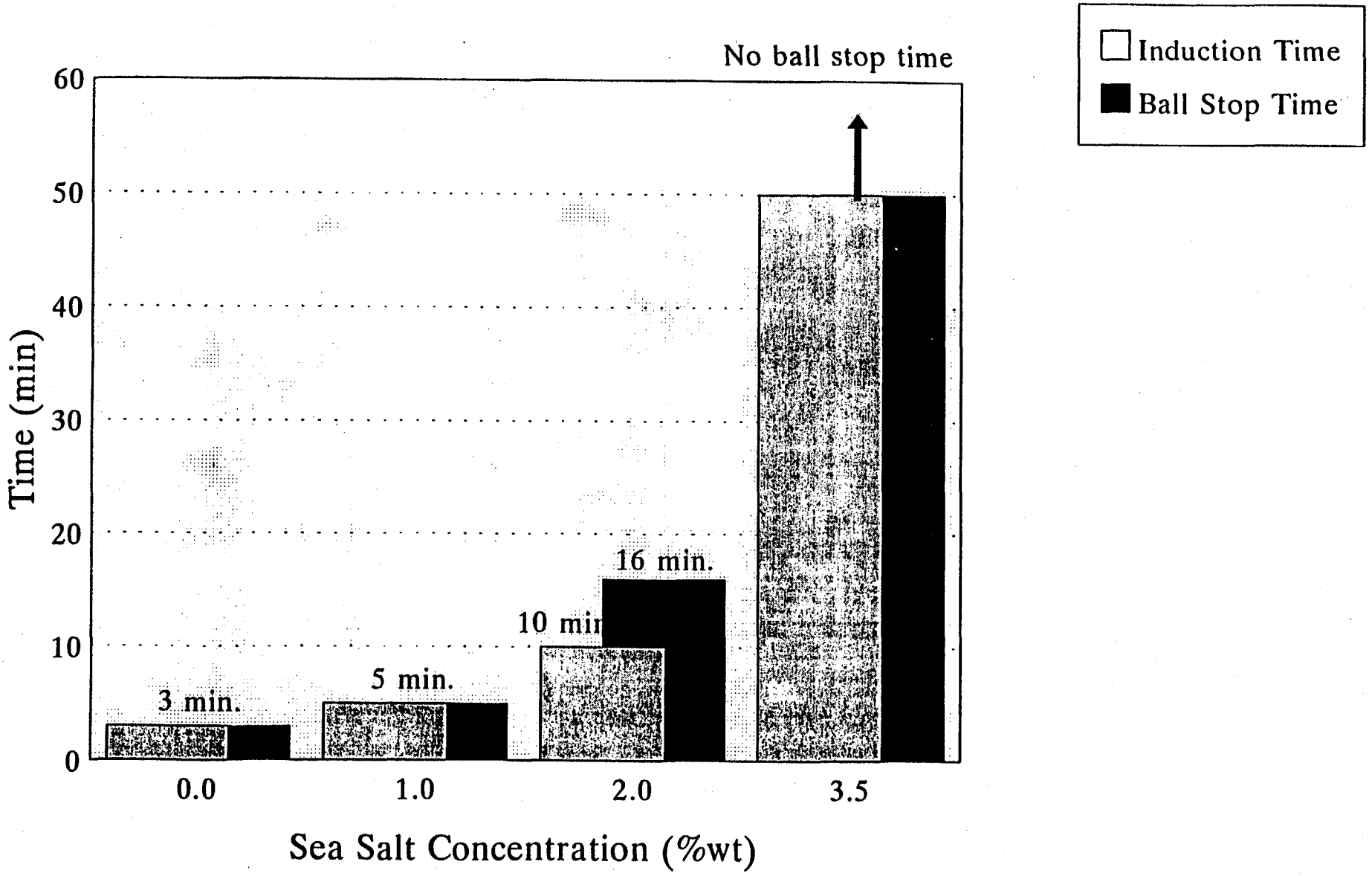

Figure 8. Results from the Screening Apparatus

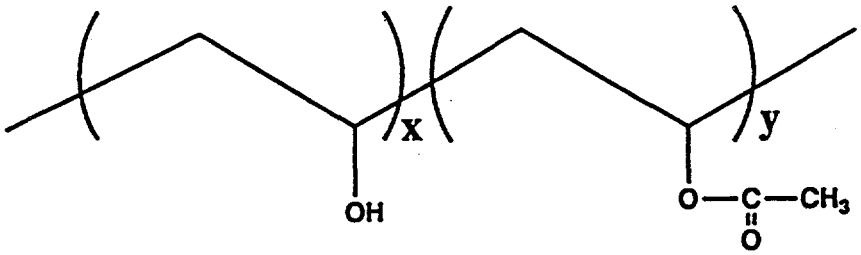

Poly(vinyl alcohol-co-vinyl acetate)

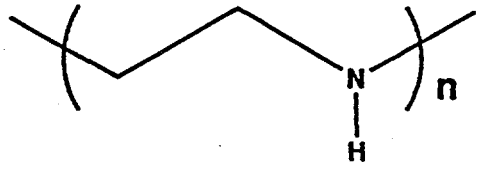

Poly(ethyleneimine)

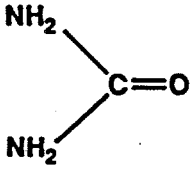

Urea

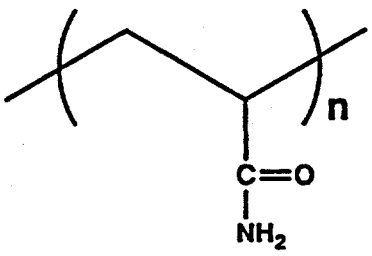

Poly(acrylamide)

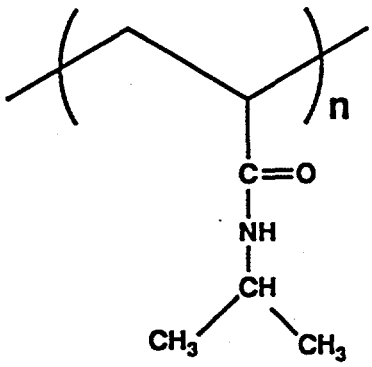

Poly(N-isopropylacrylamide)

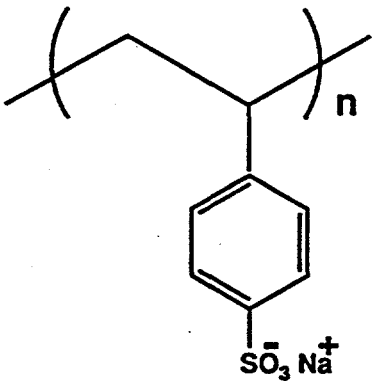

Poly(styrene sulfonate)

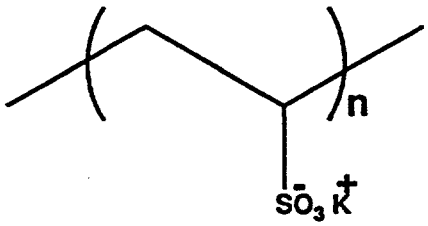

Poly(potassium-vinylsulfonate)

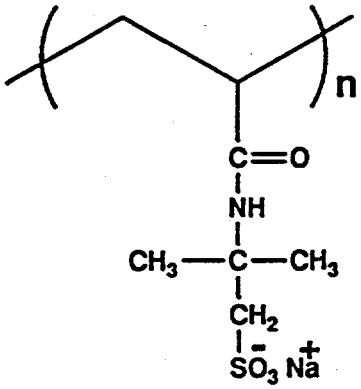

Poly(sodium-2-acrylamido-2-methylpropane sulfonate)

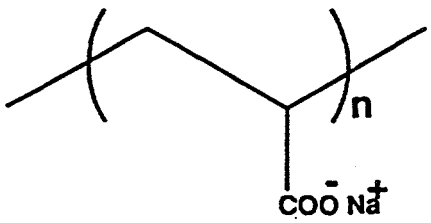

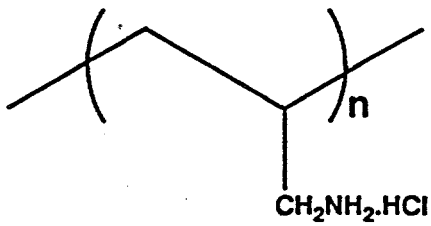

Poly(potassium-vinylsulfonate)

Figure 9a. Screened water soluble polymers.

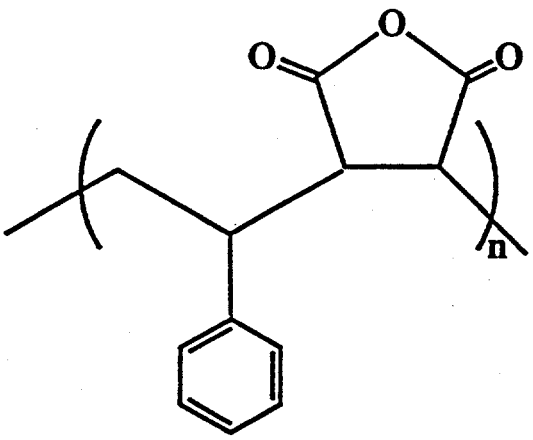

Dissolve in aq. NaOH

Anhydride to acid

Styrene-maleic anhydride copolymer

L-Tyrosine (and methyl ester)

Figure 3b. Screened aromatic water soluble polymers

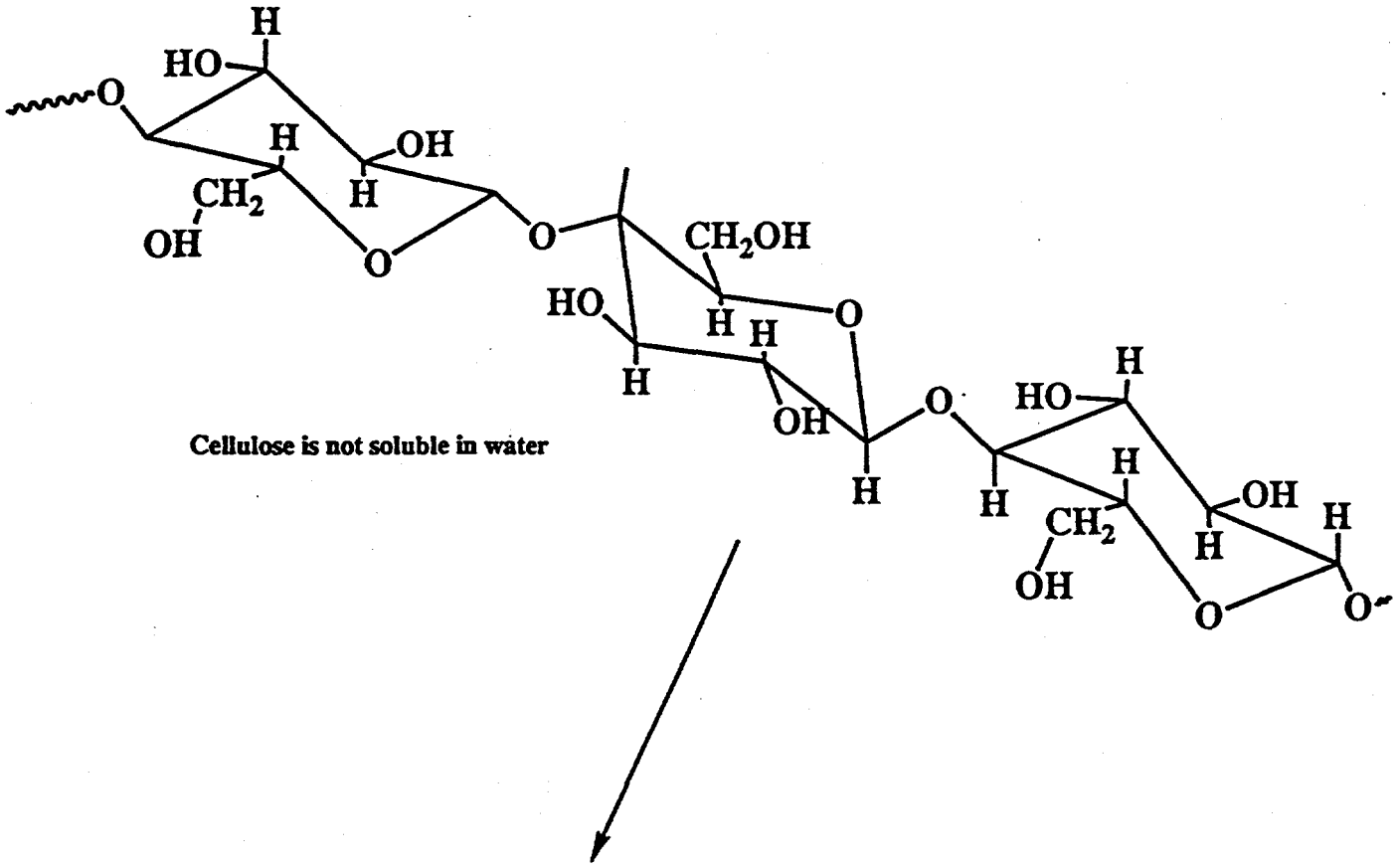

Methyl Cellulose (HO- to CH_3O-) is soluble in water

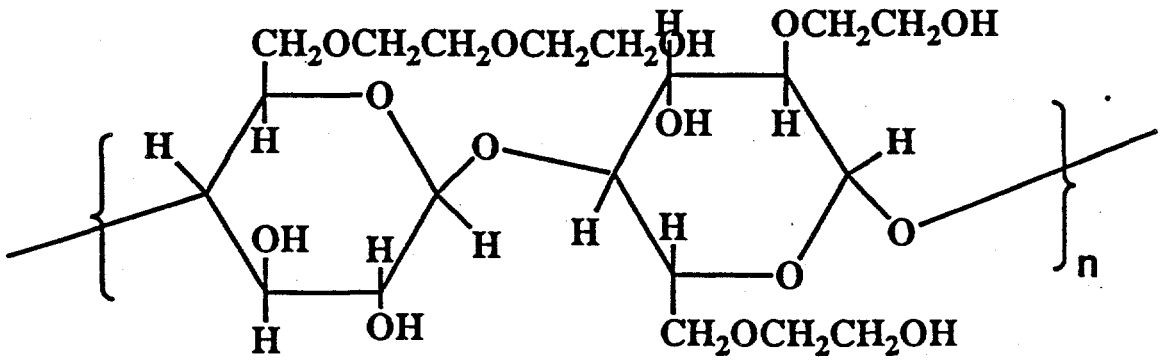

Hydroxyethyl Cellulose (HEC)

Figure 3c. Cellulose and its derivatives

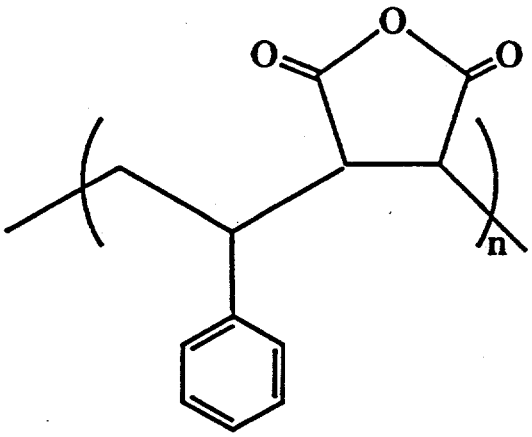

Dissolve in aq. NaOH

Anhydride to acid

Styrene-maleic anhydride copolymer

L-Tyrosine (and methyl ester)

Figure 9b. Screened aromatic water soluble polymers.

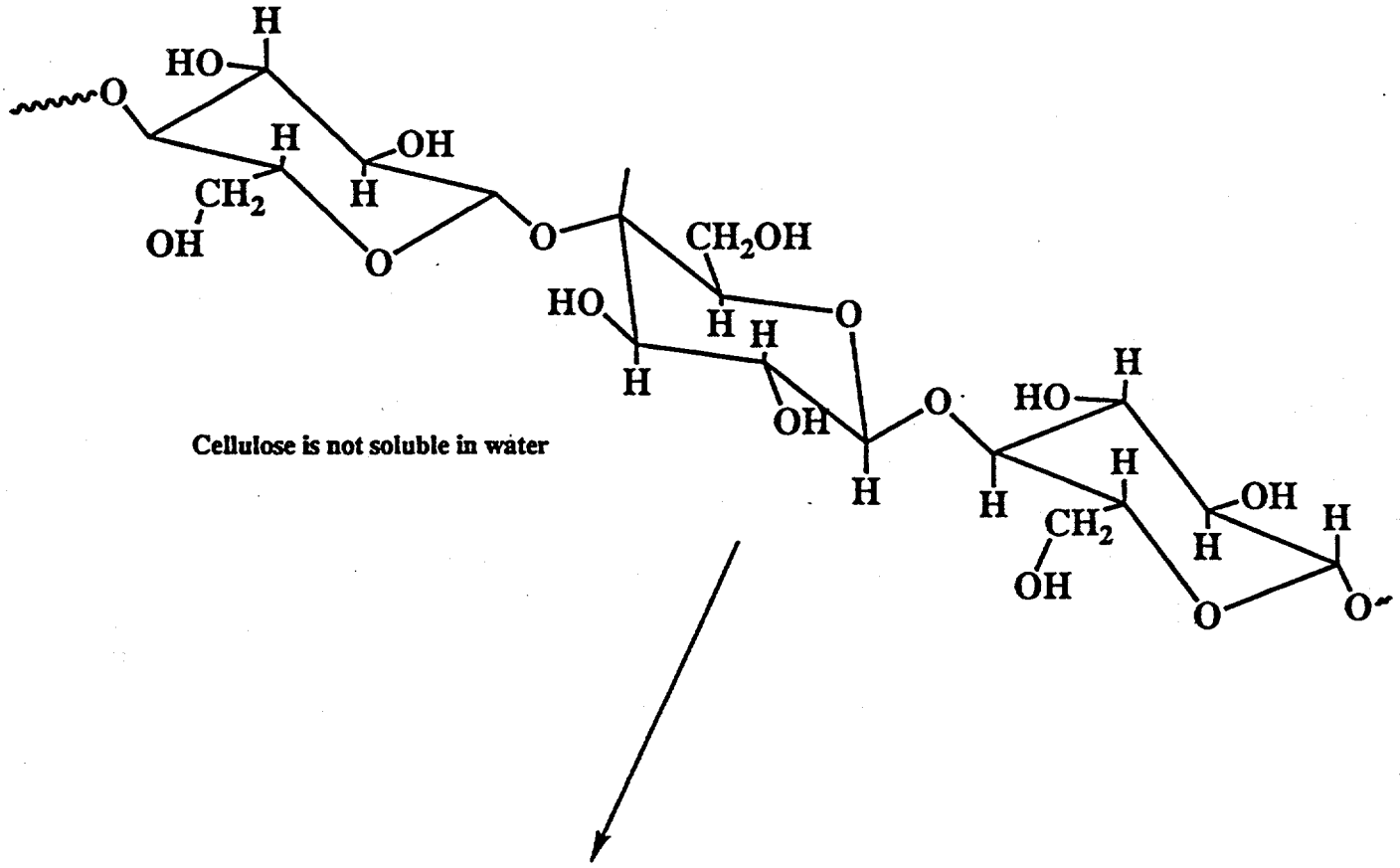

Methyl Cellulose (HO- to CH_3O-) is soluble in water

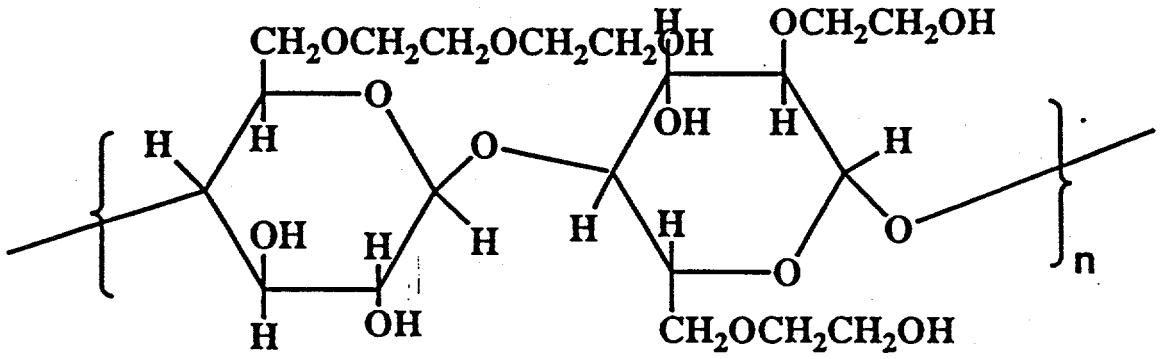

Hydroxyethyl Cellulose (HEC)

Figure 9c. Screened cellulose and its derivatives.

the polymer chain, when it is hydrated in water. This polymer can be considered an open-chain analog of PVP. However a high pressure apparatus experiment showed this polymer to be an ineffective hydrate inhibitor.

IV.B.1.b.1.b. Other Ring Polymers Tested Among the polymers with ring structures, methylcellulose, used as a drilling mud additive, showed no inhibition efficiency. Styrene-maleic anhydride copolymer (Figure 9b) has a ring structure, but is insoluble in DI water and showed no inhibition efficiency. Among the other aromatic inhibitors L-tyrosine and its methyl ester (Figure 9b) were patented by British Petroleum Co. However, neither compound was effective as an inhibitor.

IV.B.1.b.1.c. Polyelectrolytes as Inhibitor Enhancers. Polyelectrolytes such as poly(styrene sulfonate) (PSS), poly(sodium acrylate), poly(potassium vinylsulfonate), poly(sodium-2-acrylamido-2-methylpropanesulfonate) (PAMPS), and poly(allylamine) hydrochloride were tested as possible steric stabilizers (Figure 9a). An increased steric repulsion by these polyelectrolytes was expected to result from increased solvation of water molecules. Such a repulsion could possibly prevent the agglomeration of hydrate crystals. However, screening tests showed that these polyelectrolytes are ineffective.

IV.B.1.b.2. Successful Kinetic Inhibitors

All the screening results are consistent with the requirement of a non-planar ring structure with two hydrogen bonding sites for effective inhibition , such as those present in N-vinylpyrrolidone and N-vinylcaprolactam. The presence of one hydrogen bonding site may facilitate hydrogen bonding of the polymer with one face on a hydrate cavity. The presence of the second hydrogen bonding site may also bond the ring structure to a hydrate face (**docking**) and prevent the growth of hydrate unit cells, or prevent the agglomeration of the hydrate crystals. Unsuccessful screening results with aromatic polymers [e.g. poly(styrenesulfonate) and L-tyrosine] support the hypothesis that a non-planar ring structure is needed.

In 1994 we will test the "2 hydrogen bond site" hypothesis by using a synthesized or derivatized kevlar. Derivatization is required to solubilize the kevlar in water, and the presence of two hydrogen bonding sites across the aromatic rings may inhibit the hydrate growth. We will test other structures to explore this requirement.

We found a new terpolymer, HE-300 shown in Figure 2 to be a good inhibitor. This polymer contains the 5-member lactam ring structure, vinylypyrrolidone, also in one of the best inhibitors

to date. This polymer has a short induction time but no ball stop time. The induction time was eliminated by blending with other polymers. The details are presented in the following section.

IV.B.1.b.2.a. Polymer Blending Studies. Blending studies of PVP/PVCAP, PVCAP/poly(styrenesulfonate) (PSS), and HE-300 with various polymers were undertaken so that new and inexpensive inhibitors might be obtained. Blending can also provide information about the mechanism of hydrate inhibition. A 25/75 blend of PVP and PVCAP was compared with the 25/75 copolymer of vinylpyrrolidone and vinylcaprolactam (VP and VC) at 0.5 wt%. Screening results showed no induction time and no ball stop time for both systems in over 24 hours. Results from the high pressure experiment showed the blend was comparable, though somewhat lower in performance compared to the copolymer. The stock PVCAP used in the blend system was 50wt% in ethanol (BASF's sample). In the immediate future we will attempt further improvements of the PVP/PVCAP blend by using a stock PVCAP of 80wt% methanolic solution (ISP's sample).

PVCAP and PSS solutions were blended so that an inhibitor combination with docking capability and with steric ring repulsion could be obtained. As described in the polyelectrolyte section (IV.B.1.b.1.c.), PSS alone is not a good inhibitor. The combined inhibition can only be achieved if the two polymer chains are entangled in the solution. However, the blends of PVCAP and PSS were ineffective. We also observed poor performance for a blend of PVP and poly(sodium-2-acrylamido-2-methanepropanesulfonate) (PAMPS) as shown in Table 2. These discouraging results also indicated that the polymer chains are probably not intermeshed in the solution.

The above two blending experiments indicate that the combined effect of docking and steric repulsion can be achieved by a copolymer of these two monomers. Accordingly a commercially available terpolymer HE-300 was selected. This copolymer (Figure 10) has acrylamide (AM), N-vinylpyrrolidone (VP), and sodium-2-acrylamido-2-methylpropanesulfonate (AMPS) as the co-monomers. The important components are the VP and AMPS units. The role of AM units is yet to be determined, but the presence of AM was unavoidable due to its presence in the commercially available material.

New inhibitor chemical HE-300 has no ball stop time at a concentration of 0.5wt%. More importantly, this polymer has no ball stop time even at 0.25wt% whereas PVCAP (BASF) and PVP do have a low ball stop time at this concentration. Blending HE-300 with PVP or PVCAP improved the induction time marginally as shown in Table 2. The blend with PVCAP had a ball stop time. The blend of PVP had an induction time, but no ball stop time;

Table 2. Screening results of HE-300, homopolymers of its components, and blending of HE-300 with PVP, PVCAP, and N-vinylpyrrolidone/N-vinylcaprolactam copolymer [poly(VP/VC)] in 3.5% sea water.

Polymer	Concentration (wt.%) % polymer/% alcohol	Induction Time (IT, min)	Ball Stop Time (BST, min)
HE-300[a]	0.5/0	15, 13, 18, 14	no BST in 480
HE-300[a]	0.25/0	4.5, 8.0, 7.5	no BST in 480
PVP (K-90, ISP)	0.25/0	4, 7, 3	15, 15, 15
Poly(acrylamide) (PAM)	0.5/0	3.5, 2.0, 4.5, 3.0, 3.5, 2.0	10-20
PAMPS[b]	0.5/0	1.5 (3 runs)	5-20
PVP (K-90)/PAMPS	(0.25/0.25)/0	2.5 (4 runs)	30
HE-300/PVP (K-90)	(0.25/0.25)/0	8, 5, 6, 5	no BST in 1440
PVCAP-BASF[c]	0.25/0.25 (ethanol)	4, 17, 8	5, 21, 12
HE-300/PVCAP-BASF[c]	(0.25/0.25)/0.25 (ethanol)	38, 27, 25, 37	45, 40, 32, 42
Poly(VP/VC) (25/75)-ISP[d]	0.25/1.0 (methanol)	35, 300, 70	no BST in 4320
	"	35	1200
	"	no IT in 600 (6 runs)[e]	no BST in 4320 (6 runs)
	"	17.5, 90, 30, 60, 16.5, 8.5	no BST in 4320
HE-300/ Poly(VP/VC) (25/75)-ISP[d]	(0.20/0.25)/1.0 (methanol	no IT in 270 (four runs)	no BST in 270 (4 runs)
	"	no IT in1680 (6 runs)	no BST in1680 (6 runs)
	(0.25/0.25)/1.0 (methanol)	660	3600
	"	660, 35[f]	no BST in 4320
	"	>1680	"
	"	>1680	"
	"	<1500	"

[a]HE-300 contains the monomers of PVP, PAMPS, and PAM.
[b]Poly(sodium-2-acrylamido-2-methylpropanesulfonate)
[c]Polymer was supplied as a 50% solid in ethanol.
[d]Polymer was supplied as a 20% solid in methanol.
[e]Surprisingly long induction time; the actual concentration may be more than 0.25%, most likely due to a weighing error.
[f]Very short induction time; probably a contaminated test tube.

Figure 10. Mechanism of Hydrate Growth Inhibition by a Copolymer of Lactam and Electrolyte

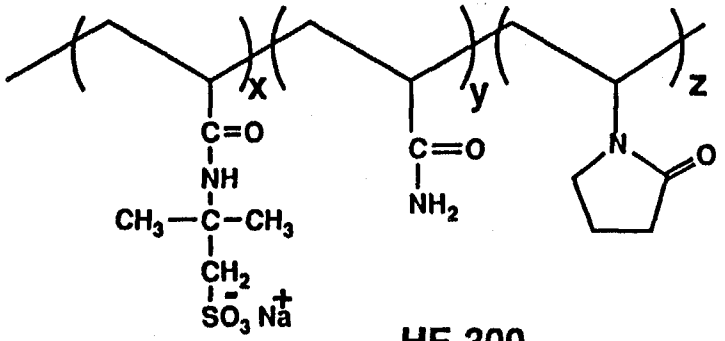

HE-300

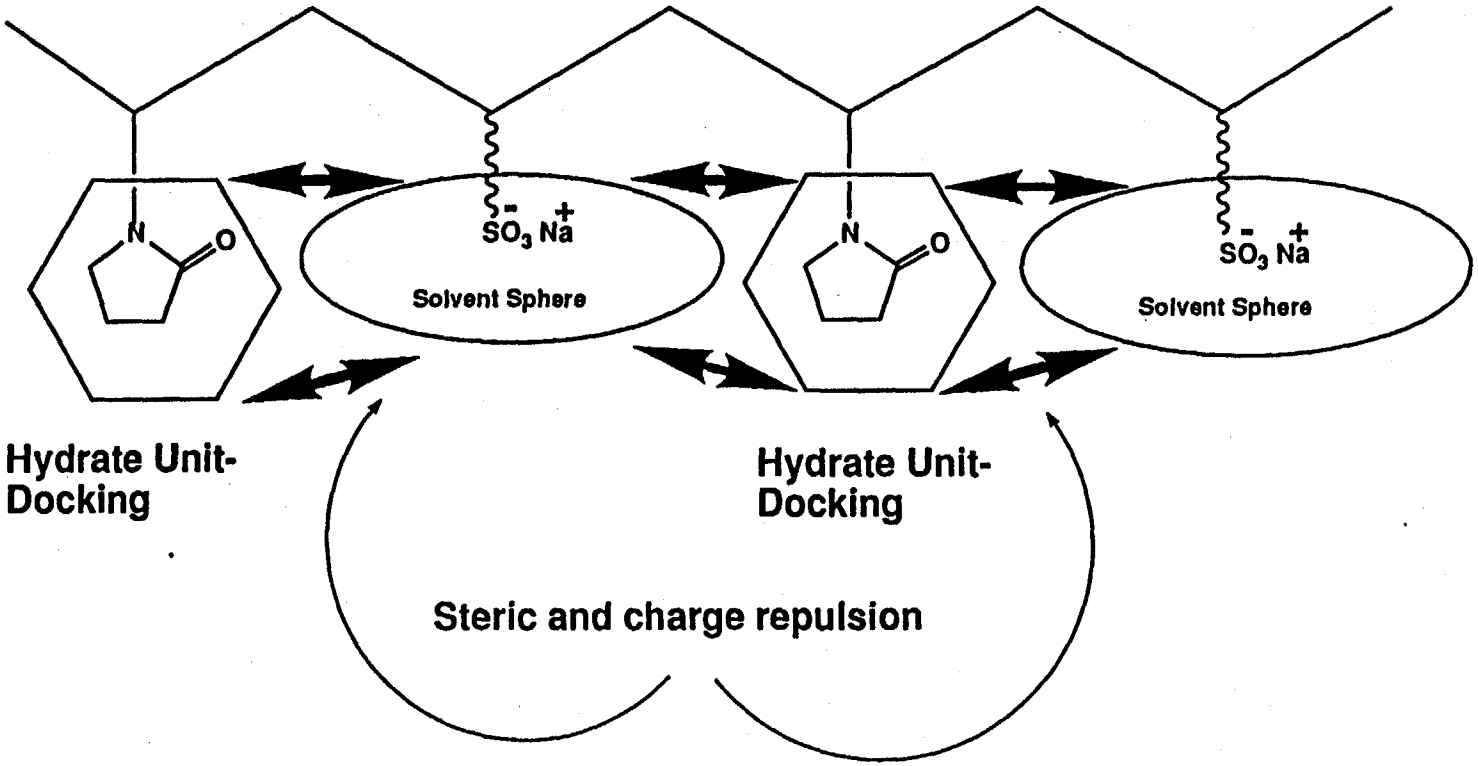

however, the PVP blend is not as good as HE-300 alone as indicated by a decreased ability of ball movement in the test tubes.

These two blending studies show that a blend of HE-300 with PVP is better than a blend of HE-300 with PVCAP. This is due to better miscibility, perhaps due to entanglement by the PVP with HE-300 polymer, because of the presence of the same monomer unit in the HE-300. The Hildebrand principle of "like-dissolves-like" applies here. As previously established in polymer science, if two polymers A and B are immiscible, they can be mixed by the use of a small amount of copolymer of A and B. This result is commonly observed in solid state mixing or in concentrated solutions. However, these phenomena may also be observed at the dilute (0.5wt%) solutions of our experiments.

Accordingly HE-300 was blended with a VP/VCP (25/75) copolymer. The data shown in Table 2 clearly indicate that the performance of the HE-300 was improved by blending it with VP/VCP (25/75) copolymer. The high pressure gas hydrate experiments also showed that this blend is comparable in inhibition to PVCAP.

It should be noted that the blend of 0.25 wt.% HE-300 and a 0.25wt% copolymer of VP/VCP (25/75) (ISP) contained 1wt% methanol. On the other hand, the blend of 0.25wt% HE-300 and 0.25wt% PVCAP (BASF) contained 0.25wt% ethanol. The amount and the type of alcohols might have influenced the results. Therefore, the influence of methanol on the inhibition efficiency is analyzed in the following section.

The above experiments suggest that a copolymer of N-vinylcaprolactam (VCAP) and AMPS might be an excellent future kinetic inhibitor. Preparation of the copolymer is underway.

IV.B.1.b.2.b. Influence of Methanol on Inhibition Efficiency. Results are shown in Table 3 for the tests of the influence of methanol. For this portion of the work screening experiments were carried out with the following chemicals:
PVP,
PVP dissolved originally in methanol,
PVCAP (ISP, from 80% methanolic solution),
VP/VCP (25/75) copolymer after the removal of solvent,
and control experiments with sea water containing methanol.

In addition the blend of HE-300 and PVCAP (ISP) from the methanolic solution showed improved efficiency in our screening apparatus. It should be noted that the blend of HE-300 and PVCAP (BASF), prepared from 50% ethanolic solution, had a disappointing ball stop time, as described in the previous section.

Table 3. Influence of methanol on the inhibition efficiency of the inhibitors in 3.5% sea water in the screening apparatus.

Polymer	Concentration (wt.%) % polymer/% CH_3OH	Induction Time (IT, min)	Ball Stop Time (BST, min)
Control	0/0	1-2	5-10
	0/1.0	1.5-20.5	no BST in 180; very viscous material
	0/2.0	1.5-4.0	no BST in 180; very viscous material
PVP (K-90), received as solid	0.5/0	12-14	no BST in 360; test tube ends were blocked and the ball movement was in the middle of the tube.
PVP (K-90)	0.5/1.0	150-270	no BST in 1060
Poly (VP/VC) (25/75)-ISP[a]	0.25/0[b]	9-25	10-32
Poly (VP/VC) (25/75)-ISP[a]	0.25/1.0	(See Table 2)	no BST in 4320
PVCAP-ISP[c]	0.25/1.0	38-120	no BST in 2820
PVCAP-ISP[c]/HE-300	(0.25/0.25)/1.0	14-150	no BST in 2820
PVCAP-BASF[d]/HE-300	(0.25/0.25)/0 (0.25% ethanol)	25-38	32-45

[a]Polymer was supplied as a 20% solid in methanol.
[b]Methanol (solvent) was removed under vacuum.
[c]Polymer was supplied as a 20% solid in methanol.
[d]Polymer was supplied as a 50% solid in ethanol.

The results of Table 3 indicate a significant improvement in the performance of the inhibitors, if the test chemicals are prepared in methanolic solutions. The comparison of the control experiments with sea water and added methanol also showed no ball stop time. However, the ball movements are slower for the control experiments compared to the tubes containing polymeric inhibitors.

These control experiments indicate that the increased induction times and ball stop times, in some cases, may not represent improved inhibition by the polymers. They may be due to a depression in freezing point of THF/water solution. Such results indicate that experiments with high pressure reactor should be made before coming to any definite conclusions regarding inhibitor efficiency.

IV.B.1.b.2.c. Supporting Evidence for Screening Results

IV.B.1.b.2.c.1.Viscosity studies of Poly(N-vinylcaprolactam).

We observed a decreased efficiency of kinetic inhibition of hydrates by poly(N-vinylcaprolactam) (PVCAP) in the presence of salts. The monomer unit of this polymer contains 8 carbon atoms, one oxygen functionality (C=O) and one nitrogen (as an amide). This chemical structure indicates that the polymer is principally hydrophobic, but it's hydrophilic functional groups (C=O and N) are responsible for polymer solubility.

Therefore, the addition of salt will increase the ionic strength of the solvent, promoting hydrophobic interactions of the polymer rings in an aqueous environment. These hydrophobic interactions between the polymer rings will cause ring agglomeration, reducing gas hydrate inhibition efficiency by making the rings less available for either hydrate docking or water bonding.

Viscosity measurements can provide information about the conformations of polymers in solution. Here we report some viscosity measurements of the PVCAP polymer in DI water and in sea water. Some viscosity results of N-vinylpyrrolidone/ N-vinylcaprolactam copolymers in methanol are also presented from ISP's technical data.

Experimental:

Viscosity measurements of PVCAP (BASF) were made using a Brookfield model LVT viscometer at 22.5°C. The measurements were also made using a Cannon viscometer (Ostwald-Fenske tube) at 25°C. All samples were prepared from a stock solution of 5wt% PVCAP in DI water. Appropriate dilutions to final concentrations were made using DI water or sea water.

Discussion:

The Brookfield viscosity measurements in Table 4 indicate that the PVCAP in DI water and in sea water have almost the same viscosities. The viscosity measurements using the Cannon viscometer in Table 5 also indicate that the PVCAP in DI water and in sea water have almost the same viscosities. It appears that the average hydrodynamic volume of the polymer has the same viscosity in DI water and in sea water.

It should be pointed out that the 5% PVCAP stock solution for these viscosity measurements was prepared from 50% PVCAP in ethanol. In the future we will compare the viscosities of solution prepared from solid PVCAP (by removing the solvent) to study the effect of pre-dissolving the polymer in alcoholic solvents. We will also determine the hydrodynamic volumes (coil dimension) of PVCAP in these various solvents by the use of low angle light scattering technique.

The viscosity data of the VP/VCP copolymers in Table 6 indicate that, as the concentration of the VP units increases in the polymer chain, the viscosity also increases in methanol. This is due to better solubility and increased chain expansion with more hydrophilic VP units in the polymer. The same trend will be expected for the copolymer in water. The increase in hydrodynamic volume will increase the hydrate inhibition efficiency by preventing the agglomeration of the hydrate crystals.

However, the 5-member lactam ring (pyrrolidone) does not provide the best docking mechanism, the 7-member ring does. In addition, these pyrrolidone units cannot adsorb a lot of water molecules and thereby provide steric inhibition to the agglomeration of the hydrate crystals. A better co-monomer for the best lactam unit (N-vinylcaprolactam) might be a an ionic monomer. In such a copolymer, the caprolactam units function according to the docking mechanism while the ionic monomer will attract a large amount of water and provide steric repulsion and charge repulsion as illustrated in Figure 10. This type of copolymer may provide better kinetic inhibition, and will be the focus of future work.

<u>IV.B.1.b.2.c.1. UV-Vis Spectroscopic Studies of PVCAP</u>. Ultraviolet Visible (UV-Vis) spectroscopy is a technique which depends upon electronic transitions of chemical bonds. The groups which are responsible for such transitions are called chromophores; in PVP and PVCAP the carbonyl (C=O) group is the chromophore. The carbonyl group has two electronic transitions. The first is an intense absorption due to $\pi \rightarrow \pi^*$ electronic transition of the carbonyl bond. A second weaker absorption at a longer wavelength is due to the $n \rightarrow \pi^*$ transition of the lone

Table 4. Viscosity results (Brookfield) of PVCAP in sea water and in DI water as a function of concentrations.

Concentration (%wt.)	In DI water (arbitrary units)	Brookfield Viscosity, in 3.5% sea water (spindle #3, 50 rpm, 22.5°C, arbitrary units)
Solvent	11.75	11.75
0.5	13.25	13.25
1.0	15.25	15.25

Table 5 . Viscosity results (Cannon Viscometer) of poly(N-vinylcaprolactam) in DI water and in 3.5% sea water

Concentration (wt.%)	$\eta_{rel.}$ in DI Water	$\eta_{rel.}$ in Sea Water (3.5%)
0.25	1.08	n/a
0.5	1.18	1.13
1.0	1.37	1.30
2.0	1.89	1.75
3.0	2.56	n/a

Table 6 . Viscosity results of N-vinylpyrrolidone/N-vinylcaprolactam (VP/VC) copolymers[a]

Copolymer (VP/VC)	$\eta_{rel.}$(Relative Viscosity), 1% in methanol (25°C)	Brookfield Viscosity, 20% in methanol (spindle #3, 50 rpm, 25°C, cps)
0/100	1.13	66
25/75	1.17	52 (?)
50/50	1.67	94
75/25	1.79	151.
100/0	n/a	n/a

[a]ISP'S technical data

pair of electrons in the oxygen of the carbonyl group; this absorption provides little information. The intensity and the wave length of the absorption signals are influenced by the solvent and interactions between the polymer chains.

In polymers, there are interactions between chains (interchain), and interactions within individual chains (intrachain). Intrachain forces will reduce the coil dimensions by contraction of the coil, while interchain forces will increase the coil dimension by attraction to other coils. These inter- and intra-chain interactions result in increased wavelength of UV-Vis absorption. With increasing polymer concentration, the interchain forces will increase. A good solvent will increase the hydrodynamic volume of the polymer chain and a poor solvent will reduce the hydrodynamic volume of the chain. Due to the sensitivity of UV-Vis spectroscopy to such phenomena, a wealth of information can be obtained regarding polymer configuration in solution. Such interactions are illustrated in Figure 11.

Experimental

The UV-Vis spectra of PVCAP were recorded on a Hewlett-Packard model 8451A diode array spectrometer. The sample solutions were prepared from 50% ethanolic solution (BASF), solid polymer (by precipitation from an ethanolic solution in pentane), and 80% methanolic solution (ISP). Spectra were also recorded on solutions prepared by adding methanol to aqueous solutions prepared from the 50% ethanolic solutions and preparing the same concentrated solution from 80% methanolic solutions.

Results and Discussion

The UV-Vis spectra of PVCAP in DI water as a function of concentrations are presented in Figures 12 and 13. The lower portion of Figure 12 shows a single peak at 210 nm for a PVCAP sample of 0.003wt%. As the concentration increases, there is an additional peak, appearing at longer wavelengths. The peak at lower wavelength is caused by the expanded polymer chains at low concentrations, as explained above. Multiple peaks and increasing wave lengths of absorption are due to polymer aggregation at increased concentrations as mentioned in the above introduction (see Figure 11).

UV-Vis spectra of PVCAP in 3.5wt% sea water are presented as a function of concentrations in Figures 14 and 15. Here again there are multiple peaks with increasing concentrations. A notable difference between the polymer solutions in DI water (Figure 12) and in sea water (Figure 14) is the absence of the shoulder at the lower wavelength in sea water. This is due to the shrinkage of the polymer coils (intrachain) in the presence of salt, as shown schematically in Figure 11. The shrinkage of the polymer chain increases the chromophore- chromophore

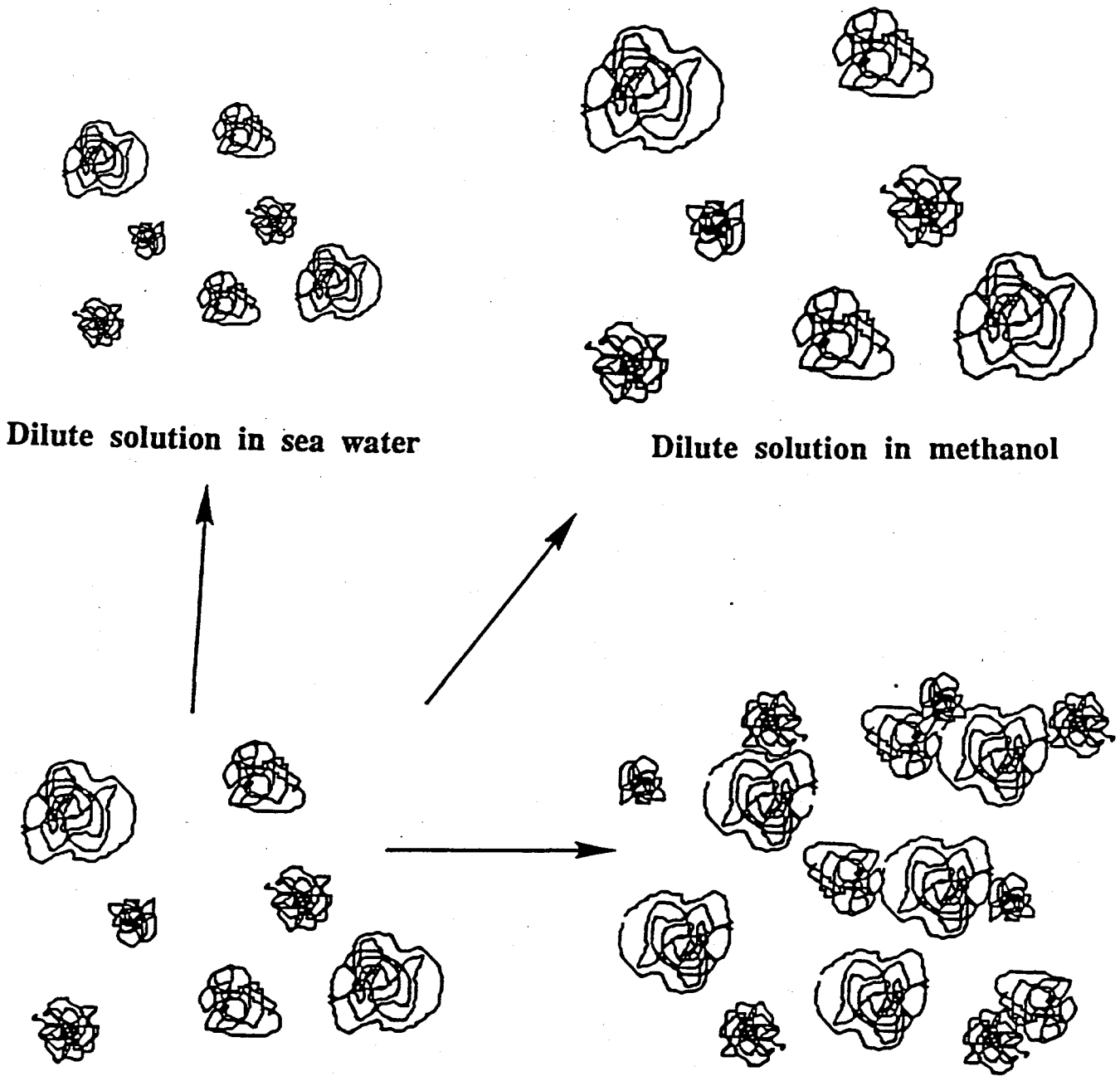

Figure 11. Hydrodynamic volumes of poly(N-vinylcaprolactam) in various solvents

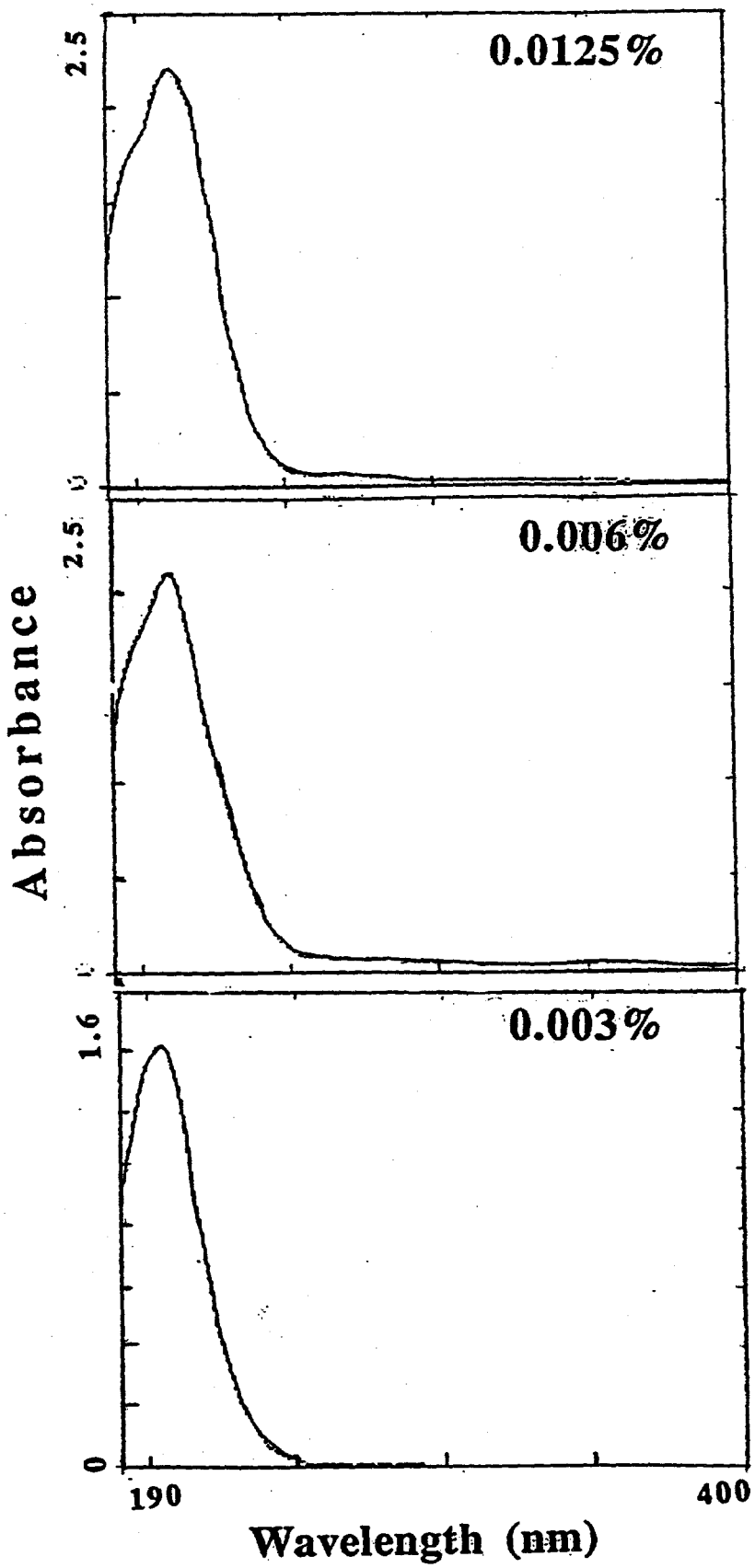

Figure 12: UV-Vis spectra of poly(N-vinylcaprolactam) in DI water as a function of concentration.

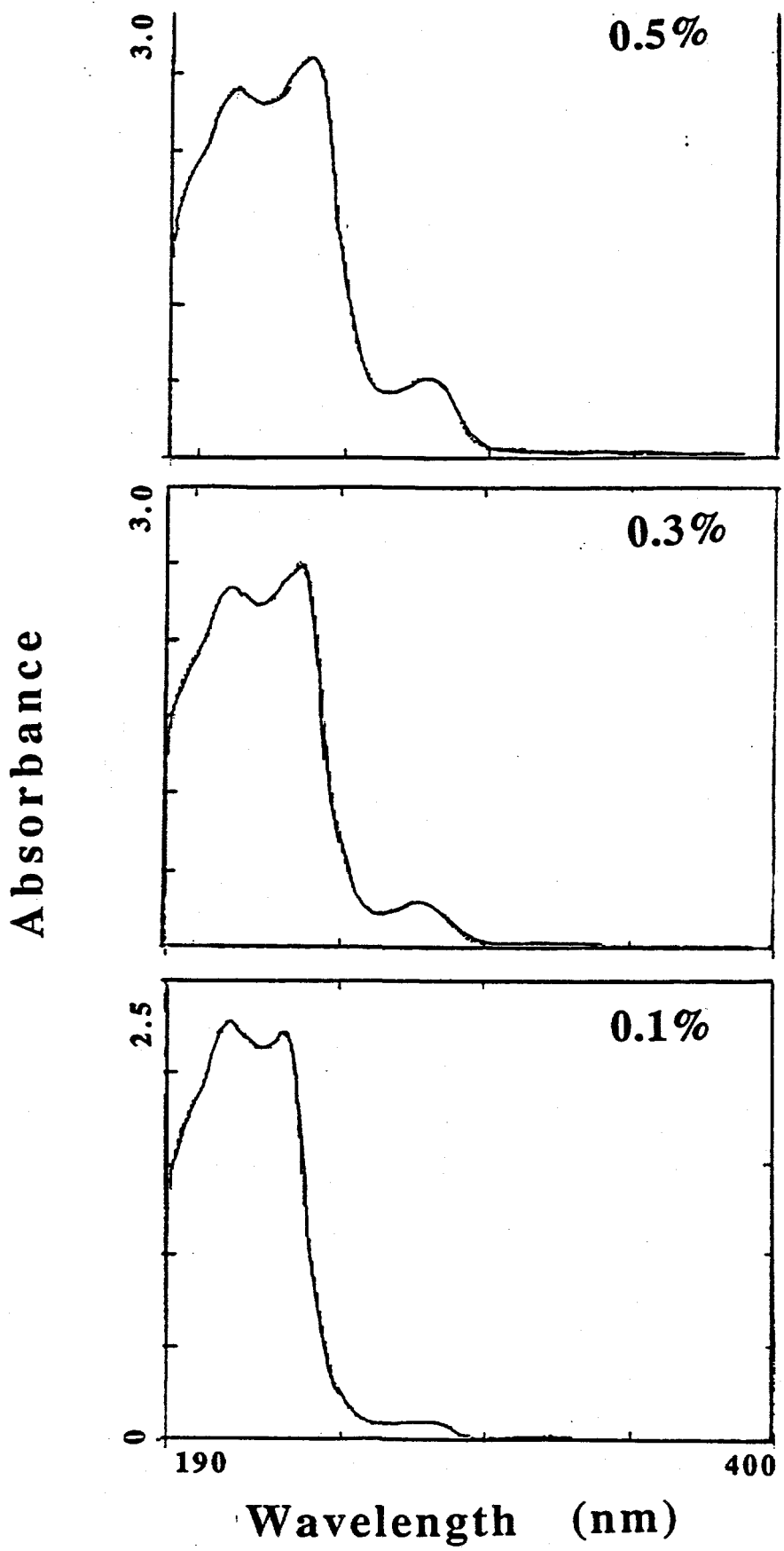

Figure 13: UV-Vis spectra of poly(N-vinylcaprolactam) in DI water as a function of concentration.

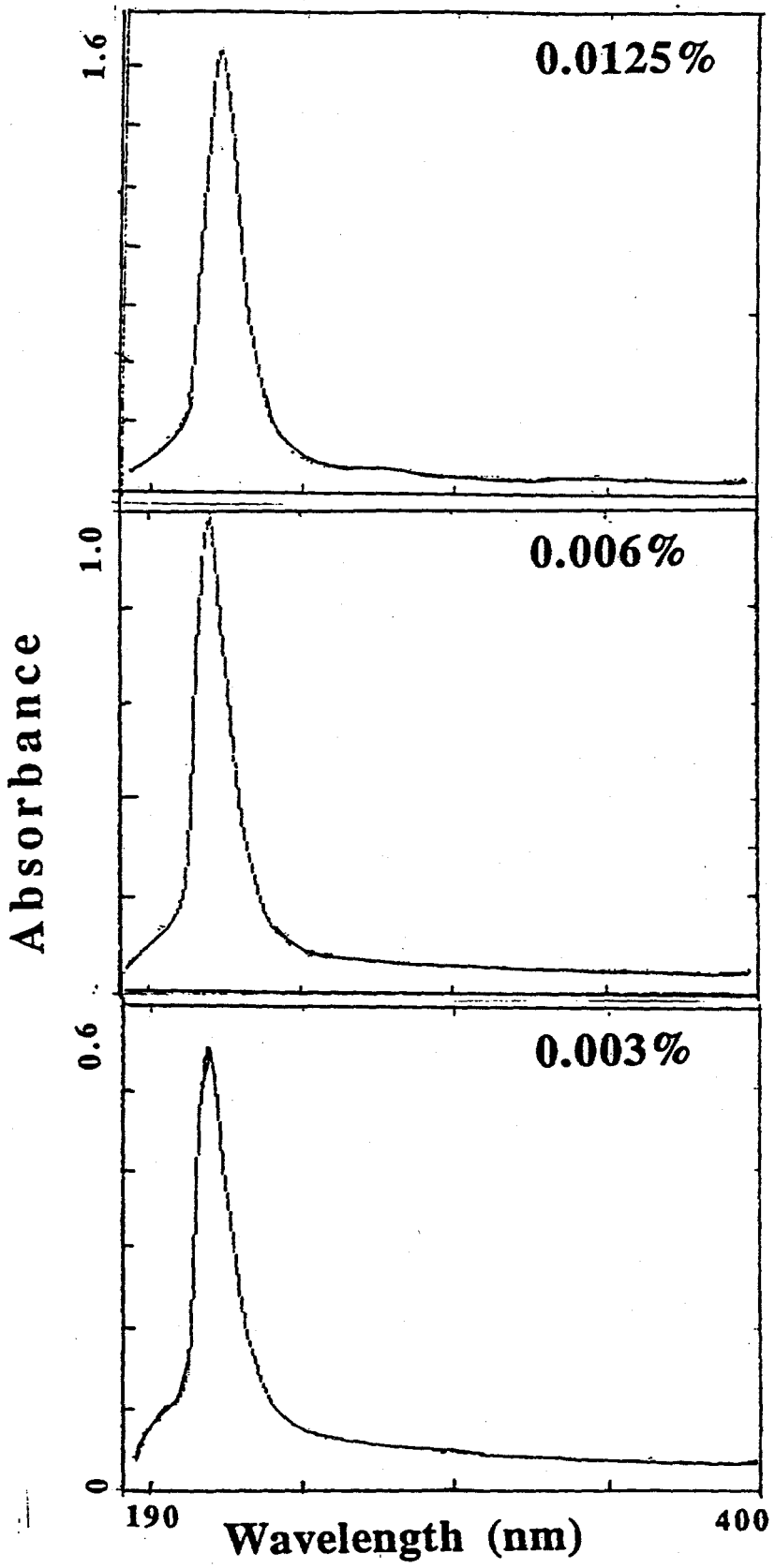

Figure 14 : UV-Vis spectra of poly(N-vinylcaprolactam) in 3.5% sea water as a function of concentration.

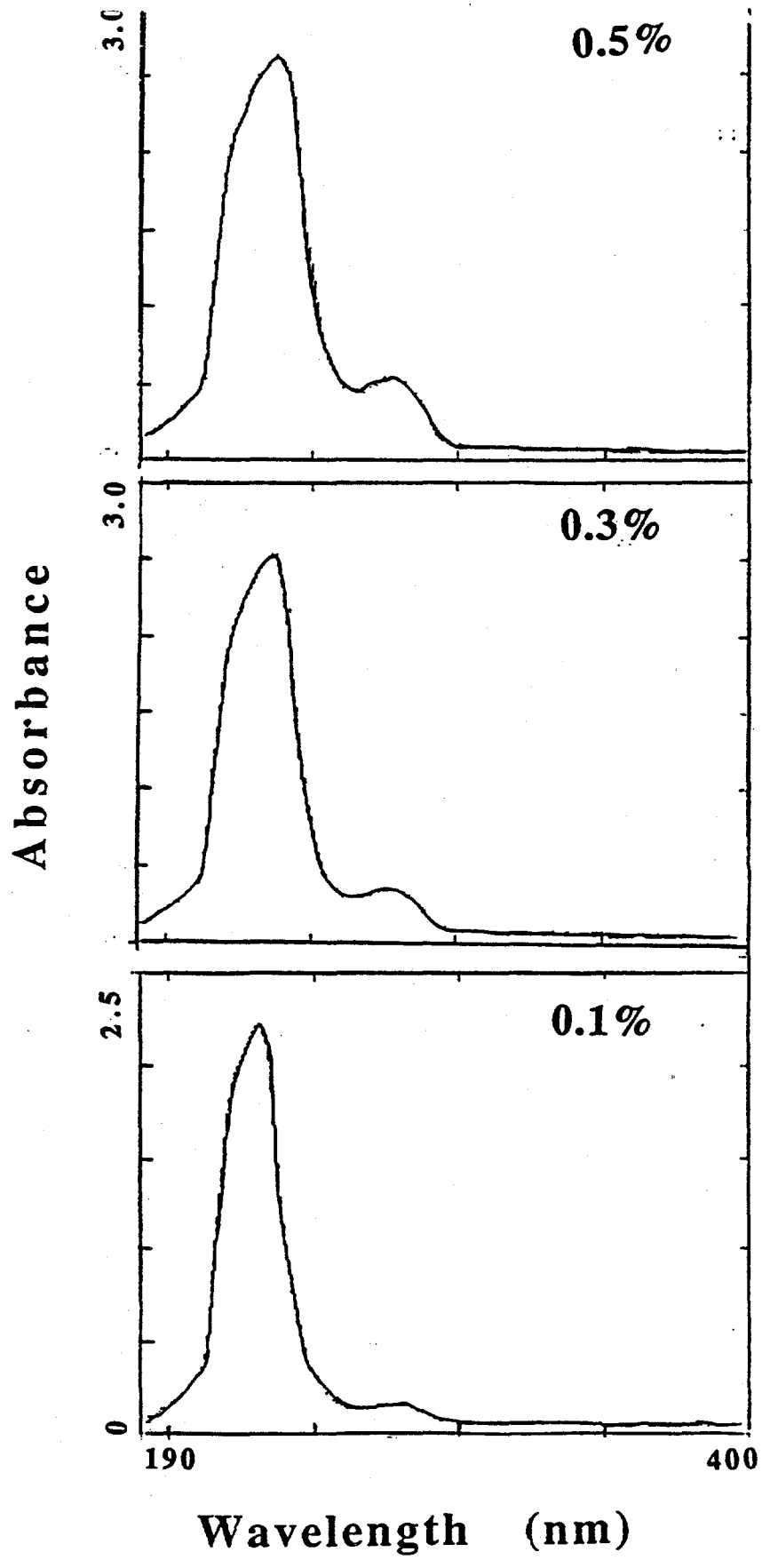

Figure 15: UV-Vis spectra of poly(N-vinylcaprolactam) in 3.5% sea water as a function of concentration.

interactions and increases the wavelength of absorption.

UV-Vis spectroscopy clearly supports the concept that PVCAP demonstrates a decreased inhibition efficiency in the presence of salt, in the high pressure reactor. This is due to the decreased availability of docking groups because of polymer internal coiling. The UV-Vis spectra of 1.0wt% PVCAP in DI water as a function of salt concentrations are presented in Figure 16. The figure shows that the addition of even 1wt% salt causes the disappearance of the lower wavelength signal; this indicates that the inhibitor efficiency can be decreased by a small salt concentration.

Experiments were carried out with salt solutions of PVCAP by adding quantitative amounts of methanol to reduce the aggregations and to increase the expansion of the polymer chains. Figures 17 and 18 indicate that there are no changes in the spectra and thus they suggest no changes in the chain conformations because of the addition of methanol.

In contrast Figure 19 compares the UV-Vis spectra of PVCAP (but prepared in an 80wt% methanolic solution) as a function of concentration in 3.5% sea water. The figure clearly indicates that the intensities of the signals are stronger than the solutions prepared from aqueous solutions which were shown in Figures 17 and 18. This may be due to an enhanced solubility of polymer in the solutions prepared by this method. Figure 19 also indicates an absence of the signal at the higher wavelength, seen in Figure 12-18 which was due to residual unreacted N-vinylcaprolactam monomer in the PVCAP samples from BASF. This signal is absent in the PVCAP sample from ISP.

These results suggest why a 0.25% PVCAP prepared from BASF's 50% ethanolic solution has a ball stop time, while our same concentrated polymer solution prepared from 80% methanolic solution does not has a ball stop time. This change in ball stop time is not due to enhanced thermodynamic inhibition by methanol (beyond that of ethanol); instead it is due to an increased hydrodynamic volume in the polymer prepared from methanolic solution.

IV.B.1.c. Future Chemicals and Experiments:

Considering the hydrate inhibition hypothesis, one might consider why poly(styrene sulfonate) or the other aromatics did not kinetically inhibit hydrates formation. The aromatics we evaluated did not have electronegative groups on the ring to provide hydrogen bonding; instead the electronegative groups were attached to the rings. As a future inhibitor candidate, poly(vinyl pyridine) which has an electronegative nitrogen on the ring may function as a hydrate inhibitor.

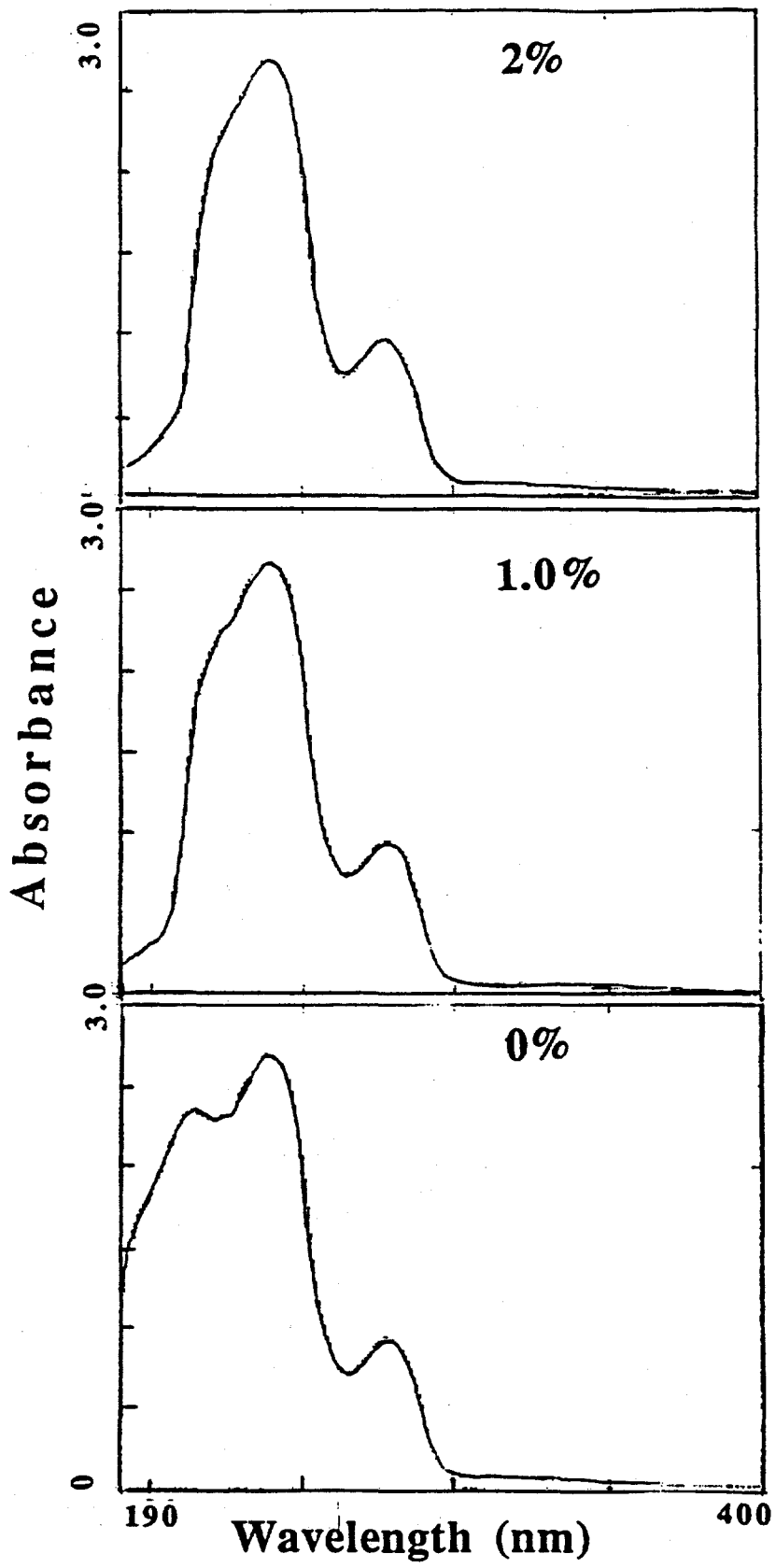

Figure 16: UV-Vis spectra of poly(N-vinylcaprolactam) (1 %) in DI water as a function of salt concentration.

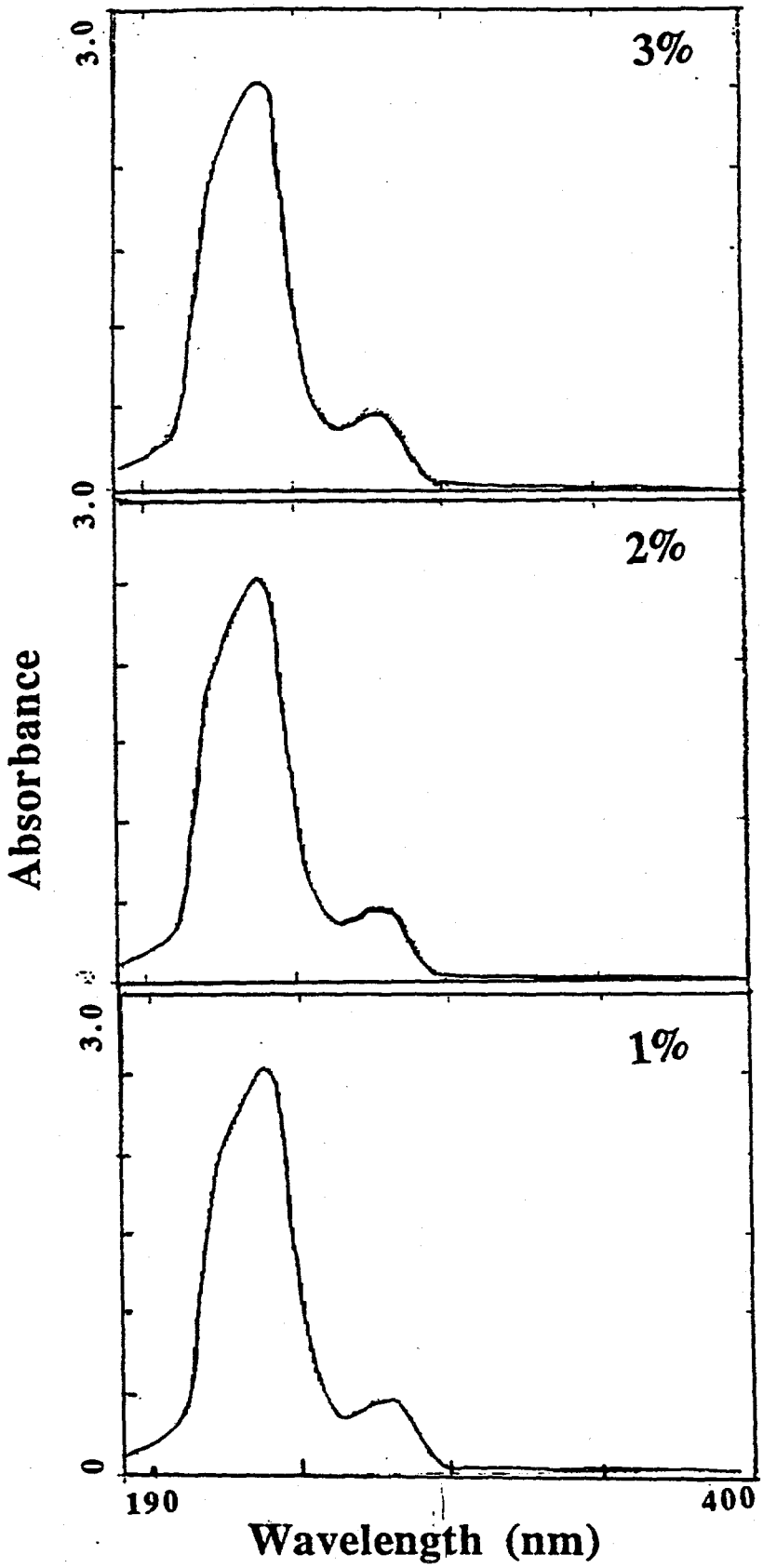

Figure 17: UV-Vis spectra of poly(N-vinylcaprolactam) (0.5%) in 3.5% sea water as a function of added methanol concentration.

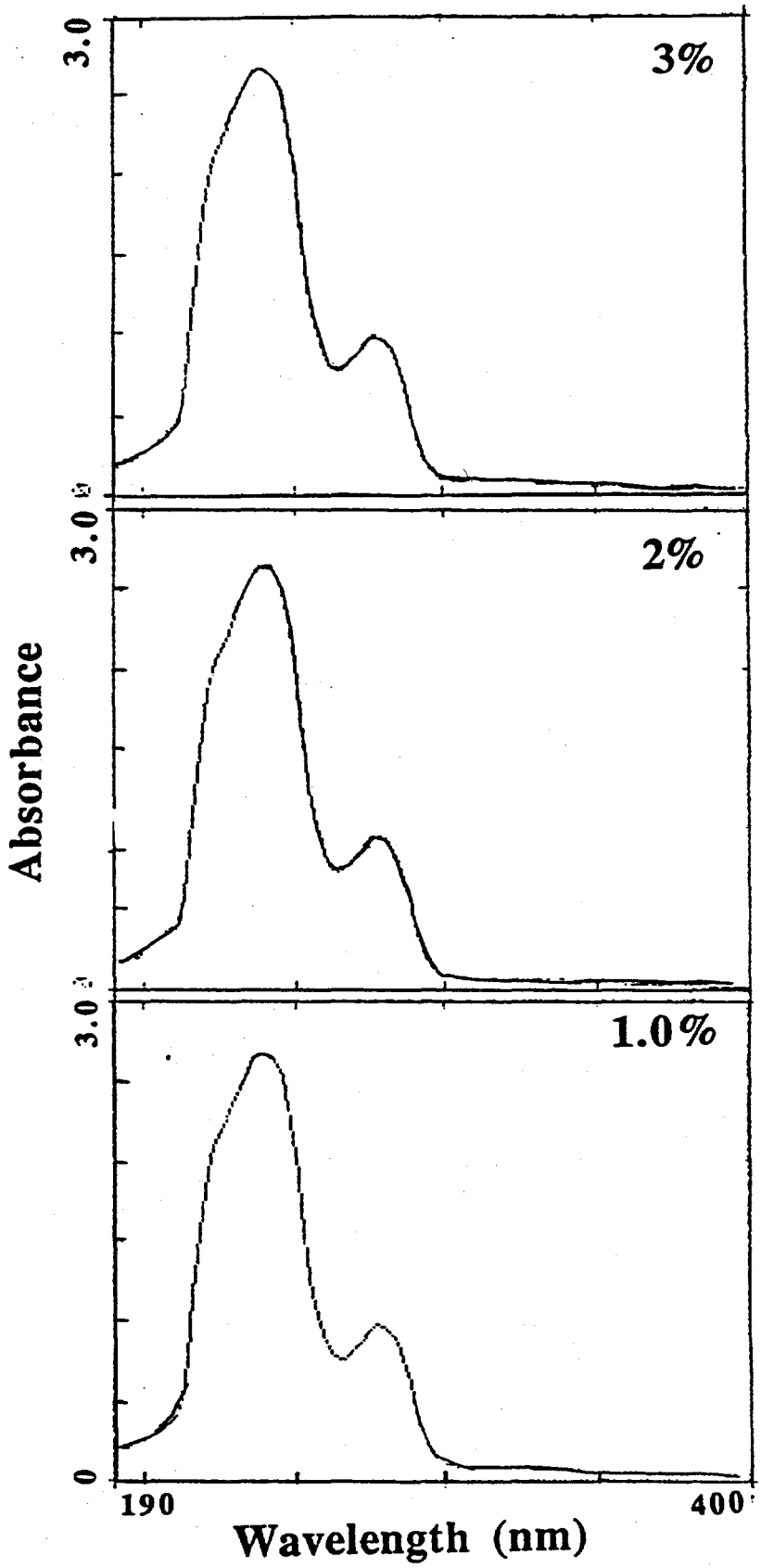

Figure 18: UV-Vis spectra of poly(N-vinylcaprolactam) (1%) in 3.5% sea water as a function of added methanol concentration.

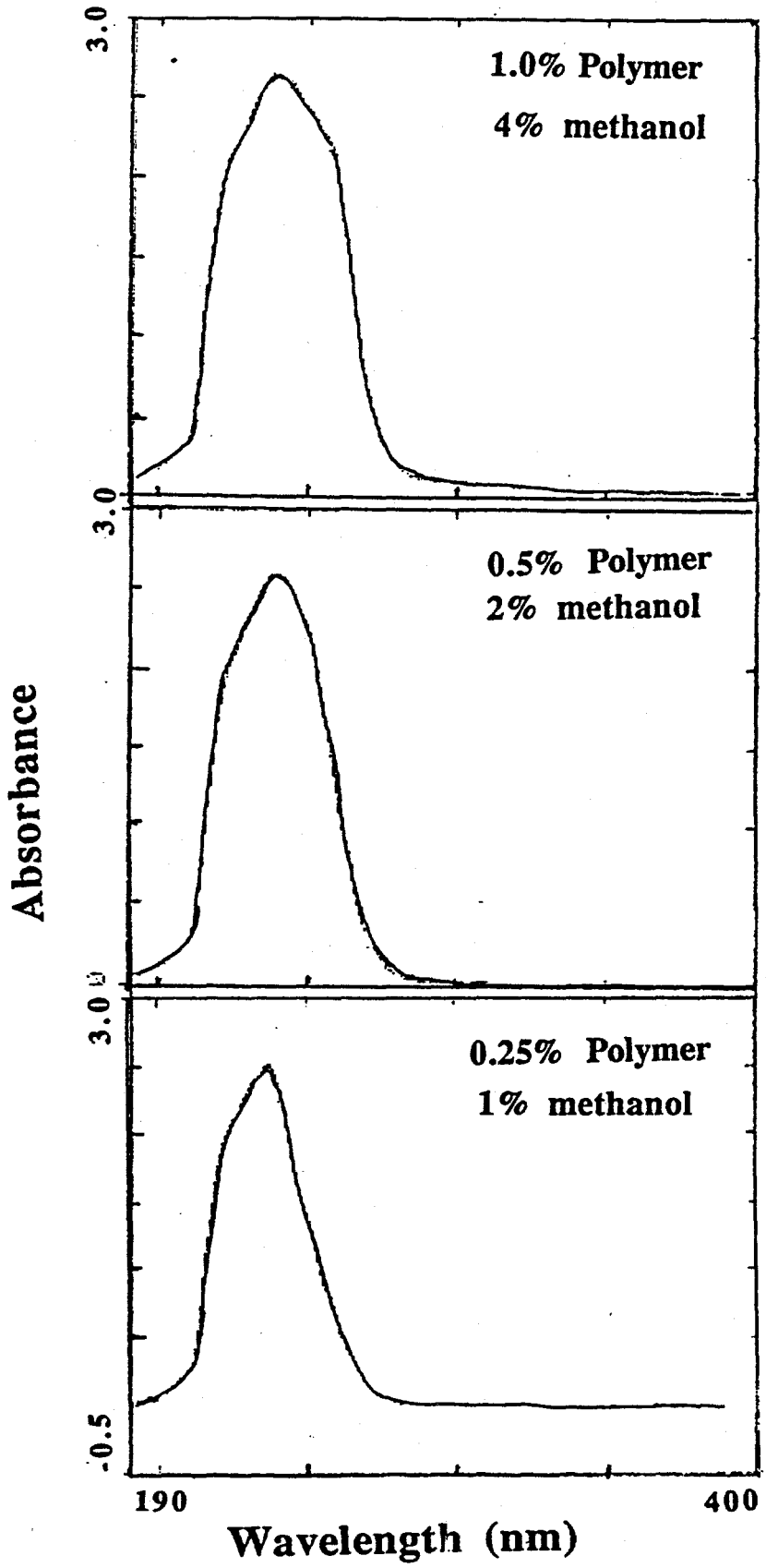

Figure 19: UV-Vis spectra of poly(N-vinylcaprolactam) in 3.5% sea water as a function of concentration (stock solution is 20% in methanol and diluted with sea water).

From the inhibition tests done to date, we have come to the conclusion that the presence of only one atom with hydrogen bonding capability may not be enough. The presence of two hydrogen bonding atoms or groups may be required for docking the ring structure of the polymer on the pentagonal or hexagonal faces of the hydrate cages. This docking seems necessary to prevent the growth of hydrate unit cells.

- We will synthesize a copolymer of N-vinylcaprolactam and sodium-2-acrylamido-2-methylpropanesulfonate to evaluate its potential as a hydrate inhibitor.
- We will partially protonate the lactam ring (C=O or N) on a known good inhibitor to remove one hydrogen bond site to determine the need for two hydrogen bond sites.
- We will derivatize VC-713, making it an electrolyte by protonation of the amine unit, to enhance its hydrate inhibition efficiency.
- We will attempt to test the current inhibitors in various solvents and use laser light scattering to correlate inhibition efficiencies with the hydrodynamic volume of the polymer in solution.
- We will investigate the possibility of solubilizing the polymers first in ethanol for comparison of performance with the solutions prepared from methanol.
- We will quantify the UV-Vis spectroscopic results to determine whether a correlation exists with polymer hydrodynamic volume.
- We will perform THF hydrate experiments with a blend of PVCAP and PVP and separate the remaining clear liquid and the solid hydrate. UV-Vis studies of the remaining clear liquid and the melted hydrate can provide information as to which lactam unit enters the hydrate phase and which one remains in the liquid phase. UV-Vis studies are possible due to the increased UV absorbance of PVCAP.

IV.B.2.a. High Pressure Experiments

IV.B.2.a.1 Apparatus.

A schematic diagram of the High Pressure Apparatus is presented in Figure 20. The principle components of the apparatus are listed below.

1. An isothermal water bath is used to contain the reactor. The

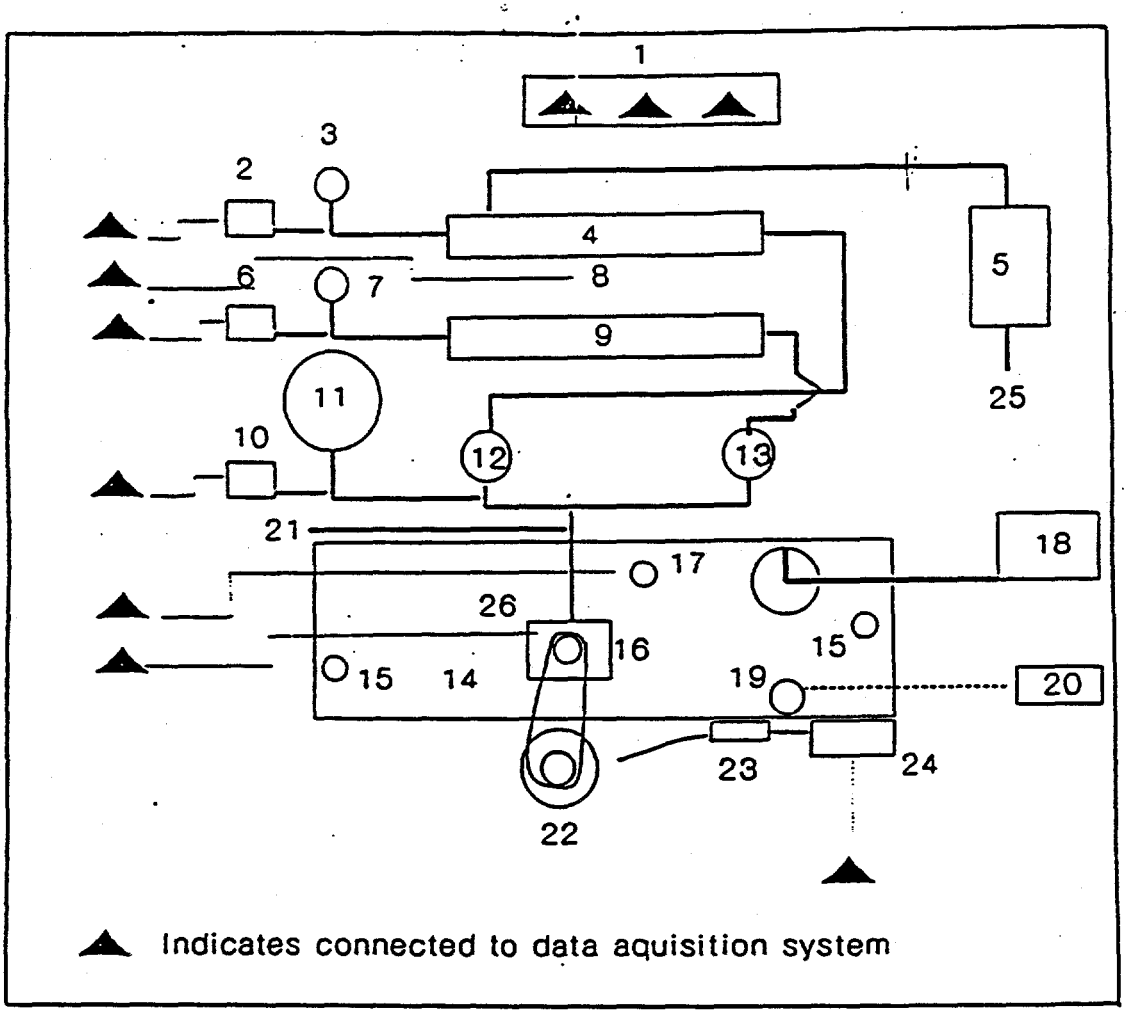

1. Keithley
2. Pressure Transducer
3. Pressure Gauge
4. High Press. Reservior
5. Gas Booster
6. Pressure Transducer
7. Pressure Gauge
8. Ambient Thermistor
9. Low Press. Reservior
10. Pressure Transducer
11. Reactor Press. Gauge
12. Press. Reducing Regulator
13. Back Press. Regulator
14. Glycol-Water Bath
15. Bath Mixer
16. Autoclave Reactor
17. Bath Thermistor
18. Bath Cooling Unit
19. Bath Heaters
20. Neslab Temp. Controler
21. System Vent
22. Motor
23. Transformer
24. Beckman
25. Gas Bottle
26. Cell Thermistor

Figure 20. Schematic of the High Pressure Apparatus.

temperature control of the water bath is to within 0.5°F.

2. A 300cc Autoclave reactor, with a magnetically-driven mixer rotated at 1000 rpm by a external motor.
3. A high pressure supply reservoir used to supply gas to the reactor, as gas is consumed in the reactor due to the hydrate formation. Thus it is possible to run the experiments at isobaric conditions (pressure is maintained ±10% of the set pressure).
4. A Heise dial pressure gauge allows monitoring of pressure in the reactor.
5. A computer data acquisition system records the data and controls the experiment. The system is composed of a KEITHLEY Series 500 Data Acquisition System, connected to an IBM XT computer. The data recorded by the data acquisition system are: temperature in the reactor, water bath temperature, high pressure reservoir temperature, high pressure reservoir pressure, and pressure in the reactor. All data are recorded in the computer for later analysis.

Data are analyzed using a computer program for gas consumption from the reservoir, which maintains constant pressure in the reactor as hydrates form. The gas consumption program uses the Peng-Robinson Equation of State to calculate z factors.

IV.B.2.a.2. Operating Procedure

1. Cleaning Procedure
   a. The Autoclave reactor is disassembled and thoroughly cleaned several times with tap water.
   b. In order to eliminate any residue left from the previous run, the reactor is washed with methanol with the aid of an air driven motor for a period of about 15 minutes.
   c. After the methanol wash is completed, the reactor is rinsed several times with tap water followed by deionized water rinse.
   d. The excess water is blown from the reactor with high pressure air, and finally the reactor is well dried with Kimwipes.

2. Preparation of Test Solution
   a. Fresh test solutions (no more than two days old) are always used in the high pressure experiments.
   b. According to the specification of the experiment, the solution make-up is as follows:
      * Concentrated solutions of the chemicals of interest are made by dissolving the chemical (resin or solution) in deionized water, making a 5 wt% solution.
      * Using the concentrated (5 wt%) solution, sea water (5 wt% salinity), and deionized water are mixed to make the final test solution.

* Care is taken that the solution is clear and no particles are observed in solution.

3. Sealing
   a. Appropriate amount of the test solution is weighed in a beaker. For most of the kinetic and thermodynamic experiments the amount of solution used is 120 grams.
   b. Sixty nine (69) stainless steel balls are placed in the reactor to provide good mixing and increase the surface area for hydrate formation
   c. The weighed test solution and condensate are poured into the reactor and the reactor is sealed.

4. Start-up

Kinetics Experiments
   a. Once sealed, the reactor is immersed in the water bath and the mixer turned on to provide faster heat transfer in bringing the solution in the reactor to thermal equilibrium with the water bath.
   b. The data acquisition system is started.
   c. After about 10 minutes, the mixer is turned off, and after 5 minutes the reactor is charged to the operating pressure.
   d. Before charging the reactor, the reactor is flushed with gas several times to eliminate the air initially present.
   e. Once the reactor is charged to the operating pressure, the system is connected to the high pressure supply reservoir.
   f. After the reactor has reached thermal equilibrium with the water bath, all the conditions are recorded at the moment and the mixer turned on. Such a point is the onset for the calculation of the gas consumption in a given run.

Thermodynamic Experiments
   a. Once sealed, the reactor is immersed in the water bath, which is initially at about 85°F.
   b. Immediately after, the reactor is flushed several times with gas to eliminate any air initially present.
   c. The reactor is charged to the desired starting pressure and the regulator closed (here the experiments are done at isochoric conditions, instead of isobaric).
   d. The mixer is started, as well as the cooling unit.
   e. The data acquisition system is started and all specifications (starting temperature and pressure, and minimum temperature and pressure) of the run are input.

5. Running
Kinetics Experiments
   a. The progress of the experiment is monitored every few hours

for any unusual phenomena.

b. The experiment is continued until the established run time determined prior to the start-up (usually 20-22 hours) is reached.

Thermodynamic Experiments

a. Once the data acquisition system is started, the run progresses on its own (control of run is done by computer).
b. Usually each thermodynamic experiment lasts two (2) days.

IV.B.2.b. Thermodynamic Experiments and Results

The thermodynamic experiments are performed using the same apparatus as shown in Figure 20, with a slight modification, which is the addition of an extra heater for better temperature control. These experiments are also carried out under isochoric conditions.

The course of thermodynamic experiments can be followed by Figure 21. Point A represents the start of the experiment, at a particular pressure (i.e., 1000, 2000 or 3000 psig) and temperature of at least 80°F. The control of the experiment is by the computer which sets the rate of cooling (usually 5°F per hour) according to the pressure drop in the reactor. Point B is the point where hydrates start to form and at this point the temperature is held constant for 5 hours. At point C, the system is heated at 1.5°F/hr and the experiment is ended after it has passed point D. The experiments last about two (2) days.

Point D is the point of interest. This point indicates the equilibrium temperature and pressure for hydrate formation.

Three (3) equilibrium points are needed for each test solution, done at 1000, 2000 and 3000 psig. Point D for each experiment represents a point on the equilibrium curve for hydrate formation. These three points should lie on a straight line on a plot of ln P versus 1/T.

Experiments have been completed for deionized (DI) water, PVCAP, and VC-713 and the results are shown in Figure 22. The amount of inhibitor used was 0.5 wt% (the PVCAP solution contained also 0.5 wt% Ethanol, and the VC-713 solution contained 0.8 wt% Ethanol).

There are many implications from the fact that the "inhibited" equilibrium curve is shifted to higher temperatures relative to the equilibrium curve for DI water. A small amount (0.5 wt%) of inhibitor shifts the equilibrium curve to higher temperatures by about 6°C, making the hydrate formation more favorable (thermodynamically). At a given pressure with the

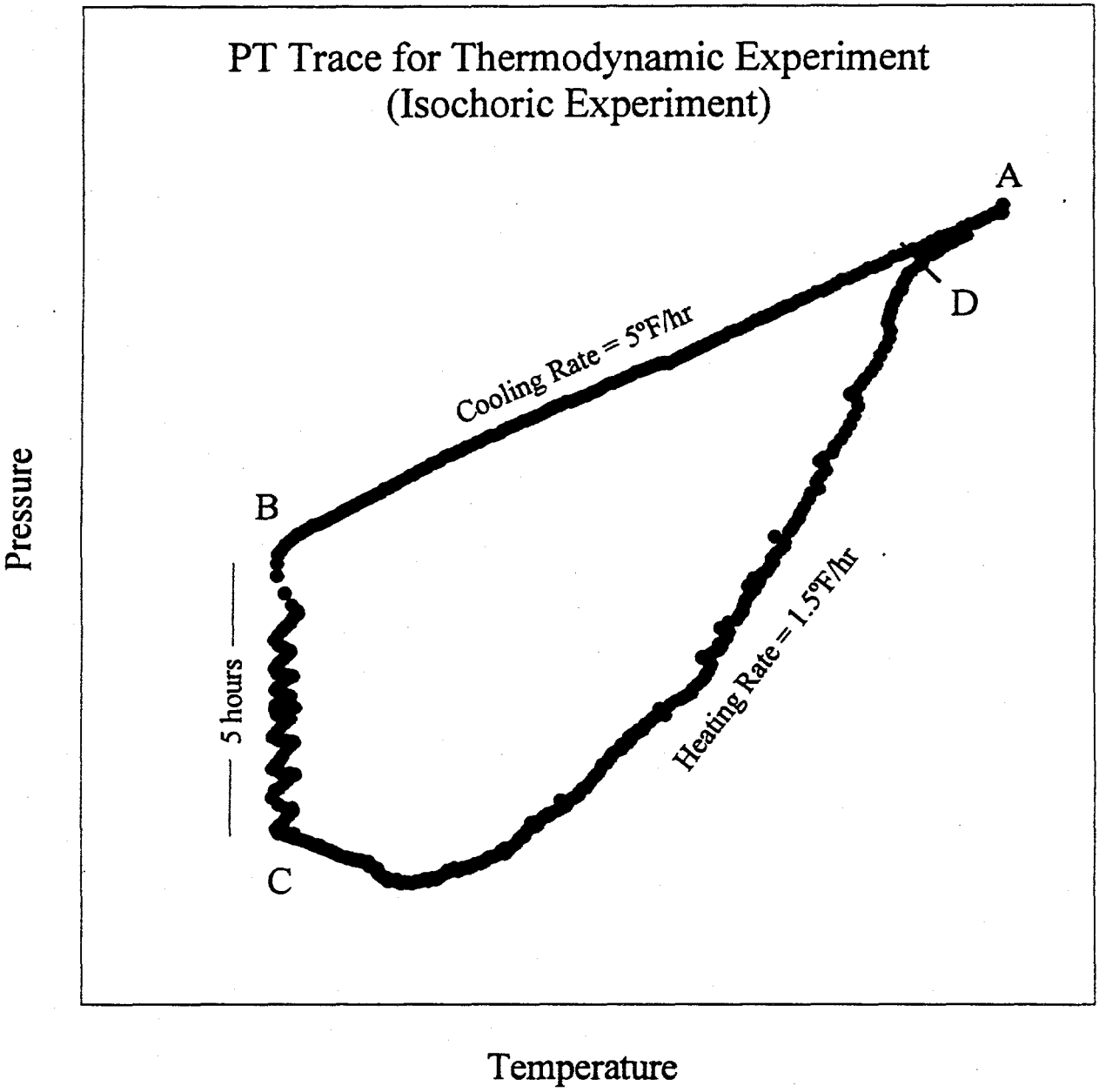

Figure 21. Schematic Temperature-Pressure Trace of a Thermodynamic Experiment

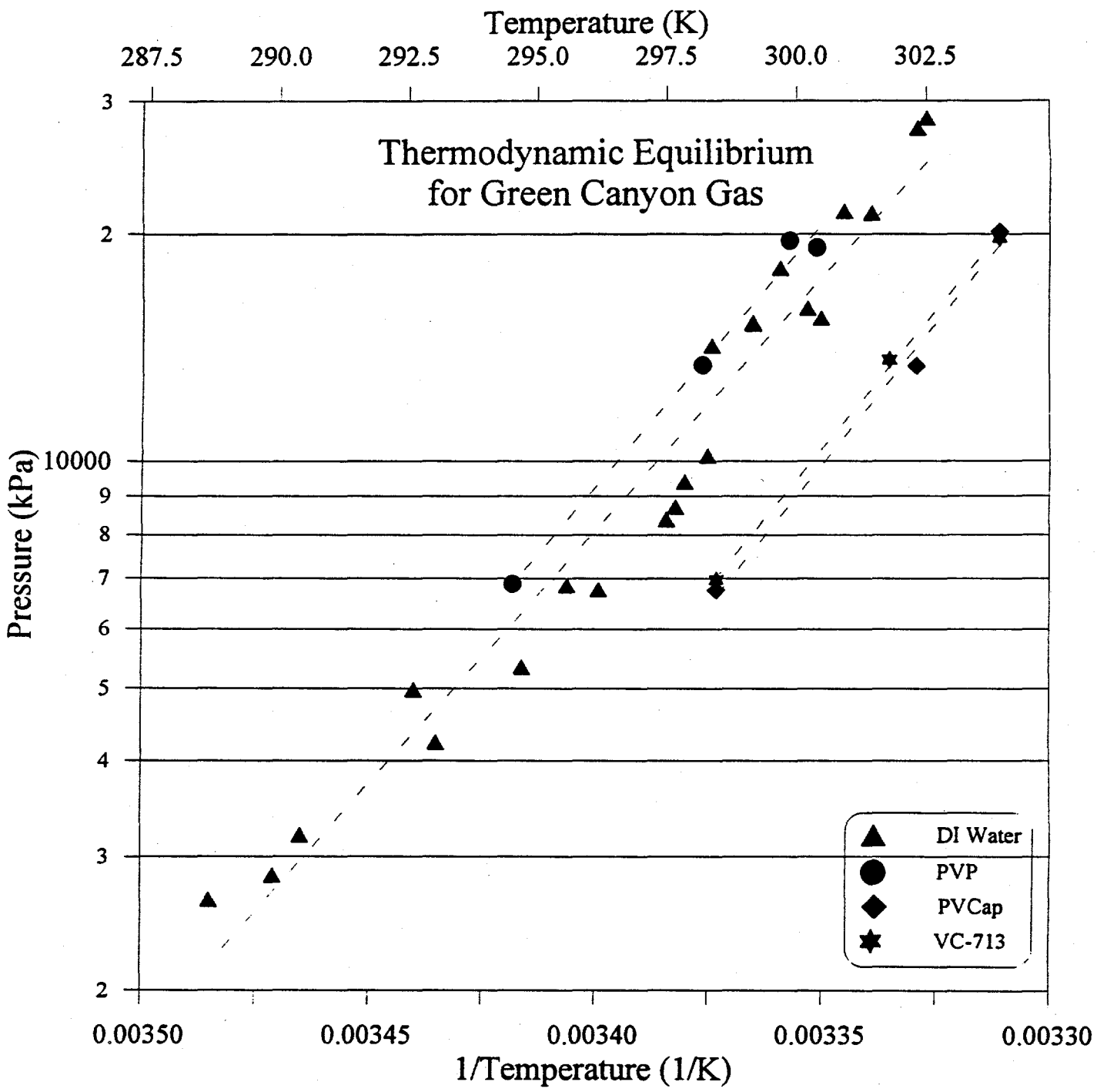

Figure 22. Hydrate Thermodynamic Points for Deionized Water, 0.5wt% PVP, 0.5wt% PVCap, and 0.5wt% VC-713.
All Inhibitor Solutions were made without salt.

inhibitor present, hydrates will form at a higher temperature, or at a given temperature, hydrates will form at a lower pressure, than the corresponding formation in DI water.

These results are of great importance because the above inhibitors markedly decrease the kinetics of hydrate formation, preventing hydrate formation in large amounts, even though the thermodynamics conditions appear more favorable for hydrate formation.

IV.B.2.c. High Pressure Kinetic Experiments and Results

The high pressure experiments are a major test of the performance of a "possible kinetic inhibitor" which is usually found in the screening apparatus. Two high pressure apparatuses run continuously, testing the effectiveness of the best chemicals found on the screening apparatus.

The high pressure apparatus simulates field conditions in terms of temperature, pressure and turbulence. In contrast with the THF used in screening apparatus, a synthetic gas mixture is used to form the hydrates in the high pressure apparatus. A synthetic Green Canyon Gas mixture was purchased from Matheson Gas Products, of the composition:

Component	Mole Fraction
Methane	0.872
Ethane	0.076
Propane	0.031
n-Butane	0.008
i-Butane	0.005
n-Pentane	0.002
i-Pentane	0.002
Nitrogen	0.004

The discussion in this report of research involving the high pressure apparatus will be divided in two parts: 1) from the beginning of 1993 through May, and 2) from June through the remainder of 1993.

The first five months of 1993 were marked by the finding of two markedly better hydrate inhibitors, VC-713 and PVCAP, which were found using the experimental conditions adopted at the start of this consortium (54.5°F and 1125 psig).

In June 1993, we decided to change our experimental conditions to 39.2°F and starting pressure to 1000 psig. This change was mainly due to the fact that our high pressure experiments needed to reflect more realistic conditions (such as ocean floor temperatures) that would provide a more rigorous test

of kinetic inhibitors. This second part of our 1993 research was performed at the more rigorous experimental conditions in order to explore the limits for VC-713 and PVCAP in terms of concentration, pressure and salinity. These last three are independent variables, the dependent variable is the time required for significant gas consumption (caused by rapid hydrate formation).

Several new chemicals were tried in the high pressure apparatuses, as listed in Table 7. However, most of the work was focussed on the study of two kinetic inhibitors, namely VC-713 and PVCAP, which have outperformed all previous inhibitors, to date, including PVP. The listing in Table 7 represents over 300 high pressure experiments carried out during the calendar year of 1993. Each solution was tested in duplicate runs; additional tests were performed with a combination of the chemicals listed in Table 7.

IV.B.2.c.1. Performance of New Inhibitors

IV.B.2.c.1.a. A. Study of Copolymers of PVP. Early in 1993 several copolymers of PVP (which was then the most promising inhibitor) were tested, as obtained from BASF and ISP. At that time, we also changed the way we were making the test solution. We made the solutions with 0.5 wt% of the active inhibitor ingredient rather than 0.5% of the solution received. Most chemicals came to us in the concentrated solution form, and by making the test solutions of 0.5 wt% of each solution, we had not previously been comparing the inhibitor performance on a basis of the same concentration of active ingredient.

Copolymers of PVP showed good inhibition at the experimental condition of 54.5°F and 1125 psig. Figure 23 and 24 show their performance relative to PVP and sea water. These copolymers were promising because they only allowed a small amount of hydrates to form (i.e. low gas consumption) but they had a short induction time.

In Figure 23, all four copolymers have a similar molecular composition (shown in the figure) differing only by the ratio of the VP ring and the second ring, and the molecular weight of the copolymers as follows:

Chemical	Ratio VP:Other Ring	Molecular Weight
FC 370	VP 70% : 30%	MW ≈ 100,000
FC 550	VP 50% : 50%	MW ≈ 80,000
FC 905	VP 5% : 95%	MW ≈ 40,000
HM 552	VP 50% : 50%	MW ≈ 800,000

Figure 24 shows results for copolymers from ISP which are composed of two of the monomer units found in VC-713 (the

Table 7. Chemicals Tested on High Pressure Apparatus during 1993

Chemical	Type of Chemical	Vendor
PVP K-30	Homopolymer	ISP
PVP K-90	Homopolymer	ISP
PVP K-120	Homopolymer	ISP
FC 550	Copolymer	BASF
FC 905	Copolymer	BASF
FC 370	Copolymer	BASF
HM 552	Copolymer	BASF
VA 73E	Copolymer	ISP
VA 55E	Copolymer	ISP
937	Copolymer	ISP
958	Copolymer	ISP
Polyox N-3000	Polymer	Union Carbide
Polyox 301	Polymer	Union Carbide
VC-713	Terpolymer	ISP
PVCap	Homopolymer	BASF
Dried VC-713	Terpolymer	ISP
VP/VCP (50/50)	Copolymer	BASF
VP/VCP (60/40)	Copolymer	BASF
VP/VCP (0/100)	Copolymer	ISP
VP/VCP (25/75)	Copolymer	ISP
VP/VCP (50/50)	Copolymer	ISP
VP/VCP (75/25)	Copolymer	ISP
HE-300	Terpolymer	Phillips
Tyrosine	Amino Acid	Fluka

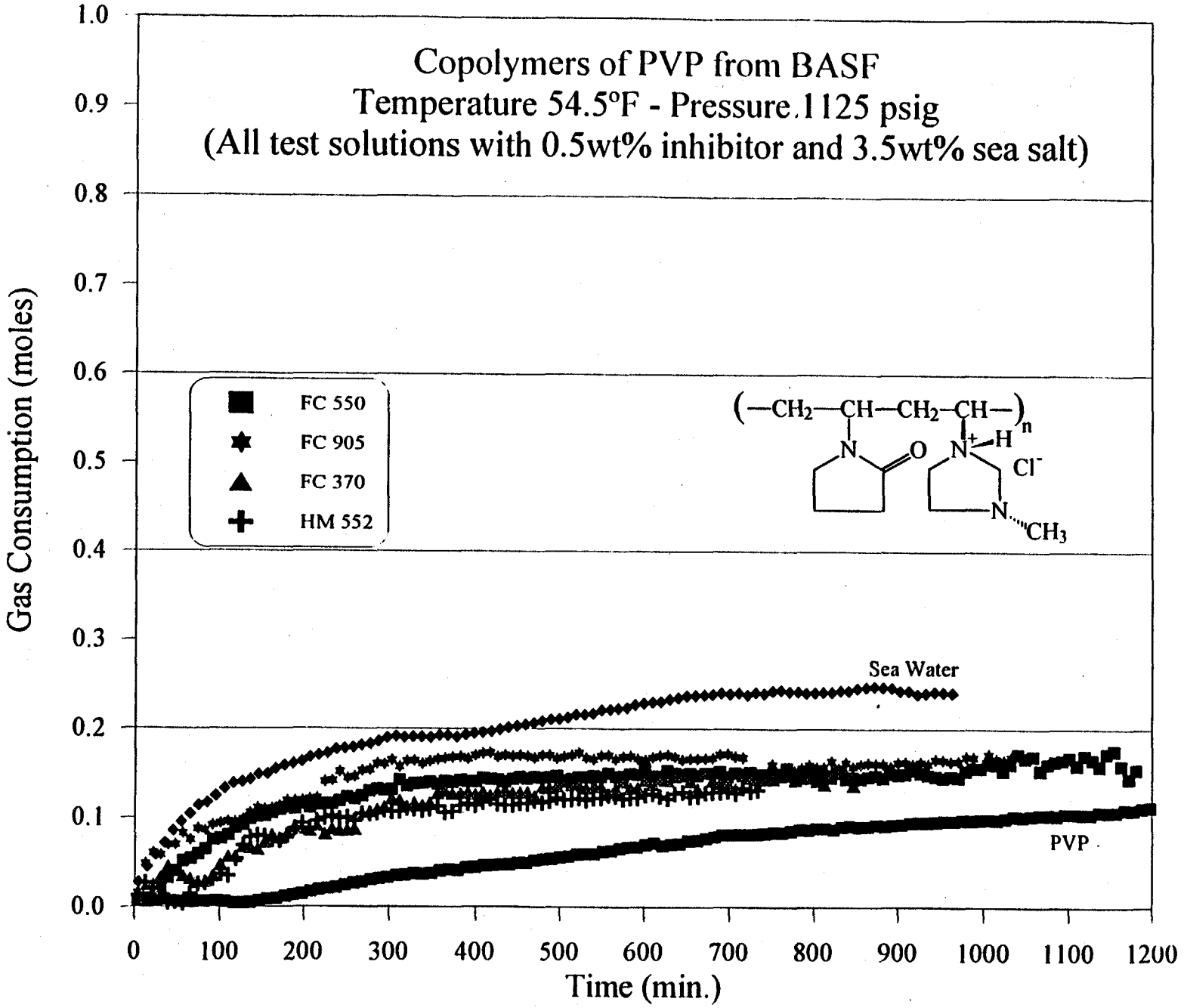

Figure 23. High Pressure Results for Copolymers of PVP from BASF

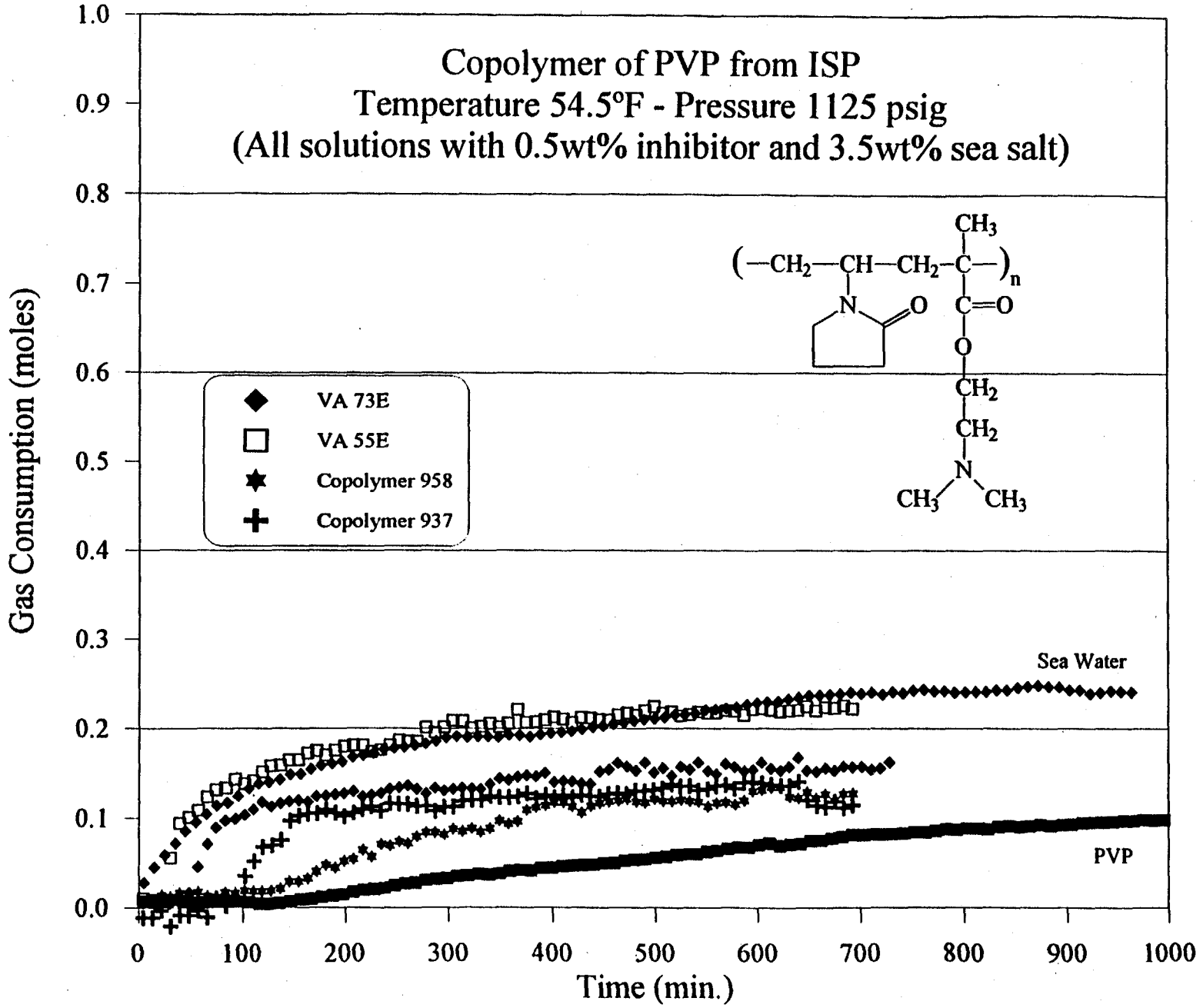

Figure 24. High Pressure Results for Copolymers of PVP from ISP

vinylpyrrolidone ring and amine group). All four copolymers only differ in their molecular weight and the ratio between the two units in the polymers. The results are not satisfactory for these copolymers.

IV.B.2.c.1.b. Study of VC-713. VC-713 (from ISP) was the first chemical found to show complete inhibition of hydrates at 54.5°F and 1125 psig. Many tests were done (at 39.2°F) to prove its effectiveness as a kinetic inhibitor. Experiments for testing the limits of VC-713 involved variations in temperature (decreased from 54.5°F to 39.2°F), pressure (1000, 2000, and 3000 psig), concentration (0.1 to 0.75 wt%), salinity (0 to 3.5 wt%), and performance from batch-to-batch.

Five batches of VC-713 (Lot 34, 65, 76, 85 and 89) in the solution form and two batches of VC-713 in the resin form were made available for tests in the high pressure Apparatus. Figure 25 shows the variations observed among these five batches of VC-713. All experiments were done under the same experimental conditions, i.e., 39.2°F and 1000 psig and VC-713 concentration of 0.5 wt% in a 3.5 wt% sea salt solution. All batches behaved very similarly, showing little variation. We noticed that VC-713 Lots 85 and 89 outperformed the other batches at about 1000 minutes, at which point all the VC-713 batches, (except for Lots 85 and 89) began to show increased gas consumption, indicating hydrate formation.

Figure 26 indicates that, while the resin did not perform as well as the solution form of VC-713, its performance was still very acceptable. A possible reason that the resin indicated higher gas consumption than the solution was due to the amount of ethanol present in the solution (37% solids) which contributed to the inhibition efficiency of VC-713.

Before decreasing the operating temperature from 54.5°F to 39.2°F, several experiments were conducted with VC-713 to determine its pressure sensitivity at 54.5°F. Figures 27 and 28 show the results for these series of experiments carried out using solutions at 0.5 wt% and 0.25 wt% with 3.5 wt% sea salt. VC-713 works very well as a kinetic inhibitor at mild conditions (54.5°F and up to 3000 psig) at a concentration of 0.5 wt%. As we will see, while good kinetic inhibitors may work well in certain regions of the pressure-temperature (P-T) diagram, the efficiency of their performance was reduced with an increase in driving force for hydrate formation (e.g. increased pressure, decreased temperature, or decreased inhibitor concentration.)

Figure 29 shows the pressure tests done with VC-713 at 0.5 wt% but at 39.2°F. Two pressures were tried at this temperature: 1000 and 1500 psig. At 39.2°F, VC-713 still performs well (low gas consumption) at 1000 psig, but it is very sensitive to

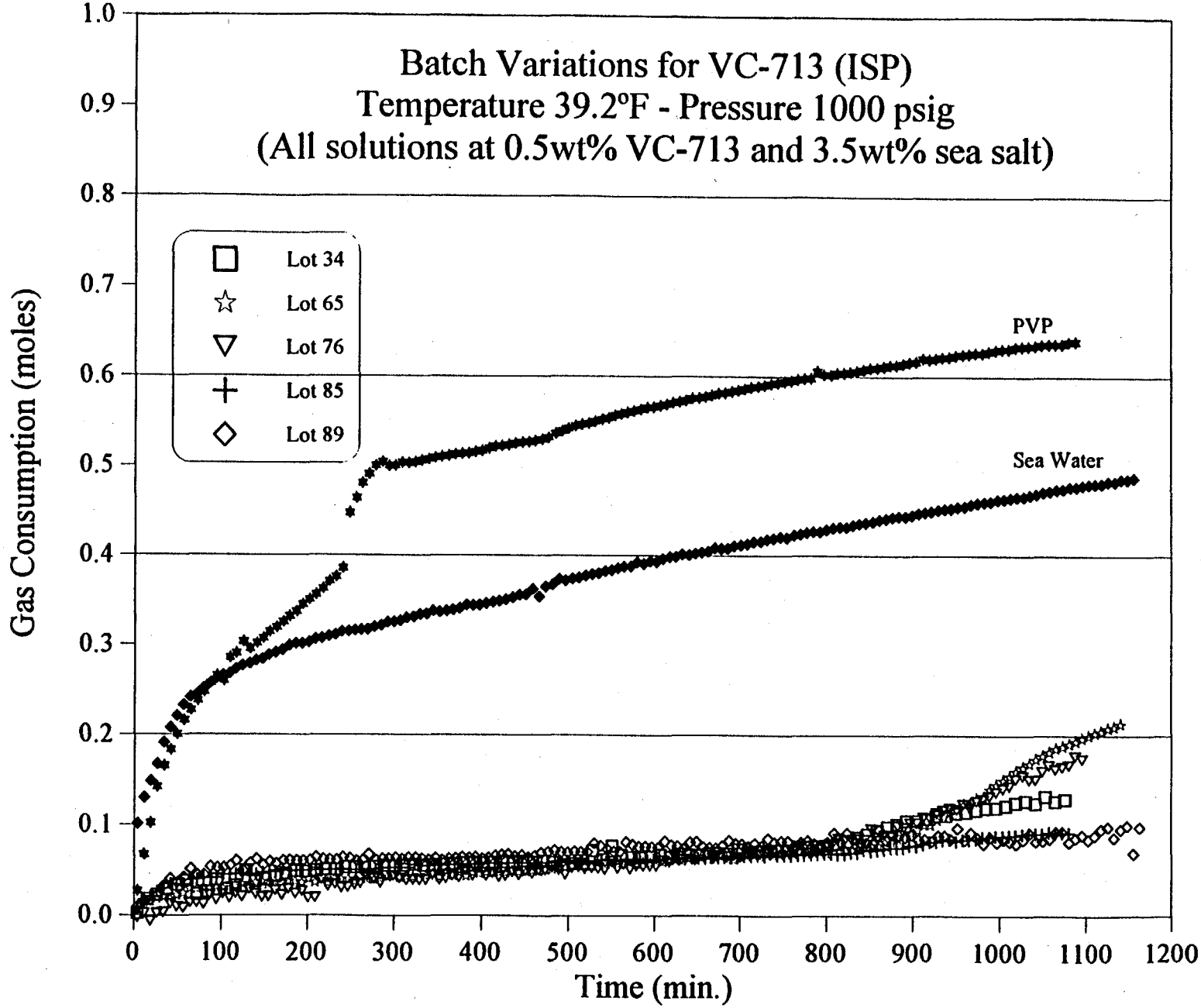

Figure 25. High Pressure Results for Comparison of Batches of VC-713

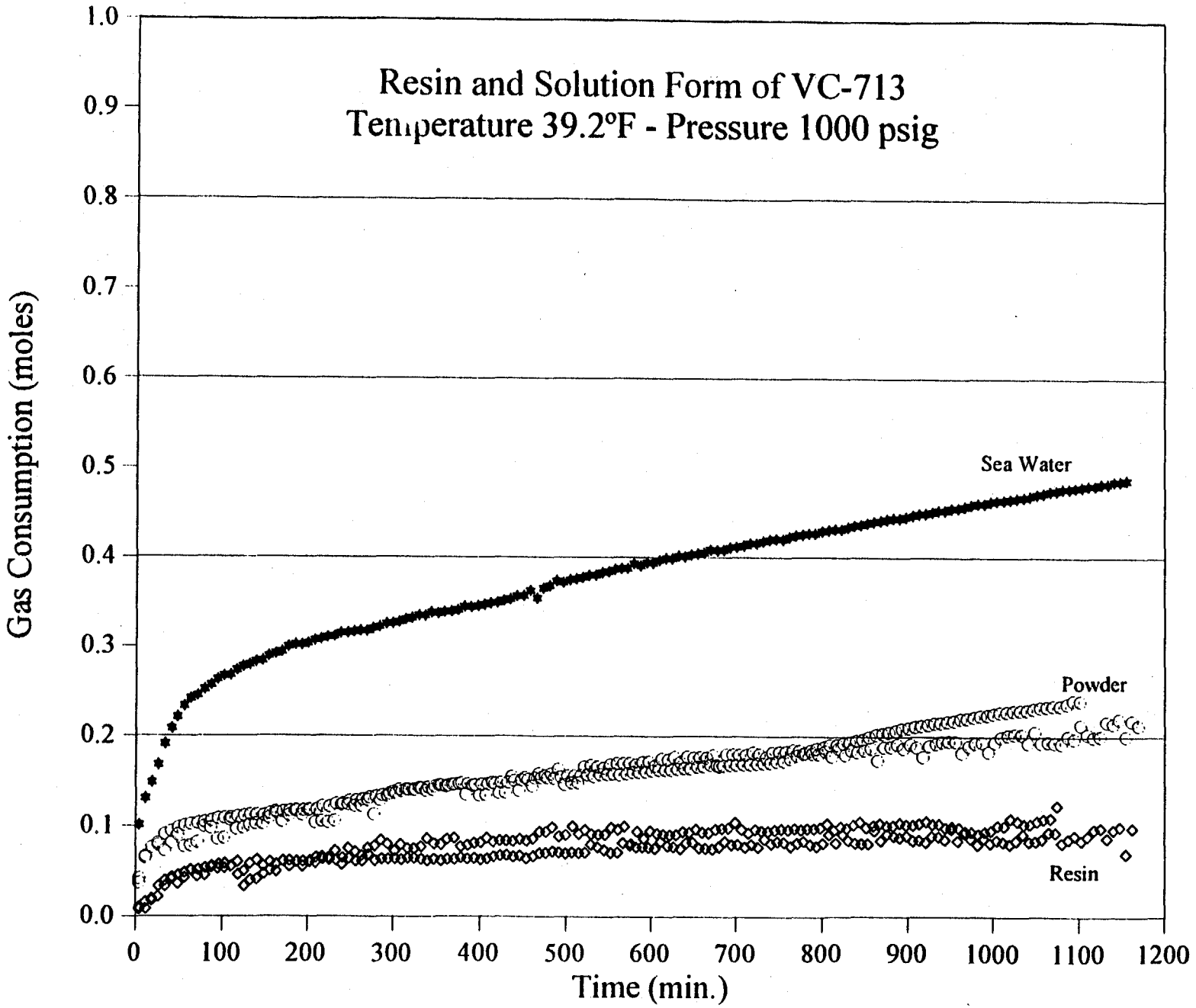

Figure 26. High Pressure Results for Comparison Between Resin and Solution Forms of VC-713

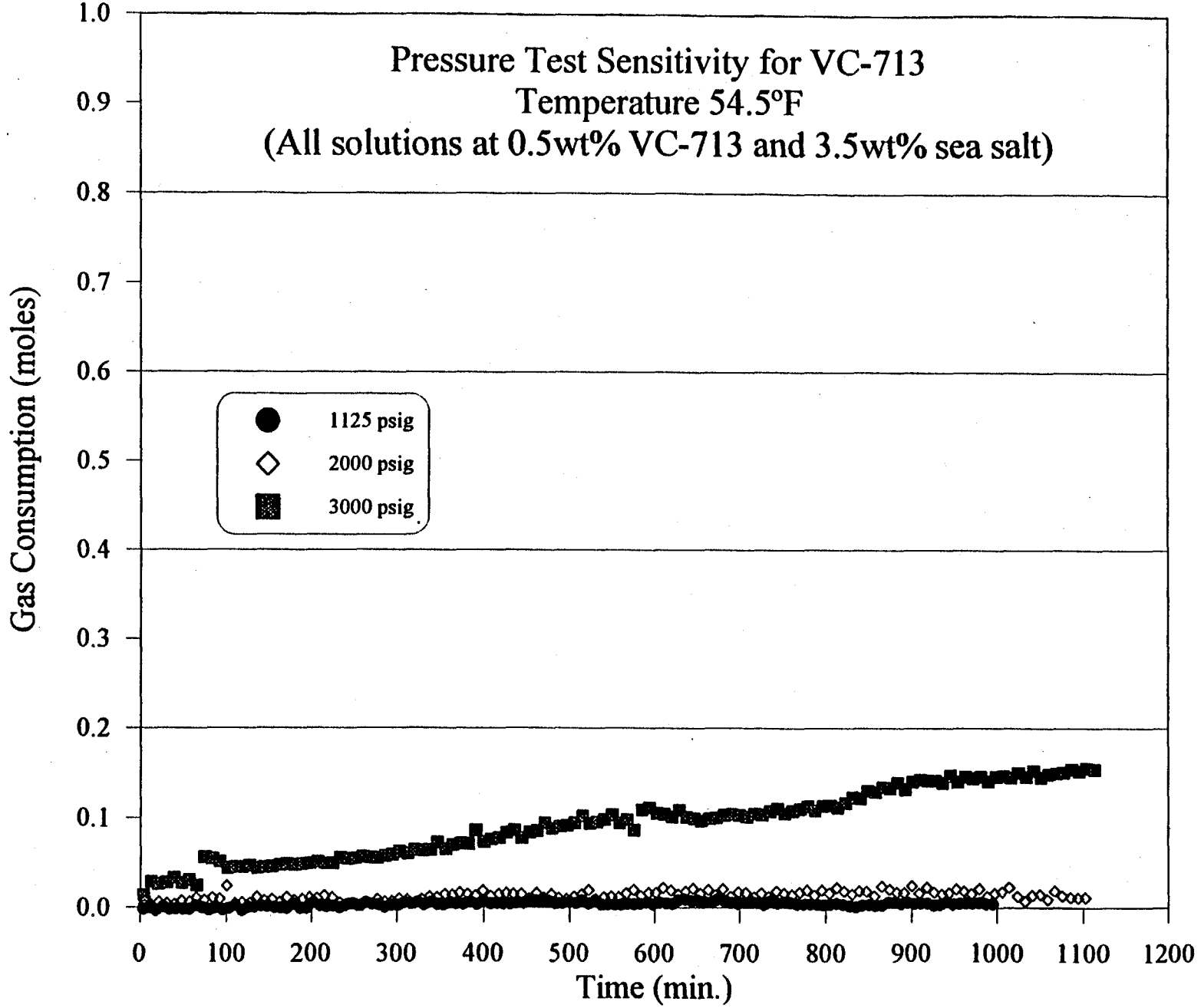

Figure 27. High Pressure Results for Pressure Sensitivity Tests of VC-713 at 54.5°F

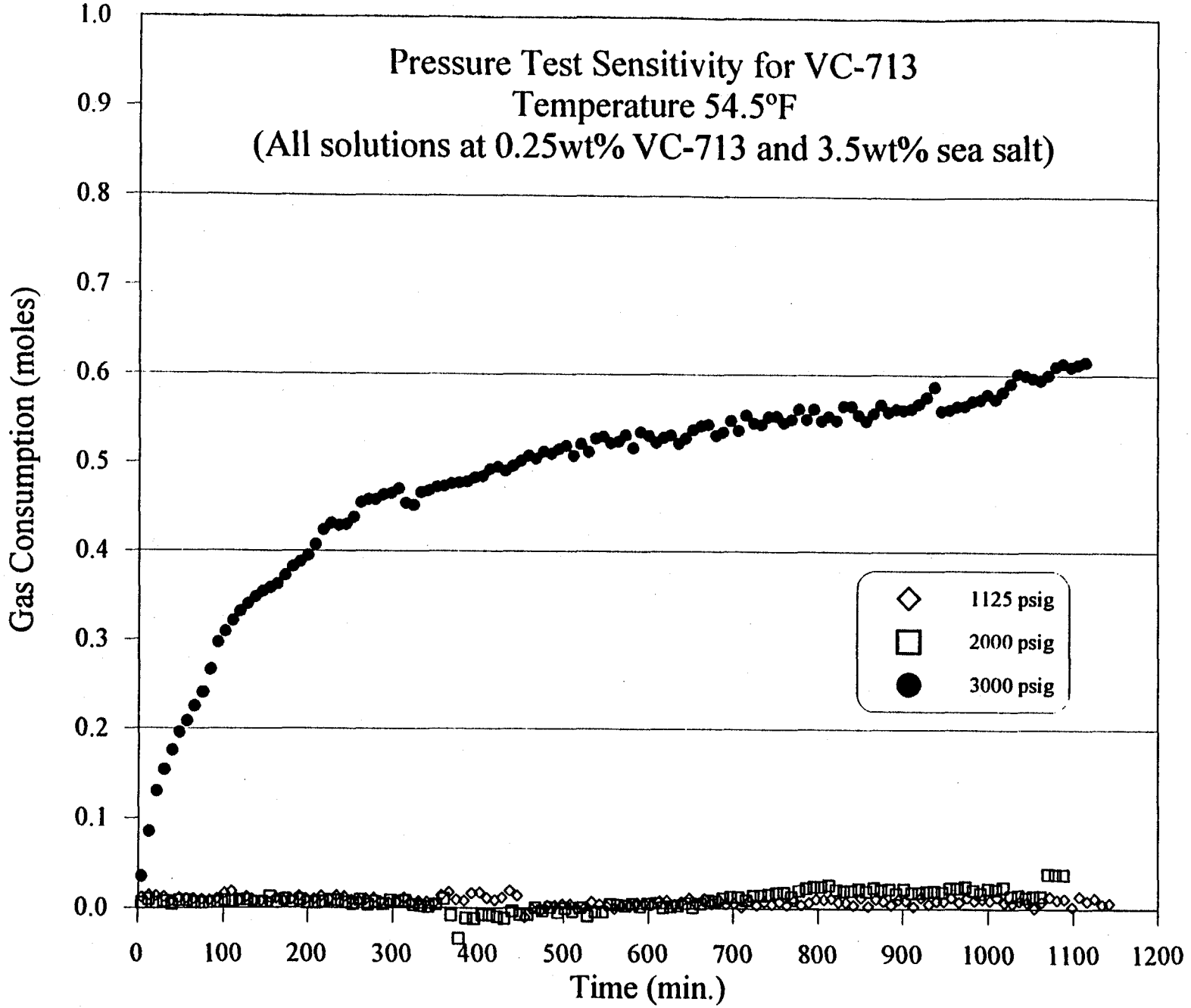

Figure 28. High Pressure Results for Pressure Sensitivity Tests of VC-713 at 54.5°F

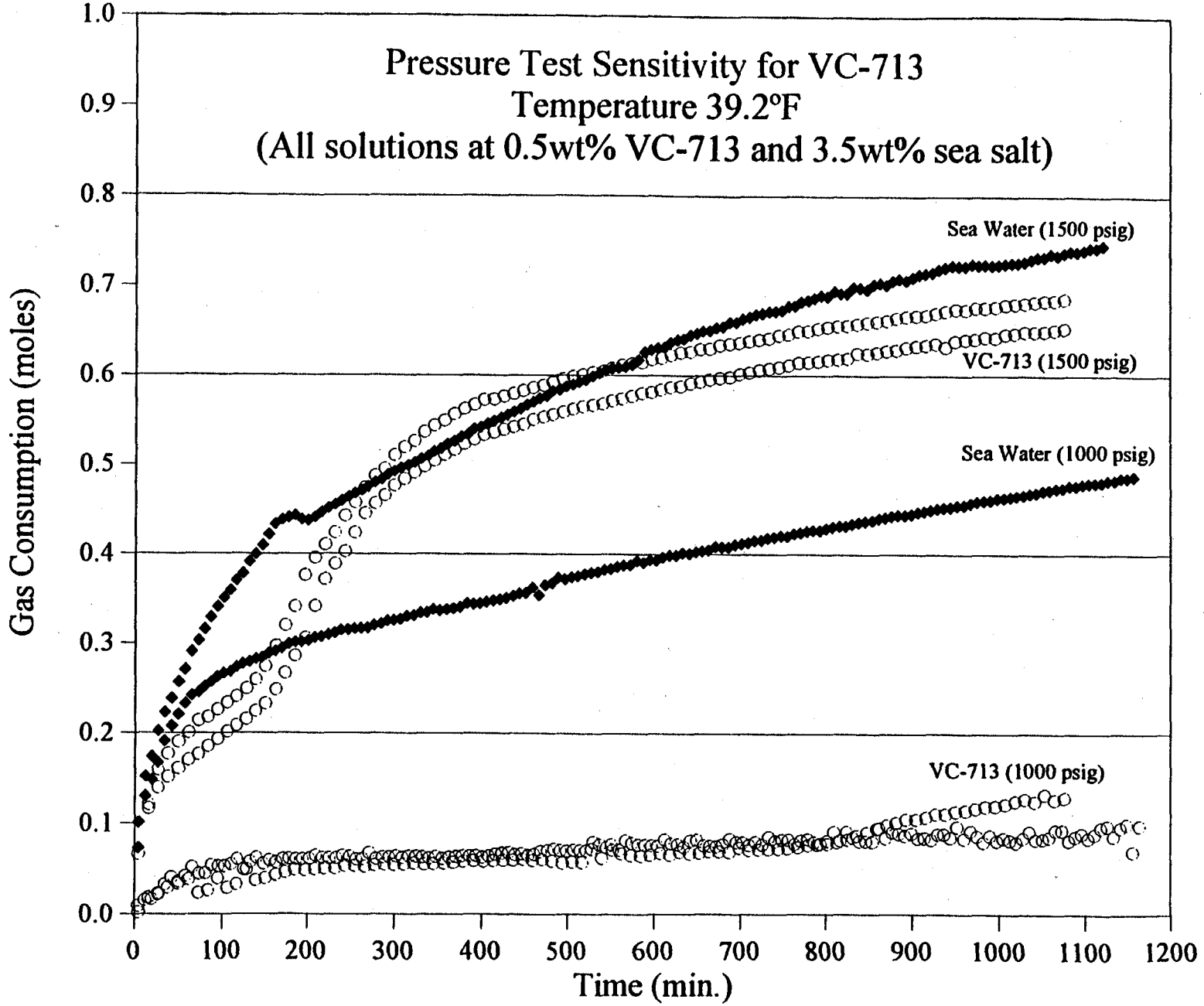

Figure 29. High Pressure Results for Pressure Sensitivity Tests of VC-713 at 39.2°F

pressure which is seen by the very large gas consumption observed at 1500 psig, close to that of sea water gas consumption.

In terms of concentration, Figures 27 and 28 indicate that not much difference was observed at 54.5°F from 0.25 to 0.5 wt% with pressures up to 3000 psig; (0.1wt% performed equivalent to 0.25 wt%). At 1125 and 2000 psig, the gas consumption was too low to determine significant differences at 0.1, 0.25 and 0.5 wt%. However, at a temperature of 39.2°F, Figure 30 shows large differences observed between the performance of 0.5 and 0.75 wt%. Initially, we had thought that inhibitor performance would be proportional to its concentration, but we were surprised to discover that the gas consumption increased (more hydrates formed) as the concentration of VC-713 increased. A reason, discussed in the hypothesis (section III.C.2.b.2.b.), is perhaps related to preferred polymer-polymer interaction rather than polymer-hydrate interaction.

Many member companies of the consortium were interested on the effect of salinity on the performance of these kinetic inhibitors. Figure 31 presents results VC-713, the first inhibitor tested at salinities from 0 to 3.5 wt% sea salt. The concentration of VC-713 was kept constant at 0.5 wt% and all experiments were carried out at 39.2°F and 1000 psig. It is worthwhile noting that the amount of salt in the system changes the thermodynamics of hydrate formation, i.e. increasing the amount of salt shifts the equilibrium curve for hydrate formation to the left (requires lower temperatures for hydrate formation) as shown in Figure 32. The increase in subcooling required is 2.5°F, as the salt concentration is increased from 0 to 3.5 wt%, while the difference in the over-pressurization required is 35 psi. In Figure 31, we see that the amount of salt is important for good performance of VC-713. The performance of VC-713 is proportional to the salinity of the solution, perhaps because the salt brings the polymer to the limits of solubility, as discussed in Section III.C.2.b.2.a.

As an alternative explanation of salt effects, it is suggested that VC-713 does not coil in the presence of salt as does other polymers, but VC-713 is able to keep its water of hydration and its expanded form in salt solution because of the amine group, which can function as an ionic part in the molecule.

IV.B.2.c.1.c. Study of PVCAP. PVCAP (Polyvinylcaprolactam) a homopolymer from BASF, also showed promising results in the high pressure apparatus. Tests done with PVCAP were the same as those done with VC-713; that is, we explored the variations in concentration, temperature, pressure, and salinity. PVCAP is a polymer which contains only the seven member ring of VC-713, and its performance is very comparable (and in some situations even better than) VC-713.

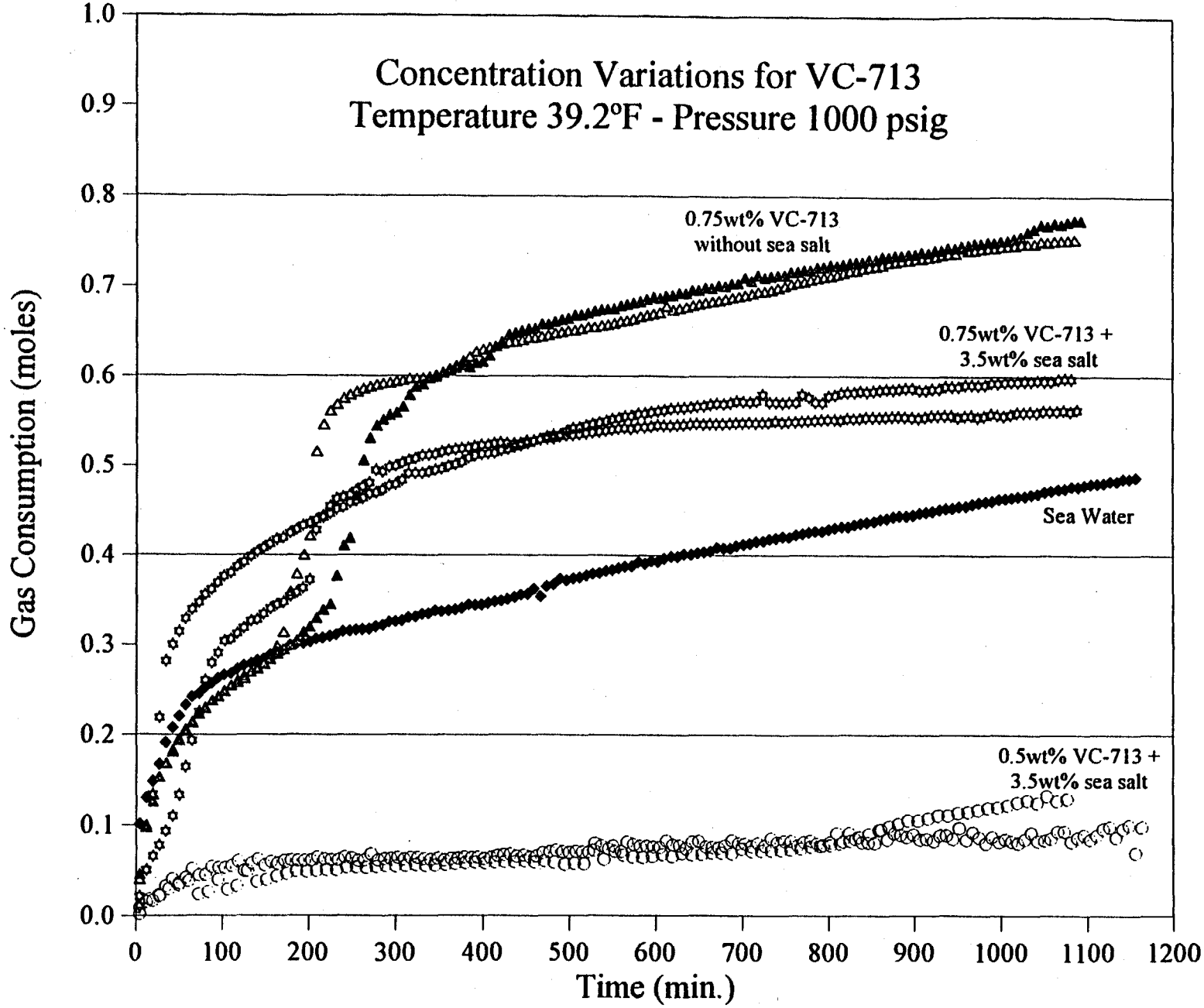

Figure 30. High Pressure Results for Concentration Sensitivity Tests of VC-713 at 39.2°F

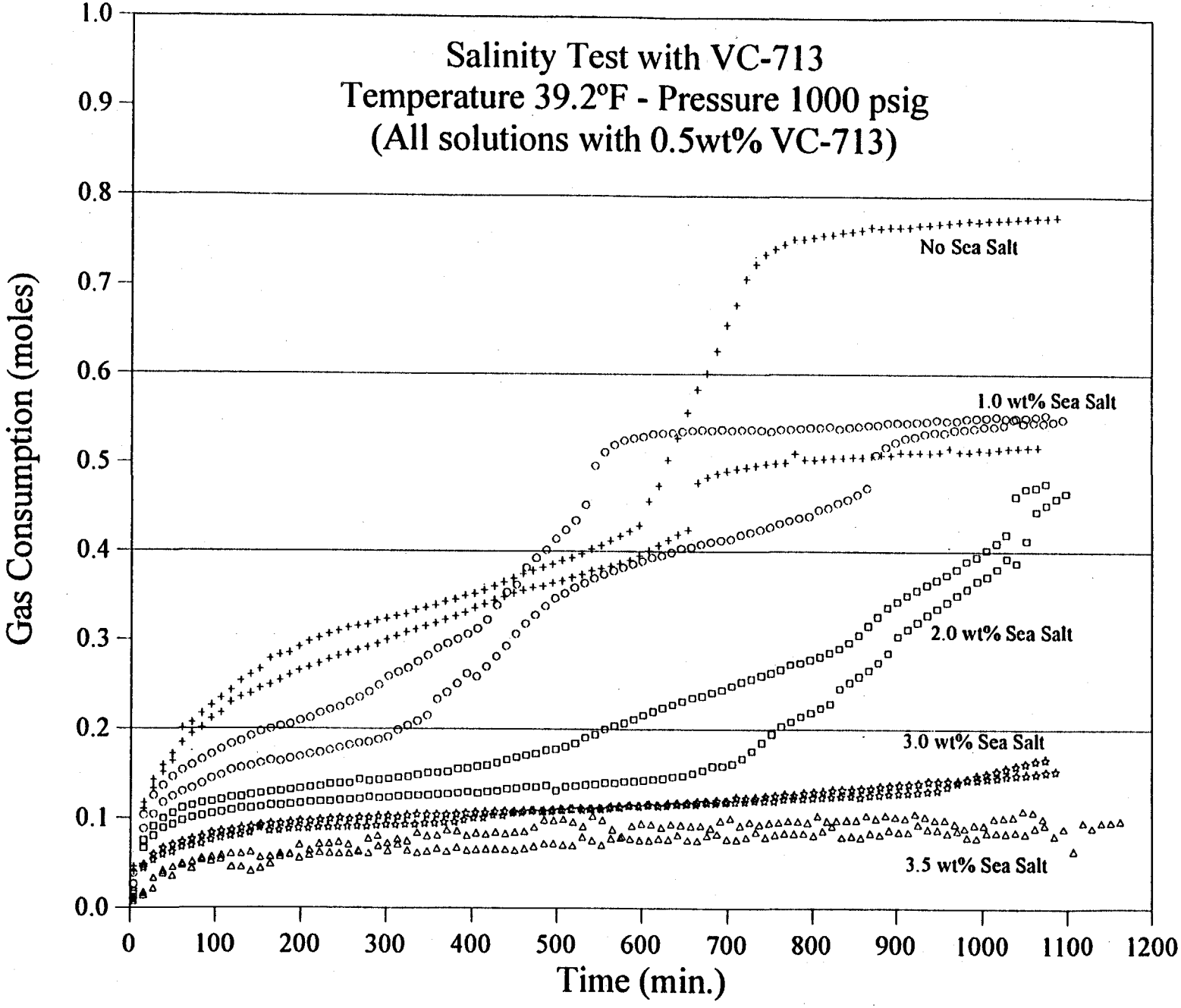

Figure 31. High Pressure Results for Salinity Sensitivity Test of VC-713 at 39.2°F

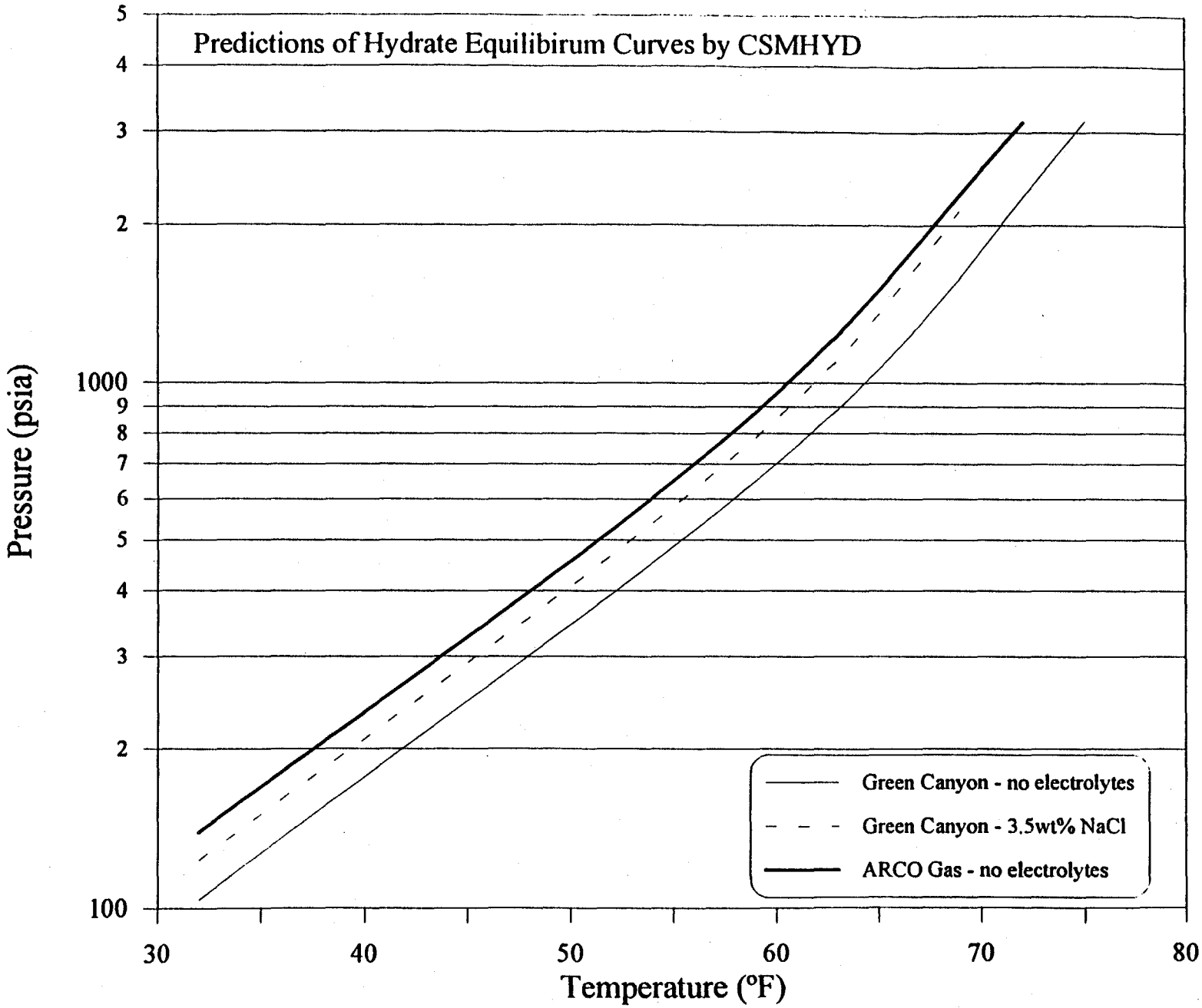

Figure 32. Hydrate Equilibrium Curves

Only a few experiments with PVCAP were done at 54.5°F; most experiments were at 39.2°F. We tested concentrations of PVCAP from 0.25 to 1.0 wt%, in solutions with 0 - 3.5 wt% sea salt and in solutions without salt. Figures 33 and 34 are the corresponding gas consumption curves for variations of PVCAP concentration without and with 3.5 wt% salt, respectively. IN contrast to the results found on the screening apparatus, PVCAP appears to inhibit hydrates very effectively without salt in solution; at 1.0 wt% PVCAP no hydrates were formed, and at 0.75 wt% a long induction time was observed followed by a low gas consumption. However, the results observed for the system with 3.5 wt% sea salt shows that the salt affects the way PVCAP inhibits hydrates, because a much larger gas consumption was seen when using PVCAP at 0.75 and 1.0 wt%.

As an alternate explanation for the effects of salt on PVCAP, the salt causes the polymer to contract or dimerize (see evidence in the UV-Vis spectra of Figure 16), making the polymer chain coil and become less effective. This is attributed to the hydration of salt ions, which remove water from the polymer. Thus the effect of salt on PVCAP is directly opposite that for salt on Gaffix VC-713.

We found that PVCAP differed from VC-713 very significantly in the absence of salt. PVCAP is effective (has a low gas consumption) at concentrations of 0.5, 0.75 and 1.0 wt% without salt in solution, while VC-713 failed as an inhibitor when no salt was present. Figures 35 and 36 compares VC-713 and PVCAP at various concentrations of sea salt.

A salinity test was also done with PVCAP. Figure 37 shows the results of tests at 0, 1.0, 2.0, 3.0 and 3.5 wt% sea salt. All salinity tests were carried out at 39.2°F and 1000 psig with a PVCAP concentration of 0.5 wt%. Changes in subcooling and over-pressurization by addition of salt were identical with those observed for VC-713, in section IV.B.2.C.1.b. We noticed that from 1.0 to 3.5 wt% sea salt, the gas consumption decreased as the salinity increases, thus following the same trend as observed with VC-713. However, with no salt, the results are different from VC-713 as shown in Figure 37.

The hypothesis s tion (III.C.2.b.2.a.) suggests why PVCAP works in the absence salt, while VC-713 does not. Our hypothesis is that PVCAP is a homopolymer with a low solubility (cloud point ≈ 27°C), in which the rings come closer together in presence of salt ions, leaving the ring aggregate less effective to dock with hydrates nuclei. When ions are present the solubility of PVCAP decreases (the polymer is "salted out" of solution) causing particles suspended in solution to serve as nucleation sites for hydrates growth, thus causing the gas consumption to be greater in the presence of salt. At higher salt concentrations (3.5wt%) the driving force for hydrate

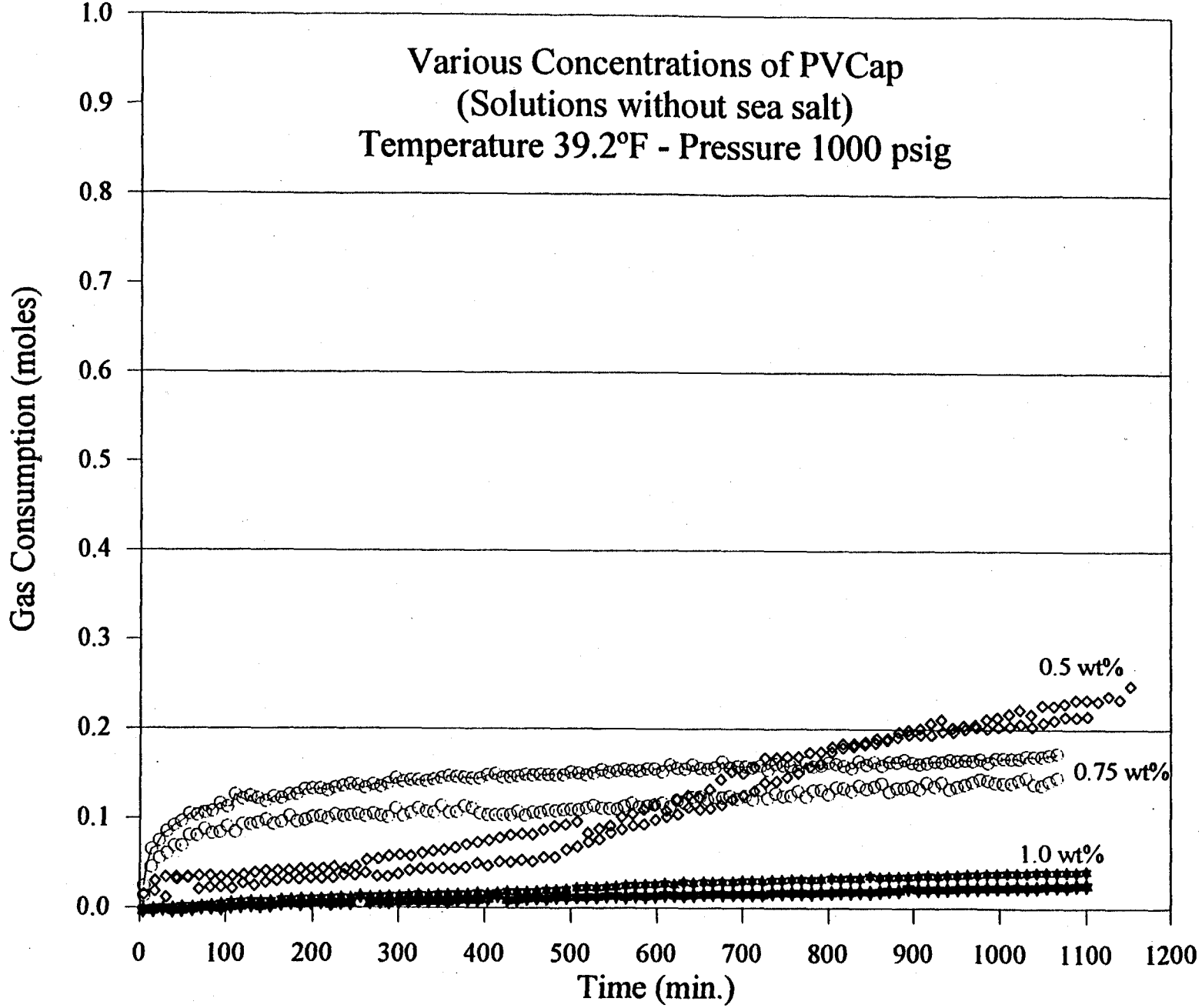

Figure 33. PVCap performance at various concentrations in the absence of salt

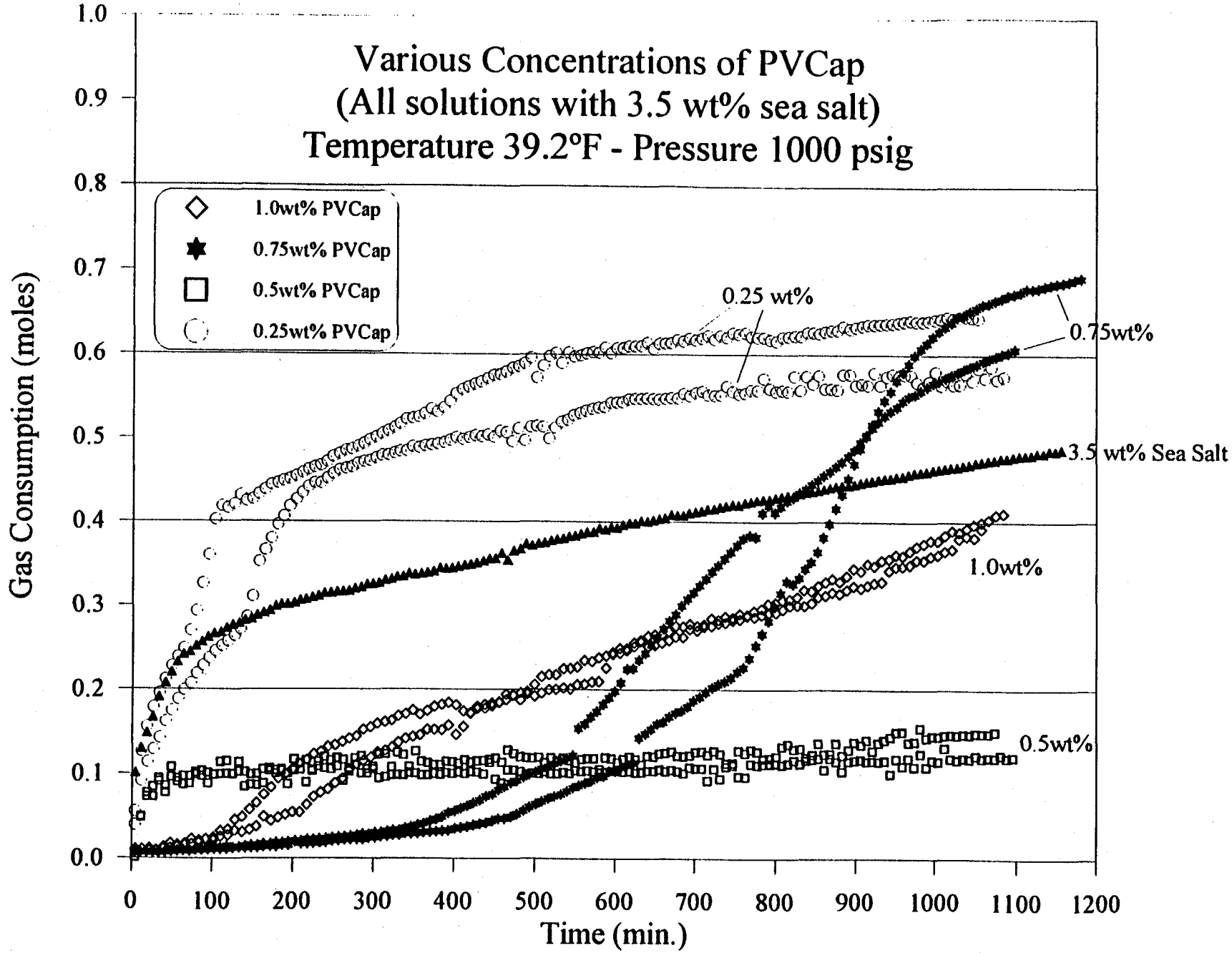

Figure 34. PVCap Performance at Various Concentrations in the Presence of Salt

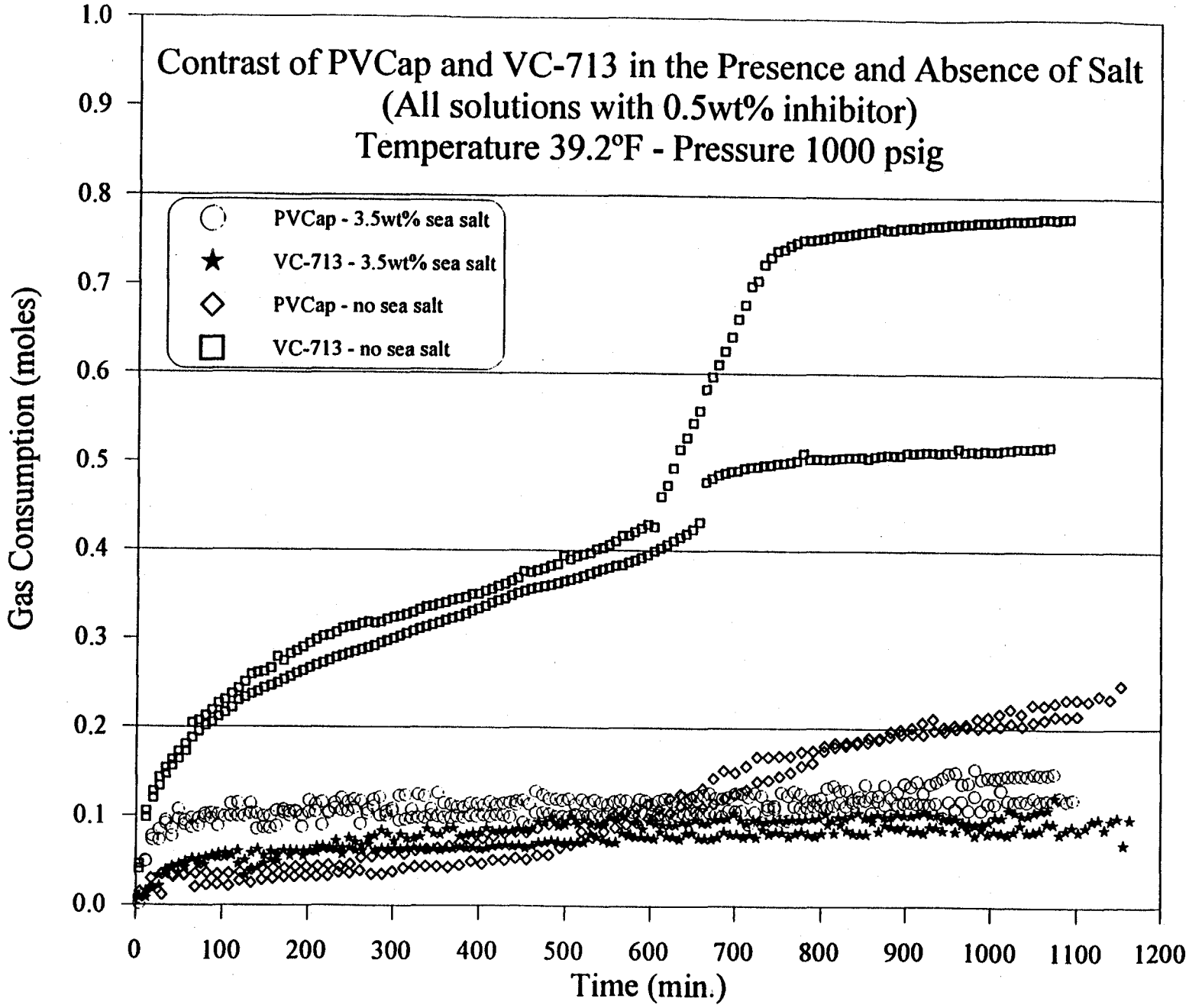

Figure 35. Comparison of PVCap and VC-713 at 0.5wt% in the presence and absence of salt

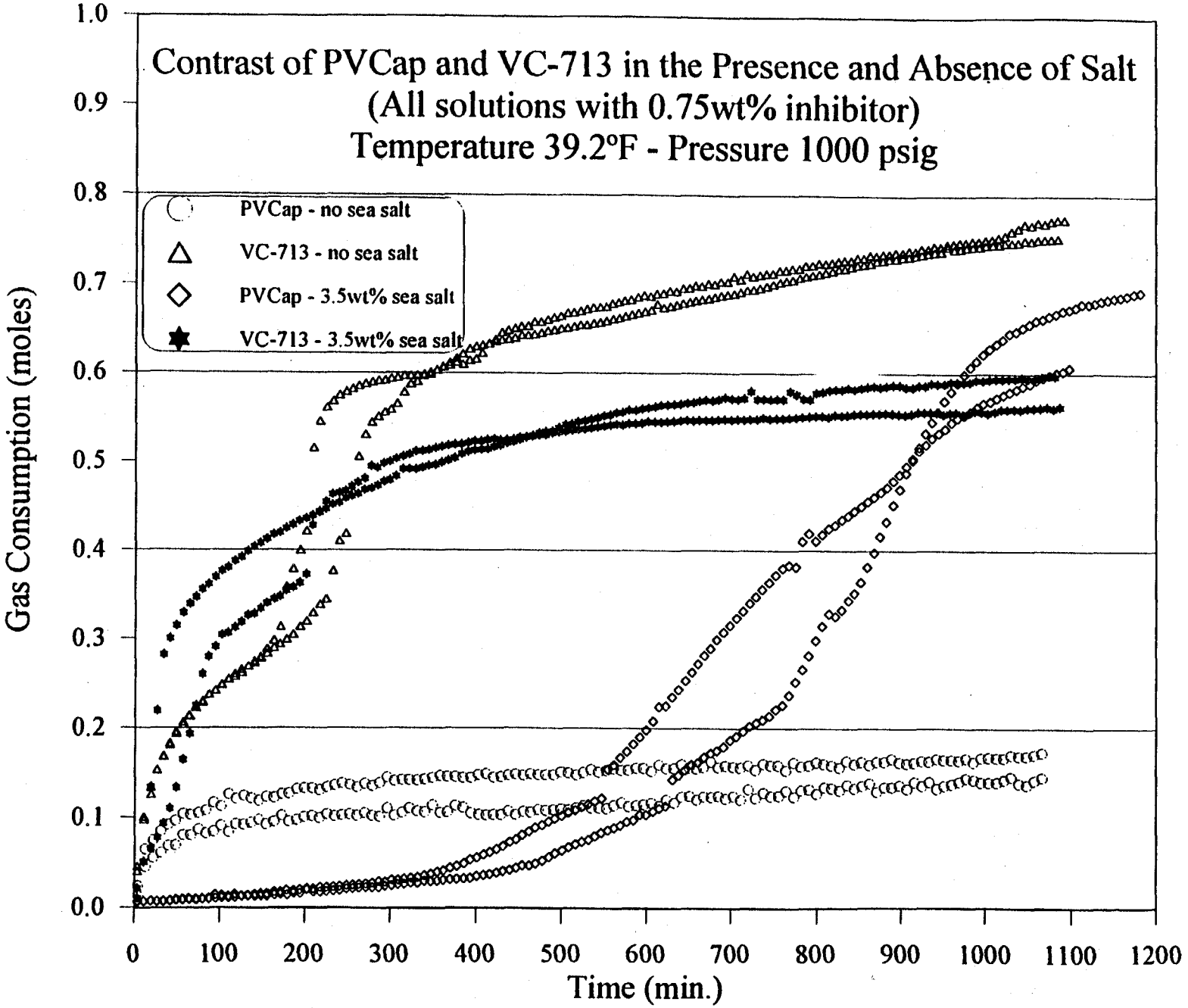

Figure 36. Comparison of PVCap and VC-713 at 0.75wt% in the presence and absence of salt

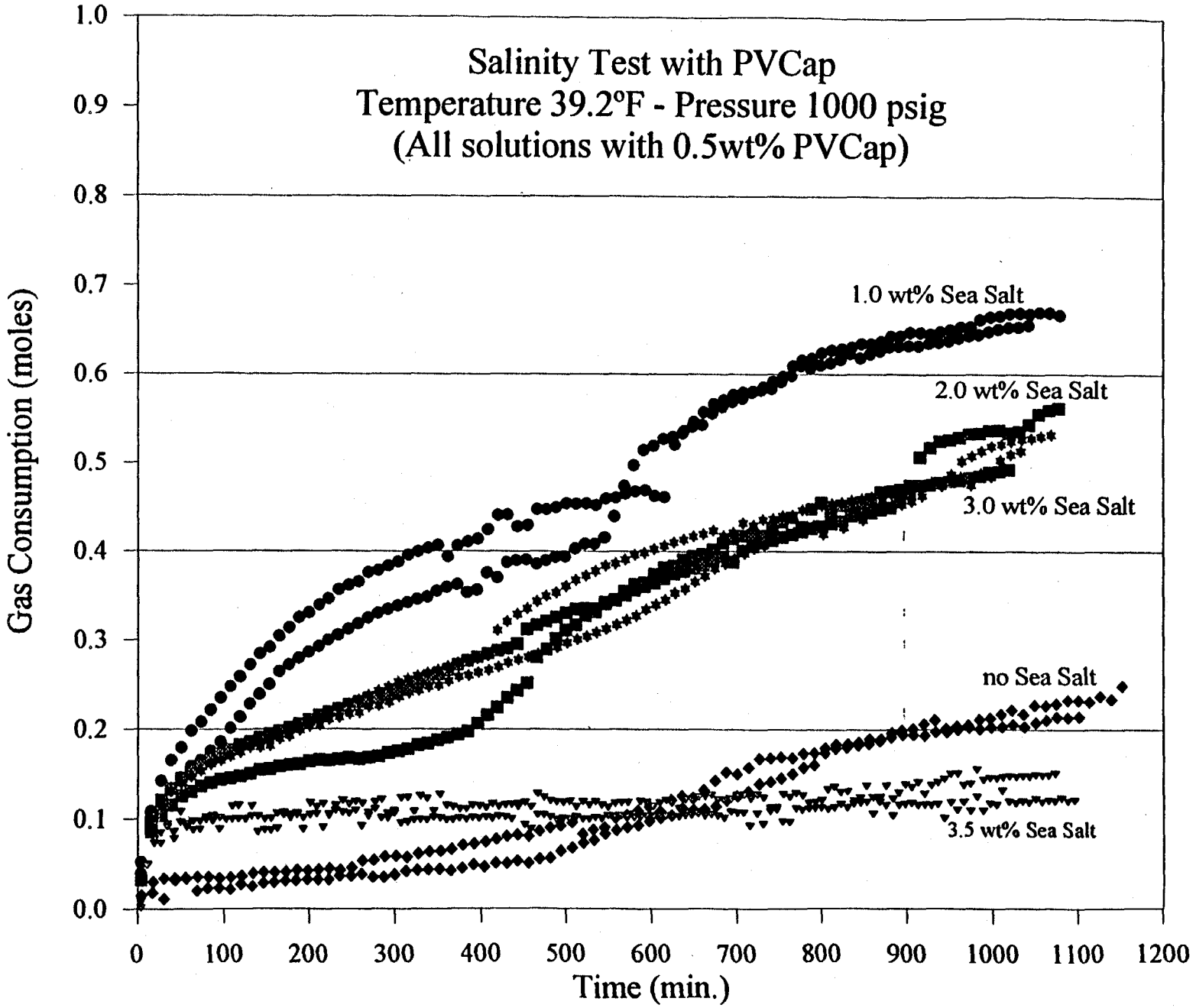

Figure 37. Salinity Test with PVCap

formation is decreased, resulting in lower gas consumption. No tests have yet been done at a higher salinity than 3.5 wt% for both PVCAP and VC-713. There seems to be optimum concentrations of PVCAP or VC-713 with optimum salt concentrations, where performance is best.

A pressure sensitivity study was also done with PVCAP (Figure 38) at 0.5 wt% PVCAP and 3.5 wt% sea salt. In this study, we went a to higher pressures (1200 and 1500 psig); however, not much difference is seen in the gas consumption for those four experiments, which actually reflects four experiments at about the same (1500 psig) pressure. Unfortunately during the experiments at 1200 psig, the pressure regulators did not work properly, thus causing the pressure in the reactor to go beyond its set point. Therefore our conclusions about the PVCAP pressure sensitivity are based only on 1000 psig and 1500 psig experiments, which indicate that a very large amount of hydrate are formed by a 500 psig increase in pressure. Other tests will be conducted with PVCAP at pressures between 1000 and 1500 psig to determine how the upper pressure limit for PVCAP inhibition.

Figure 39 shows the gas consumption observed for this system at 1000 and 1200 psig using 1.0 wt% PVCAP with and without sea salt. PVCAP provided good inhibition at 1.0 wt% without sea salt at 1000 psig. PVCAP provided better results than at 1000 psig with 1.0 wt% PVCAP with 3.5 wt% sea salt. Even though one of the runs shown in Figure 39 for PVCAP at 1200 psig shows an initial increase in gas consumption at 1000 minutes, the performance of PVCAP at these conditions was very impressive and further tests are underway.

PVCAP is presently the inhibitor on which we have focused, and subsequent sections discuss the results obtained with copolymers of PVCAP, blends of chemicals with PVCAP and combinations of PVCAP with methanol.

IV.B.2.c.1.d. Study of Copolymers of PVP/PVCAP. VC-713 is a terpolymer composed of VP (vinylpyrrolidone), VCP (vinylcaprolactam) and dimethyl amino ethyl methacrylate. PVCAP is a homopolymer of vinylcaprolactam. Since these two chemicals showed the best hydrate inhibition among all chemicals tested, we decided to test copolymers of VP and VCP, with the idea that the caprolactam ring is of great importance in the inhibition mechanism (it is present in both chemicals), while the pyrrolidone ring serves to increase the solubility of the chemical (VC-713 and PVCAP both have a very low cloud point: VC-713 at 34°C, and PVCAP at 27°C).

Several copolymers of VP/VCP were made available by BASF and ISP at various ratios of VP to VCP. Following is a listing of the copolymers of VP/VCP which were tested.

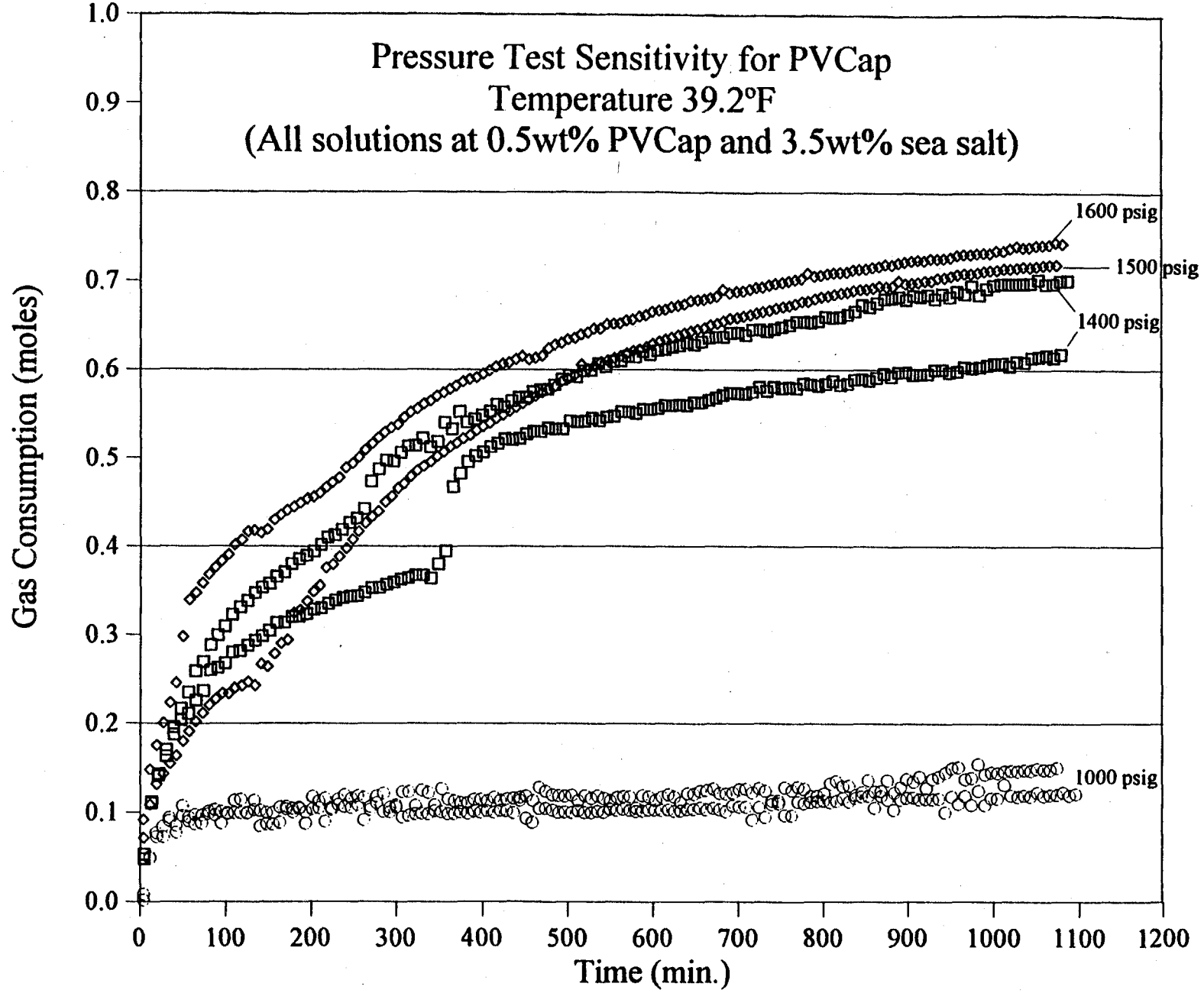

Figure 38. Pressure Sensitivity Test with PVCap at 0.5wt%

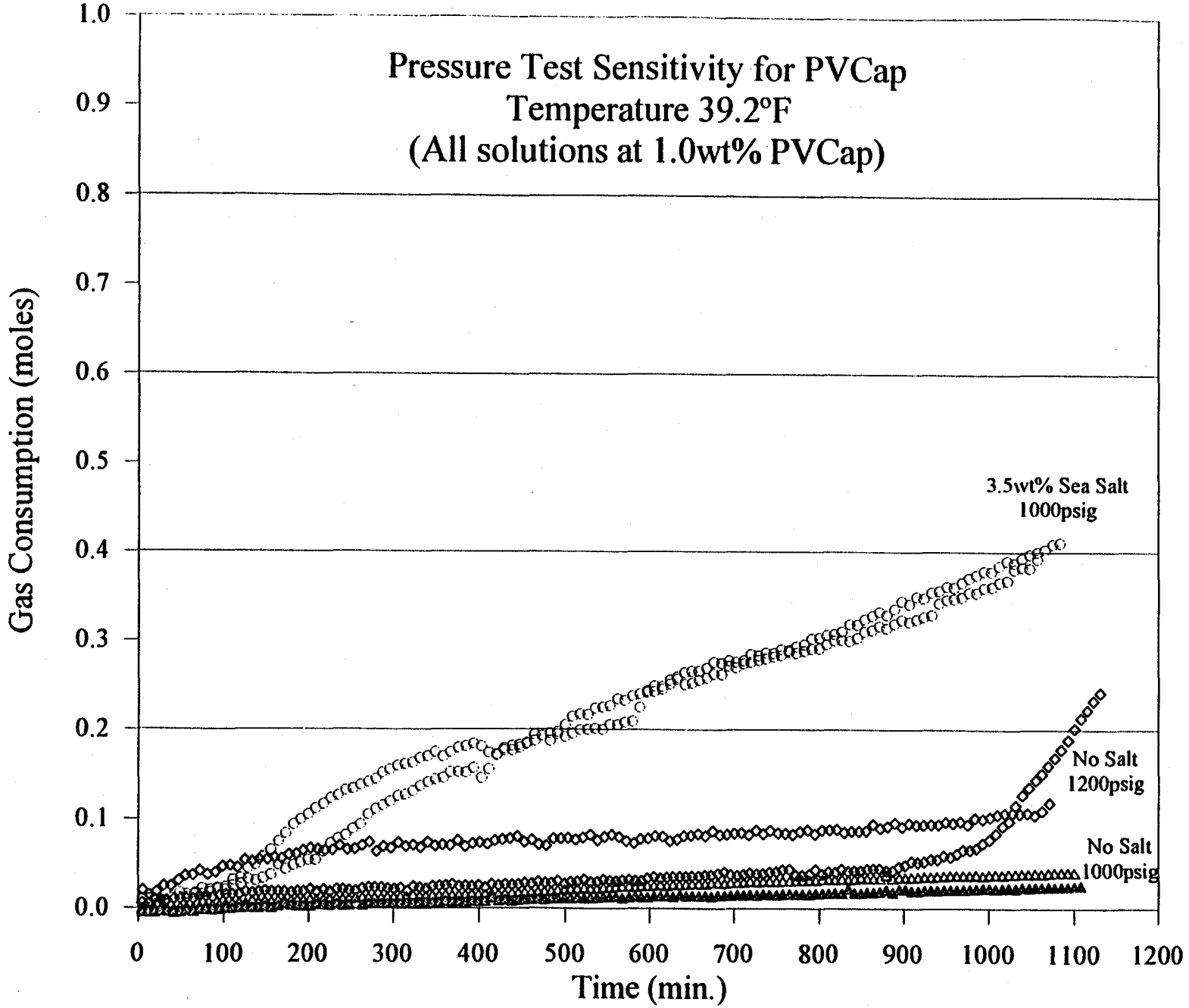

Figure 39. Pressure Sensitivity Test with PVCap at 1.0wt%

Identification Name	Ratio VP:VCP	Vendor
VP/VCP (50/50)	50:50	BASF
VP/VCP (60/40)	60:40	BASF
VP/VCP (0/100)	0:100	ISP
VP/VCP (25/75)	25:75	ISP
VP/VCP (50/50)	50:50	ISP
VP/VCP (75/25)	75:25	ISP

Experiments with these copolymers were conducted at 39.2°F and 1000 psig. Figures 40 and 41 compare the gas consumption for the copolymers from BASF and the copolymers from ISP, respectively. In each figure, the gas consumption for VC-713 and PVP are also included for comparison at the same conditions. Note that the two copolymers from BASF are solutions containing 37% solids in methanol, and the four copolymers from ISP are also solutions containing 20% solids in methanol, therefore the results shown might be confounded by methanol present in solution.

In Figure 40 a 10% change in the ratio of VP:VCP is shown to cause a substantial difference in the amount of hydrates formed during the first 600 minutes. The PVP gas consumption curve lies above that of the sea water line (3.5 wt% sea salt), indicating that more hydrates are formed when PVP is present than when it is not. A possible explanation for this fact was determined through an observation of the hydrates formed in the presence of PVP (with similar observations for other good kinetic inhibitors). Immediately after the experiment was shut down the reactor may be opened very quickly, and one may observe the remaining hydrates. In the presence of inhibitor(s), the remaining hydrates appeared to be finely dispersed crystals, while hydrates from uninhibited sea water formed a big crystalline mass which was difficult to break. Thus hydrates formed in the presence of inhibitor(s) were composed of a larger quantity of smaller, more dispersed hydrates causing a larger gas consumption than sea water (because some water is probably occluded when large "chunks" of hydrate form.

Figure 41 shows results from all copolymers from ISP. In Figures 40 and 41 there is a trend observed for gas consumption by the copolymers. The performance of the inhibitor was directly proportional to the proportion of the caprolactam ring in the polymer. For example, it is clear that PVP is not as good an inhibitor as the 75:25 (VP:VCP ratio) polymer, which in turn is worse than 50:50 (VP:VCP co-polymer). For the 25:75, 0:100 copolymers or for PVCAP, we see that there is no difference in gas consumption, indicating that the VCP ring is the main component responsible for the inhibition of hydrates, while the concentration of the pyrrolidone ring increases the copolymer solubility, and perhaps also aiding as a spacer between the caprolactam rings.

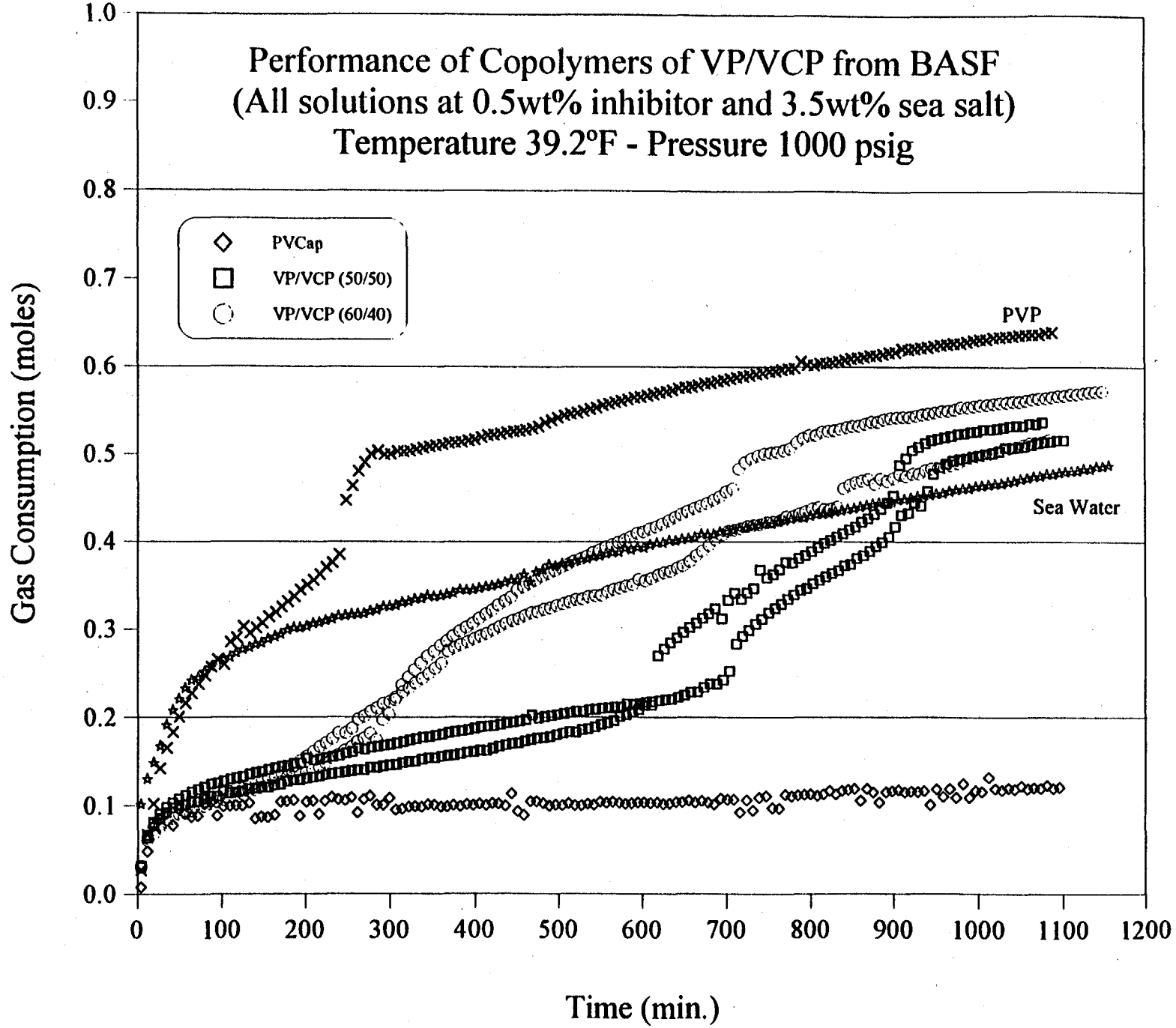

Figure 40. Copolymers of VP/VCP from BASF

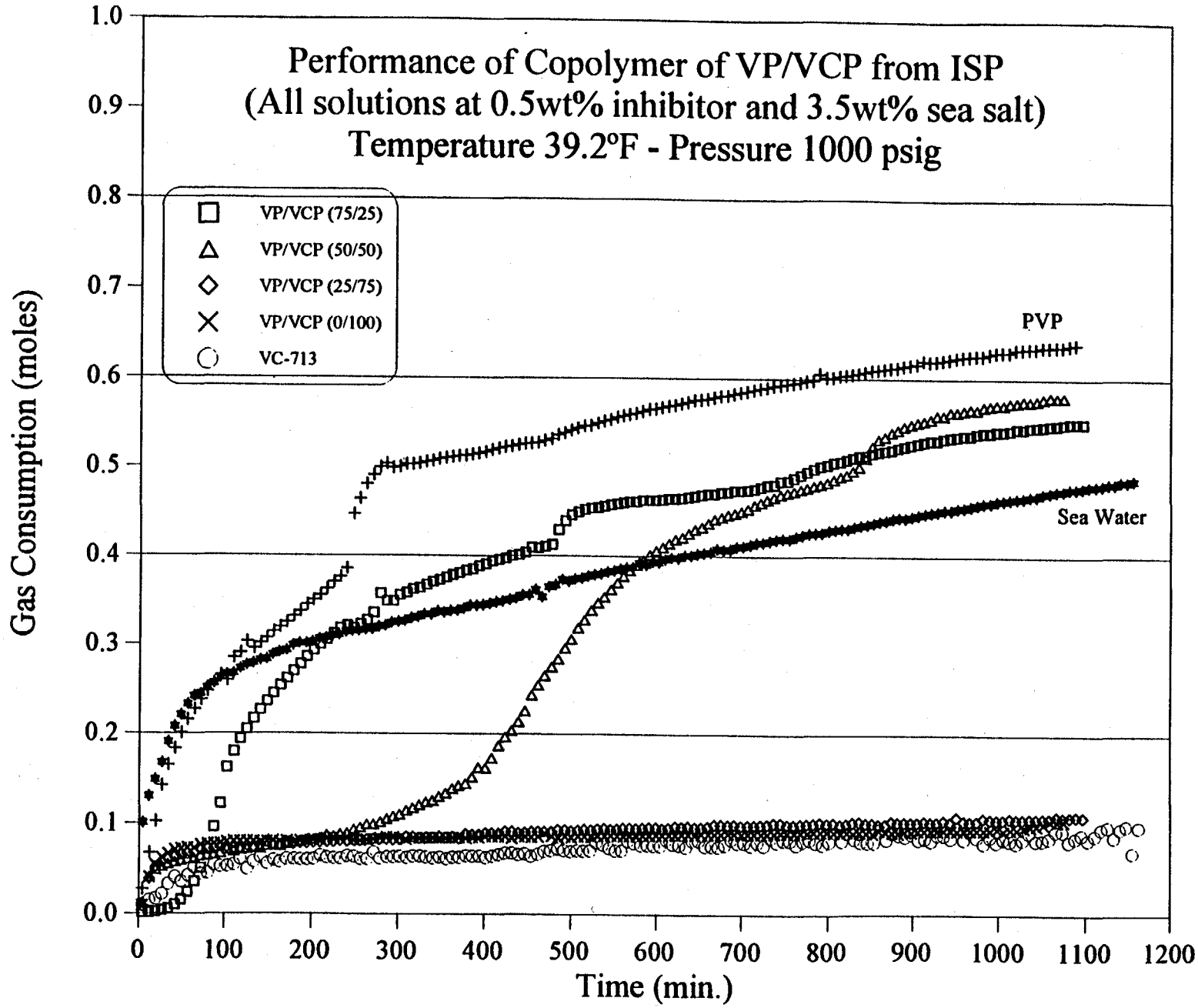

Figure 41. Copolymers of VP/VCP from ISP

It is important to note that in the presence of these inhibitors (PVCAP, VC-713, VP/VCP (25/75)) small amounts of hydrates did form at the beginning, but for the next 20 hours or so, no more hydrates were formed (as indicated by the flat gas consumption curve). This observation suggests that inhibitors prevented hydrate nuclei from agglomerating and causing a massive amount of hydrate growth.

IV.B.2.c.1.e. Studies of Combination of PVCAP and Methanol. According to field test results by the some consortium member companies, the new kinetic inhibitors are injected with methanol, thus the prevention of hydrates is through a combination of kinetic and thermodynamic inhibitors.

In this preliminary study we investigated the effect of methanol on the inhibition performance of PVCAP. Our objective was to determine whether a thermodynamic inhibitor (in this case methanol) will have a synergistic effect when combined with a kinetic inhibitor (in this case PVCAP.)

Only two sets of experiments have been completed to date, both at 39.2°F and 1000 psig. One duplicate run used a system of PVCAP at 0.5 wt% and 5.0 wt% methanol; another run used the same concentration of PVCAP but 2.5 wt% methanol.

Figure 42 shows the results for both sets of experiments. The gas consumption indicates that methanol at 5.0 wt% did not aid the inhibition of hydrates, and 2.5 wt% methanol may even promote hydrate formation. On a lnP versus T plot, the addition of 5.0 wt% of methanol to an aqueous solution did shift the hydrate equilibrium curve to the left of (but still parallel to) the equilibrium line for pure water; that is, lower temperatures and higher pressures will be required for hydrate formation when methanol is present in the liquid.

The above results are preliminary and more tests are scheduled to determine why the presence of methanol causes more hydrates to form.

IV.B.2.c.1.f. Studies of HE-300 and Blends of PVP with PVCAP. Some new kinetic inhibitors which gave good results in the screening apparatus, have subsequently been tested in the high pressure apparatus. One of the new chemicals is HE-300 a polyelectrolyte whose chemical structure is shown in Figure 2.

The initial results from the high pressure apparatus for HE-300 are plotted in Figure 43. HE-300 alone did not show promise as a good inhibitor, as indicated by the large gas consumption and an extremely large rate of formation during the first 200 minutes. However, since we had previously determined that the

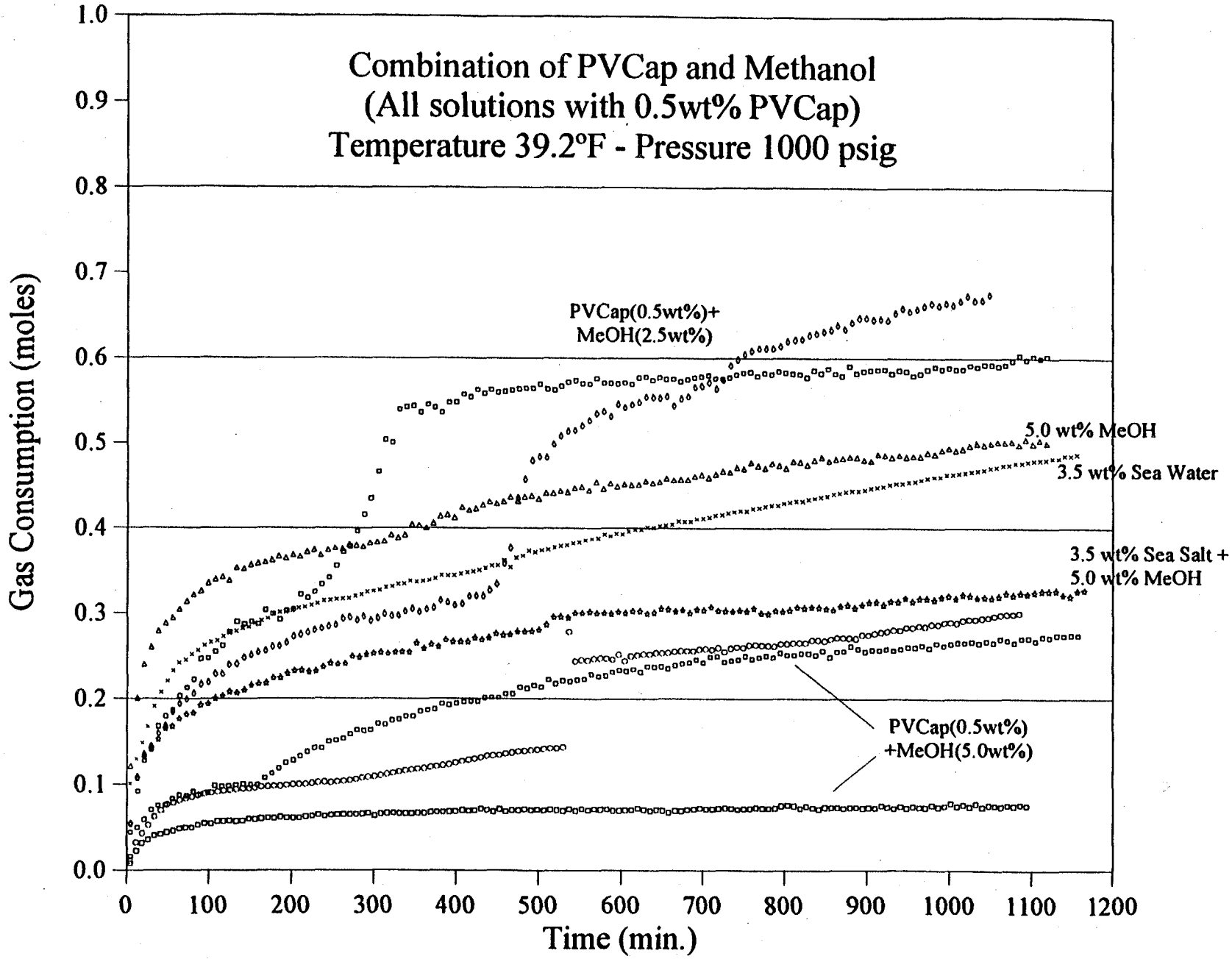

Figure 42. Combination of PVCap and Methanol

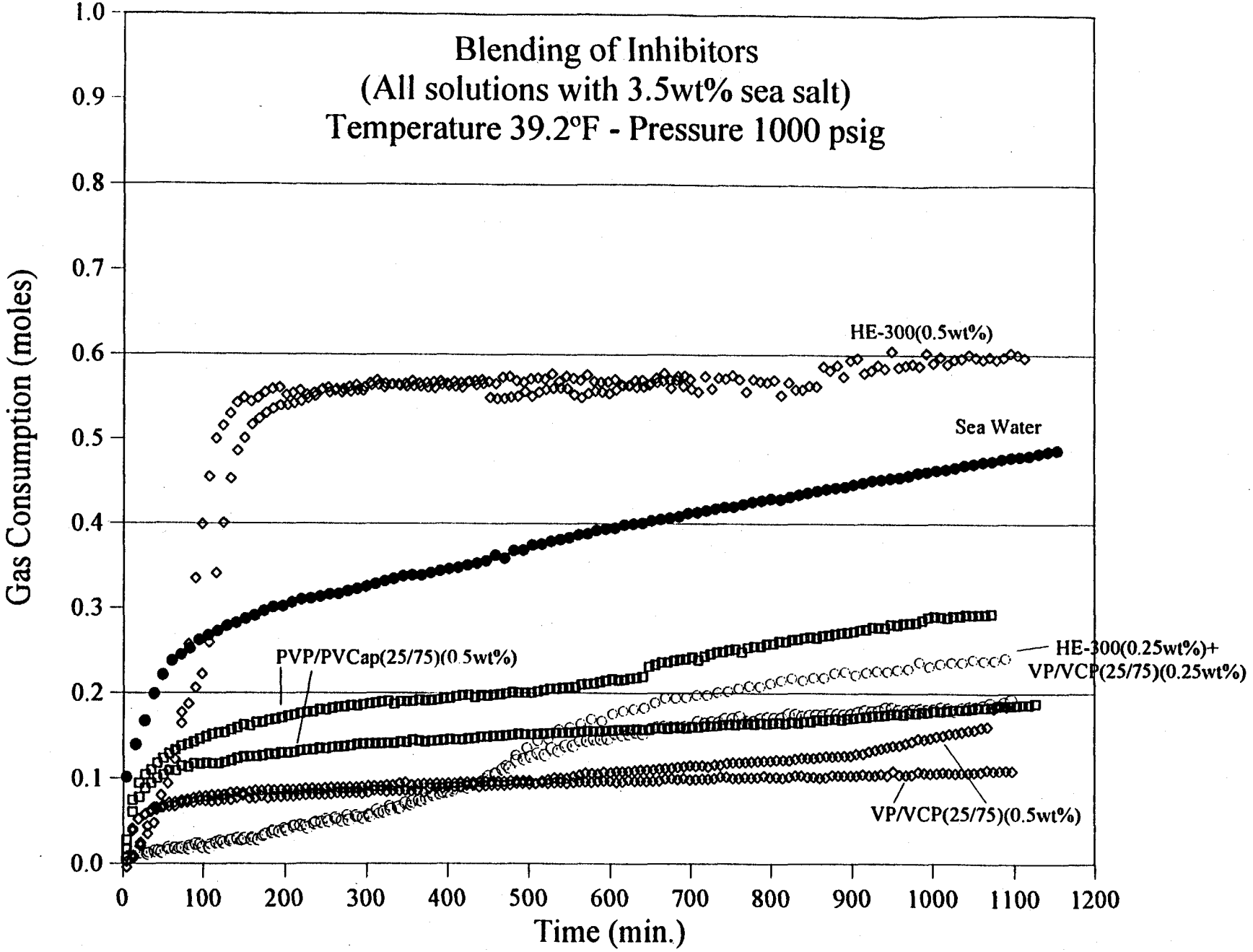

Figure 43. Blending of Kinetic Inhibitors

caprolactam ring was a major factor in the kinetic inhibition of hydrates, we decided to blend HE-300 and VP/VCP (25/75) to determine whether some improvement occurred in performance of HE-300.

A substantial kinetic inhibition improvement was observed, as shown in Figure 43. HE-300 and VP/VCP were blended at 0.25 wt% HE-300 and 0.25 wt% VP/VCP (25/75) in a 3.5 wt% sea salt solution. Blending was our only option in this case because we did not have a copolymer of these two chemicals. HE-300 is not a significant hydrate kinetic inhibitor by itself, but there seems to be a promising future for this chemical when combined with other copolymers of caprolactam. We note here that HE-300 is less expensive than the lactam ring polymers (PVP or PVCAP).

Figure 43 also has the results for a blend of PVP and PVCAP in the ratio of 25:75. In this experiment we wanted to test whether a copolymer of VP/VCP was needed; in other words whether the presence of a soluble Caprolactam unit would suffice to inhibit hydrates. The combined blend concentration was 0.5 wt% of inhibitors in a 3.5 wt% sea salt solution. The difference between a blend of PVP and PVCAP and a copolymer VP/VCP (25/75) is confounded by the presence of methanol, because the copolymer VP/VCP (25/75) was a solution of 20% solids in methanol, causing the final test solution to contain both 2.0 wt% of methanol and 0.5 wt% copolymer inhibitor.

One might account for the difference by the fact that methanol causes the equilibrium curve of hydrate formation to shift to the left, and we would expect a lower gas consumption for the solution with 2.0 wt% methanol because of lower driving forces for hydrate formation (smaller deviations from the equilibrium line). Therefore, the polymer blend appears to be as good as the copolymer. This experiment indicates that the solubility of the Caprolactam ring has a vital role in the hydrates inhibition.

IV.B.2.d. Extended Time Inhibition Tests of Chemicals

ARCO North Sea Operations requested that our laboratory perform tests for kinetic inhibition of hydrates using VC-713 and PVCAP as kinetic inhibitors. They funded this work independently, but ARCO has graciously made their results available to the consortium members in the form of this report.

The series of tests were done with gas and n-Decane representing a liquid condensate. A gas of the following composition was acquired through Matheson Gas Products:

Component	Mole Fraction
Methane	0.8663
Ethane	0.0492
Propane	0.0151
n-Butane	0.0042
i-Butane	0.0028
Nitrogen	0.0321
Carbon Dioxide	0.0303

The equilibrium curve for the above gas is shown in Figure 32, as calculated by CSMHYD. As shown by the displacement of the equilibrium line to the left, hydrates are harder to form with the ARCO gas mixture than with our standard Green Canyon Gas.

In these tests, 1500 ppm of Petrolite, a corrosion inhibitor provided by ARCO, and 500 ppm of salt was used. Table 8 lists the results for experiments conducted for ARCO, including compositions of test solutions, as well as induction times. All experiments were done with 60 grams of n-Decane and 60 grams of the test solution. Figures 44 and 45 show results of all experiments listed in Table 8. Note that the initial gas consumption in both Figure 44 and 45 is due to the solubility of the gas in n-Decane.

In the ARCO study, only two experiments (shown in Figure 44) were done with PVCAP, both at conditions of 39.2°F and 1000 psig. Both experiments indicated that PVCAP can provide acceptable inhibition performance. PVCAP inhibited hydrates for a period of a day using 5000 ppm of PVCAP and 500 ppm of sea salt. PVCAP provided still better inhibition (for a period of almost two days) when its concentration was increased to 7500 ppm and no sea salt was present in the system.

Figure 45 shows the results of VC-713 tests at four different pressures. Only at low pressure (900 psig), did VC-713 inhibit hydrates for five days. At higher pressures (1300 and 1500 psig), hydrates formed more rapidly than anticipated; VC-713 did not appear to prevent hydrates from forming, even at higher concentration of sea salt (3.5 wt%), but it did slow the growth of hydrates. At 1000 psig, VC-713 inhibited hydrates for a period of about a day, which was followed by a massive amount of hydrates formation (indicated by the gas consumption).

These nine experiments were very interesting; we decided to continue testing with a similar system to determine whether the liquid condensate, corrosion inhibitor and gas caused the inhibition to be less than that anticipated.

In future tests we plan (with a similar system) to remove the liquid condensate and then increase the salt concentration, before further studying the effects of PVCAP , the best single

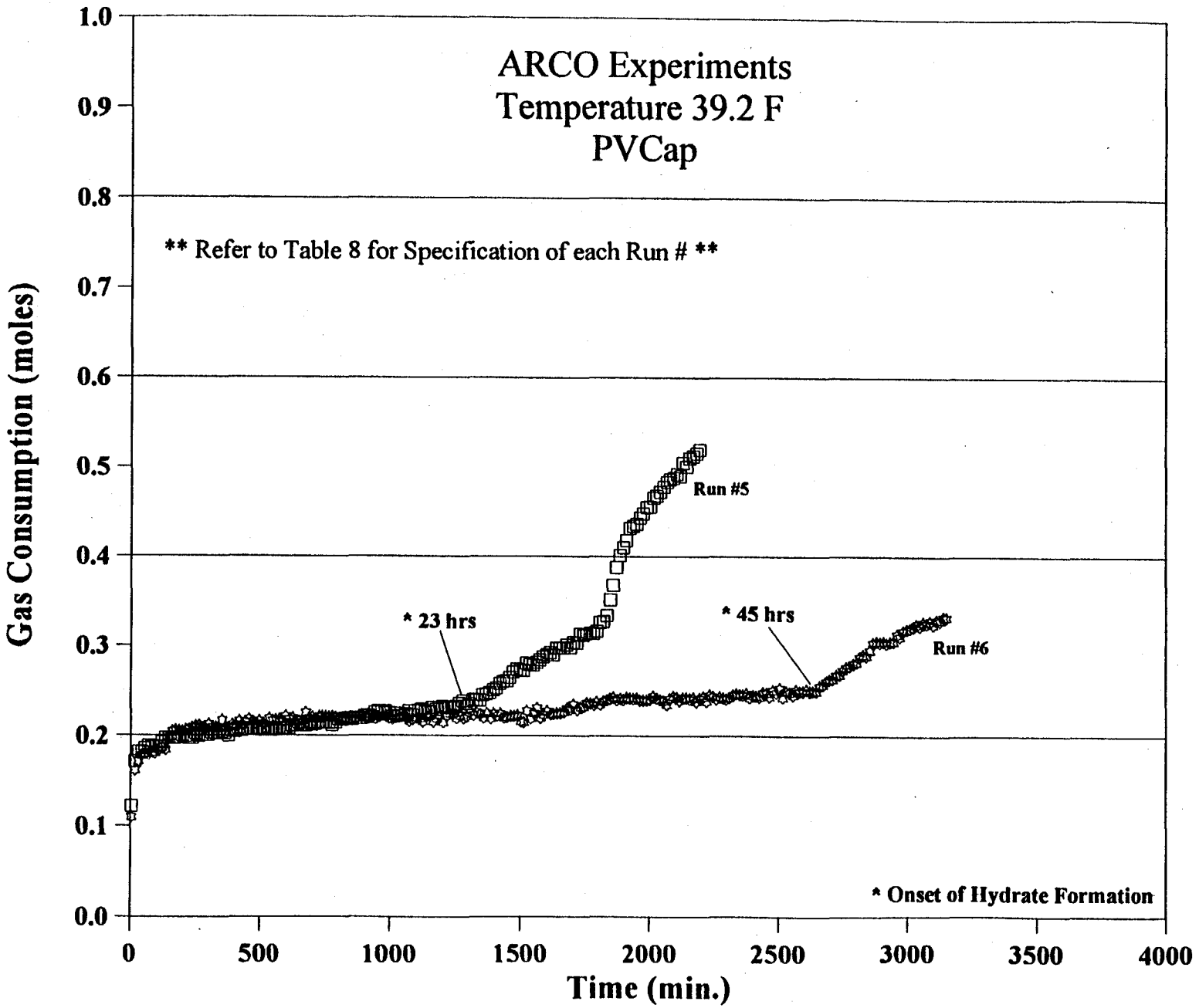

Figure 44. ARCO Experiments with PVCap

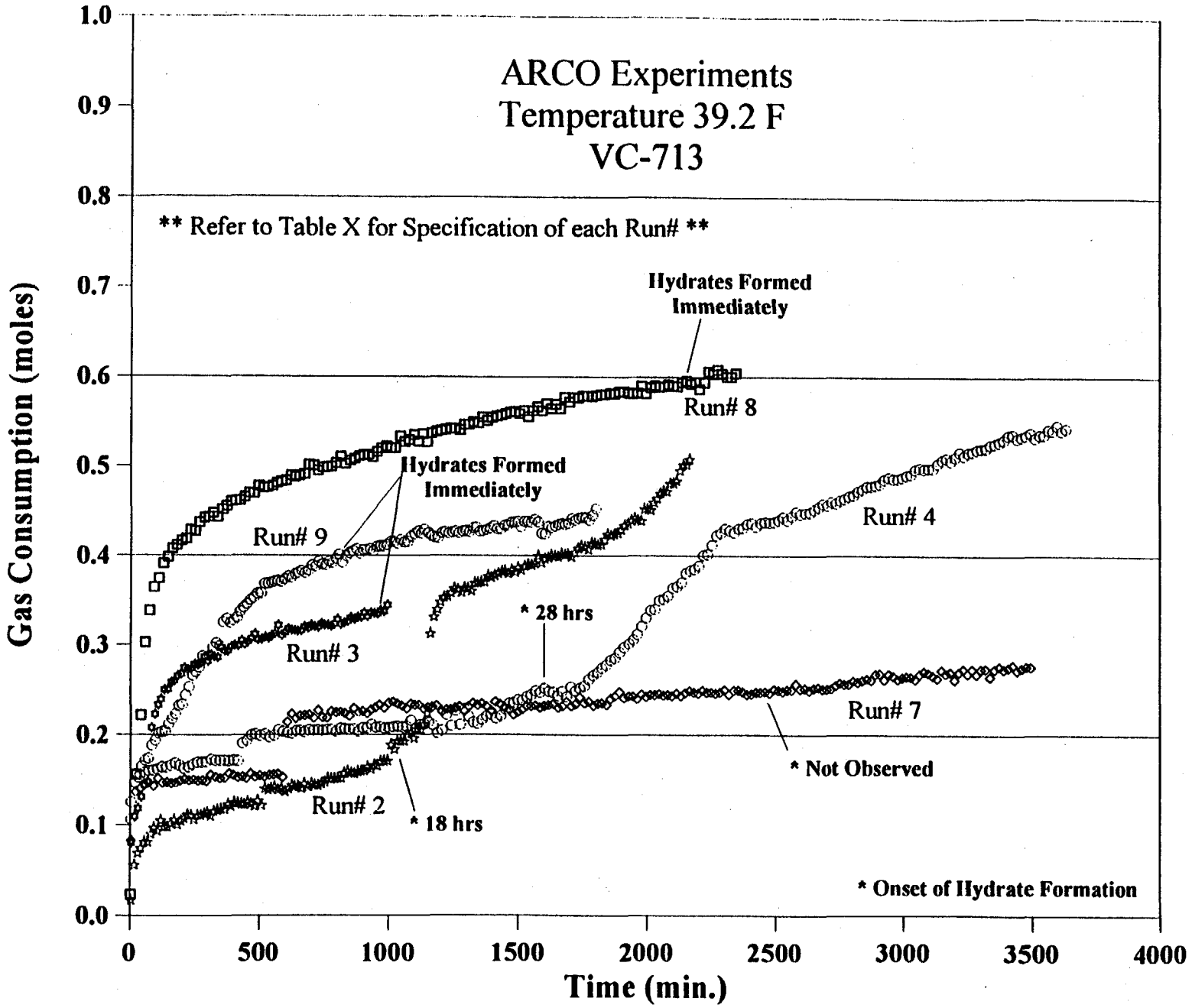

Figure 45. ARCO Experiments with VC-713

Table 8. Summary of ARCO Experiments

Standard Solution: 5000 ppm inhibitor + 500 ppm sea salt + 1500 ppm corrosion inhibitor

All test at 39.2°F

Test solution: 60 grams n-decane + 60 grams standard solution

Run #	Kinetic Inhibitor	Solution (as different of standard)	Pressure (psig)	Time of Hydrate Formation	Duration of Test
1	DI Water	-	1500	immediately	1 day
2	VC-713	standard	1500	18 hrs	2 days
3	VC-713	standard	1300	immediately	1 day
4	VC-713	standard	1000	28 hrs	3 days
5	PVCap	standard	1000	23 hrs	2 days
6	PVCap	7500 ppm PVCap w/o sea salt + 1500 Petrolite	1000	45 hrs	2½ days
7	VC-713	5000 ppm VC-713 + 500 ppm sea salt and no corrosion inh.	see note*	Not Observed	5 days
8	VC-713	5000 ppm VC-713 + 500 ppm sea salt and no corrosion inh.	1500	immmediately	2 days
9	VC-713	5000 ppm VC-713 + 35000 ppm sea salt no corrosion inh.	1500	immediately	1½ days

*Note: For this test the pressure was 800 psig for the first 11 hrs, then the pressure was boosted to 900 psig and at this pressure the test continued for 3 days. At the end of the third day, the mixer was shut down and the pressure increased to 1000 psig, where the test proceeded for another day without the mixer on. On the fourth day, the pressure was decreased to 900 psig and the mixer turned on, and the test continued for one more day.

kinetic inhibitor at present.

IV.B.2.e. Viscosity Effects on Kinetics of Hydrate Formation

In the 1992 Annual Report, we reported that the HEC series of chemicals demonstrated kinetic inhibition of gas hydrate formation. Unfortunately, the best inhibitor solution had a relatively high viscosity, but these results indicated that further study was warranted. The study of viscosity effects served two purpose; (1) it provided insights concerning the mechanism of hydrate formation and inhibition, and (2) it enabled our examination of kinetic inhibition effects of other viscosity modifiers which were commonly used in oil/gas industry.

In our early work, we found that a high molecular weight of HEC provided good inhibition for hydrate growth, demonstrated by low gas consumption, but it had a short induction time. It was hypothesized that an increased viscosity might provide kinetic inhibition by limiting mass transfer of molecules (or clusters of molecules) necessary for hydrate agglomeration. The following four classes of experiments were designed to study viscosity effects on hydrate formation:

(1) Different molecular weight HEC chemicals with the same weight concentration (0.5 wt%),

(2) Identical molecular weight HEC samples with different concentrations (different viscosities),

(3) Different molecular weight HEC chemicals and different concentrations (identical apparent viscosities), and

(4) Different molecular structures of HEC with different concentrations (identical apparent viscosities).

Viscosity measurements used a Brookfield viscometer at 600 rpm, close to the mixing rate in our high pressure apparatus. Figure 46 shows gas consumptions for different HEC molecular weights at the same concentration (0.5 wt%). The data in the figure demonstrate that viscosity influences hydrate formation, with higher viscosity producing dramatically lower gas consumption. However these data might also be explained by the suggestion that higher molecular weight HEC (larger molecular structures) provide better kinetic inhibition.

As shown in Figure 47, when we varied the concentrations of the same molecular weight samples of HEC, gas consumptions were much less for higher HEC concentrations than for lower HEC concentrations. This result gives additional credence to our hypothesis that hydrate growth rate is less in higher viscosity solutions. The HEC used in this set of experiments was a low

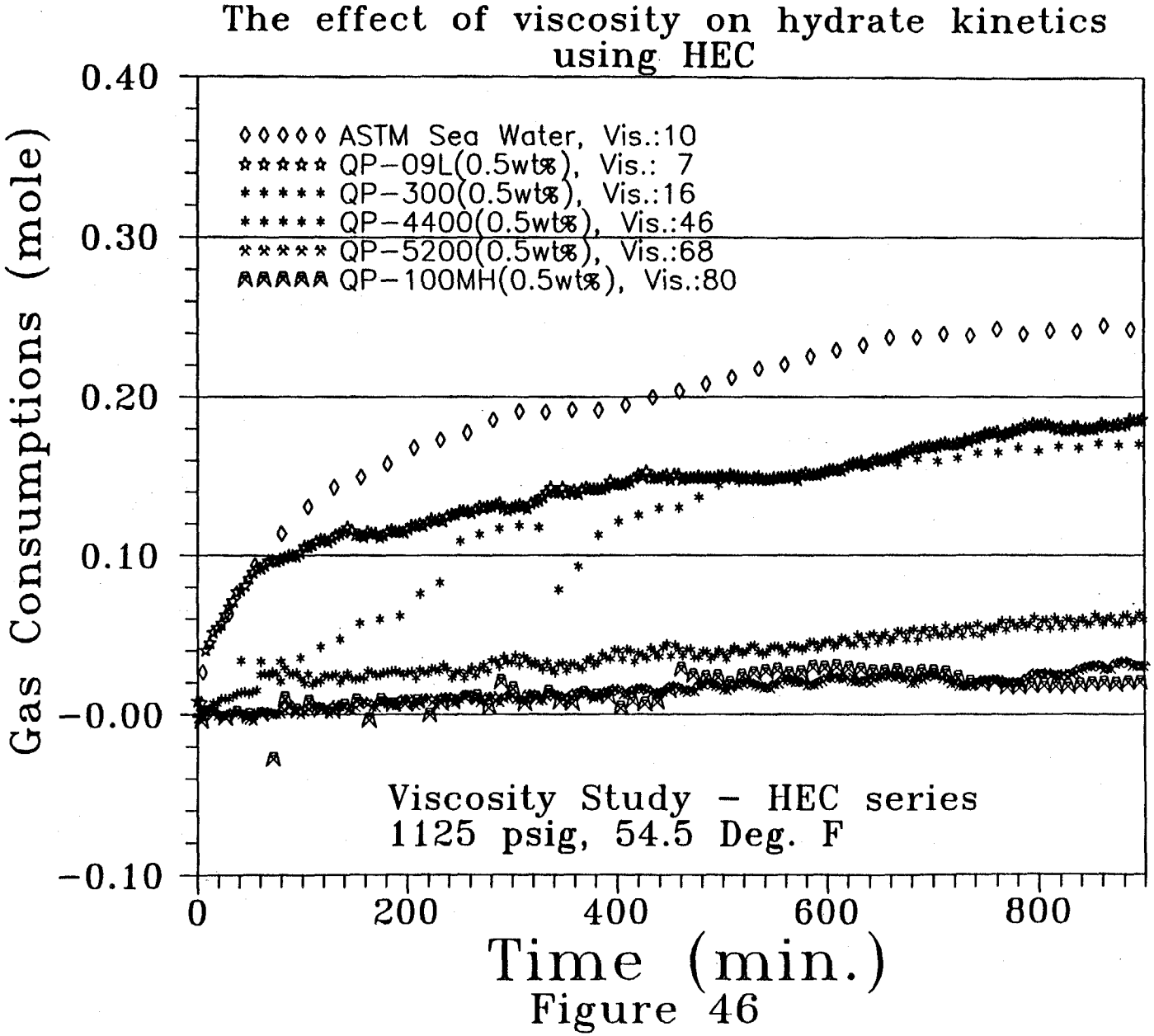
The effect of viscosity on hydrate kinetics using HEC
◊◊◊◊◊ ASTM Sea Water, Vis.:10
☆☆☆☆☆ QP-09L(0.5wt%), Vis.: 7
***** QP-300(0.5wt%), Vis.:16
***** QP-4400(0.5wt%), Vis.:46
***** QP-5200(0.5wt%), Vis.:68
AAAAA QP-100MH(0.5wt%), Vis.:80
Viscosity Study - HEC series
1125 psig, 54.5 Deg. F
Gas Consumptions (mole)
0.40
0.30
0.20
0.10
-0.00
-0.10
0
200
400
600
800
Time (min.)

Figure 46

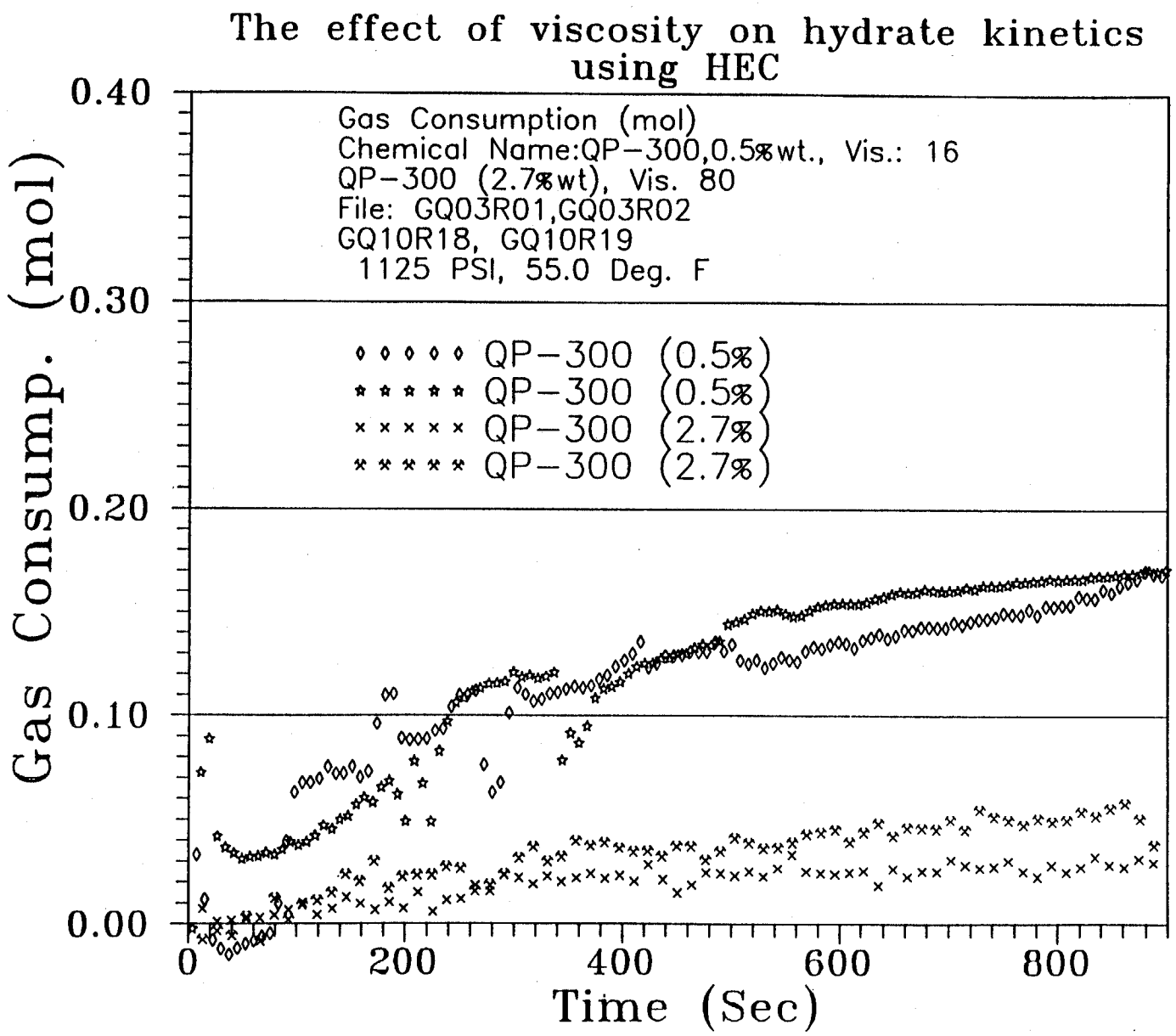
The effect of viscosity on hydrate kinetics using HEC
Gas Consumption (mol)
Chemical Name:QP-300,0.5%wt., Vis.: 16
QP-300 (2.7%wt), Vis. 80
File: GQ03R01,GQ03R02
GQ10R18, GQ10R19
1125 PSI, 55.0 Deg. F
QP-300 (0.5%)
QP-300 (0.5%)
QP-300 (2.7%)
QP-300 (2.7%)
Gas Consump. (mol)
0.40
0.30
0.20
0.10
0.00
0
200
400
600
800
Time (Sec)

Figure 47

molecular weight HEC.

Since we used the same chemical throughout the above experiments, it was possible that the chemical structure was the principal reason for kinetic inhibition. In order to test this hypothesis, we tested a different molecular structure, Polyethyleneoxide (PEO), from Union Carbide. We prepared the PEO solution at 2.0 wt% to obtain the same viscosity as that of HEC 100 MH at 0.5 wt%. Figure 48 shows similar, low gas consumptions for all high viscosity solutions, in comparison to sea water with no viscosifier.

Based on the above experiments, we concluded that solution viscosity significantly impacts hydrate growth. In fact, a viscous solution might provide a principal resistance to hydrate growth. Gas consumptions curve showed that none of the high viscosity solutions prolonged the induction time for hydrate formation.

With increased viscosity, and increase is observed in mass transfer resistance, thereby preventing the agglomeration of molecules or clusters of molecules in the bulk liquid phase. However, if nucleation is not mass transfer limited, then induction time would not be affected strongly by viscosity.

There are at least three possible mechanisms (or combinations thereof) for providing mass transfer limitations as follows:

(1) the large inhibitor molecules block smaller hydrate particles from contacting each other in the liquid phase, so that there is reduced opportunity for them to collide for combination/growth.

(2) a viscous inhibitor may "tie up" a large amount of water molecules, for example via hydration of water around the polymer molecule. At the temperature and pressure tested, it might be difficult to strip the water molecules from the polymer, in order to form hydrates.

(3) Very small gas diffusion coefficients provided by high viscosity solutions might also slow the growth process.

Unfortunately, high viscosity solutions are difficult to handle in the field. In order to use such solutions as kinetic inhibitors, the solution viscosity must be reduced to enable easier handling. One possible way to solve this problem is to employ a non-Newtonian fluid which has a lower viscosity at lower shear rates. During the initial storage period of low shear, the solution would have a relative low viscosity, but it would have a high viscosity in the pipeline when the shear rate was high.

In summary, chemical inhibitors which were able to prevent

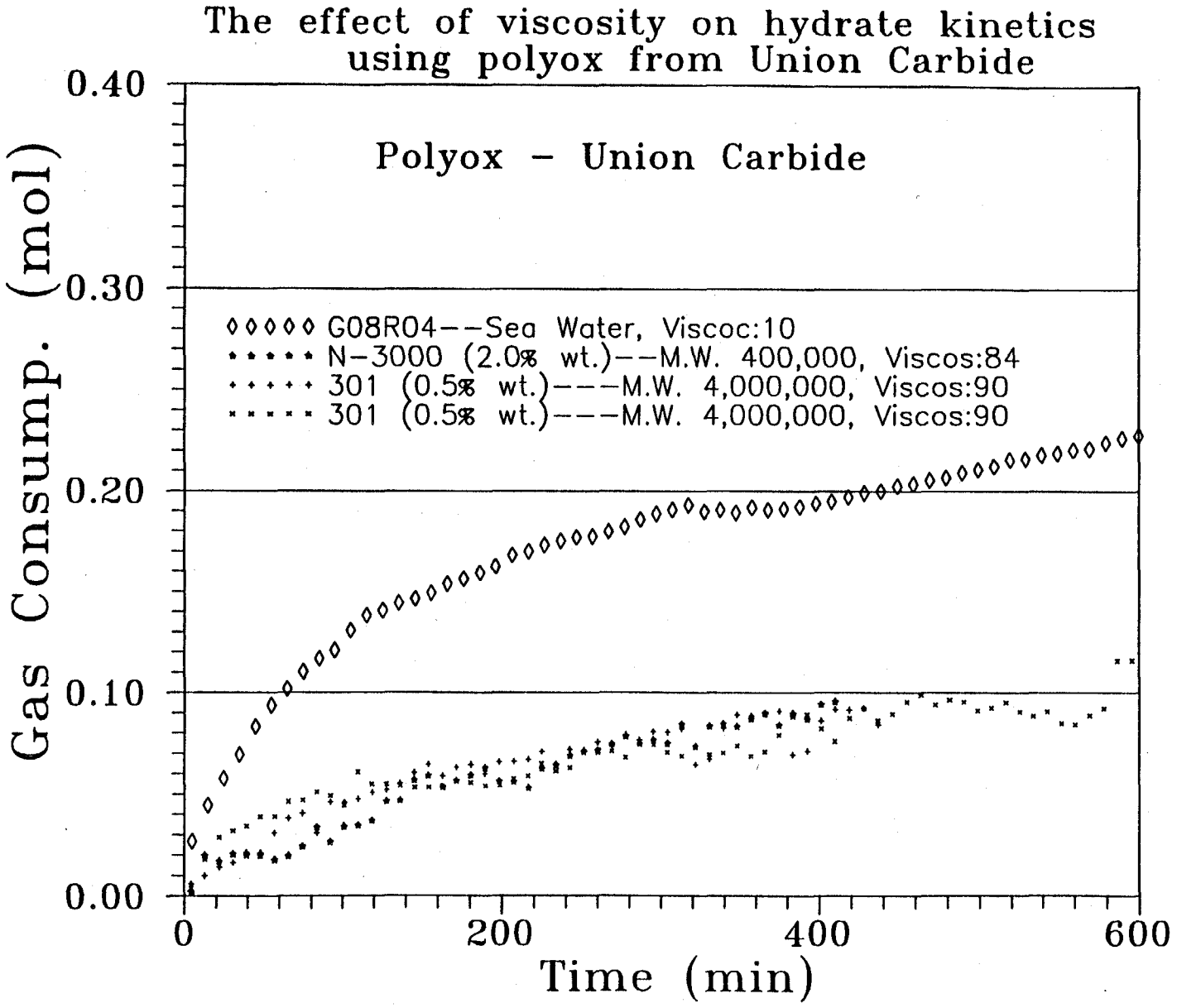
The effect of viscosity on hydrate kinetics
using polyox from Union Carbide
Polyox - Union Carbide
◊◊◊◊◊ G08R04--Sea Water, Viscoc:10
* * * * * N-3000 (2.0% wt.)--M.W. 400,000, Viscos:84
+ + + + + 301 (0.5% wt.)---M.W. 4,000,000, Viscos:90
- - - - - 301 (0.5% wt.)---M.W. 4,000,000, Viscos:90
Gas Consump. (mol)
0.40
0.30
0.20
0.10
0.00
0
200
400
600
Time (min)

Figure 48

hydrate growth were high molecular weight, long chain organic polymers. Specific chemical structures were not important, provided they were highly soluble in water and able to increase the solution viscosity. This observation may also imply that a strong association exists between water and polymer molecules.

IV.B.2.f. Inhibition of Both sI and sII Hydrates with PVP

While sI hydrates may not be commonly found in the pipeline, it would be very interesting to examine effects of inhibitors on the formation of two different crystal structures. Structure I (sI) hydrate growth is believed to occur through the sharing of vertices, while structure II (sII) hydrate growth is believed to result from face-sharing of the 5^{12} cavity. If the kinetic inhibitor was able to block the specific sites (such as vertices or faces) for hydrate growth, the performance of kinetic inhibitor with different system might be different. The experiments below were done to probe our hypothesis.

The 1992 Annual Report summarized evidence that PVP provided good kinetic inhibition of sII at 1150 psig and 54.5°F. In the work during 1993, we used ethane as our model gas to study sI hydrate formation and inhibition with PVP.

The data in Figures 49, 50, and 51 indicate that PVP solution did provide good kinetic inhibition for sI hydrates by prolonging the induction time; however PVP did not reduce the total gas consumption significantly. The length of the induction time was a strong function of temperature (subcooling), and pressure (over-pressurization). In contrast both induction time and growth were inhibited for structure II hydrates.

IV.B.2.g. Effect of Mixing & Materials in High Pressure Cell

In our high pressure apparatus and in our screening apparatus we had previously found that foreign surfaces (e.g. metal balls etc.) played a very important part in hydrate formation (see pp. 16-17 of the 1992 Annual Report.) In this portion of the work we used stainless steel powder to study whether an active, high area metal surface would promote hydrate formation.

We used a stainless steel powder (316L, 140 mesh) provided by Dr. John Cayias of Oryx Energy. Initially we tested different amounts of the powder in the THF screening apparatus. To our surprise, the stainless steel powder slowed down the THF hydrate formation process, providing a much longer induction time than observed with the stainless ball. When a small amount of stainless powder was used, the THF solution did not form hydrates at all, even though the surface area of metal powder was several orders of magnitude higher than that of the ball.

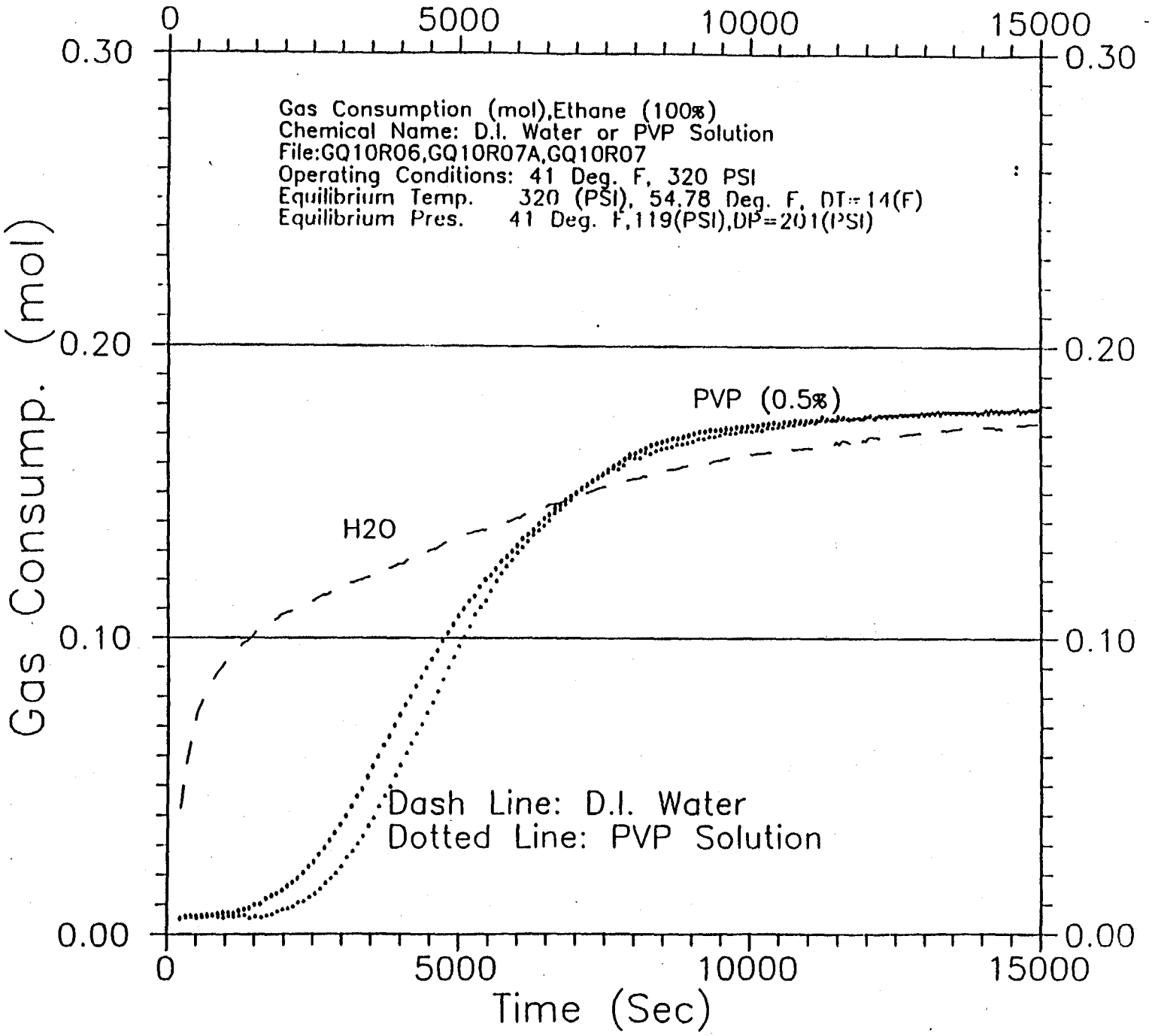

Figure 49. Kinetics of ethane hydrate formation.

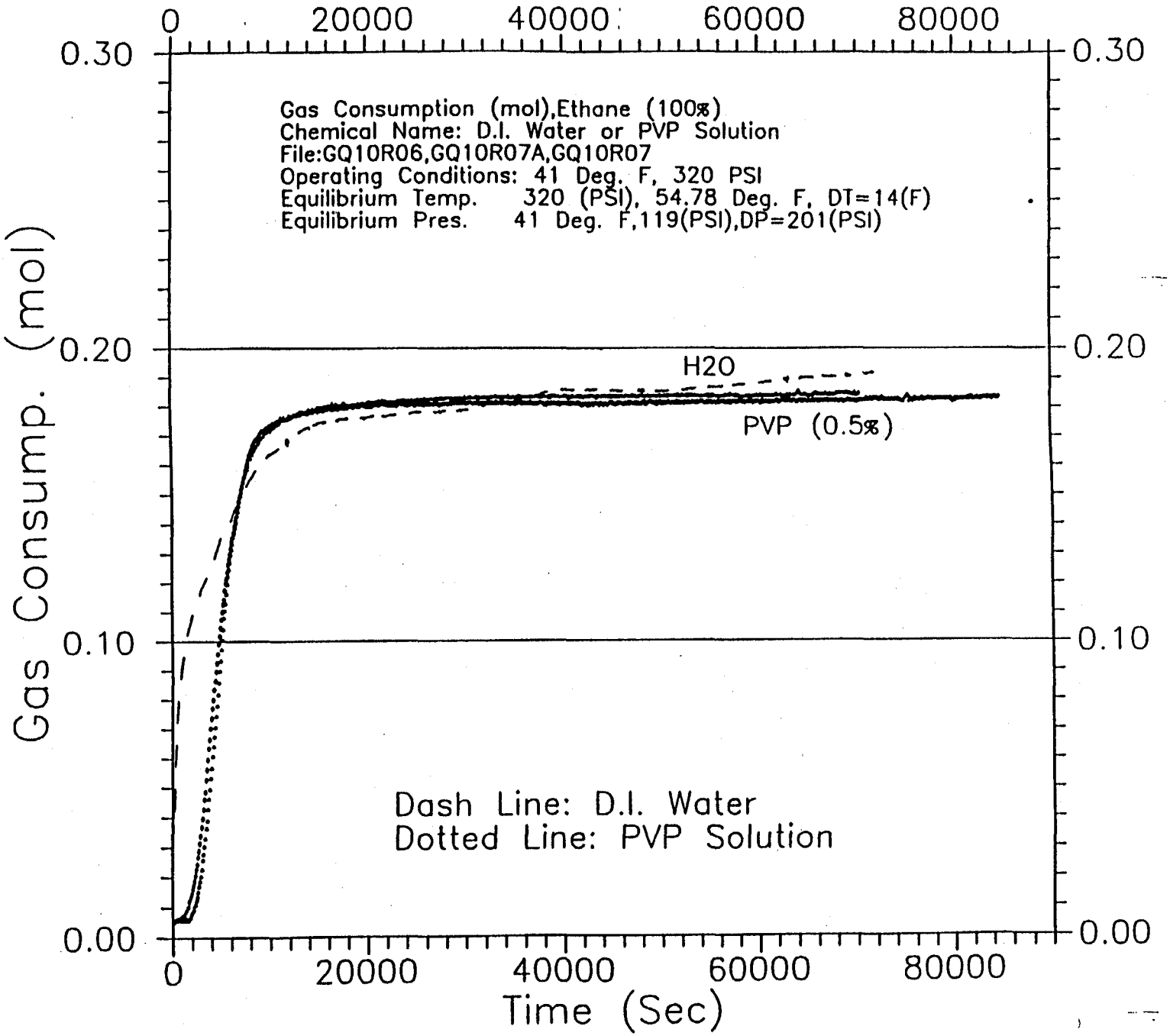

Figure 50. Kinetics of ethane hydrate formation.

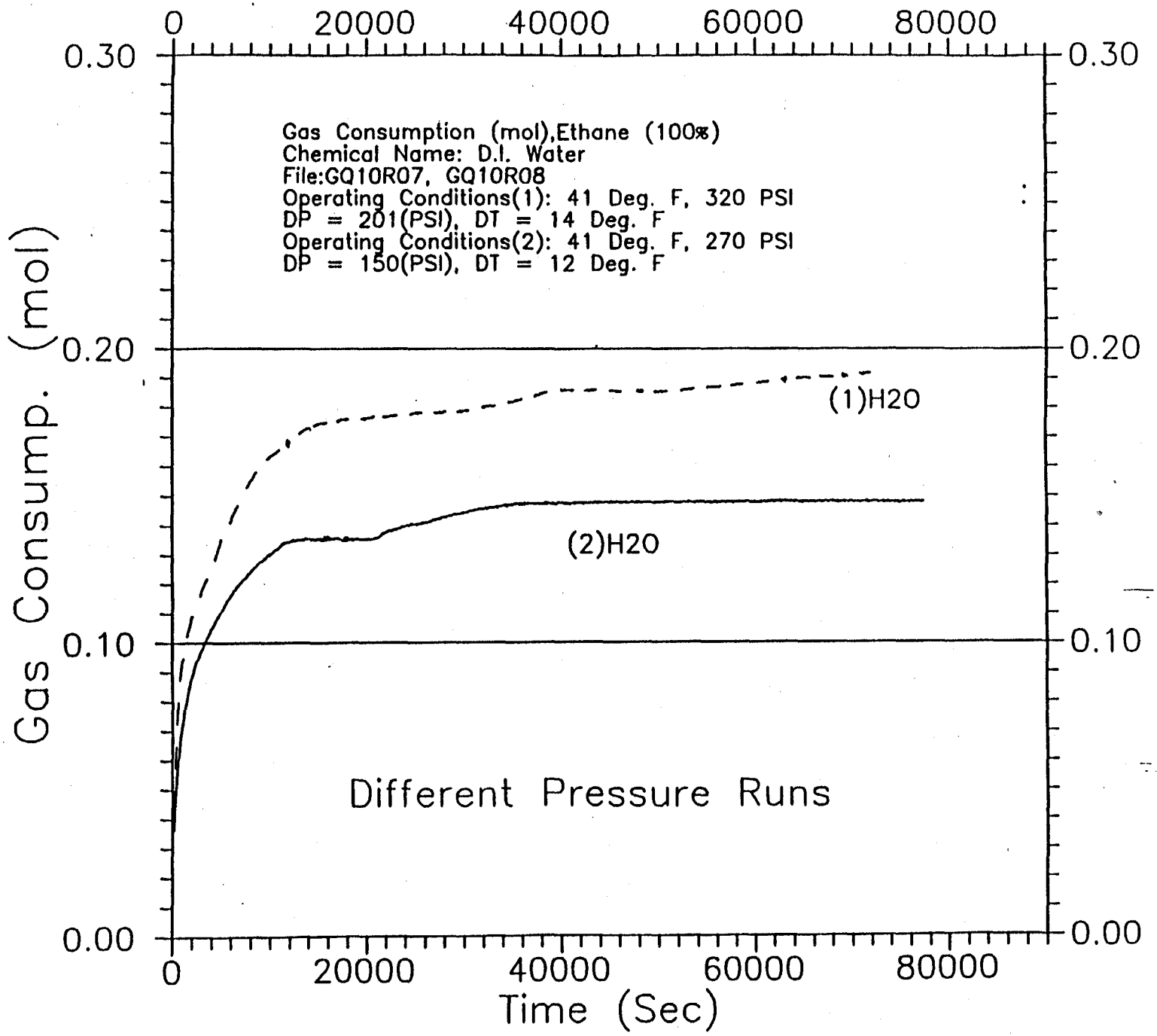

Figure 51. Kinetics of ethane hydrate formation.

In high pressure apparatus, three different cases were examined, (1)69, 316SS metal balls, (2) 4 grams of 140 mesh stainless steel powder, and (3) no stainless material. The gas consumption and pressure drop curves were almost identical as shown in Figures 52 and 53.

The results of this study suggested that mixing rate, rather than the metal surface was the important factor in hydrates initiation. The heavy metal ball provided better mixing in the Multiple Reactor Apparatus, which induced hydrate formation. In our pressure apparatus, the mixing at 1000 rpm was so strong that small amounts of additional materials (such as metal balls or metal powder) did not make much difference.

Hydrate formation process may be a flow induced nucleation phenomena caused by rapid mixing. Vigorous mixing renews the gas-water interface very rapidly, perhaps providing a surface renewal at the same time as interring the older surface in the bulk solution.

IV.B.2.h. Inhibition of Systems Containing Liquid Condensate

In most industrial applications of hydrate inhibitors a condensate phase will be present. In order to test the applicability of the kinetic inhibitors in these situations two of the best kinetic inhibitors to date were tested in the presence of n-decane. For simplicity, n-decane was chosen as a model hydrocarbon condensate for this work. As a continuation of the work started in 1992 in which the effect of n-decane on the kinetics of hydrate formation from sea water was investigated, in 1993 we extended this work to include the effectiveness of both VC-713 and PVP in the presence of n-decane. All inhibitor solutions were 0.5wt% inhibitor in synthetic sea water and were prepared as described in Section IV.B.2.a.2. In all tests 30g of n-decane were used with 120g of aqueous inhibitor solution.

The n-decane was purchased from Aldrich Chemical Co. and used without further refinement at a specified purity of 99.0^{+}%. As with the other constant pressure experiments the simulated Green Canyon gas was used. However, the actual gas phase composition in the cell differed slightly from that of Green Canyon gas due to the solubility of the gas in the n-decane. The gas phase compositions were predicted for each of the three operating conditions using the Peng-Robinson equation of state as shown in Table 9. For the equilibrium flash prediction, the gas volume was estimated as 400ml and the n-decane volume was taken as 21.9ml; the solubility of both hydrocarbon phases in the aqueous phase was ignored.

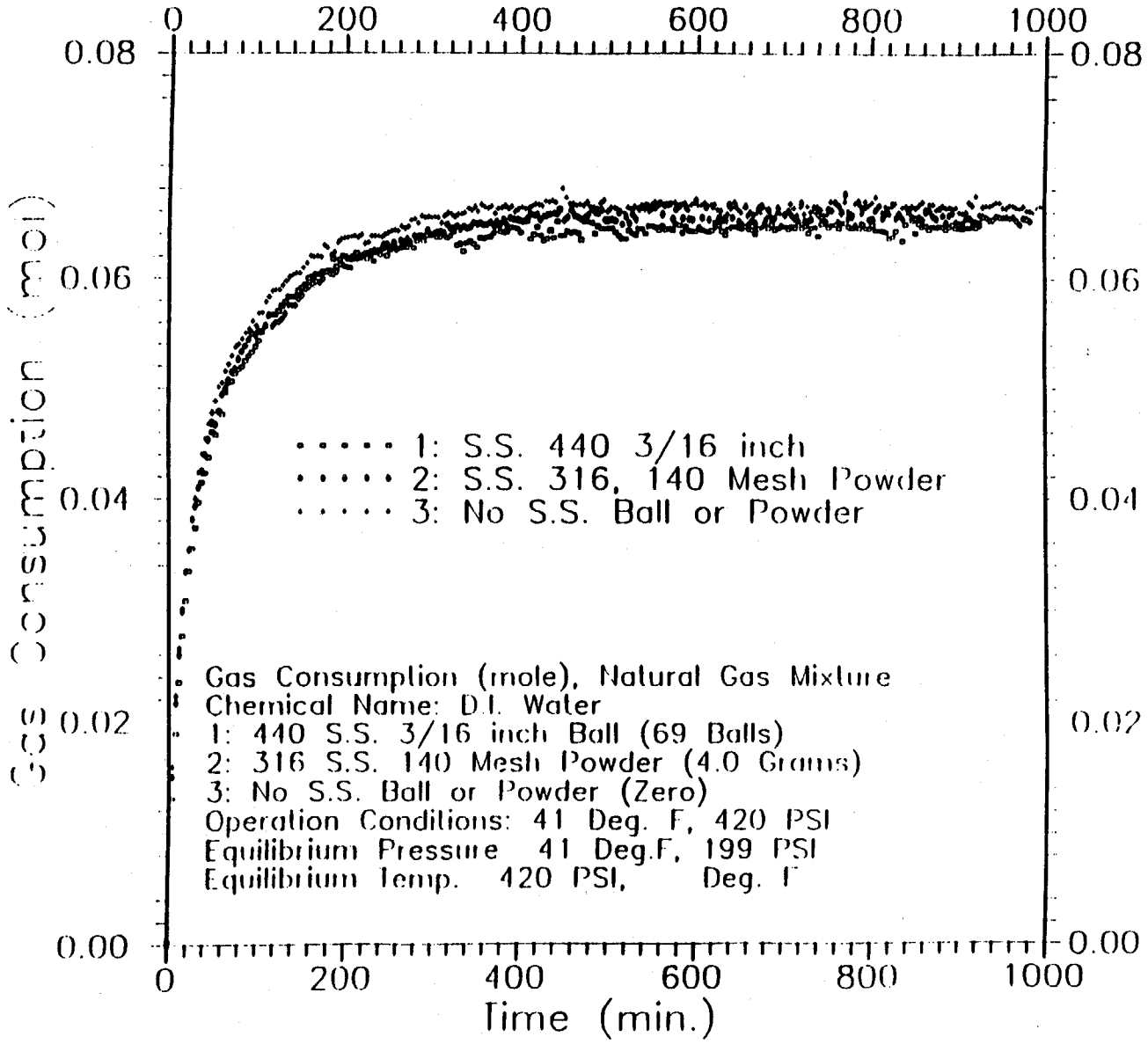

Figure 52. The effect of stainless steel balls and stainless steel powder on hydrate kinetics

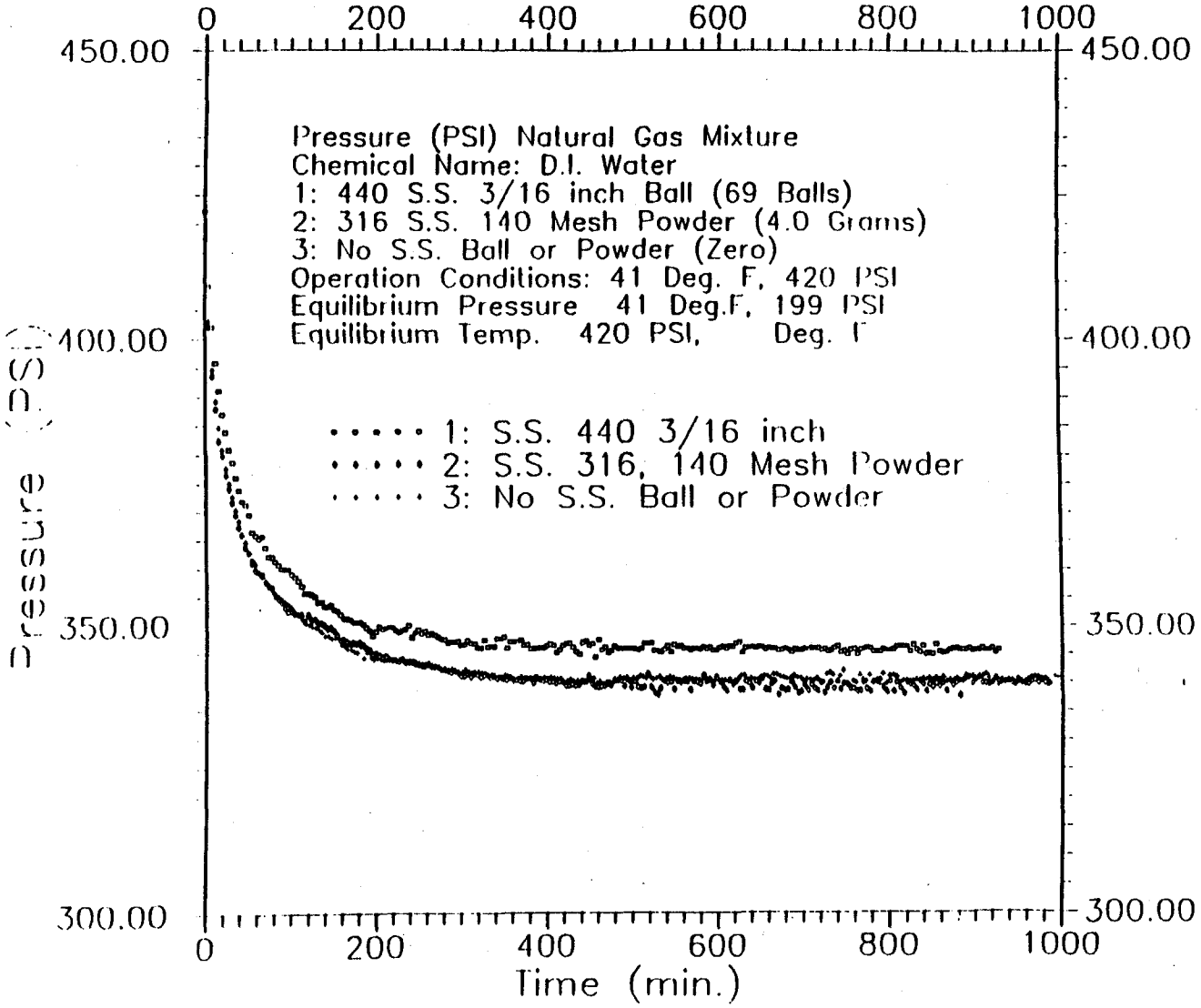

Figure 53. The effect of stainless steel balls and stainless steel powder on hydrate kinetics

Table 9. Gas phase composition (mol fraction) for the three operating conditions.

Component	Green Canyon Composition	700psi 40°F	900psi 40°F	2000psi 54.5°F
Case		A	B	C
Methane	87.2	92.98	92.80	91.51
Ethane	7.6	5.13	5.19	5.54
Propane	3.1	1.07	1.14	1.57
i-Butane	0.8	0.141	0.17	0.31
n-Butane	0.4	0.059	0.06	0.13
Pentane	0.4	0.03	0.03	0.09
Nitrogen	0.5	0.589	0.6	0.63
n-Decane	0	0.001	0.01	0.22

In Figure 54, the predicted L_w-H-V phase equilibria is shown for each of the four gas compositions in Table 9. As can be seen from this figure, the presence of n-decane shifts the hydrate equilibrium line to the left requiring a higher pressure (or lower temperature) to enter the hydrate stability zone.

The results for PVP and VC-713 are presented in Figures 55, 56, and 57. In each of the figures a jump in the gas consumption can be observed at time zero, followed by a leveling off for the inhibited n-decane runs; this initial jump in the gas consumption corresponds to the start of stirring in the cell. On starting cell agitation gas consumption increases due to the fact that n-decane quickly becomes saturated with gas. The predicted equilibrium saturation of the gas in the n-decane is shown as a solid horizontal line in each of the figures.

For the PVP experiments two operating conditions were investigated. In Figure 55 the results for the 900 psig and 40°F operating condition are presented. The addition of 0.5wt% PVP to the n-decane+sea water system results in an increase of approximately 50 minutes in the induction time over that observed for the n-decane+sea water system. The effect of PVP with and without n-decane present is shown in Figure 56 for the operating condition of 2000 psig and 54.5°F. This figure shows that the induction times for both systems are approximately the same.

For the VC-713 experiments, only one operating condition was investigated, namely 700 psig and 40°F. Figure 57 presents the VC-713 results. The addition of VC-713 to the n-decane+sea water

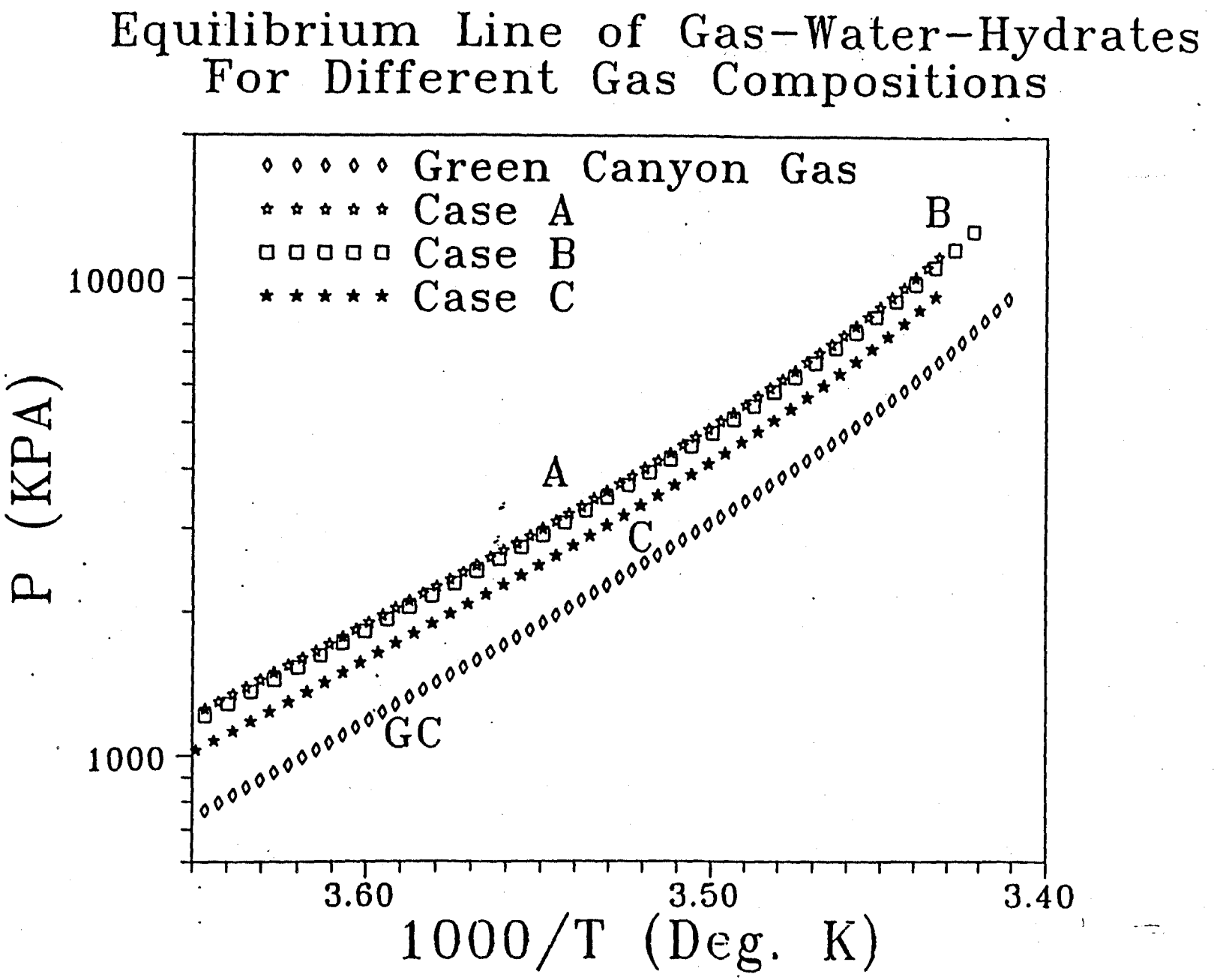

Figure 54. Predicted sensitivity of hydrate equilibrium to gas composition.

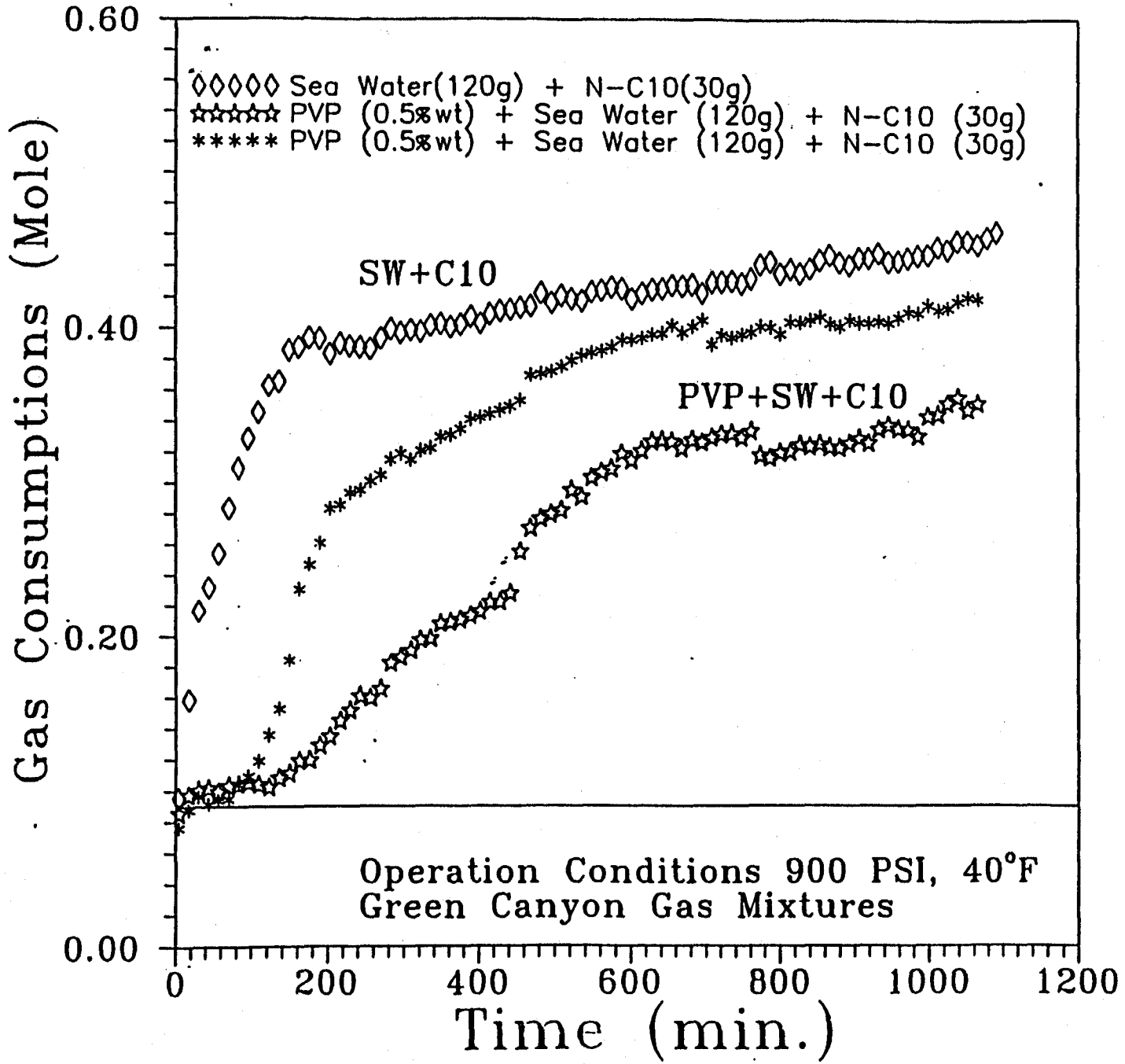

Figure 55. PVP performance in the presence of n-decane.

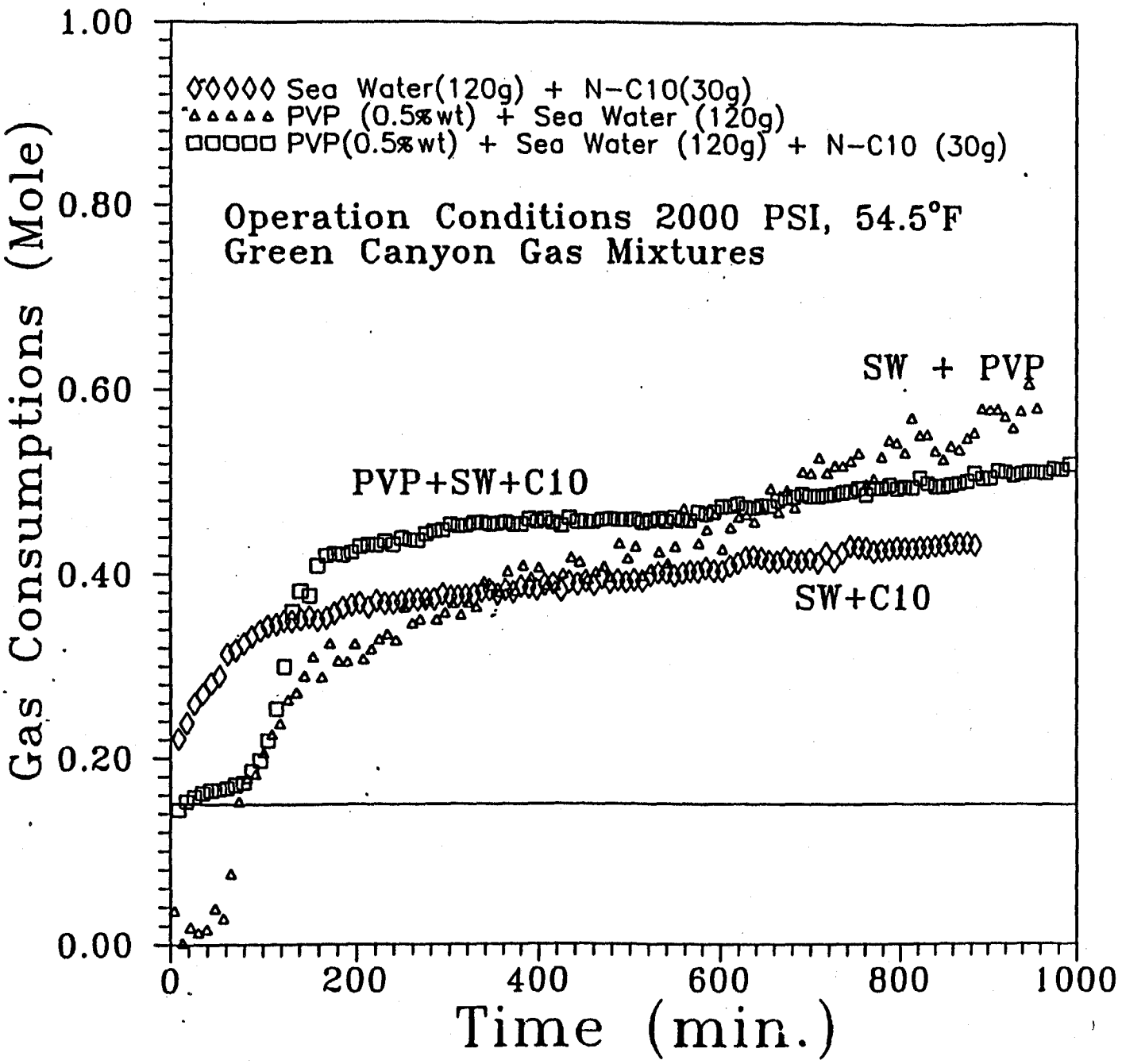

Figure 56. PVP performance in the presence of n-decane.

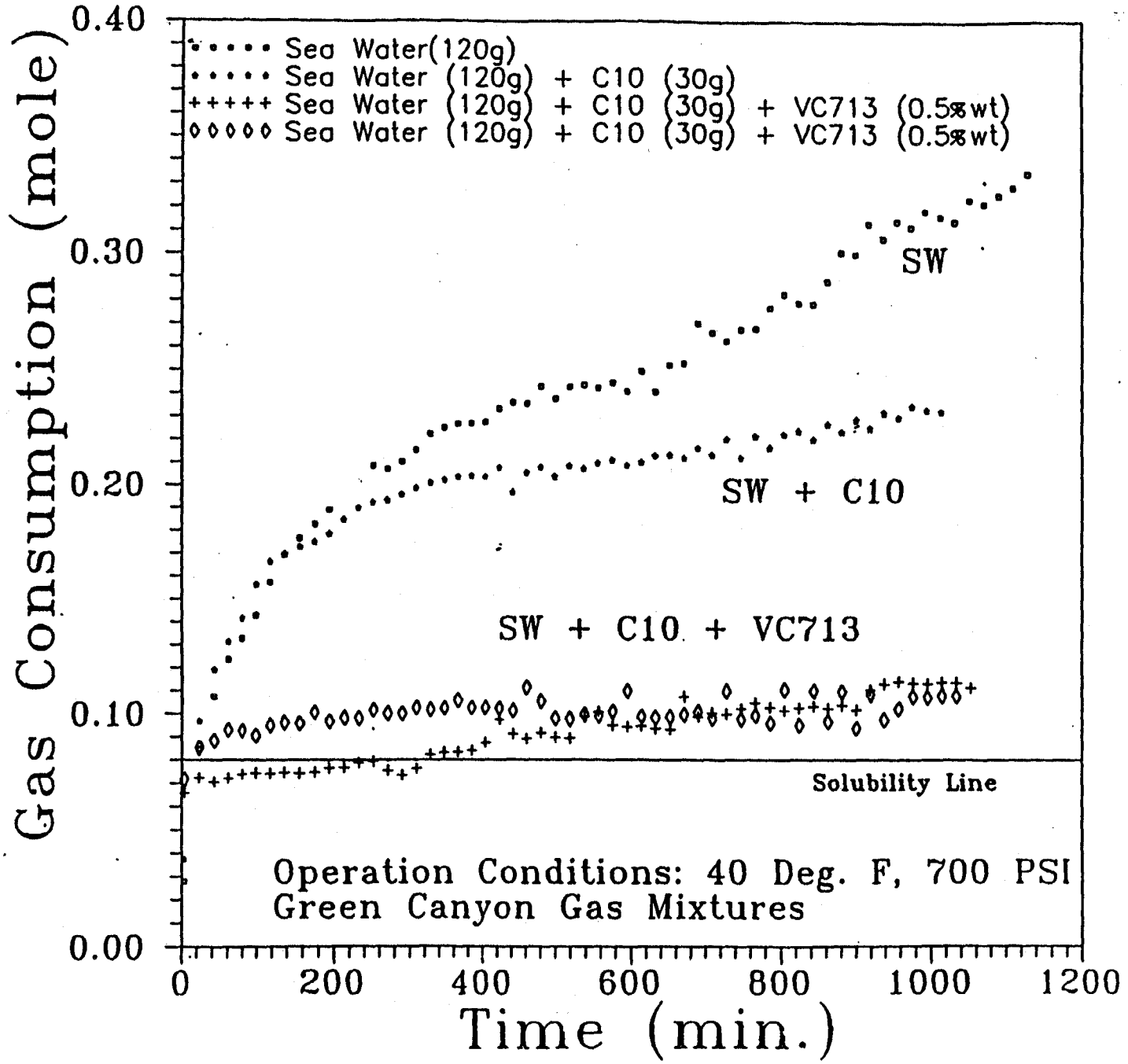

Figure 57. VC-713 performance in the presence of n-decane.

system results in a very low (< 0.12gmol) gas consumption. This may be a very promising area for future experiments, at the discretion of the consortium.

IV.B.2.i. Inhibition of Hydrates in Drilling Muds

The purpose of this work was to investigate whether the kinetic inhibitor VC-713 also works in drilling muds. Two different drilling muds were studied in this work. For both muds it was found that severe operating conditions were required to form hydrates even without the use of an inhibitor. Operating conditions for drilling mud runs was 3000 psig and 40°F.

One of the drilling muds tested was furnished by Oryx Energy (referred to as MC401) and the other mud was that developed during the previous DEA project (DEA-30; 1987-1990) - referred to as the Base mud. Compositions of muds are presented in Table 10.

Table 10. Composition (wt%) of Two Drilling Muds Tested.

Component	Base Mud	MC401 Mud
Water	53.58	29.75
Barite	31.53	43.65
NaCl	12.59	21.16
Bentonite	2.10	0
PHPA	0.1	0
XCD	0.1	0
Blacknight	0	1.59
Starch	0	1.57
Gel	0	0.79
CMS	0	0.79
ECD	0	0.17
CMC	0	0.09

It was difficult to dissolve the VC-713 into the drilling muds and thus there is some ambiguity concerning the actual amount of the inhibitor present. The amount of VC-713 added was based on the weight fraction of water in the mud; for all inhibited runs 0.5wt% VC-713 was used. The experimental run procedure was the same as that discussed previously, but 120 grams of mud were loaded into the cell.

For each mud two base runs were made with no inhibitor before making two runs with 0.5wt% VC-713. All results were scaled to reflect 120 grams of water present. Results for the

Base mud are presented in Figure 58 which shows that effectively no hydrates were formed for either the inhibited or uninhibited systems. The addition of VC-713 to the base mud resulted in approximately a 1.5-fold increase in the viscosity of the mud.

In contrast to the Base mud, the MC401 mud did form hydrates as shown in Figure 59. This figure shows that the addition of VC-713 to the MC401 mud results in no hydrate formation. There was little change in the viscosity observed when VC-713 was added to the MC401 mud.

The above experiments of mud inhibition are promising, but preliminary. A Consortium discussion will determine the future studies of the mud branch of hydrate inhibition.

IV.B.3. New Sapphire Cell for Observation of Hydrate Formation

Since the beginning of gas hydrate research, there has been a controversy concerning whether gas hydrates initiate on the gas-water interface, in the bulk liquid water, or at some other interface such as the container wall. A high pressure visual sapphire apparatus equipped with a stereo microscope and a video recorder was designed to investigate this problem. Following is a brief description of the experimental apparatus and the results obtained from its operation in the last quarter of 1993.

The objective of this study was three-fold; (1) to visually identify where hydrate nucleation and growth occurs; (2) to examine the morphology of gas hydrates; (3) to study macroscopic features of the inhibition mechanism for the most promising kinetic inhibitors by visual observation.

IV.B.3.a. Apparatus Design and Operating Procedure

A diagram of the new apparatus is shown in Figure 60. The apparatus consists of a 1/4 inch I.D. sapphire tube that is 1 inch long and is supported by a brass housing with windows for viewing the cell contents. The maximum designed operating pressure is 10,000 psig.

Temperature control of the cell was accomplished by immersing the cell in a small Lexan bath which is connected to a NESLAB cooler. A magnetic coil located outside the cell and magnetic stirrer located inside the cell are used to agitate the contents of the cell. The magnetic stirrer oscillates axially as the power to the coil is activated/deactivated.

Measurement of the cell pressure can be made either visually via a Heise gauge or a Heise pressure transducer. Both the pressure transducer and the bath temperature thermistor are connected to a Keithley data acquisition system which

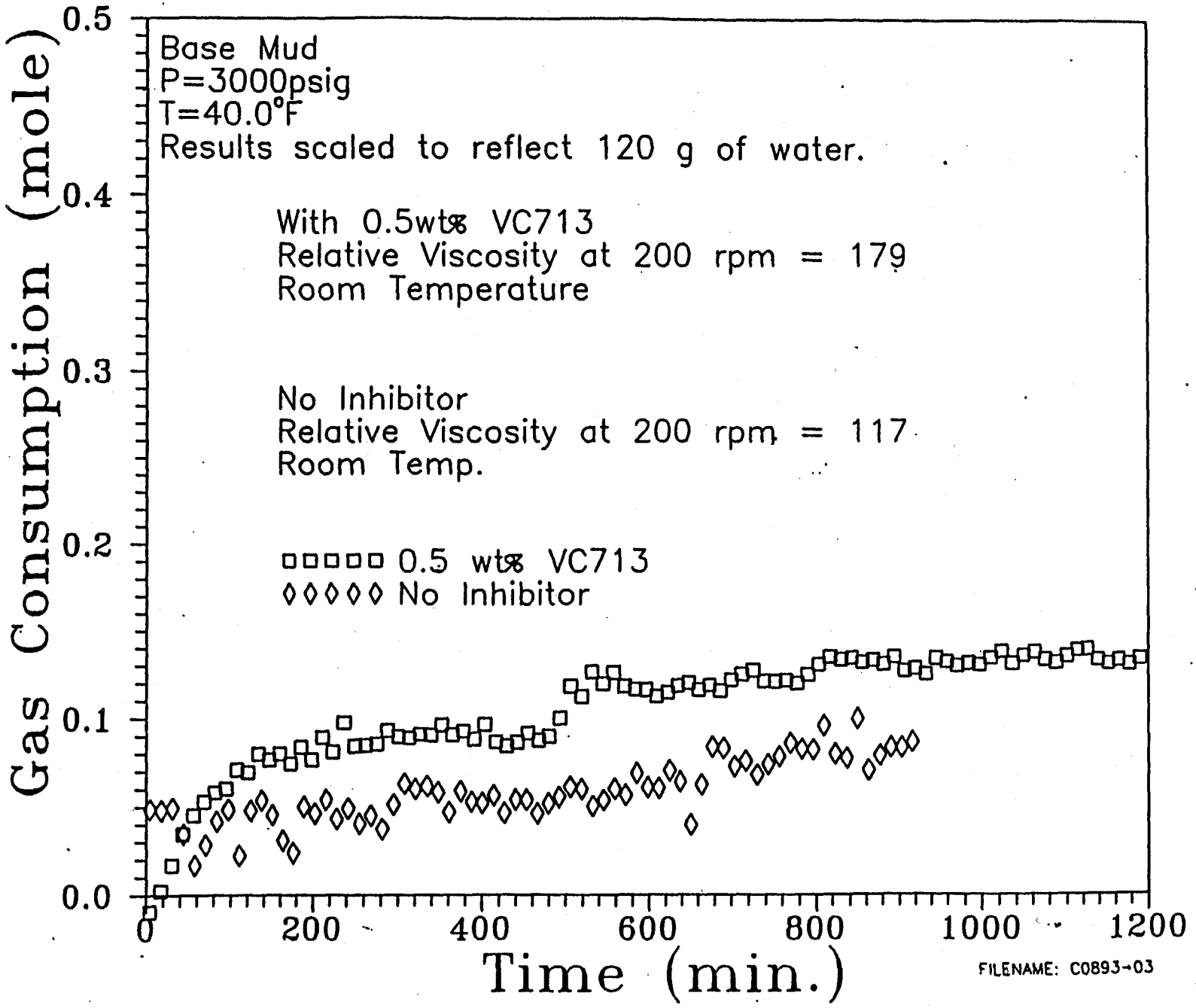

Figure 58. VC-713 performance in base drilling mud.

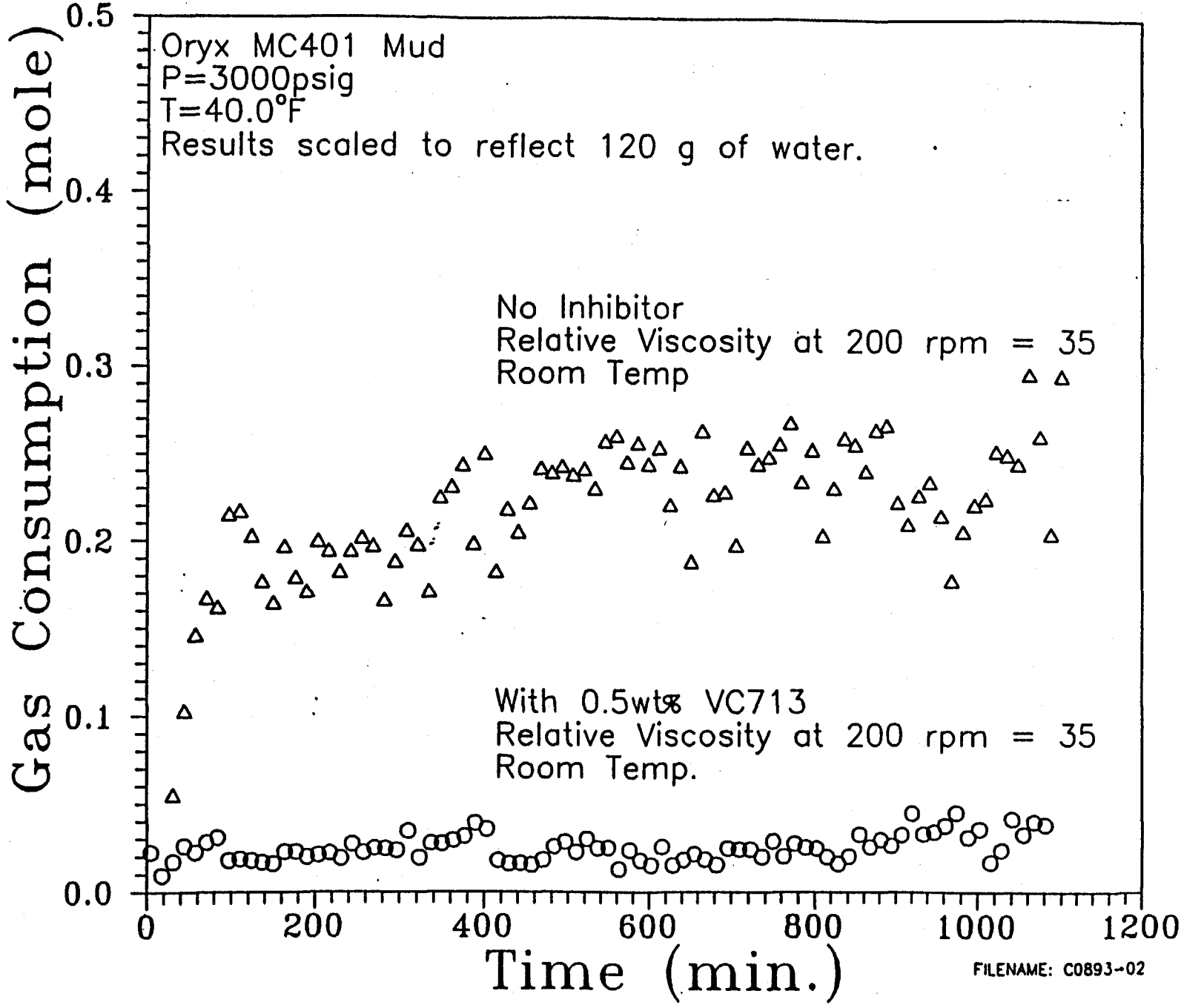

Figure 59. VC-713 performance in Oryx MC401 drilling mud.

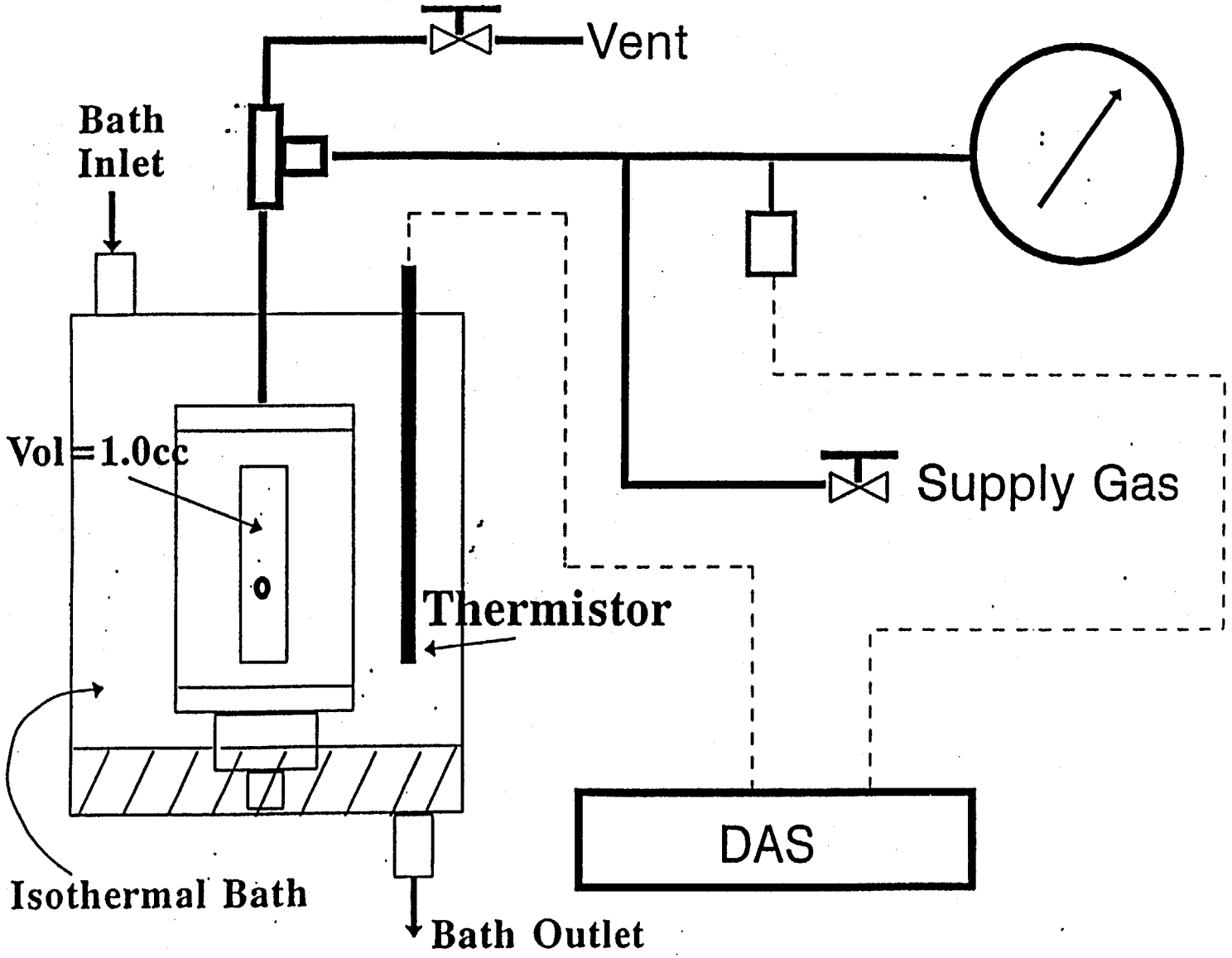

Figure 60. Schematic of the sapphire cell apparatus.

continuously monitors the progress of the experiment.

The experimental procedure was as follows:

(1) The reactor was thoroughly cleaned with deionized water and dried with high pressure air.
(2) 0.5ml solution was added to the reactor via a 3cc syringe.
(3) The system was sealed and brought to the operating pressure with the experimental gas at the room temperature.
(4) The system was equilibrated for 1 approximately hour, allowing natural gas compounds to dissolve into the water, perhaps in order to promote water cluster formation in the bulk water. This process was necessary to obtain good reproducibility in the subsequent experiments.
(5) The reactor was then vented and recharged with gas to the operating pressure. This process required less than 1 minute, and ensured that air is exolved from the water.
(6) The cooling water valve was opened to start the experimental run, with the simultaneous initiation of data acquisition.
(7) Observations were made with both microscope and video recorder.
(8) All experiments were done at 4.0°C and 1000 psig, except where noted.

The time between the beginning of the cooling water flow and the time of the visual appearance of the first hydrate crystal was regarded as the induction time. After induction time, the hydrate formation process entered the second stage, that of crystal growth.

IV.B.3.b. Visual Observations in the Sapphire Cell

Fascinating observations were recorded with the new system which answers many of our previous questions about the nature of hydrate formation. With the new system visual observations were made on the site and morphology of hydrate formation for the following cases:

1. Natural Gas and Deionized Water
2. Natural Gas and Sodium Dodecyl Sulfate Solution
3. Natural Gas and Sea Water
4. Natural Gas, Amorphous Silica, and Deionized Water
5. Natural Gas, n-Decane, and Deionized Water
6. Natural Gas, 0.5 wt% VC-713, and Seawater
7. Natural Gas, 0.5 wt% VC-713, and Seawater
8. Carbon Dioxide in Deionized Water and in Seawater

Hydrate appearance is described in the following sections for each of the above eight systems, in subsections with corresponding numbers. A video tape, provided with this report, also documents some of these interesting effects. In subsequent portions of this section, segments of the single video tape are referenced; the video tape has a table of contents inscribed to direct the viewer to the appropriate section of the tape.

IV.B.3.b.1. Natural Gas and Deionized Water

Six runs were made with this system at 4.0°C and 1000 psig. As shown in Figure 54 the hydrate equilibrium pressure is 130 psig for this gas at 4°C. Usually (in 5 of 6 experiments) hydrate growth initiated from the gas-water interface as shown in the first segment of the video tape, provided with this report.

The first hydrate crystal grew rapidly above the gas-water interface, to give a balloon-like shape. In another case hydrate growth initiated at the gas+water+wall surface, as illustrated in the first segment of the video tape. After first hydrate crystal formed on the interface, the hydrate propagated across the whole surface within 10 seconds, as indicated in the first segment of the video tape. The hydrate growth process in this period seemed to be reaction rate controlled, since there were no mass or energy transfer barriers in the system. While a very small amount of hydrate formed in the surface region (pressure drops less than 1.0 psig), it appeared that the hydrate formed a completely solid barrier at the surface. At that point, transport of gas through the hydrate film (and the hydrate growth process) essentially stopped.

After surface growth, a small amount of water came from below the gas+water+hydrate interface along the wall of the reactor into the gas phase. Hydrates crystals then formed around wall of the sapphire cell as shown in the first segment of the video tape. In the bulk water phase only a very small amount of needle hydrates grew from the bulk water, due to dissolved gas in the water as shown in the first segment of the video tape. The major portion of the liquid water remained clear, indicating no crystals were in the solution.

It is worth noting that a very small amount of hydrate formed initially, with no further hydrate growth for 24 hours. The cause of extremely slow growth was the impermeable solid hydrate film, which acted like a physical barrier preventing gas+water contact. The diffusion of gas or water molecules through the solid film was extremely small (less than 10^{-9} cm/min), which made the hydrate growth essentially zero. The bulk liquid water remained effectively clear during the experiments.

IV.B.3.b.2. Natural Gas and (SDS)

As we know from catalytic reaction engineering, a reaction requires more severe conditions (high temperatures and high pressures) to proceed if the catalyst surface has been deactivated by coking or poisoning. By analogy in the hydrate formation process, if we could deactivate or block active sites for hydrate nucleation at the gas+water interface, further hydrate nucleation and growth would require much lower

temperatures or higher pressures.

Sodium Dodecyl Sulfate (SDS) was employed as a surface active agent in this study to block the gas+water interface, since its properties as a surface active agent are well documented in the literature. SDS with a purity of 98% was purchased from Aldrich Chemical Company, Inc. The critical micelle concentration of SDS in pure water at 25°C and 1 atmosphere is 0.234 g/100ml (R.J. Williams, J.N. Philips, K.J. Mysels, Trans. Faraday Soc. 51, 728, 1955). Typical properties of SDS versus concentration are shown in Figure 61 (from Adamson Physical Chemistry of Surfaces, 5th edition, Page 509, Harper-Row, New York, 1989).

The SDS concentration used was 0.001g in either 0.4 or 0.5 ml deionized water, corresponding to 0.25g/100ml and 0.20g/100ml, which spans the critical micelle concentration (CMC) of SDS at room temperature and 1 atmosphere. There were no corresponding experimental data for the CMC of SDS at the temperature and pressure of hydrate formation.

However, the surface coverage is far beyond a monolayer due to the high concentration of SDS in solution. If we assume the cross-sectional area of SDS to be 20Å^2 and all of the SDS molecules to be at the interface, the monolayer coverage would only require 1.6E+14 SDS molecules for a 1/4" inner diameter sapphire cell. This is equivalent to 7.5E-08g, an amount too small to be measured by an ordinary balance. The amount we used was 12,000 times greater than that required for monolayer coverage. The density of SDS on the interface would be equivalent to a condensed liquid, as shown in Figure 62.

A total of six experiments were done using SDS with deionized water, which deactivated the gas-interface in the experiments. Gas hydrate nucleation initiated at three places: (1) the gas+water+bottom metal surface (Type A), (2) the gas+water+sapphire wall surface (Type B), and (3) in water immediately below gas+water+SDS interface (Type C). Each of these phenomena are discussed in the following sections.

(1) Type A: Hydrate Nucleation at the Gas+Water+Metal-bottom Surface.

There were two experiments in which hydrate nucleation began at the gas+water+metal-bottom surface at the lower end of the reactor. In both experiments, the gas appeared to be concentrated as bubbles at the bottom brass reactor end plate.

In the first experiment hydrates did not form within 15 hours at 4.0°C and 1000 psig. Thus, in order to achieve hydrate formation, we lowered the temperature to 0.5°C, while keeping the pressure constant. The quenching process from 4.0°C to 0.5°C took less than 5 minutes. Because the microscope was focused at

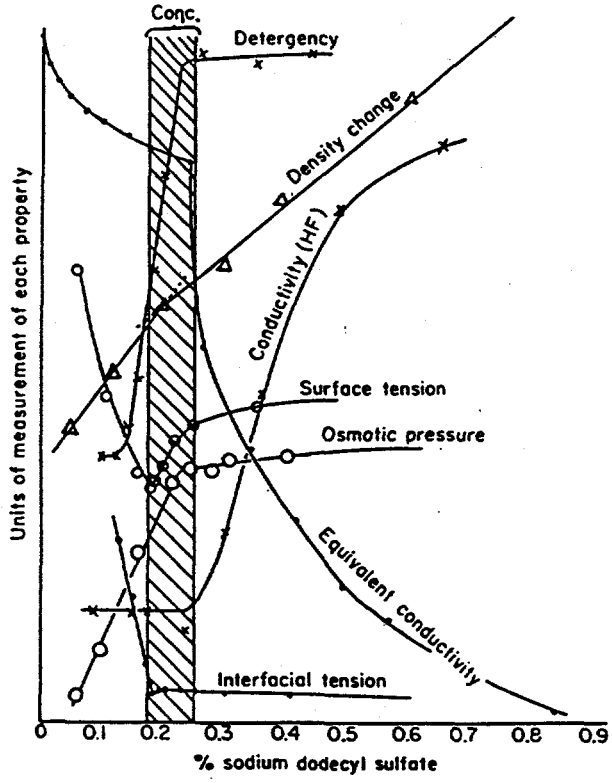

Figure 61. Properties of colloidal electrolyte solutions - sodium dodecyl sulfate. (From Ref. 56.)

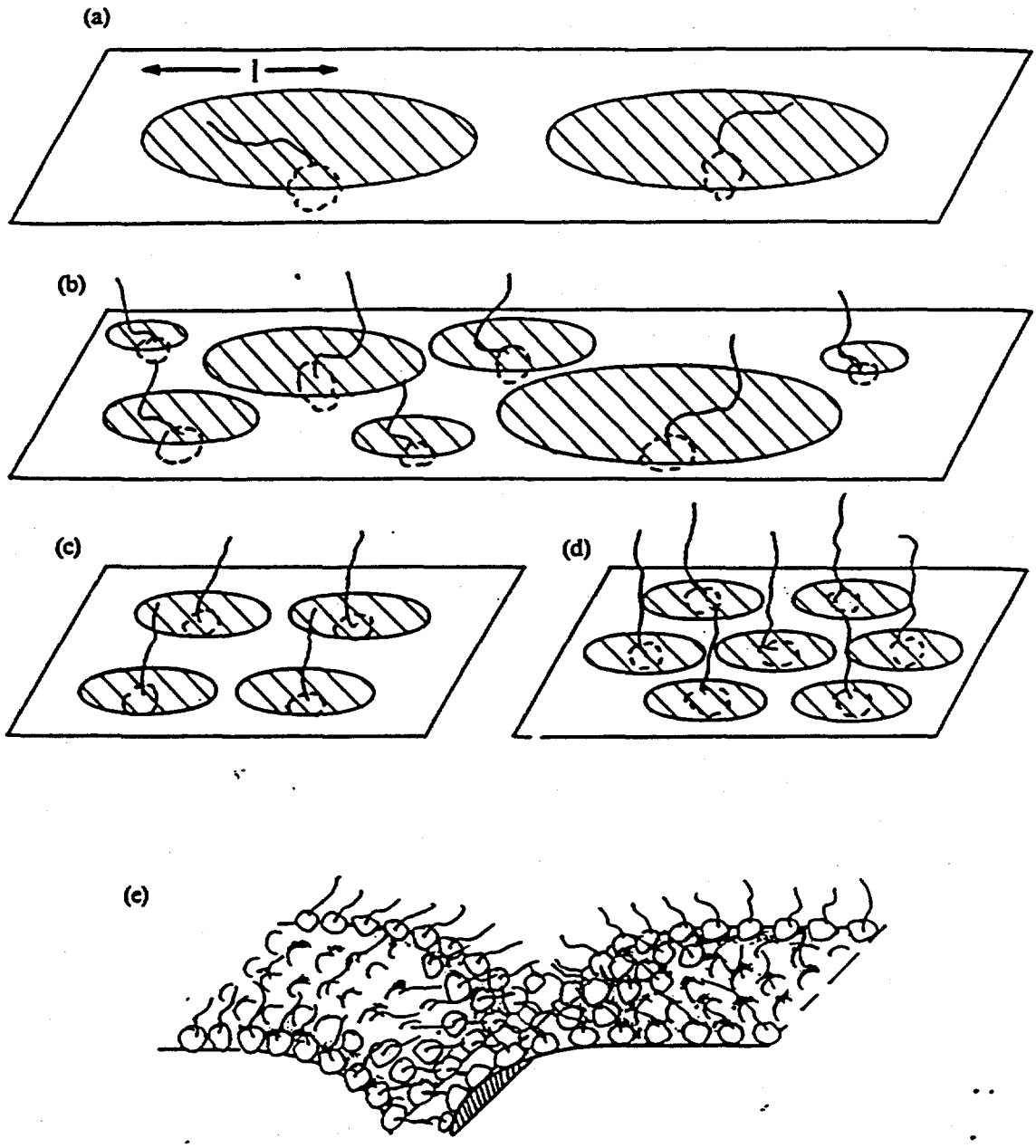

Figure 62. Schematic illustration showing by shading the effective area per molecule at various stages of monolayer compression: (a)gaseous state, (b) liquid expanded state, (c) liquid condensed state, and (d) solid state. In (e) the collapse of the film is illustrated.

the gas-water-SDS interface, the bottom of the sapphire cell was not observed. Therefore, the time of hydrate formation onset was not known exactly after the temperature decreased to 0.5°C.

After several hours, a translucent hydrate crystal "tree" which was about a half inch in length, appeared in the bulk water as shown in the second segment of the video tape. Hydrate formation appeared to have started at the bottom of the reactor, requiring more than 9 hours to reach the gas+water+SDS interface after the temperature reached 0.5°C. During this process, crystal growth in bulk water did not consume a significant amount of gas as indicated by a small pressure drop. One cause of such slow hydrate growth in the bulk water was a slow mass transfer of gas into bulk water, with a diffusion coefficient of about 10^{-5} cm/sec. Only a portion of the bulk water was consumed to form gas hydrates as illustrated in the second segment of the video tape.

However, in the above case, after the hydrate crystal penetrated the gas+water interface, destroying the stability of the surface, a massive hydrate growth occurred in the gas phase, resulting in a large pressure drop in a short period of time (<2 minutes). The liquid level dropped as the water was transferred to the gas phase (around the gas+water+SDS interface) to promote rapid hydrate growth. The rapid rate of hydrate growth was controlled by mass transfer, in this case by the transport of water to the gas phase by convection. This process is described in the third segment of the video tape.

The second experiment was performed at 4.0°C and 1000 psig. It took 3 hours for the first hydrate crystal to nucleate on the gas+water+metal-bottom surface as shown in the fourth segment of the video tape. Eight (8) additional hours were required for hydrate growth from the bottom of the cell to the gas+water+SDS interface. The hydrate crystal formed in the bulk water was a translucent "tree-like" structure, similar to that formed in the first experiment. After the hydrate crystal reached and penetrated the gas+water+SDS interface, the remaining phenomena were identical with the first experiment, as shown in the fifth segment of the video tape.

(2) Type B: Hydrate Nucleation on the Gas+Water+Sapphire-Wall Surface

The results of two experiments suggested that hydrate formation occurred at the gas+water+sapphire wall surface. In these experiments, hydrate propagated along the sapphire wall and penetrated the gas+water+SDS interface. When the surface lost its stability, convection occurred along the edge of the sapphire wall, resulting in large quantities of hydrate formation above the gas+water+SDS interface. The water interface dropped until

it reached the bottom of the cell. The hydrate formation rate was mass transfer limited, controlled by the rate of water transport. The whole process required less than 1 or 2 minutes and very large, rapid pressure drops were observed in a short period of time, as digitally encoded in the sixth segment of the video tape.

The tape also shows that, after the rapid hydrate growth process was completed, the hydrate morphology slowly appeared to change to a more coherent solid-like structure. There is no quantitative information about this process.

In the above cases, to make sure there was no water left around the wall of the cell, the solution was carefully injected to cell. Apparently, water diffused through the vapor and condensed on the cell wall providing sites for hydrate formation in the gas phase along the cell wall.

(3) Type C. Nucleation Immediately Below the Gas+Water+SDS Interface.

Two experiments showed that hydrate formation occurred at the active site of the gas+water+SDS interface. Gas diffused to contact the water to form hydrate crystals at the water+SDS side of the gas+water+SDS interface. In both cases, the first hydrate crystal appeared in the bulk water immediately below the gas-water-SDS interface. The hydrate crystal grew downward, perpendicular to the interface, with growth occurring at the interface in order to push the dendritic needle into the bulk water phase, illustrated in the seventh segment of the video tape. When hydrates grew at the interface, the interface was deformed significantly.

Eventually hydrate formation destroyed the stability of the gas+water+SDS interface, and a large amount of water flowed out of that point on the interface and contacted gas phase, resulting in a large amount of hydrates formed. In both cases, it took less than 5 minutes to destroy the stability of the gas+water+SDS interface. Then rapid hydrate growth was completed in a few minutes, resulting in a large, rapid pressure drop.

In summary, SDS does provide some inhibition of hydrate growth if the surface coverage is dense and uniform. Simple surfactants, like SDS, can block a majority of the active sites on the gas+water interface. Surface instability of the gas+water+SDS interface introduces a convective flow which enhances the mass transfer rate significantly as illustrated in Figure 63. This process also provides a good reaction environment for hydrate growth by supplying the maximum surface contact between gas, water, and hydrate formation. The surface instability and convective flow were induced by Marangoni effects caused by surface tension gradients.

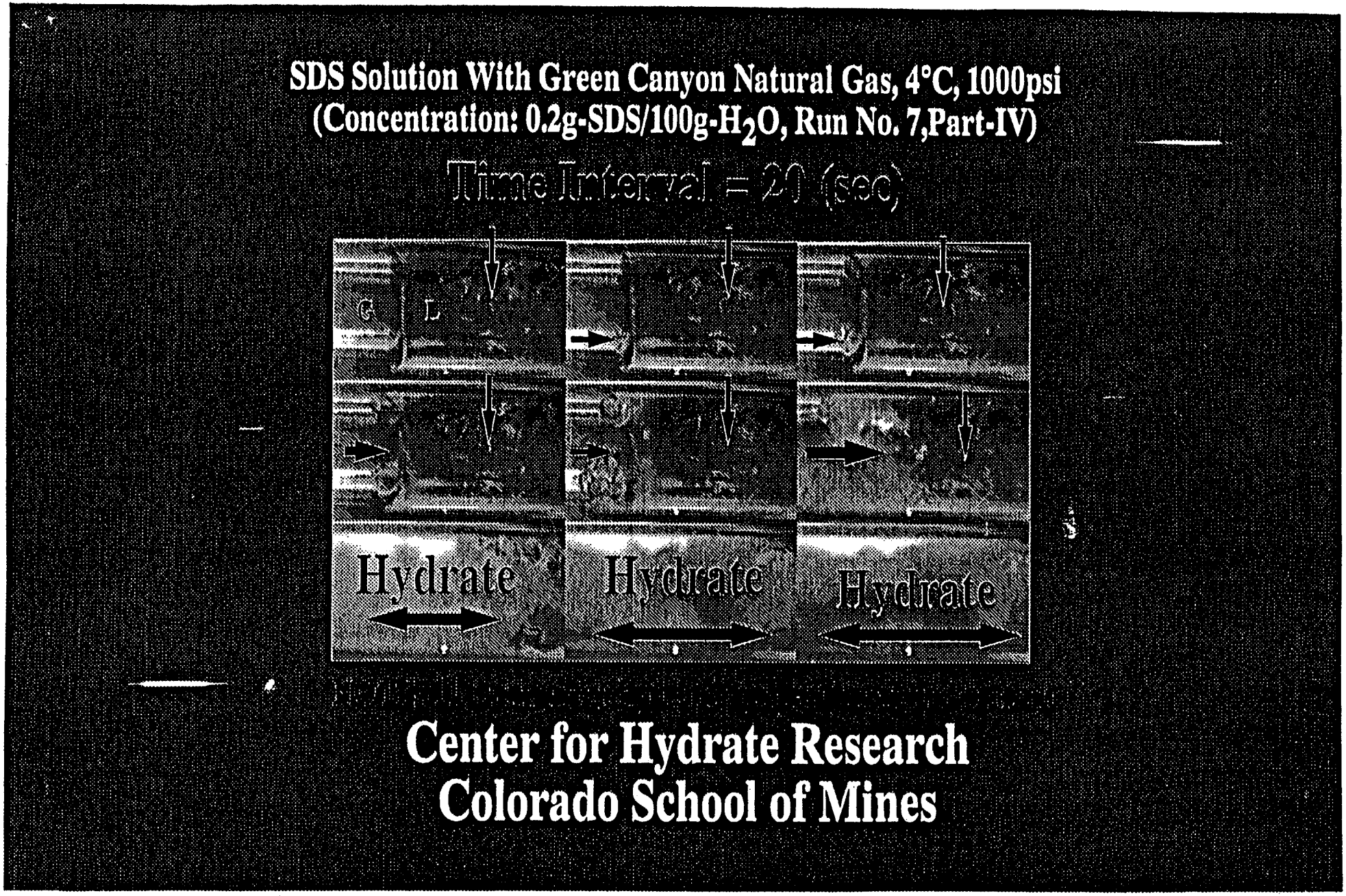

Figure 63. Time lapse of hydrate formation in the presence of SDS.

The stability of the surface in the presence of surfactants is a very difficult subject to study, especially at the temperature and pressure of hydrate formation. The problem is also compounded by the physical reaction of gas hydrate formation at the interface.

While the system with SDS was not our central focus, we learned the following four facts from the above studies:

(1) Hydrate growth is normally a surface phenomena. A small amount of surfactant plays a significant role in the hydrate formation process. If hydrate formation were a bulk phenomena, a surface active agent would not change the reaction so drastically.
(2) A simple surface active agent alone cannot work as an inhibitor due to surface instability at the gas+water+surfactant interface. IN fact no simple chemical surfactant structures were found to be effective inhibitors in our screening studies.
(3) With good surface coverage, we were able to initiate gas hydrate from the gas+water+metal-bottom surface and grow hydrates in bulk water. This may be a single crystal which could be used for other studies, such as X-ray, or Raman spectroscopy.
(4) In most cases, hydrate growth is a mass transfer limited process, in common with other crystallization processes. The initial growth of hydrate crystal at the gas+water+interface is reaction limited, rather than mass transfer limited.

Since the stability of the surface depends on the surface tension gradient and viscosity (Marangoni number), we may be able to use a combination of higher viscosity solution (such as HEC) and surfactant (such as SDS) to maintain the interface stability which would further inhibit hydrate nucleation.

IV.B.3.b.3. Natural Gas and Sea Water

Two experiments were carried out with ASTM synthetic sea water with the objective of determining how electrolytes (or ionic strength) change the nature of the hydrate formation. The observations were almost identical with deionized water except that longer induction times occurred. Hydrate growth initiated at the gas+water interface. Only a small amount of hydrate formed at the gas+water interface (indicated both visually and by a very small pressure drop) but it was sufficient to block gas transport through the solid hydrate film. The formation process can be found in the eighth segment of the video tape.

IV.B.3.b.4. Natural Gas, Amorphous Silica and DI Water

Another project of this laboratory (V. Bansal, "Kinetic Study of Clathrate Hydrates," M.S. Thesis, 1993) showed that hydrate formation can occur at a bulk water+metal surface when amorphous

silica is used as a hydrate formation promoter. We also tested amorphous silica in our visual apparatus for two runs. We used about 0.1ml of synthetic silica in the sapphire cell (25% by volume compared with the total solution). This total amorphous silica concentration was beyond the solubility limit (ca. 100 ppm) and resulted in precipitation of a small deposit of amorphous silica at the bottom of the cell.

In both instances, hydrate formation occurred at the gas+water interface. In one run, only a small amount of hydrate formed at the interface. In the other run, a relatively large amount of hydrate formed and grew toward the amorphous silica deposit at the bottom of the sapphire cell. A record of these runs with amorphous silica may be found in the ninth segment of the video tape.

For future work, we plan to use the same concentration (200ppm) used by Bansal in her experiments.

IV.B 3.b.5. Natural Gas, n-Decane, and Deionized Water

To complete our study on the location of hydrate formation, we added 0.01 ml of n-decane to the reactor, to determine the effect of a liquid condensate on hydrate formation. The oil/water ratio was very low(1/40 - weight basis). At the consortium's discretion, in the future we may increase the oil/water ratio to 1/4.

The experiments (the tenth segment of the video tape) in the sapphire cell with n-decane in 1993, resulted in hydrate formation at the condensate+water interface. Since the amount of n-decane was so small, the hydrate formation process eventually destroyed the liquid condensate phase. In each of these runs, only a small amount of hydrates were formed.

IV.B.3.b.6. Natural Gas, VC-713 (0.5wt%), and Sea Water

Four experiments were conducted at 4.0°C and 1000 psig. A typical example of hydrate formation is shown in the 11th segment of the video tape. Resulting induction times ranged from 7 to 30 minutes. It appeared that VC-713 did not prolong the induction time significantly at this operating condition.

However, when hydrate growth began at the gas+water interface, the growth rate was significantly slower with VC-713 than in deionized water, even for the initial growth stage at the interface (1.0 minute versus 10 seconds). The hydrate crystal on the surface had relatively good permeability which allowed the

gas molecules to diffuse to the bulk water to form hydrates. The growth front was at the hydrate+water interface. The majority of hydrate growth was downward in the bulk water.

The rate of continued growth was relatively slow compared with the initial growth at the interface. As illustrated on the video tape, a gas bubble formed between the hydrates and water after hydrate growth for 3 hours. The bubble grew until it completely separated the hydrate phase from the bulk water phase. With the presence of a gas bubble separating the liquid water from hydrates, the hydrate growth mainly occurred on the hydrates side, rather than the liquid water side. At the termination of hydrate growth, the solid hydrate prevented pressure communication between the bulk gas and the gas bubble. The hydrate growth process stopped at that point. For three of the runs, after about three additional hours, the hydrate crystal phase and solution phase were entirely separated by the gas phase. Subsequently, all three phases (gas, hydrates, and liquid water) appeared to be very stable over a long period of time (> 20 hours).

IV.B.3.b.7. Natural Gas, PVP(0.5wt%), and Sea Water

In late 1993, we only had time for a single run to be made with PVP, Green Canyon gas, and sea water. The 12th segment of the video tape summarizes the experiment, in which hydrate growth started at the gas+water interface and propagated across the surface rapidly. Only a very small amount of hydrate formed over a period of 7.5 hours.

IV.B.3.b.8 CO_2 in Deionized Water

One might theorize that gas solubility in the bulk solution is the controlling parameter for the kinetics of hydrate formation. We used CO_2 to examine this concept, since the solubility of CO_2 is two orders of magnitude larger than CH_4, C_2H_6, C_3H_8, etc.

The second justification for its use was that CO_2 hydrates are denser than water (1.07g/cm^3) and would thus precipitate when they achieved a size of 1mm (personal communication 10/6/93 by Dr. Kamarta of Mitsubishi). This would address the issue of whether the hydrate crystal nucleates in the bulk water but floats to surface as a less dense phase.

Two runs were made with CO_2 in deionized water. Typical results are shown in the 13th segment of the video tape at the experimental conditions of 0.5°C and 500 psig. The dew point pressure is 520 psia, based upon the Peng-Robinson equation. Carbon dioxide hydrate started its growth at the gas-water

interface. The hydrate propagated toward the bulk very rapidly (less than 15 seconds) with the initial growth along the wall of the reactor. Over a long period of time, crystal relaxation occurred in the hydrate phase. The final segment of the video tape shows changes in crystal morphology. One may conclude that the hydrate growth in the bulk is only observed for gases of very high solubility.

IV.B.4. Collaborative Flow Loop Effort at Exxon

In the last quarter of 1993 Mr. J.P. Lederhos, one of the senior graduate students in the Hydrate Center, went to Houston to begin testing some of our inhibitors on the Exxon Production Research Laboratory's hydrate formation loop. The Center for Hydrate Research expresses its gratitude for Exxon's generosity in providing the opportunity to perform research using the loop and to share those results with the consortium.

The Exxon facility is unique in that, while it represents a capital and operational investment beyond that of a normal academic institution, it is also the best pilot plant facility available for scale-up. The Exxon flow loop itself is a 4 inch stainless steel, 275 foot-long, temperature-controlled line.

IV.B.4.a. CSM Experiments on Systems Proposed for Loop.

Before starting tests at Exxon's facility in Houston we tested systems similar to those proposed at Exxon on both our screening and high pressures apparatuses, to determine transferability of results. Because of time delays we began our effort at the Exxon facility late in the year, and we were only able to establish a baseline for hydrate formation in the flow loop at the time this report was written. The complete exposition of our experiments on the flow loop will be detailed in the 1994 annual report.

Since the screening tests had already been done to the extent possible, the initial phase of the collaboration consisted of running a series of kinetic experiments on the CSM constant pressure apparatus using a representative field condensate.

In this series of experiments we tested the sensitivity of the VC-713 system to inhibitor concentration and sea water fraction (wt% sea salt in a solution / 3.5wt% sea salt). In all experiments 120g of aqueous solution and 30g of condensate were used. Three different inhibitor concentrations were investigated ranging from 0.1 to 0.75 wt% in the aqueous phase. In addition, we used three sea water fractions ranging from 0 to 1.2. The gas used was our standard synthetic Green Canyon gas and the condensate composition is given in Table 11.

Table 11. Exxon Condensate Composition

Component	Weight Fraction
n-C4	0.0012
i-C4	0.0003
neoC5	0.0043
n-C5	0.1282
i-C5	0.1340
C6	0.2624
C7	0.2807
C8	0.1503
C9	0.0315
C10 plus	0.0071

In Figure 64 the sensitivity of the system to inhibitor concentration is shown. At the two higher concentrations of 0.5 and 0.75 wt% there was little to no hydrate formation; however, upon reducing the concentration of VC713 to 0.1wt% hydrates formed rapidly. The sensitivity of the system to sea water fraction is shown in Figure 65. For all of these runs the inhibitor concentration was kept constant at 0.5wt%. As can be seen in Figure 65, little difference was observed in the gas consumption results for sea water fractions of 1 and 1.2, but with no salt present the total gas consumption dramatically increased, to 0.9gmol.

Following the above series of experiments on the high pressure apparatus at CSM, a series of experiments were started using the Exxon 4 inch diameter flow loop and the Exxon 0.5 inch diameter mini-loop in Houston. These results will reported in the 1994 annual report.

IV.B.5. Raman Spectroscopic Studies

Raman spectroscopy has been used intensively in this laboratory for understanding the kinetic inhibition mechanism. The experimental results show that this technique is one of the most useful and valid techniques for this application.

In this research tetrahydrofuran (THF) hydrate has been used as a model hydrate. The reasons for using THF hydrate follows: 1) experimental simplicity (THF can form hydrate around 278.1 K at 1 atm and THF is totally miscible with water) 2) experience (the THF-water system has been used extensively in this lab for the past 15 years.)

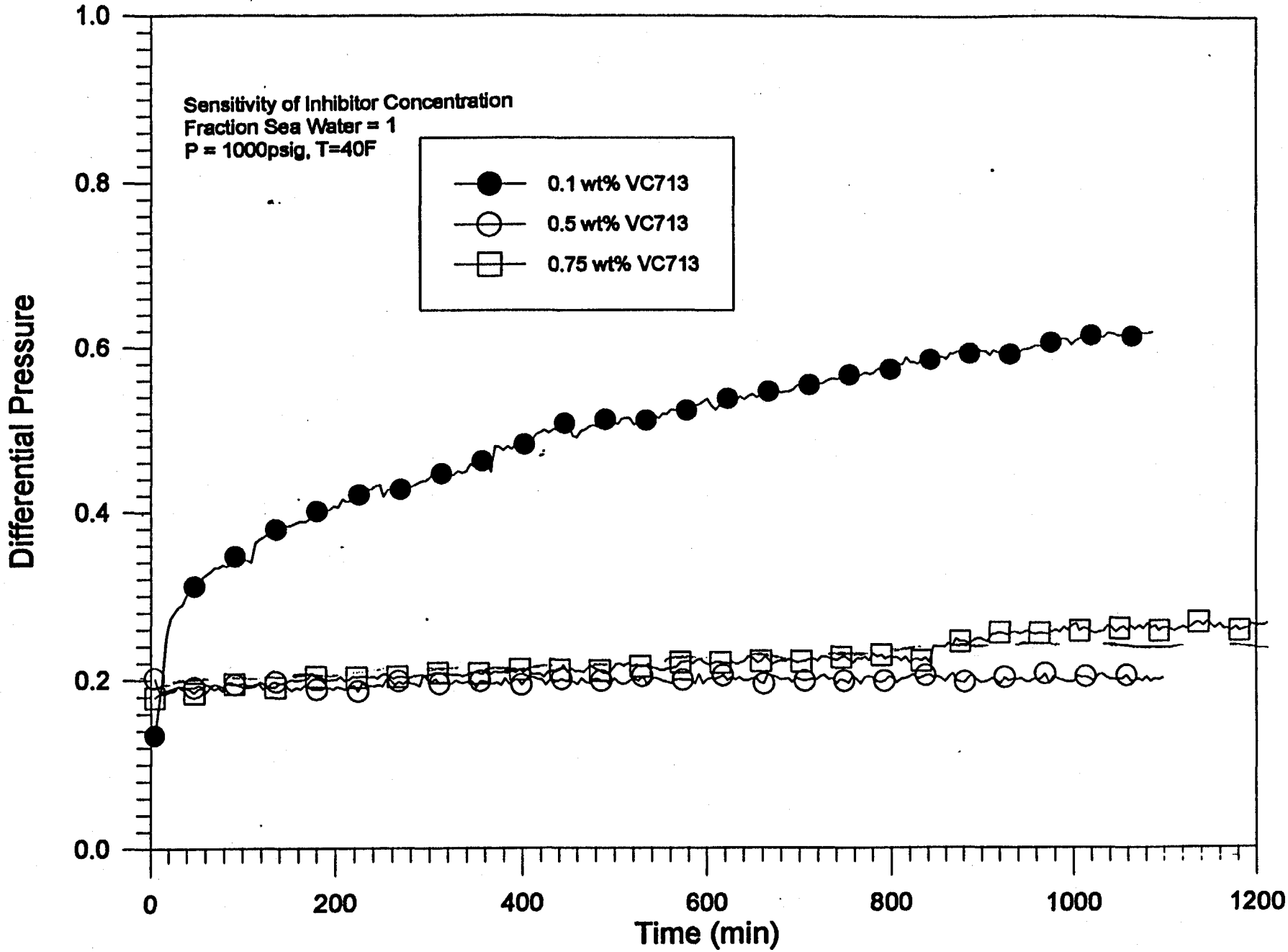

Figure 64. Sensitivity of VC-713 performance to concentration for the Exxon gas/condensate system.

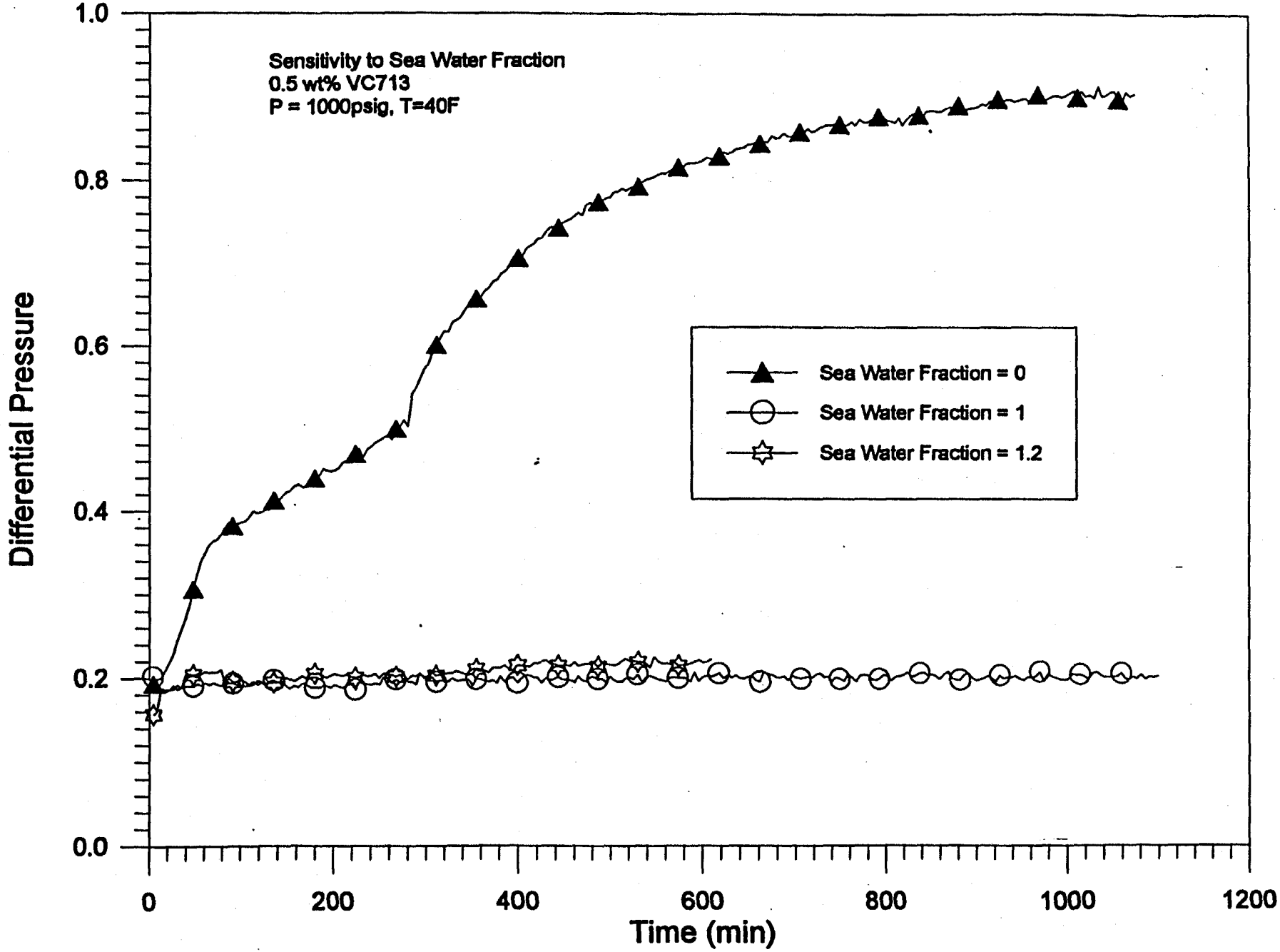

Figure 65. Sensitivity of VC-713 performance to sea water fraction for the Exxon gas/condensate system.

In this portion of the report, Raman spectra of THF-water are presented, deconvoluted and analyzed for inhibitors: VC713, PVP and PVCAP. The inhibitor concentrations are at 0.5 wt% for all the systems - with and without 3.5 wt% ASTM sea salt.

IV.B.5.a. Experimental Procedure

The instrument used for this work is located at the U.S. Geological Survey in the Denver Federal Center and future work in will be done under a cooperative agreement (CRADA) between the Center for Hydrate Research and that U.S.G.S. laboratory with Dr. R.C. Burruss.

A spectra-Physics Ar^+ cw laser, model 2025-5, capable of generating ten visible wavelength and two ultraviolet lines, was used in this study. The visible green line with wavelength 514.53 nm was used, with an operating power of 170 *mw* for studying THF-water-inhibitor-salts and THF-water-inhibitor solutions. An Instruments SA, Inc. Ramanor U1000, 1m double-dispersed monochrometer system equipped with different holographic grating systems was used for the spectroscopic measurements.

The signal was detected with a single-channel, photon-counting system (RCA 31034A PMT cooled to -20°C and a Pacific Instruments amplifier-discriminator) connected to an ISA Spectralink module which was interfaced to an IBM-AT computer running ISA PRISM software.

The three systems studied in this research were:
VC-713+THF+Water (with and without salt),
PVP+THF+Water (with and without salt), and
PVCAP+THF+Water (without salt).

Concentration of THF in all tests was 23 wt% in aqueous solution; that of the inhibitors was 0.5 wt% ; if NaCl was present its concentration was 3.5 wt%.

Spectra were measured for all systems at two different temperatures, 0.0°C and 25.0°C. Because hydrates should form for the THF+water and the inhibitor+THF+water system at 0°C, the spectra reported here for that temperature represent a metastable state.

IV.B.5.b. Experimental Results from Raman Apparatus

In the literature, several different ways to interpret the water OH stretching band are described. The one used in this research is the Walrafen et al. approach (J. Chem. Phys., **85**, 6964 (1986)). Walrafen determined that there were several components that contributed to the water OH band. These contributions were separated by the isosbestic point. Any

contribution below the isosbestic point was due to unbroken hydrogen bonding, while contribution above the isosbestic point was due to broken hydrogen bonding. Three Gaussian bands were determined to comprise OH stretching phenomena via digital computer deconvolution.

Initially, to gain experience with the analysis routine, the OH stretching band of pure liquid water was deconvoluted and analyzed using the above approach. The results of this baseline determination were satisfactory when compared to Walrafen's results.

IV.B.5.b.1. Raman Results for VC-713 + Water + THF System

The spectra of VC-713+THF+water with and without 3.5 wt% salts at 25.0 °C and 0.0 °C are shown in Figures 66 and 67. As shown in these two figures, there are obvious changes in the band positions, especially for the water OH intramolecular stretching band between 3100 and 3600 cm^{-1}. However, as the temperature is lowered, the difference decreases between solutions with and without salts.

Deconvolution analysis was done on both THF C-O-C ring stretching band and water OH stretching band. The results for C-O-C ring stretching bands showed that the inhibiting polymers do not affect the vibrational frequencies of the solute molecules in the solution. This result implies that the interactions between polymer molecules and solute molecules are negligible. However, the intensity of the THF C-O-C ring stretching mode is smaller in the presence of salts than in the absence of salts.

However, both the frequencies and the intensities of the OH stretching band, are sensitive to VC-713. The frequency shifts, which indicate hydrogen bond strength are shown in Figure 68. The intensities which reflect hydrogen bond population are shown in Figure 69.

As shown in Figure 68, the center position of the unbroken hydrogen bond band for both systems (with and without 3.5 wt% salt) shifts to higher wavenumbers compared to that of both pure liquid water and water+THF solution. The center frequency for the broken hydrogen bond bands, which is not shown in the figure, move to lower wavenumbers. These results indicate that, in the presence of the VC-713, the strength of the hydrogen bond increases. Whether this increase is due to the hydrogen bonding between VC-713 molecules and water molecules or due to water-water molecules is not known at this time.

The effect of VC-713 on the hydrogen bond population varies with temperature as shown in Figure 69. At 0°C, the population increases with addition of VC-713 to a THF+water solution, while at 25°C, the population decreases. This result suggests that

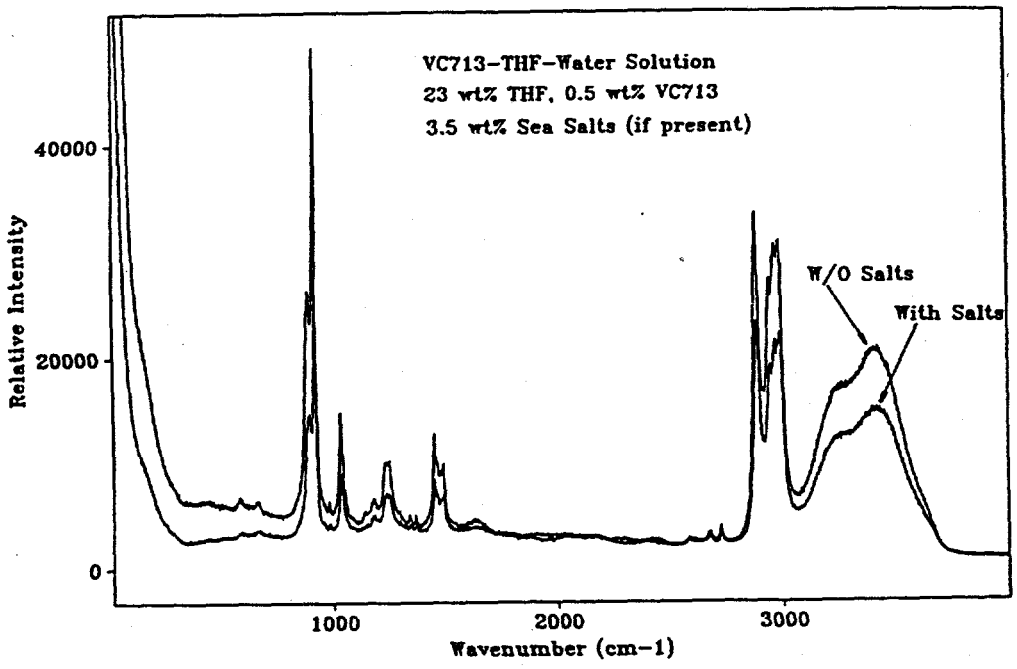

Figure 66. Spectra of VC-713/water/THF with and without salt at 25°C.

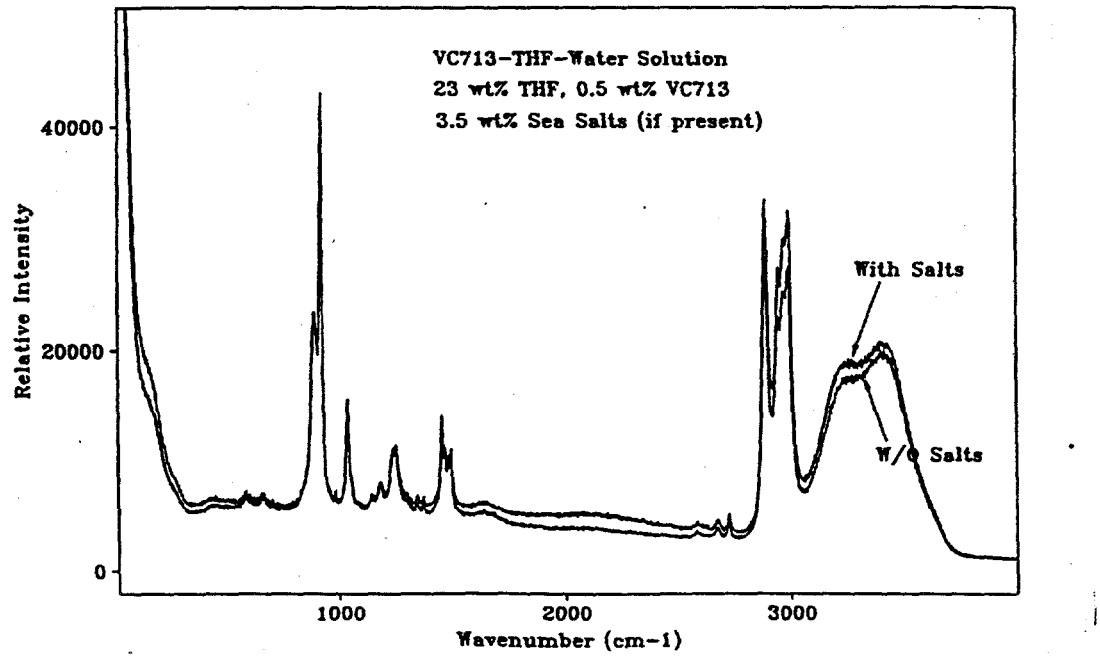

Figure 67. Spectra of VC-713/water/THF with and without salt at 0.0°C.

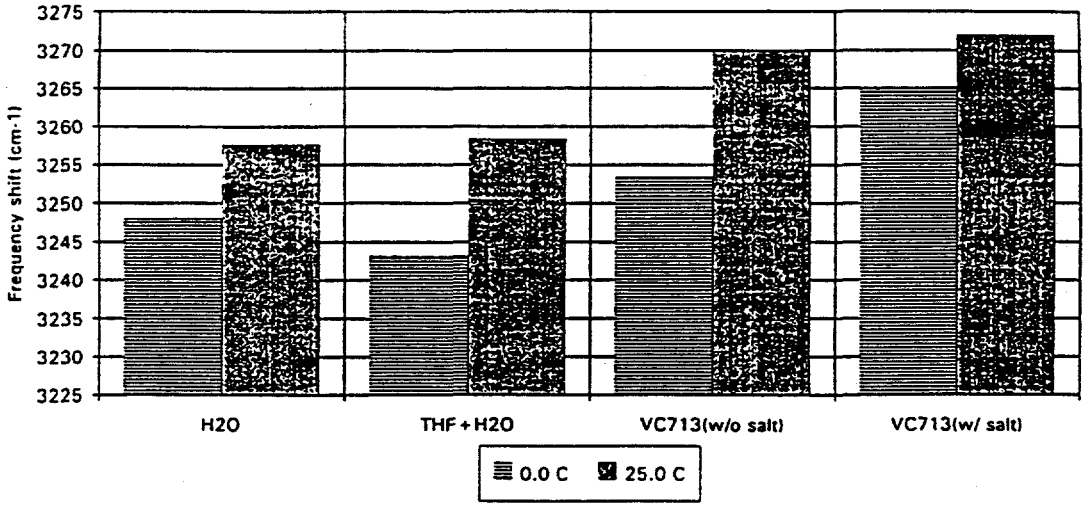

Figure 68. Hydrogen bond strength of VC-713/water/THF system with and without salt.

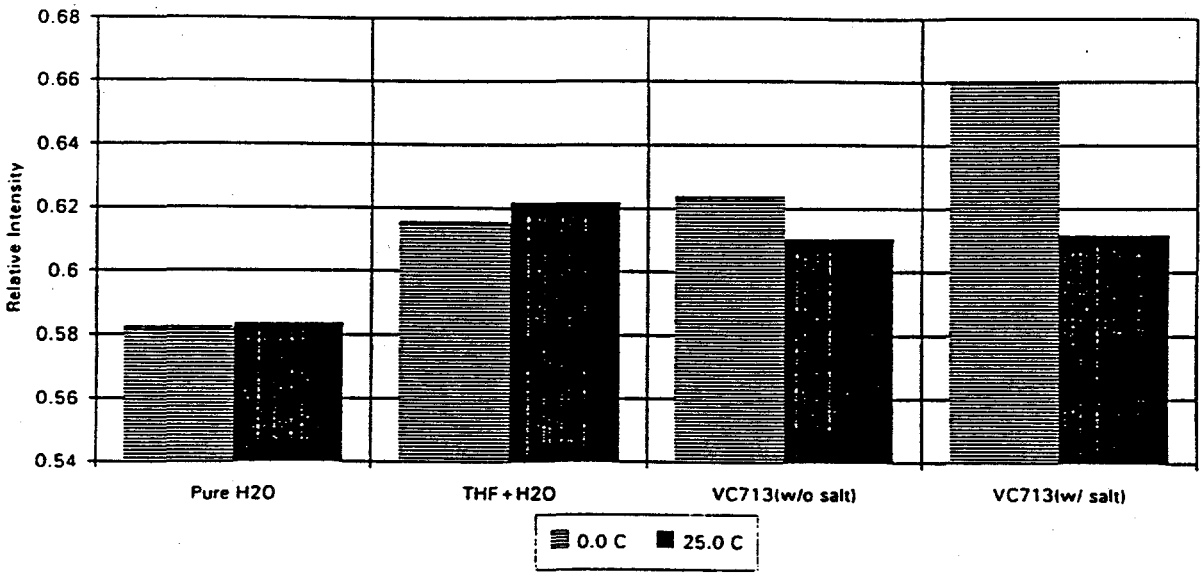

Figure 69. Hydrogen bond population of VC-713/water/THF system with and without salt.

there is not a contribution of unbroken hydrogen bonding for the VC-713 solution compared to that of pure liquid water, however, there is not much increase compared to that of water+THF solution.

Note that for VC-713, the salt affects the solution hydrogen bond population and strength more than the solution without salt, particularly at low temperatures, probably because of VC-713 expansion in 3.5% salt.

IV.B.5.b.1.a. Possible Interpretation of VC-713+THF+Water Results The increase in the water hydrogen bond strength and population by VC-713 might be caused by either of the following two effects: (1) water molecules might be induced to cluster around polymer segments, or (2) H_2O molecules might be hydrogen bonded to the O atoms in VC-713 causing an increase in unbroken hydrogen bonding. This process might seem counter-intuitive in the process of hydrate formation, since one might think that an increase in hydrogen bonding, would cause hydrates to be easier to form.

It is evident that for pure hydrate and ice, there are more hydrogen bonds than pure water. However, the hydrate formation process might be conceived as a two-step process: bond-breaking and bond formation. If this is the case, then an increase in both the hydrogen bond population and strength will decrease the bond-breaking step.

We cannot tell the source of the increase of strength and number in water hydrogen bonding. A second interpretation is that the H-bonding increase is due to water-polymer interactions rather than water-water interactions. This will be investigated further in 1994.

A third possibility to interpret these results is that increasing the population of hydrogen bonds present in the subcooled solution may also result in a change in the ring number/distribution of hydrogen bonded water molecules. That is, Rahman and Stillinger (J. Am. Chem. Soc. **95**, 7943, 1973) indicated that 5 and 6-member hydrogen bond rings predominate in pure water. (Note that hydrates are composed of such 5- and 6-member faces.) The addition of a polymer such as VC-713 might change the number/distribution of the rings away from that favorable for hydrate formation (say to 7 or 8-member rings).

With the polymer, the salt presence enlarges the population and strength of hydrogen bonding in the inhibitor system compared to that of both pure water and water+THF solution. This can be explained in the following way. Salt is known as a water structure breaker. The presence of salt will decrease the contribution from the unbroken hydrogen bonding and increase the contribution from broken hydrogen bonding. That is why salt can be used as a hydrate thermodynamic inhibitor; salt ions attract

water molecules, making them less available for participation in the hydrate structure. When salt and VC-713 are both present, part of the requirement by VC-713 to form hydrogen bonds is satisfied by the salt. The hydrate formation mechanism is an two-step process, involving both bond breaking and bond forming. VC-713 enters this process at some point which leads to the inhibition of hydrate formation.

In conclusion, the OH band changes for VC-713 are significant. An increase in both population and strength of hydrogen bonds effectively decreases the possibility of water molecules forming a lattice-like structure, since it has to break the bonds formed by water molecules in the presence of VC-713. This can only be done under more stringent conditions, such as lower temperature and higher pressure. The above explanation may account for the hydrate inhibition function of VC-713 and is thus included in the hypothesis description in Section III.C.

IV.B.5.b.2. Raman Results for the PVP+Water+THF System

While not as effective an inhibitor as VC-713 or PVCAP, PVP was one of the first water-soluble polymers found to have a good inhibition effect. As seen from the chemical structures (shown in the screening apparatus section) PVP has only the 5-member lactam ring of the VC-713 molecule as the structural unit, and is thus a homopolymer. The spectra of PVP+THF+H_2O system with and without 3.5 wt% salt at 25.0 °C and 0.0 °C are shown in Figures 70 and 71.

The hydrogen bond population and hydrogen bond strength profiles for PVP are shown in Figures 72 and 73. Although VC-713 provides enhanced water hydrogen bond structure in the presence of salt, the effect of PVP is different. In the presence of the salt, PVP shows neither a significant increase of hydrogen bond population nor strength compared to water+THF solution. (However, there are small changes in comparison to pure water.) In the absence of salt at 0°C, both the hydrogen bond population and strength increase compared to that of both pure liquid water and THF-water solution, implying that salt affects the mechanism for PVP inhibition different from that of VC-713 inhibition, suggesting a review of the effect of salt on PVP's performance in the high pressure apparatus.

IV.B.5.b.3. Raman Results for PVCAP + THF + Water

The PVCAP+THF+water system was also studied in this research only for the case without salt. The spectra for this system at 25.0°C and 0.0°C are shown in Figure 74. The figure shows are some differences in both the intensities and the positions of water OH stretching band. The intensity at 25.0°C is higher than

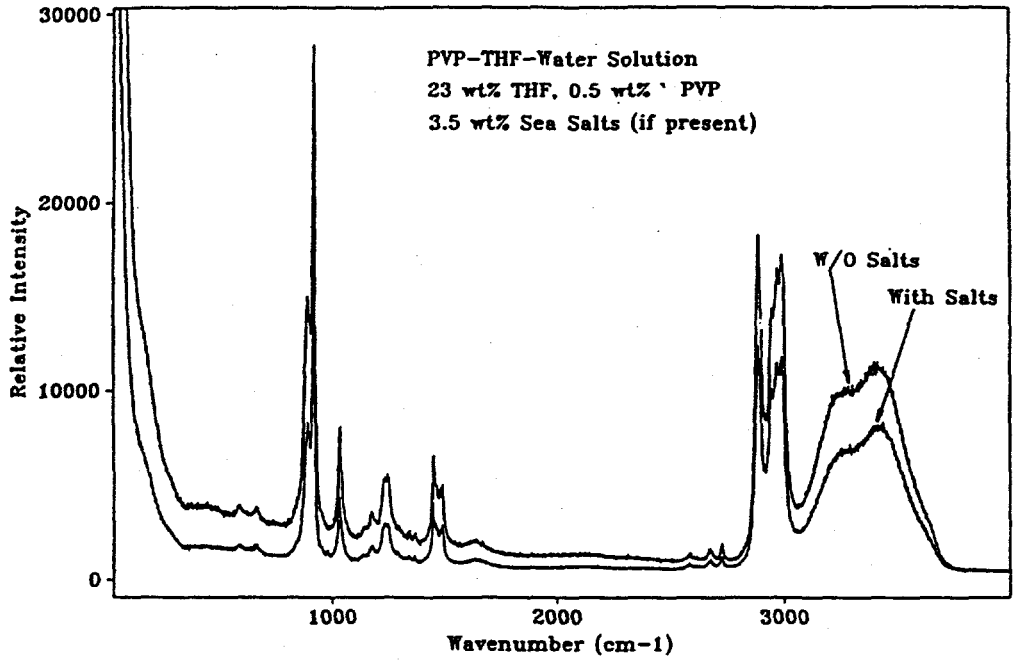

Figure 70. Spectra of PVP/water/THF with and without salt at 25°C.

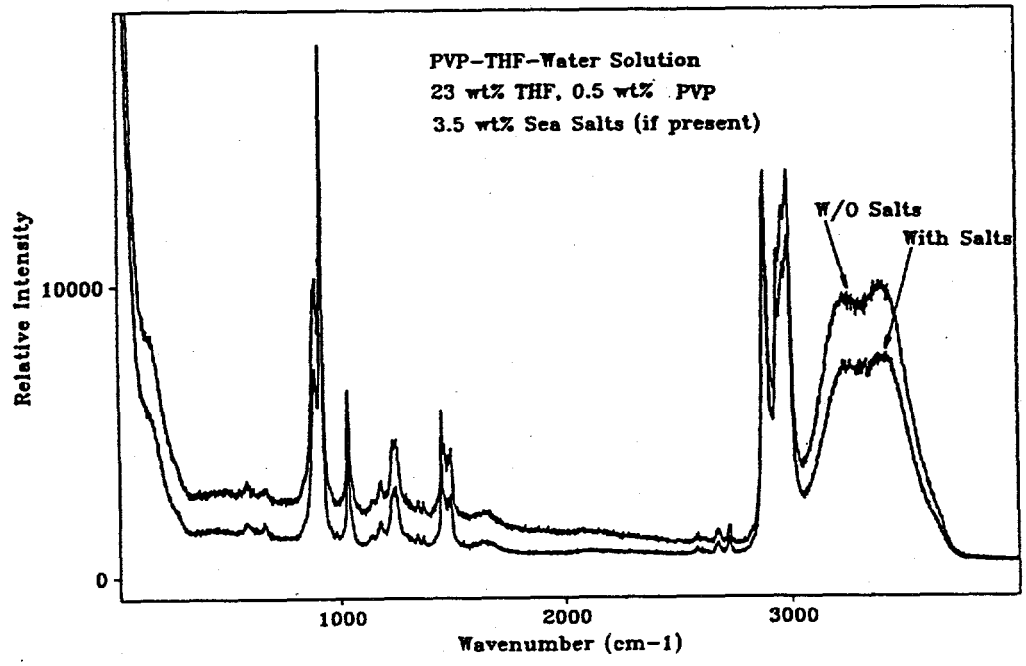

Figure 71. Spectra of PVP/water/THF with and without salt at 0.0°C.

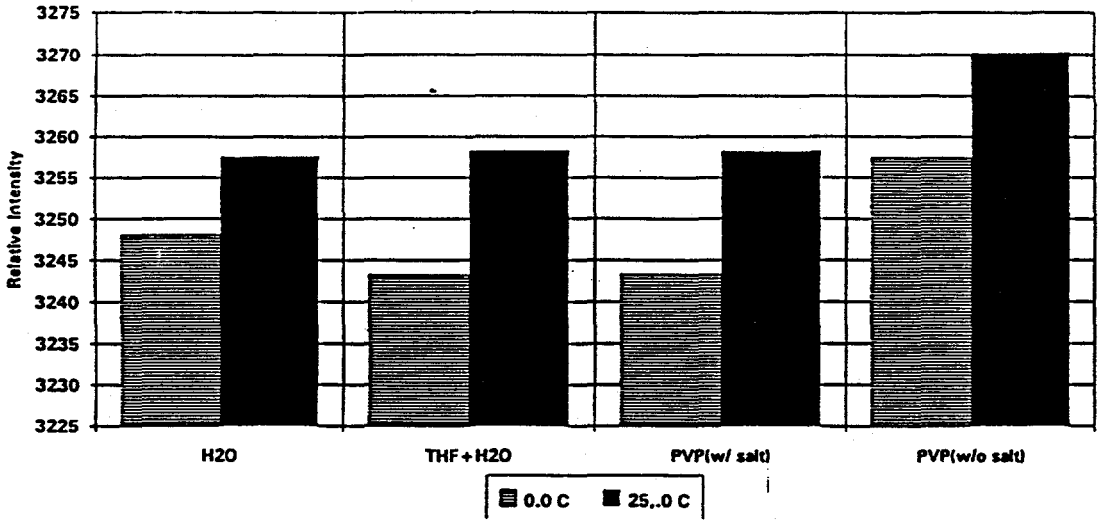

Figure 72. Hydrogen bond strength of PVP/water/THF system with and without salt.

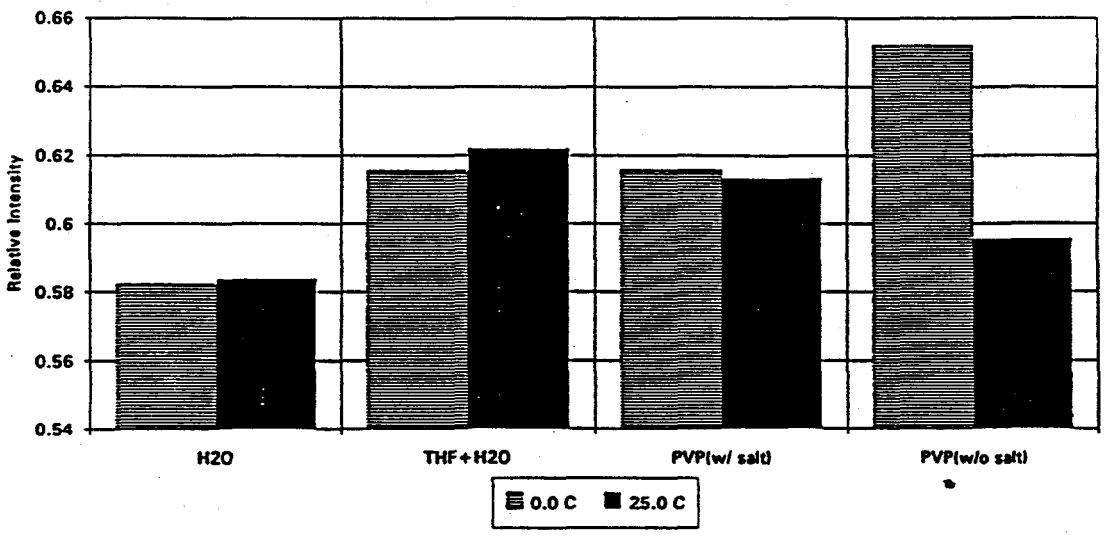

Figure 73. Hydrogen bond population of PVP/water/THF system with and without salt.

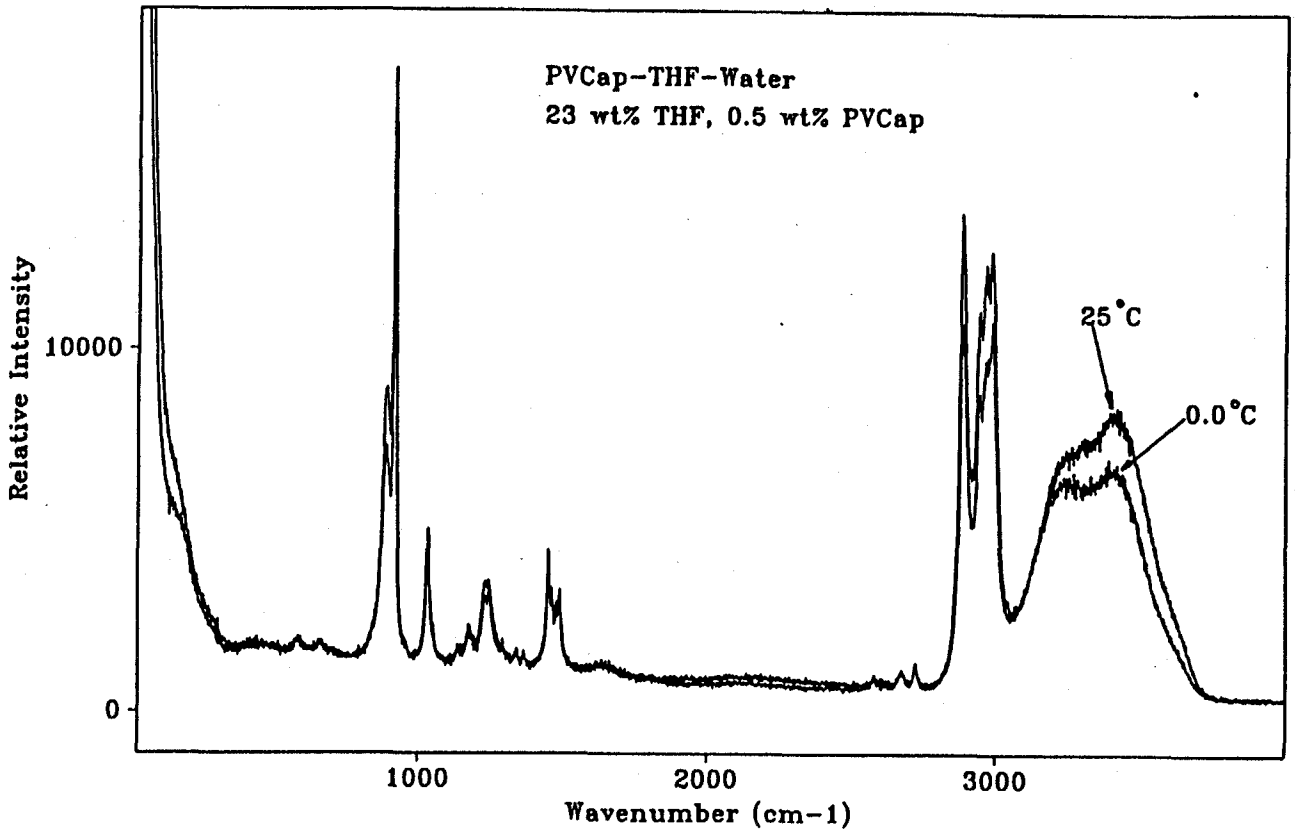

Figure 74. Spectra of PVCap/water/THF system at 25.0°C and 0.0°C.

at 0.0°C.

The hydrogen bond strength and population are shown in Figures 75 and 76, respectively. At 0°C, (close to the hydrate formation temperature) the bond strength and population both increase only slightly when PVCAP is added to the THF+water solution. However, away from the hydrate formation temperature at 25°C, the bond strength increases very slightly, while the bond population decreases upon the addition of PVCAP to the water+THF solution.

The PVCAP system has yet to be measured with salts, so it is not possible to say anything about the effect of PVCAP on hydrogen bonding of the water+THF in the presence of salts. However, from the results of the thermodynamic inhibition in the high pressure cell, one might expect similar Raman results to those obtained with VC-713 - that is salt may have a substantial impact.

IV.B.5.c. Conclusions from Raman Work

In conclusion, VC-713, PVP and PVCAP change the subcooled water+THF solution structure as a function of the salt present. The very low concentration of polymer indicates this type of interaction between VC-713, PVP, PVCAP and water changes the overall water hydrogen bond configuration. This change causes water to deviate from the normal structure for hydrate formation to some unfavored configuration. The hydrogen bond population and strength are changed (as a function of salt concentration) in the presence of these polymers. The salts effect differs for VC-713 and PVP. For VC-713, salt promotes more and stronger hydrogen bond formation, without much effect in salt's absence (with similar results for PVCAP). For PVP, the presence of salt does not have a very significant influence, yet PVP increases the hydrogen bond strength and population in the absence of salt.

At this point, we do not know the mechanistic details of the water structure change by these polymers; it may be due to polymer expansion. However, we do have a much better microscopic and macroscopic hypothesis that we did previously. This hypothesis, set forth initially in this report in Section III.C. has led to the construction of new and better hydrate inhibitors, indicated in other sections of this report.

IV.B.6. Computer Simulation of Hydrate Formation/Inhibition

In this work, we attempted to generate a microscopic simulation of hydrate formation and inhibition using both original and commercial programs. If successful, it was hoped that a simulation could provide qualitative answers to phenomena which were not easily observed via experiments.

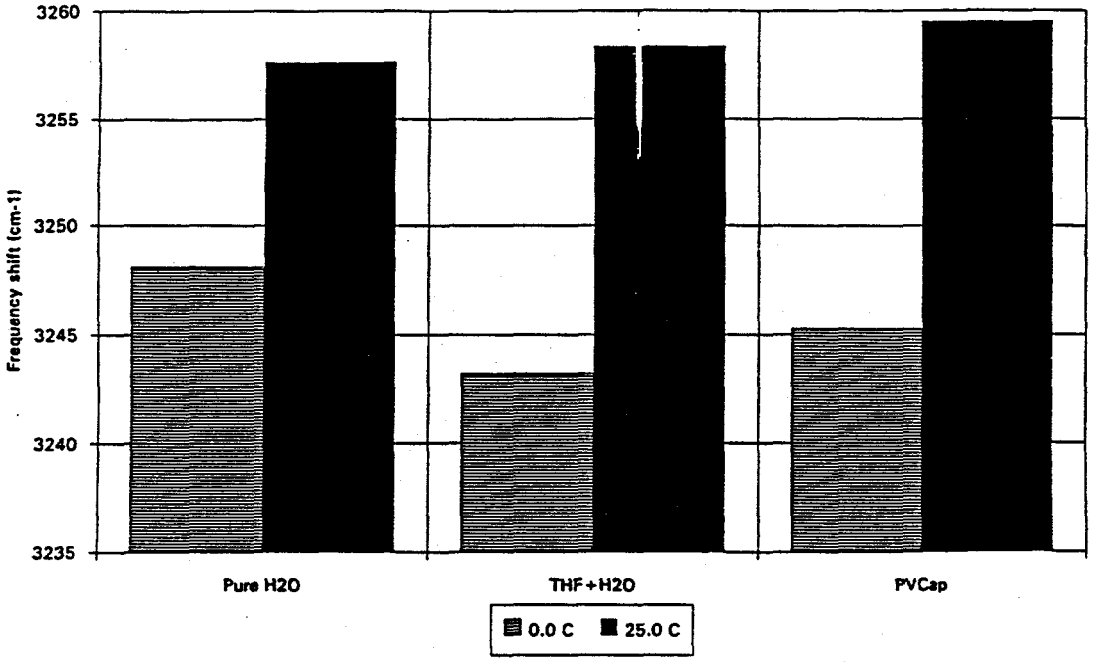

Figure 75. Hydrogen bond strength of PVCap/water/THF system with and without salt.

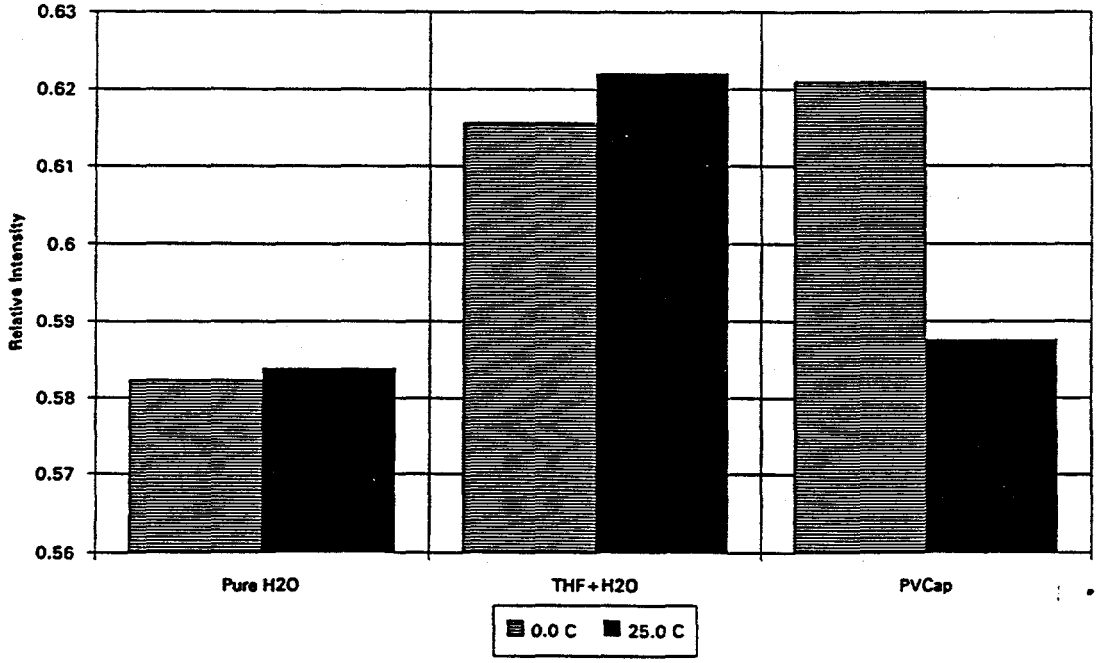

Figure 76. Hydrogen bond population of PVCap/water/THF system with and without salt.

The first portion of the section describes our use of two commercial software packages (HYPERCHEM AND SYBYL) to simulate the interaction of two polymers (VC-713 and a winter flounder polypeptide) first with hydrate and ice surfaces (Section IV.B.6.a) and then with water solutions (Section IV.B.6.b).

The second portion of the work was an attempt to use our own programs to determine if we could simulate the aggregation of water clusters. This work was done to examine the hydrate nucleation/growth hypothesis which was reported in the introduction section of this report. At first we examined the possibility for hydrate formation at an interface, or in small quantities of molecules (Section IV.B.6.c); then we considered the possibility of modeling the joining of water clusters (Section IV.B.6.d).

IV.B.6.a. Docking of Polymers on Hydrate and Ice Surfaces

1. Method of Computation

A computer molecular simulation program named Sybyl from Tripos, Inc. was used to perform the docking studies. This program was made available through a "partnership" purchase with Shell, Inc. In this work a crystal surface (either ice or hydrate) and polymer macromolecule were "docked" in a vacuum; that is the energy of interaction between the crystal and polymer was compared for different conformations.

The surfaces of sI, sII and hexagonal ice lattice were prepared in Sybyl by reading in the experimental coordinates of the oxygen and hydrogen atoms (in three dimensions) and connecting them to make water molecules. The size of the surface was 5x5x1 unit cells for sI, 4x4x1 for sII, and 9x9x2 for ice. The dimension of each surface was 61+ Å along the x and y axes, chosen in order to optimize the space to accommodate the winter flounder polypeptide (59 Å length), 9-link chain of the VC-713 polymer (61 Å length) while limiting the computation time.

Polymer chains of VC-713 and flounder polypeptide were generated on an IBM 486 using Hyperchem (version 2.0 for Windows software by Autodesk.) The polymers were then transferred from the 486 PC to the RISC-6000 computer in Brookhaven format. The coordinates for both macromolecule and crystal surface were then read into the Sybyl software. Charges for water molecules in crystal and for the macromolecule were computed using the method of Berthoud and Pullman (J. Chem. Phys., **62**, 942 (1965)). Periodic boundary conditions were used in the system, calculated via a intermolecular energy lattice field, for various relative positions of the macromolecule and the crystal surface.

Docking of a macromolecule on the crystal surface was performed by varying x, y, z, θ and ϕ coordinates for the

macromolecule; x, y and z specify the position of center of the macromolecule relative to the crystal surface, θ is the angle between the center line of the macromolecule and the initial position on the crystal surface, ϕ is the angle of the macromolecule rotation about its center line relative to the initial position. Each macromolecule was place in a position with its major axis parallel to that of the surface.

Intermolecular energies (that is, the potential energy between the polymer and the surface relative to that at infinite distance) was analyzed during this process. After manually placing many different configurations of the polymer on the surface, the conformation with the lowest intermolecular energy was chosen as the preferred orientation . This step was followed by an energy minimization of the whole system (relaxation of the macromolecule on the crystal surface). The final energy of the system was recorded for comparison with other configurations.

For each run the following final values are presented in Table 12:

a) the number of hydrogen bonds between the macromolecule and water molecules of the crystal.
b) the conformation geometry, represented by repeated docking sites on the crystal (if any), and
c) the energy of intermolecular interaction.

Table 12. Analysis of Docking of Macromolecules on Crystals

	Intermolecular energy, kcal/mole	Number of hydrogen bonds *	Pattern of adsorption sites
Winter flounder polypeptide on			
ice 011	1742	4 (100%)	yes (16.9Å)
ice 101	-19850	4 (100%)	yes (16.9 Å)
ice 110	-19924	4 (100%)	yes (16.9 Å)
sI hydrate	7504	0 (0%)	yes (16.9 Å)
sII hydrate	-12696	4 (100%)	yes (16.9 Å)
VC-713 on			
sI hydrate	751600	0 (0%)	some (36.9 Å)
sII hydrate	731594	1 (1.59%)	no

* - percentage of bonding at available sites on macromolecule

2. Discussion

Docking the winter flounder polypeptide was performed on five types of crystal surface: the 011, 101 and 110 crystal surface planes of ice, and the surfaces of sI and sII hydrate. The best results were obtained for docking the flounder polypeptide on the ice surfaces - an expected outcome because winter flounder

polypeptide prevents the freezing of this fish at sub-zero temperatures down to -2.3°C by adsorbing on ice crystals and preventing them from agglomeration.

However, docking the polypeptide on hydrate sI and sII gave lower interaction energies, indicating that it may provide effective inhibition. However, docking (adsorption) of VC-713 on sI and sII hydrate resulted in a very high, unfavorable interaction energy. This suggests that the kinetic inhibition mechanism of VC-713 might not be adsorption of polymer on the hydrate surface, but rather by the creation of unfavorable hydrogen bonded structures in bulk water.

Example figures of the polymer molecules are shown in Figures 77 through 80. The numbers on Figure 77 show the distance between repeating groups which may participate in hydrogen bonding. The distance between the macromolecule and crystal surface in Figures 78 through 80 indicate that this is an adsorbed state. The preferred position of the components on the macromolecules can be learned from these figures. One may notice the repeating pattern of adsorption sites in flounder polypeptide on ice and on hydrate. However such a pattern is not present in the case of docking of VC-713 on hydrate.

IV.B.6.b. Interaction of Kinetic Inhibitors with Water

This research was directed towards further understanding the mechanism of kinetic inhibition of hydrates. Two main possibilities were investigated: 1)prevention of hydrate formation by the polymer through adsorption on the active (growing) surface of the crystal, and 2) by promoting structure in the bulk water and preventing it from forming hydrate. In order to determine the inhibition mechanism for a particular polymer the results will be compared for both cases.

In order to verify that water properties are modelled adequately, a comparison of three water models available in Sybyl was made: (1) SPC (single point charge), (2) TIP3P (transferable intermolecular potential 3 point charge) and (3) the proprietary Tripos model.

A lattice of 216 (6x6x6) water molecules was set for each model with the density of 1.0 g/cc. Periodic boundary conditions were applied. Charges on water molecules were set as pre-computed (+0.41 on each hydrogen and -0.82 on oxygen). The first part of each run was an equilibration of the water in periodic box, consisting of three stages:
1) 1000 time steps in the microcanonical NVE ensemble (constant number of particles N, constant volume V, and constant energy E) to equilibrate kinetic and potential energies of water,
2) 1000 time steps in canonical NTV ensemble (constant N, constant temperature T, constant V) to set the temperature

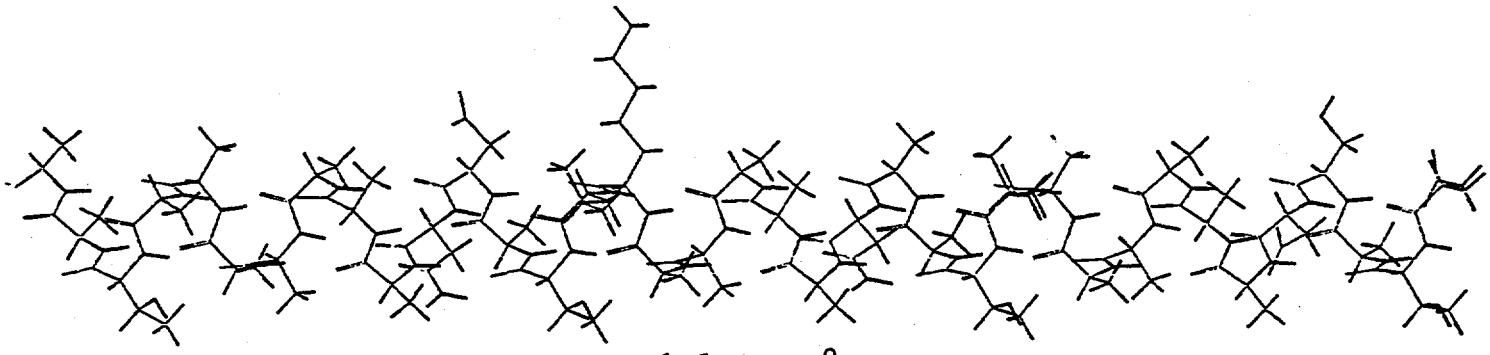

16.86 Å

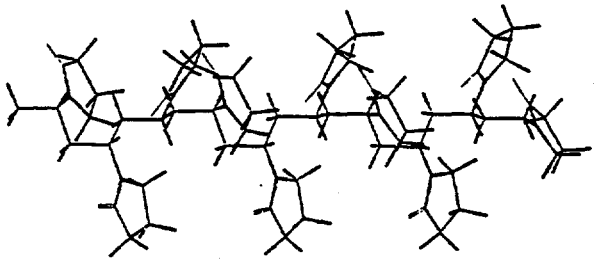

6.22 Å

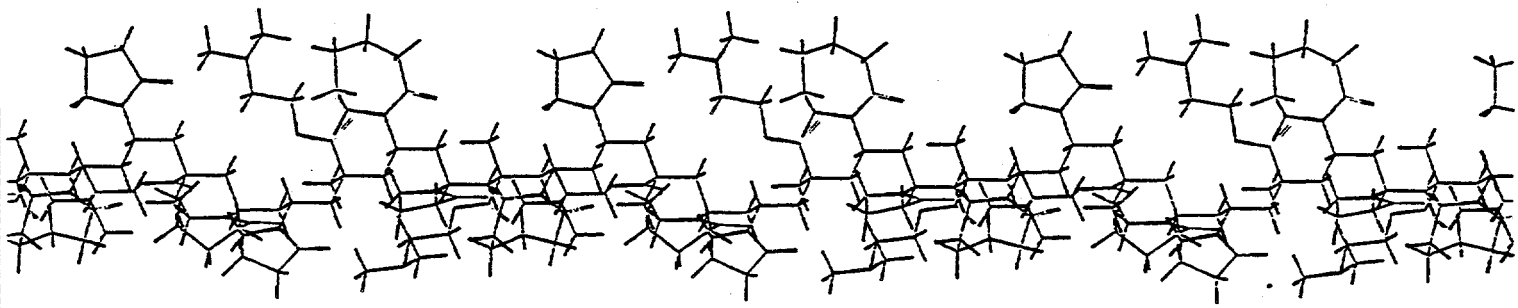

18.45 Å

Figure 77,

WINTER FLOUNDER POLYPEPTIDE, PVP, AND VC-713 POLYMERS

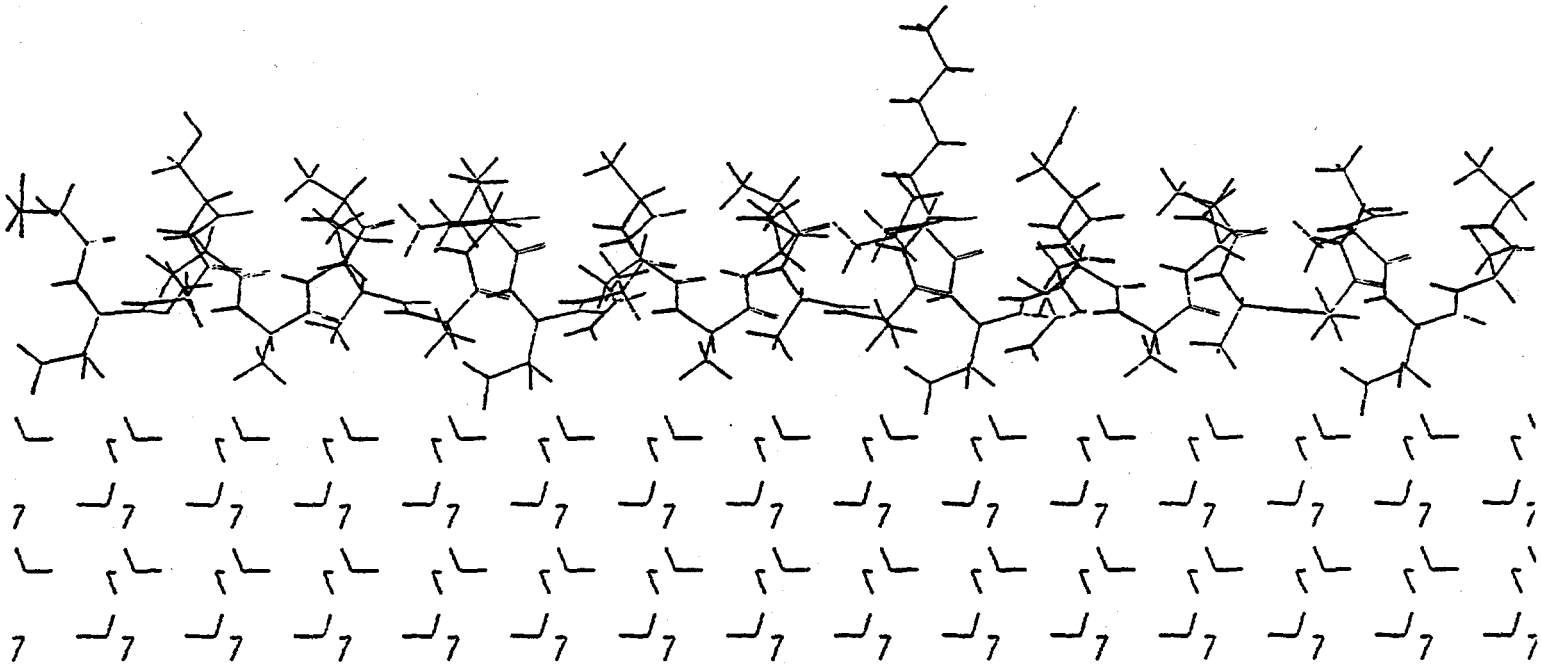

Figure 78.

WINTER FLOUNDER POLYPEPTIDE FITTING ON ICE

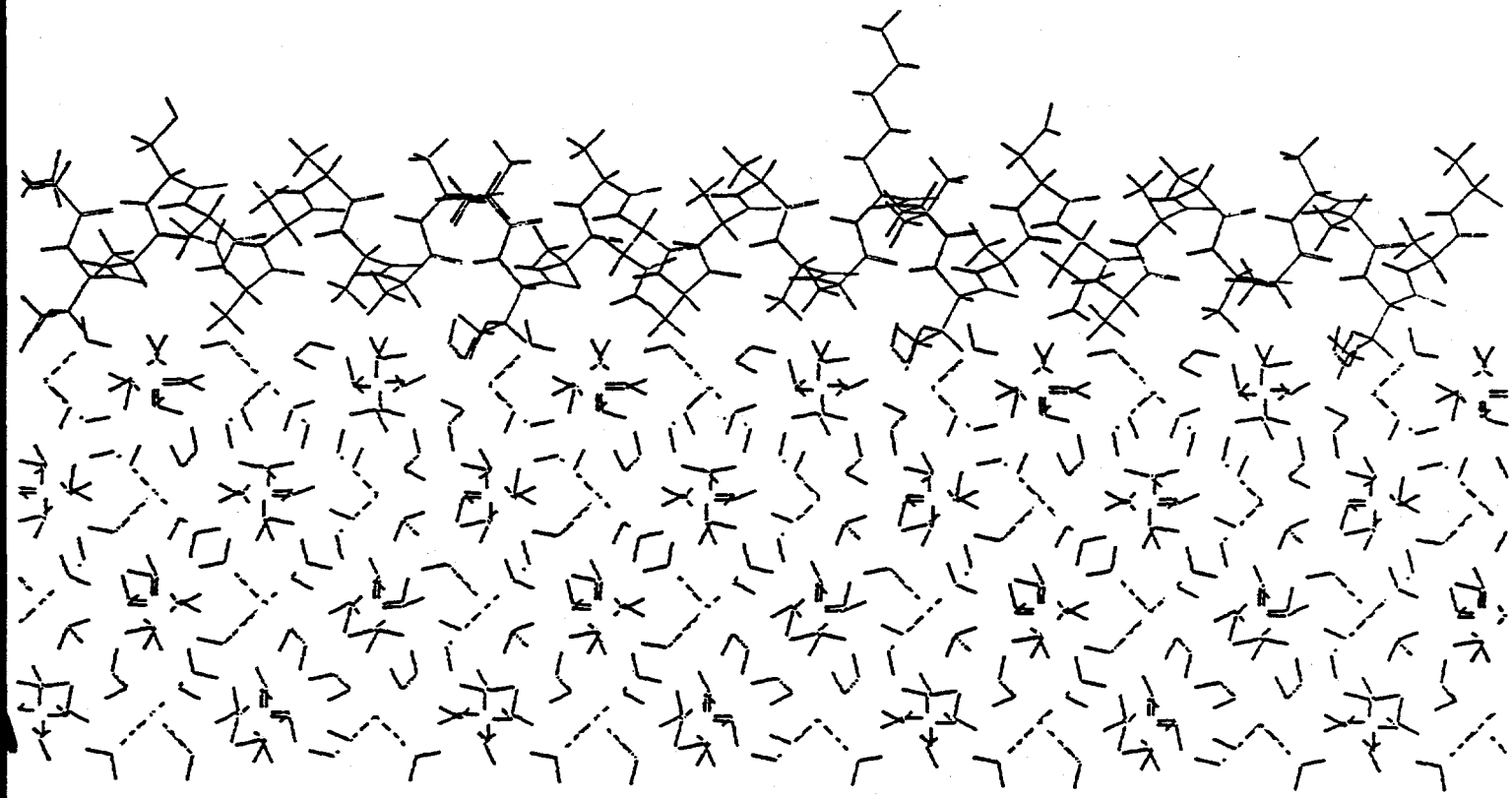

Figure 79.

WINTER FLOUNDER POLYPEPTIDE FIT ON STRUCTURE II

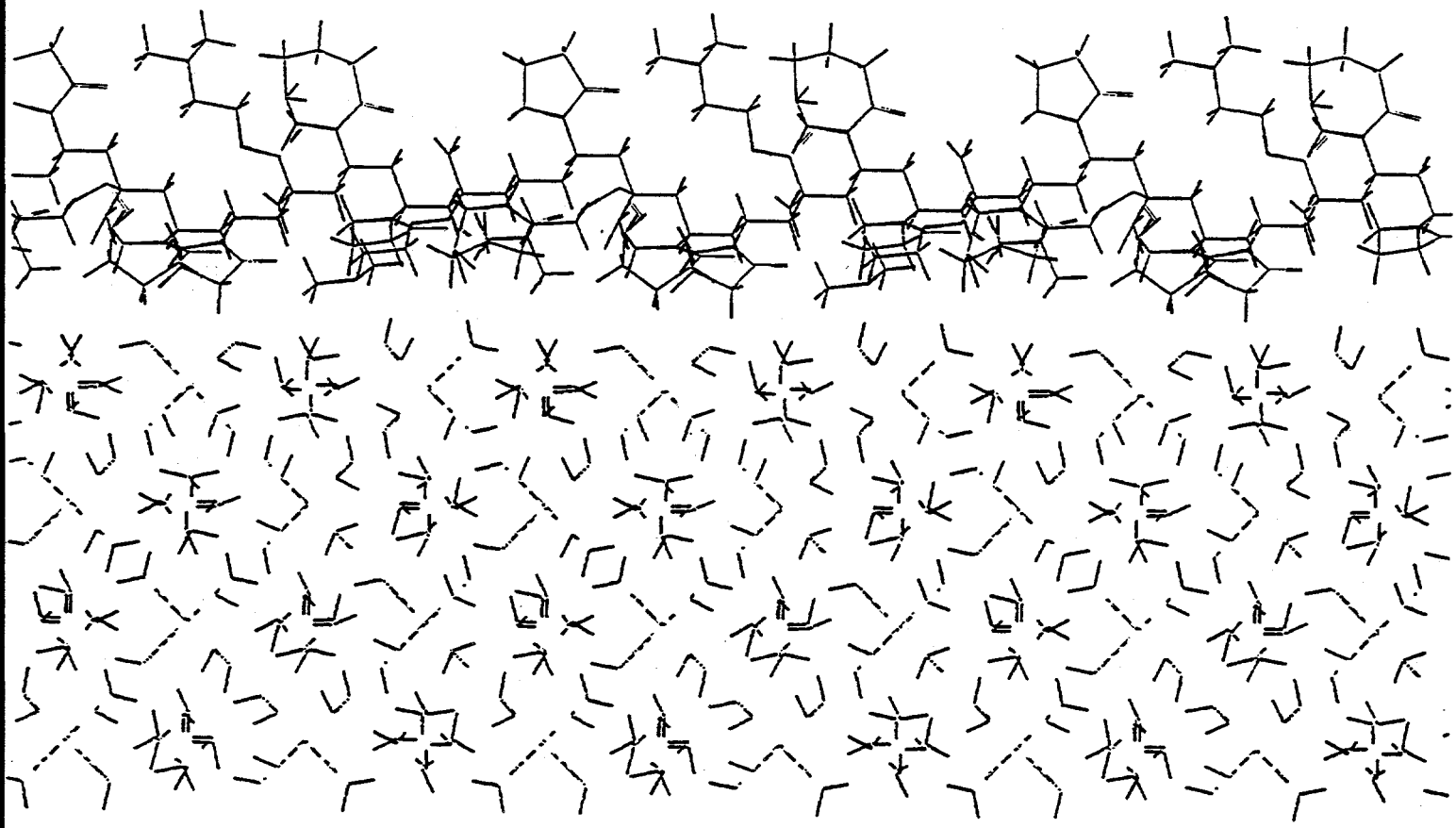

Figure 80.

FITTING OF VC-713 POLYMER ON STRUCTURE II

(300K), and
3) 1000 time steps in microcanonical NVE ensemble.

The second part of each run was the data collection for 10000 time steps in NVE ensemble.

Data Analysis

As a first step in our analysis we compared the simulated water to experimental values of water, to determine the physical reality of the system. After each run was finished, an ASCII file with coordinates of particles in time was generated and processed with a Fortran program to obtain the oxygen-oxygen radial distribution function (RDF). The RDF is an indicator of the density of water on a molecular scale by indicating the probability of finding a water molecules at any distance from another particle.

Radial distribution functions for three models were compared against the experimental data of Narten and Levy (J. Chem. Phys., 55, 2263 (1971)) for water at density (1.01 g/cc) and temperature (298 K). A comparison of simulations with the data, shown in Figure 81, indicates that SPC and TIP3p models are in good agreement with experiment while the Tripos model doesn't represent the water structure well.

Water molecules are H-bonded to each other and form ring-like structures. Two programs have been developed for determining the H-bond patterns in water. These program will permit a determination of the effects of inhibitors on the number distribution of H-bonded water molecules in rings.

Solvation of the 10-link chain PVP polymer in 860 TIP3P water molecules was performed and the whole system was equilibrated as described above. Data on hydrogen bonding to the solute was analyzed in this run, resulting in 5 oxygens of the PVP molecule which were hydrogen bonded to the water solvent. Similar run will be performed for PVP which is solvated in SPC water.

Conclusion

It was determined that SPC and TIP3P models for water incorporated in Sybyl give adequate representation of the structural properties of water. The tools for analyzing the structure of water were developed and are being enhanced.

IV.B.6.c. Interfacial Studies of Hydrate Nucleation

These studies were initially aimed at the construction of a hydrate-water interface, as a preliminary measure to the insertion of a polymer at the interface. This year the solid -

Figure 81. Radial distribution function for different water models

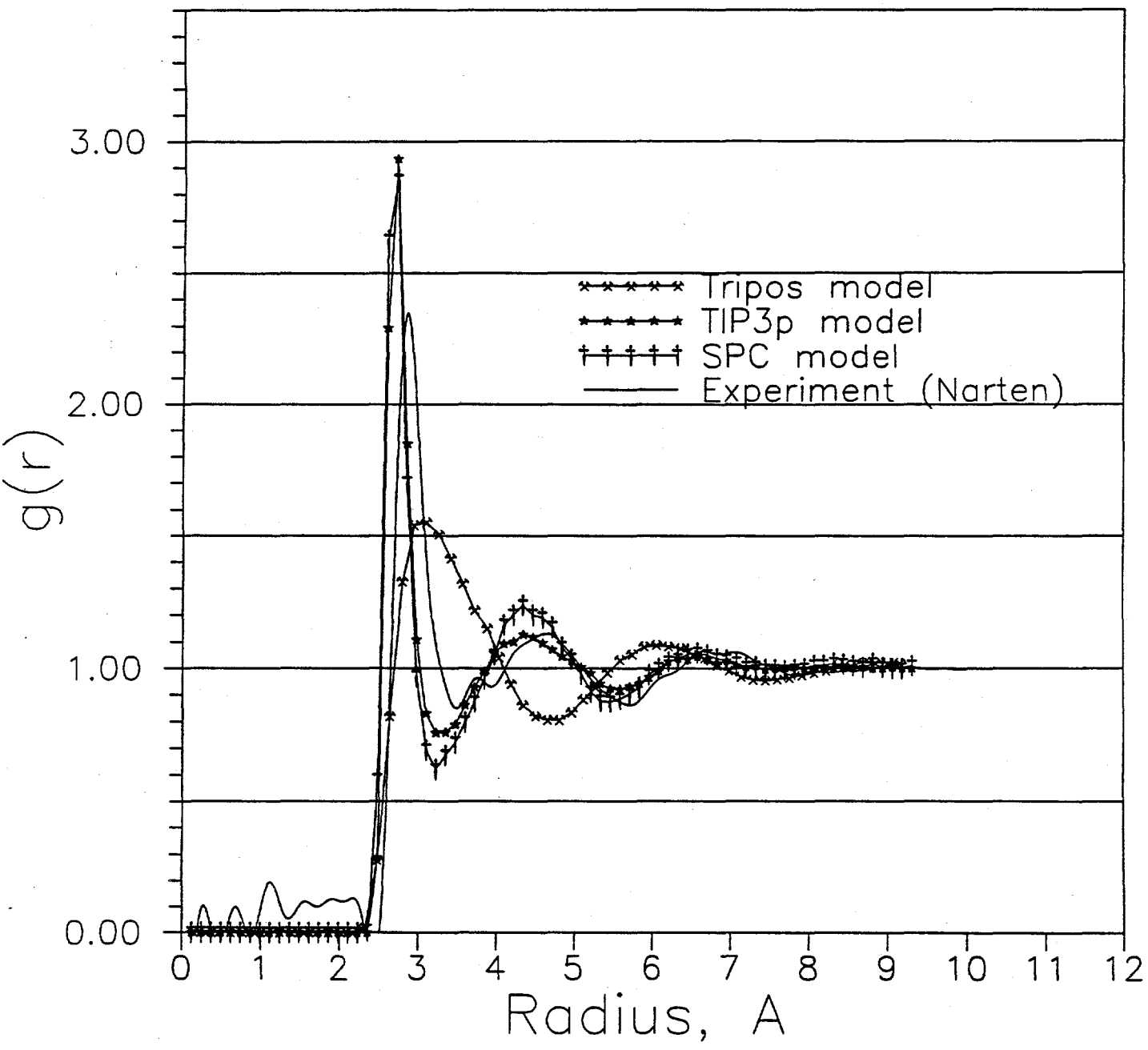

liquid interface computer simulation studies were extended to structure II clathrate hydrates. As in the studies for the solid ice and structure I hydrate interfaces, two quantities were calculated: the oxygen density profile (an indication of how many oxygens are found in thin slabs parallel to the interface) and the translational mean square displacements (an indication of the degree of translational motion of the molecules). These are shown in Figures 82 and 83.

In addition, two additional properties were calculated to give an indication of the orientation of the molecules across the interface. First these is an orientational mean square displacement. This is identical to the translational mean square displacement except it reveals how far the orientation of a molecule has changed from an initial time. This result applied to the ice interface is shown in Figure 84 and those for the hydrate interfaces are shown in Figures 85 and 86. The results are qualitatively similar to those of the translational mean square displacement; the rotation of molecules in the liquid near the interface is impeded from that in the bulk. The orientation of molecules in the crystal lattices is held quite rigid by the intermolecular forces.

The second quantity studied is the orientational autocorrelation factor which is an indication of the "memory" of a molecule to remember its initial orientation. In a crystal, molecular orientations vibrate around some fixed spatial position, so the memory effect is infinitely long, hence the autocorrelation factor does not vary over time significantly from unity. For a liquid, however, the orientations are always changing, and the autocorrelation factor eventually decays to near zero. Figures 87, 88, and 89 show the autocorrelation factor as a function of time for the slabs across the interfaces of the three systems. The effect of the interface as revealed by this parameter is observed several angstroms into the liquid, and scarcely at all in the solid.

There was no significant variation in the behavior of the structure II hydrate system from the structure I system studied earlier. The principle result of this study is that molecules in the liquid near the interfaces are perturbed in an orientational sense, but their center of masses to not show any tendency to want to assume the positions characteristic of the nearby solid. This indicates that crystal growth simulations involving water may be quite difficult.

IV.B.6.c.1. Crystal Growth Studies

Originally, an integral part of this study was to investigate ice and clathrate hydrate growth. If hydrates could be observed to grow in a molecular system, this would provide a molecular tool to answer many questions about their growth.

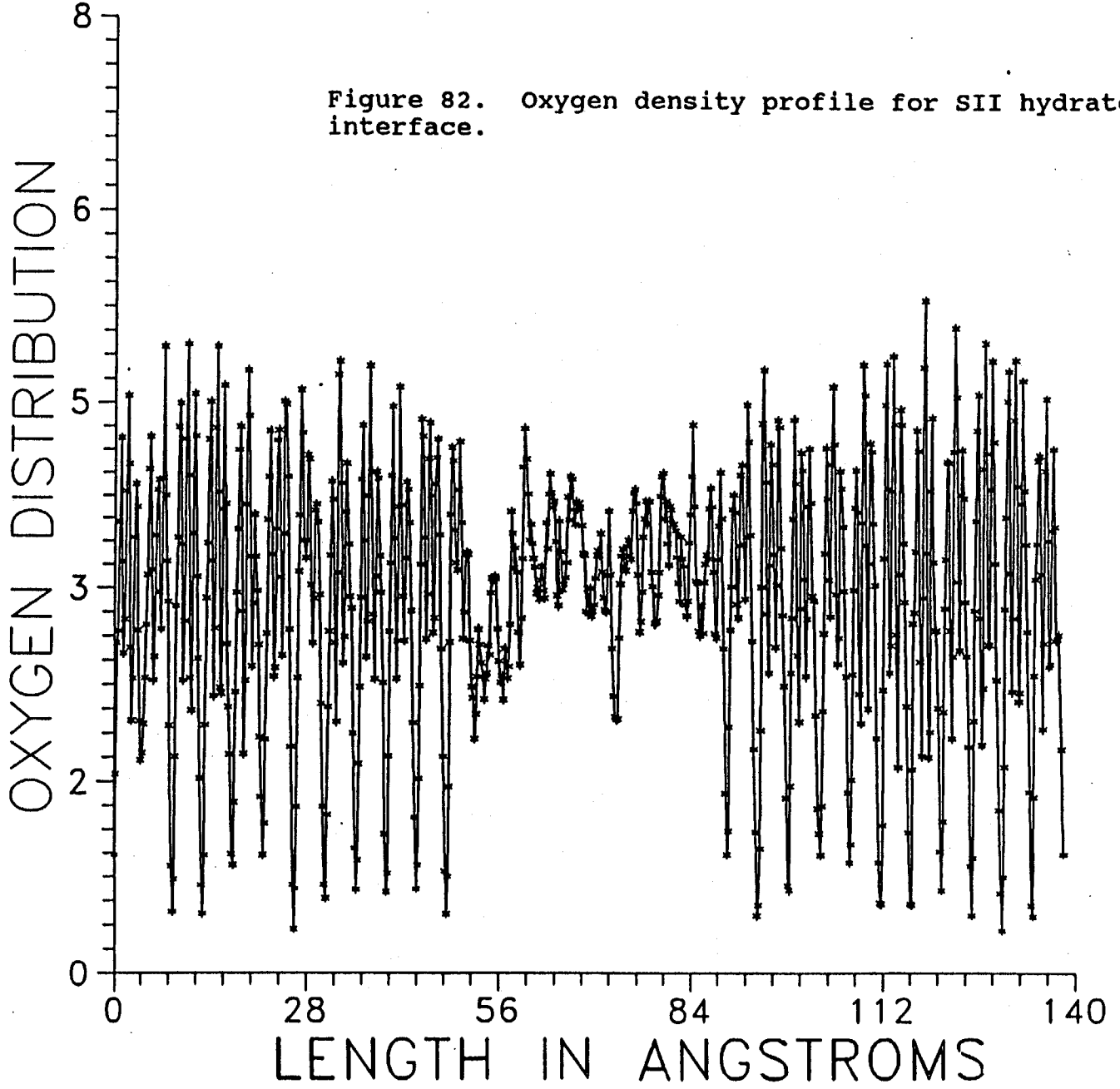

Figure 82. Oxygen density profile for SII hydrate/water interface.

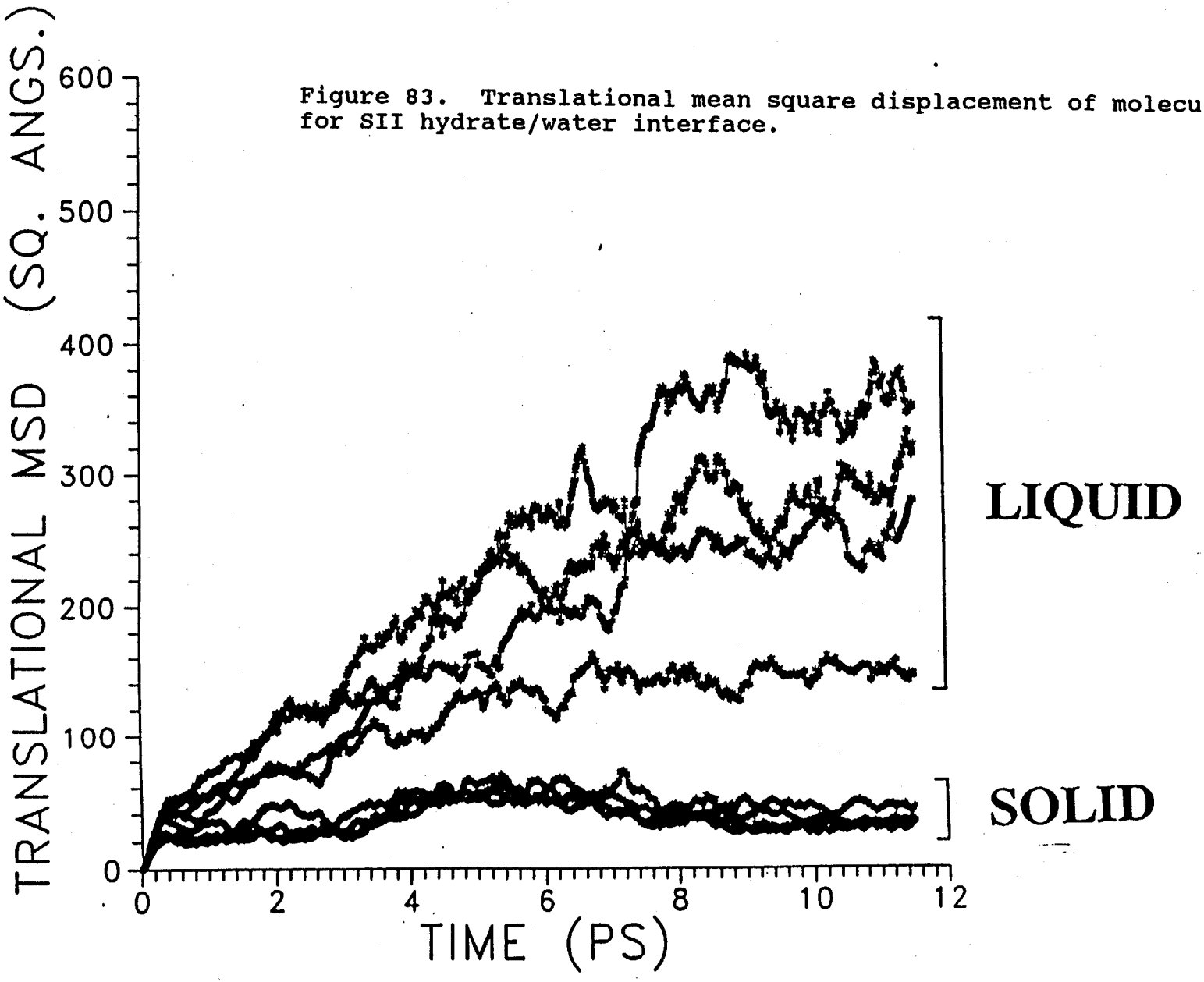

Figure 83. Translational mean square displacement of molecules for SII hydrate/water interface.

Figure 84. Orientational mean square displacement of molecules for ice/water interface.

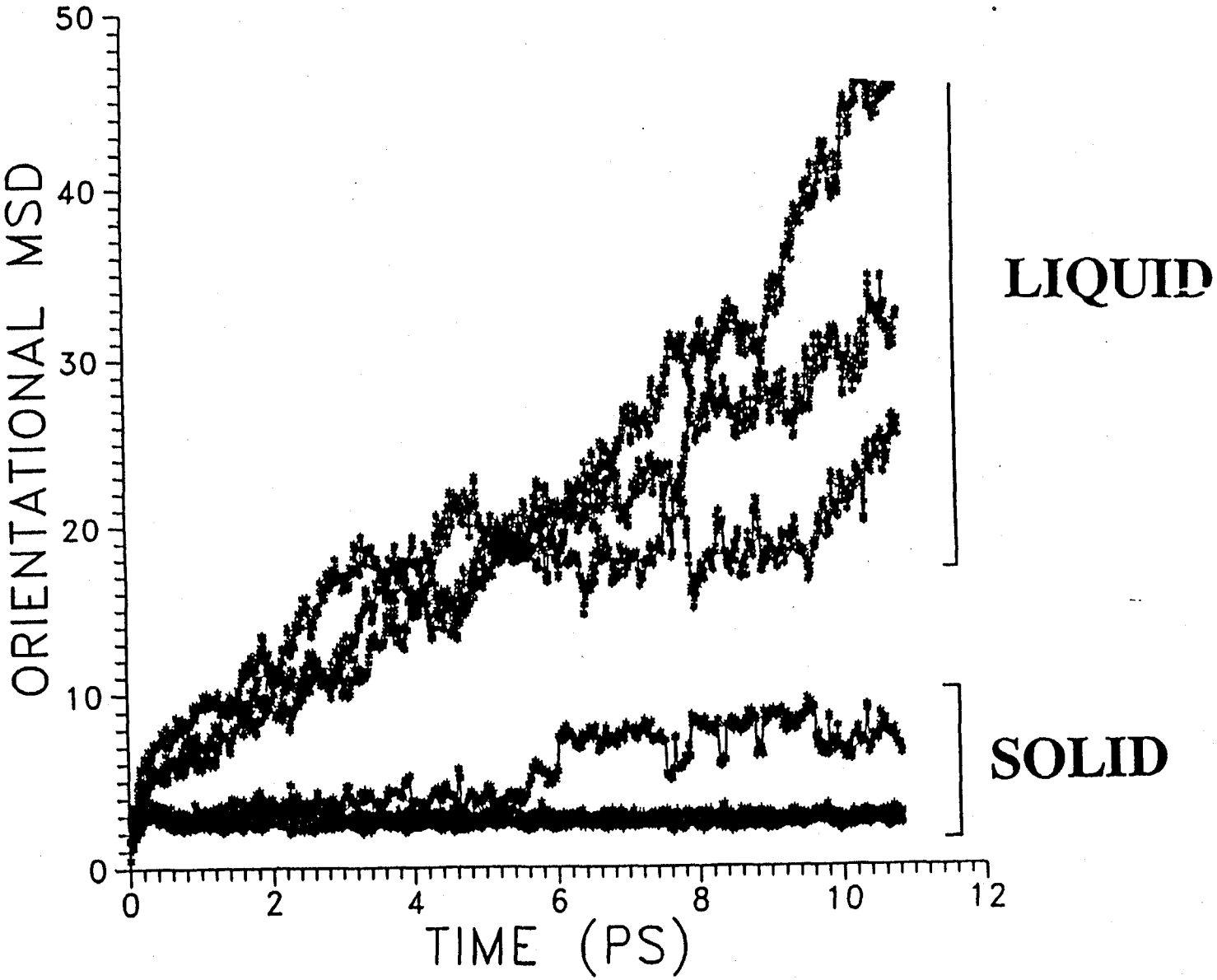

Figure 85. Orientational mean square displacement of molecules for SI hydrate/water interface.

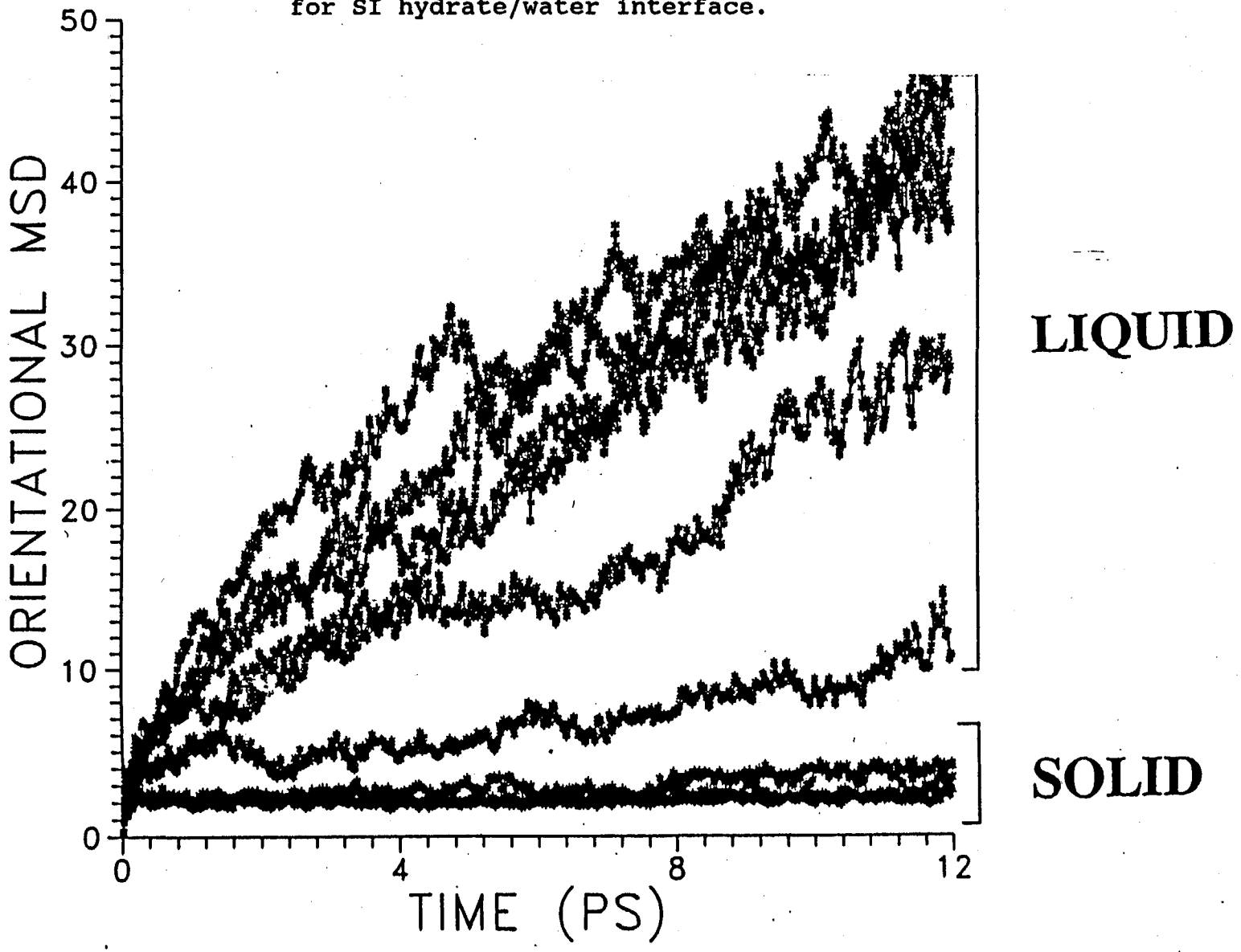

Figure 86. Orientational mean square displacement of molecules for SII hydrate/water interface.

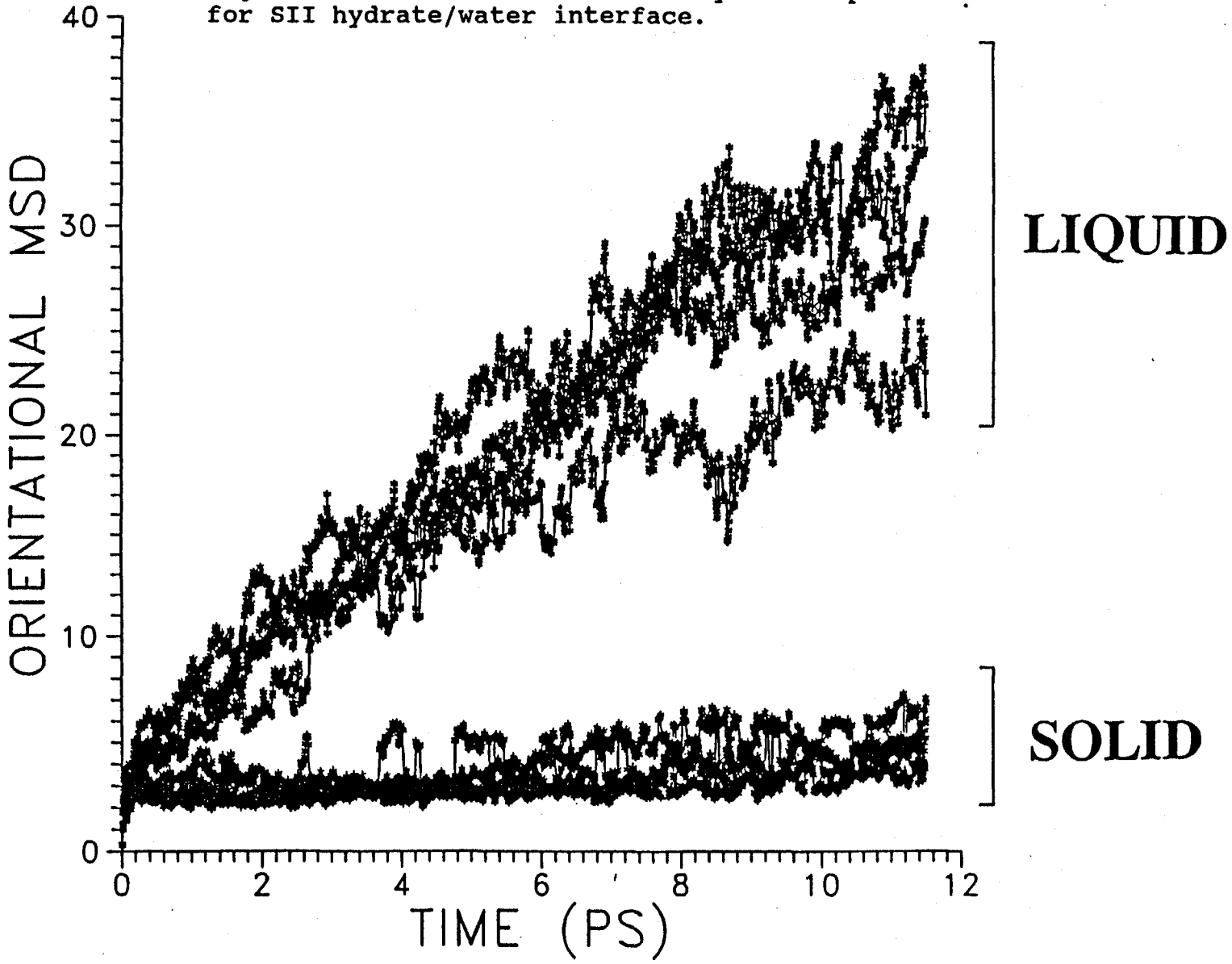

Figure 87. Autocorrelation factor for orientation of molecules for ice/water interface.

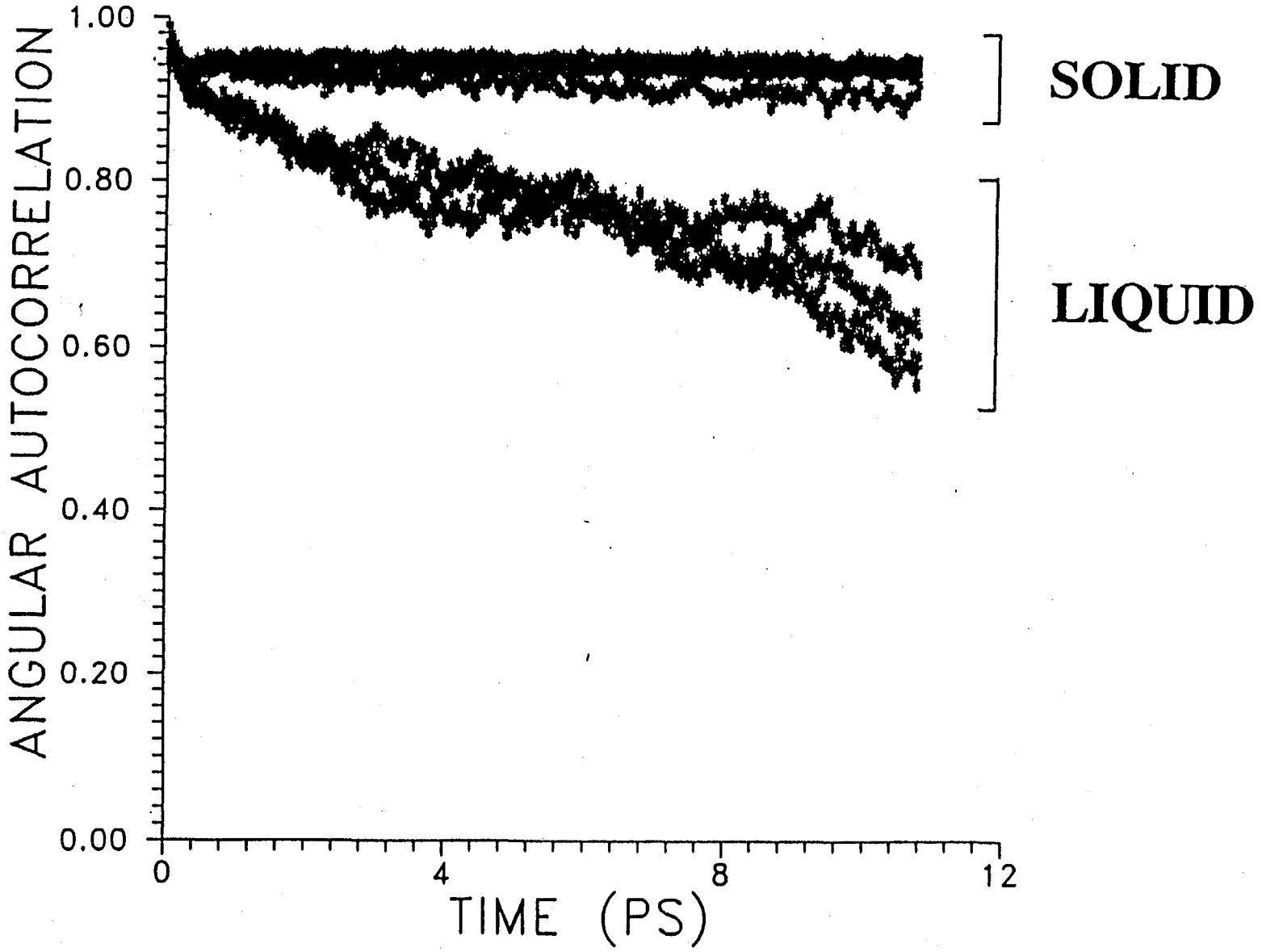

Figure 88. Autocorrelation factor for orientation of molecules for SI hydrate/water interface.

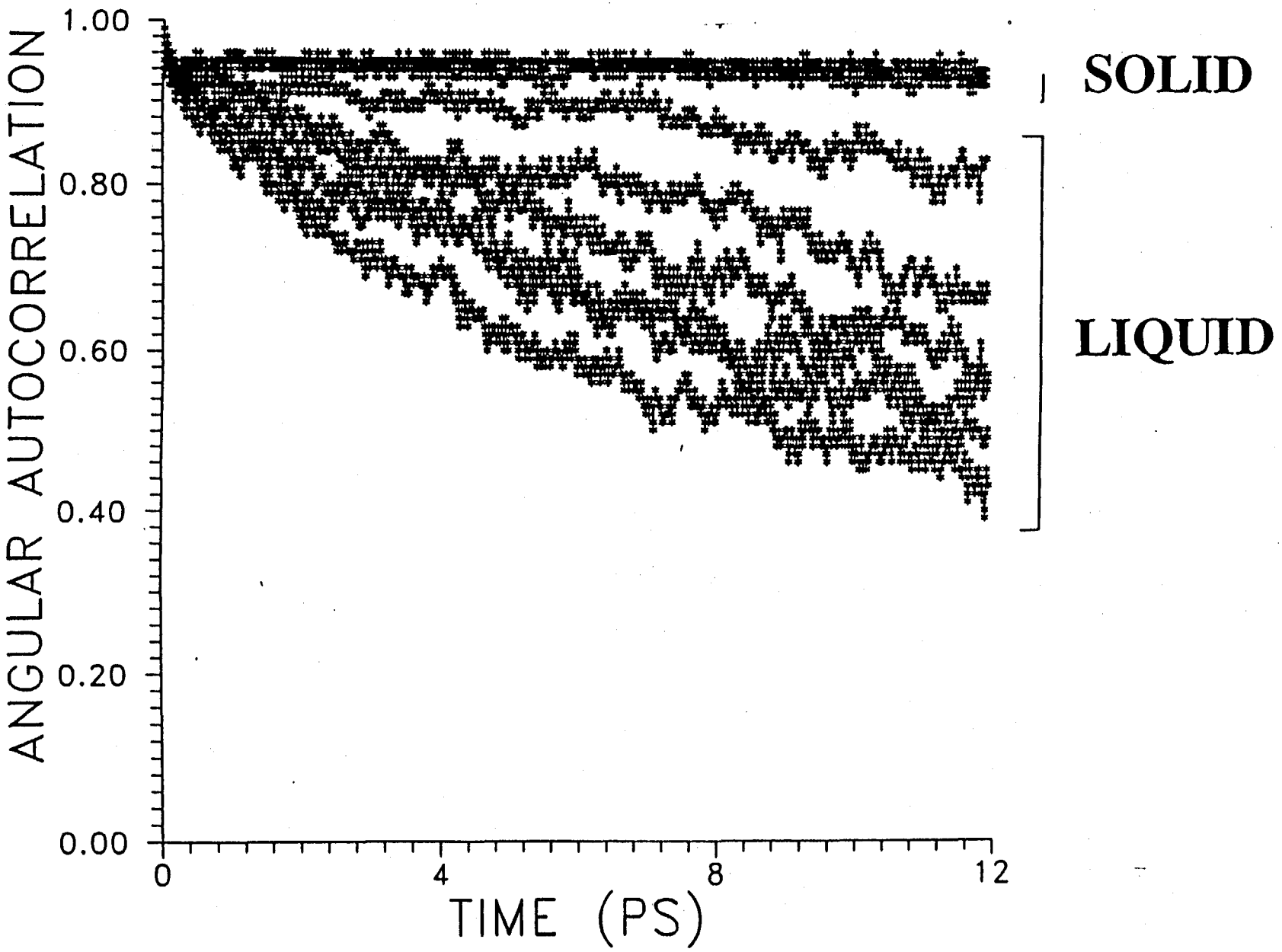

Figure 89. Autocorrelation factor for orientation of molecules for SII hydrate/water interface.

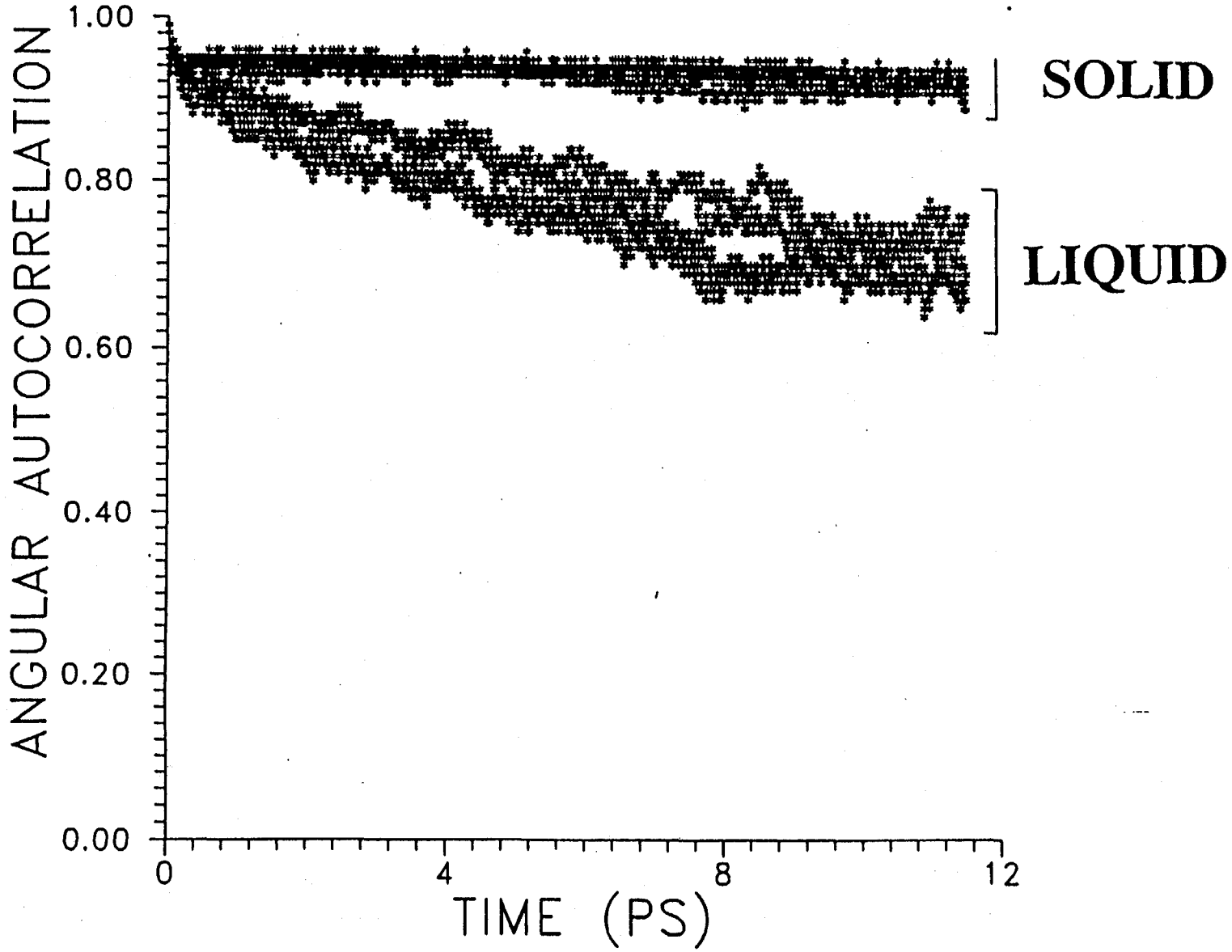

An initial system consisted of a solid structure I hydrate seed consisting of about 400 molecules placed in a super saturated water - hydrocarbon liquid solution. The immediate formation of many small water clusters around each hydrocarbon molecule gave hope that the growth of hydrates could be observed.

However, during the period of time investigated, no further similarities to solid hydrates were observed. Specifically, the problem seems that it is not possible to get the labile cages to differentiate between pentagonal dodecahedral and tetrakaidecahedral forms. This would be a key mark to distinguish formation of clathrate hydrates from a spurious simulation result. A similar work, by Luis Baez at Cornell University was presented at the New York Academy of Sciences meeting in June, 1993. The results were at best equivocal, and did not receive support from the attending molecular dynamics community. Because of these results prior to the conference, and the objections posed at the conference, no further work has been done on directly trying to observe hydrate growth via molecular simulation.

To date, there have been no reports in the literature of the successful growth of ice 1h from a water melt using computer simulation, an analogous system to hydrate growth. However, since we have software set up to readily investigate this phenomenon, we attempted to observe ice growth in a couple of relatively small systems. Since well equilibrated ice - water interface planes existed in earlier simulation, it was attempted to observe planar growth by lowering the temperature into the subcooled region and allowing the system to evolve over a long period of time. Simulations at 500 picoseconds failed to revel any growth or enhancement of ice-like order in the liquid water near the interface. As in the interface studies, there was an orientational tendency, without a translational tendency for the water molecules near the interface to align themselves to resemble ice.

It was attempted to perturb eight water molecules away from their ice lattice position and orientations and allow them to reorganize themselves over time back to an ice - like configuration. The eight molecules were placed in the center of a solid ice mass consisting of around 1600 molecules, such that the overall density of the system was consistent with solid ice at its melting point. Even this small number of molecules was unable to recover its structure over a time of about 30 picoseconds. The results of these studies show that any degree of perturbation may be made to the **orientational** configuration of an ice lattice, and the hydrogen bonding will cause the lattice to relax into a stable ice 1h configuration. However, even a small **translational** perturbation made to the ice system causes the ice to "melt" into an amorphous, glassy substance. Further attempts to grow crystals have been put aside.

IV.B.6.d. Hydrophobic Interactions

The hypothesis previously advanced by this laboratory suggests that hydrocarbons dissolved in water form water clusters as a precursor to hydrate formation. Because the solubility of the hydrocarbons in water is so low, it is difficult to carry out spectroscopic measurements on these systems, thus it was felt that molecular simulation might be a viable tool to investigate these phenomena.

The question to be answered was whether these clusters have a tendency aggregate together, and if so, does this mass show a tendency to assume the structure of clathrate hydrates. Much of the literature to date shows that the agglomeration tendency becomes stronger at higher temperatures and lower pressures. The simulation results of Skipper (Chem. Phys. Let., 207, 424, 1993) for a water mixture at 320K, 1 g/cc indicate a tendency to form an aggregate, while the same system at 300 K forms a transient labile mass, and the system at 270K shows a tendency for the hydrocarbons to repel each other. At the same time, a super concentrated solution at lower pressures will tend to form a two phase liquid mixture, while the system at higher pressure remains a uniform mixture. As mentioned earlier, there was also no tendency for differentiation between cavity types from a supercooled agglomeration of these clusters.

Our work to date has been largely devoted to verifying phenomena found in the literature, but as of yet our simulation results do not support the concept of hydrate formation by agglomeration at their temperature/pressure conditions. Future work will be concerned with answering this question.

V. What is Proposed in 1994

In 1994 we will come much closer to resolving the best kinetic inhibitors through a series of objectives, aided by several personnel changes.

V.A. Objectives for 1994

The following four major objectives will shape the work in 1994:

V.A.1. Define a Rational Approach for Inhibitor Design.

We will define a better inhibitor mechanism, principally through modification of the one set forth in this report. We will supplement the macroscopic work in Objective 3 (below) with microscopic Raman and UV-Visible spectroscopy, and we will begin

to consider light scattering. The computer simulation of hydrate growth will be reduced in scope for 1994.

V.A.2. Improve Inhibitor Performance.

In 1994 we will design and fabricate inhibitors in accordance with the approach found in Objective 1. We will complete the survey of all chemical commercially available as well as begin to synthesize and test new polymers/surfactants in our laboratory. Section IV.B.1.c. gives examples of chemicals to be synthesized.

V.A.3. Test Inhibitors on CSM Apparatuses and Exxon Flow Loop.

We will continue to use the screening, high pressure, and sapphire apparatuses. A senior graduate student will complete a test of the best 1993 chemicals on the Exxon flow loop in Houston and resulting transferability between the CSM apparatuses and the flow loop will be defined.

V.A.4. Act as a Forum for Sharing Field & Pilot Plant Results.

At our two consortium meetings, we will provide a forum for sharing the field results from each company which has tested the chemicals. In addition all of the Exxon flow loop results will be examined in Consortium meetings.

V.B. Personnel Changes to Accomplish Objectives

The area of most substantial personnel change is the area of inhibitor concept and synthesis, with the addition of two professional chemists in late 1993, Dr. V. Panchilingham (full time) and Dr. Howard Angstadt, as a consultant. Dr. Panchilingham joins the group as a postdoctoral fellow, with more than 8 years of organic polymer chemistry experience in other postdoctoral positions. Dr. Howard Angstadt comes to the group as a organic chemical consultant, after retiring from a substantial, productive career as an organic chemist with Sun Company, Inc.

Since the area of Raman spectroscopy has proved beneficial to our molecular understanding, we have entered into a cooperative research agreement (CRADA) with Dr. Robert C. Burruss of the U.S. Geological Survey (Denver Federal Center). This agreement will enable us to continue the use of the sophisticated and expensive Raman device at U.S.G.S. while protecting the proprietary nature

of the inhibition chemicals generated on this project.

A number of graduate student personnel changes will also occur. Joe Lederhos will return to the laboratory after completing work on the Exxon flow loop in Houston. Jinping Long (sapphire apparatus), Xiaoping Long (Raman spectroscopy), and Ron Pratt (molecular simulation) will graduate from the laboratory. Mr. Y. Du will join the laboratory as an experienced, older graduate student, who has completed a Master's thesis and published in the area of hydrate prediction.

APPENDIX A

COMPANIES IN THE CONSORTIUM AT THE CENTER FOR HYDRATE RESEARCH
Colorado School of Mines

NAME & ADDRESS	PHONE NO.	FAX NO.
1. Dr. George Shoup **Amoco Production Co.** Tulsa Research Center P. O. Box 3385 Tulsa, OK 74102	(918) 660-4349	(918) 660-3274 (918) 660-4163
2. Mr. Ben Bloys **ARCO Oil & Gas Co.** E&P Technology Services 2300 West Plano Parkway Plano, TX 75075	(214) 754-3261	(214) 754-3280
3. Dr. John L. Cayias **Oryx Energy Company** 13155 Noel Road Dallas, TX 75240-5067	(214) 715-4423	(214) 715-4419
4. Dr. William Young **Exxon Production Research Co.** Production Operations P. O. Box 2189 Houston, TX 77402	(713) 965-4362	(713) 966-6387
5. Mr. Kerry J. Van-Son **Mobil R & D Corp.** 13777 Midway Road Dallas, TX 75244-4312	(214) 851-7120	(214) 851-8349
6. Dr. V. R. Kruka **Shell Development Co.** P. O. Box 1380 Houston, TX 77251-13807	(713) 544-7118	(713) 544-8826
7. Dr. Luis Chu **Conoco Inc.** Research & Development P. O. Box 1267 Ponca City, OK 74601	(405) 767-4184	(405) 767-6533

NAME & ADDRESS	PHONE NO.	FAX NO.
8. Mr. Phil Notz **Texaco Inc.** P. O. Box 425 Bellaire, TX 77402	(713) 432-2281	(713) 432-6929
9. Mr. Pat Shuler **Chevron Oil Field Res.** P. O. Box 446 La Habra, CA 90633-0446	(310) 694-7572	(310) 694-7746
10. Dr. Rodney D. Malone **Dept. of Energy** Morgantown Energy Tech. Centr. Collins Perry Road Morgantown, WVA 26505	(304) 291-4723	(304) 291-4469
11. Dr. R. G. Thompson **Marathon Oil Company** Petroleum Technology Center P. O. Box 269 Littleton, CO 80160-0269	(303) 794-2601	(303) 794-1720
12. Dr. W. R. Parrish **Phillips Petroleum Co.** Research & Development Bartlesville, OK 74004	(918) 661-9651	(918) 662-2870
13. Mr. Alexandre Mussumeci **Petrobras** Production Engineer CENPES/DIPLOT Cidade Universitaria - Quadra 7 Iiha do Fundao CEP 21910 -RJ BRAZIL	55-21-598-6548	55-21-598-6796

APPENDIX B

Colorado School of Mines
Center for Hydrate Research

Budget Summary for the Consortium Account

Expenses inccurred in 1992	**Amount $**	**Expenses for 1993**	**Amount $**
Salaries Academic Faculty $70,000 Undergrad. students 14,000 Graduate students 68,000 P/T Sec. & Technician 31,000	183,000	Salaries Academic Faculty $70,000 Undergrad. students 14,000 Graduate students 70,000 P/T Sec. & P/T Technician 25,000 Post Doctoral Fellow - Salary & Fringe 37,000 Patents 20,000	236,000
Equipment and Supplies	30,000	Equipment and Supplies	30,000
Travel (10 Hydrate Lab members travel expense to attend the ISOPE Conf. in San Francisco in June 1992)	12,000	Travel (10 Hydrate Lab members travel expense to attend the Int. Hydrate Conf. New Paltz, NY in June 1993)	12,000
Other Costs	51,000	Other Costs (Courier, Freight, Official Functions, etc.)	50,000
Overhead	84,000	Overhead	83,000
Total	**360,000**	**Total**	**411,000**

APPENDIX C

CONCEPTUAL DESIGN OF POLYMER RECOVERY

KINETIC HYDRATE INHIBITORS VC713 AND PVP

Senior Design Group:

Michael Gordon
Heidi Gusich
Rocky Hill

October 26, 1993

Presented to:

Dr. Veenkant
Special Research Associate
Amoco Production Company

Executive Summary

The Chemical Engineering & Petroleum Refining class of Fall 1993 has been asked to design and economically justify a polymer / water separation scheme for Amoco. The polymer will be in an aqueous solution and injected into a gas process pipeline to inhibit the formation of hydrates. This system must concentrate the aqueous phase in polymer at a level adequate to assure a pipeline *in situ* concentration of 0.4 w/w%. The system of choice will be economically more favorable than the current inhibition system.

Two polymers, PVP and VC-713, have been chosen as likely candidates to replace the current inhibitor MEG. This design team has investigated a separation scheme specific to each polymer and a third system applicable to both. The underlying method of separation for all systems is based on size exclusion. The best method of separation specific to VC-713 utilizes its cloud point at 100 °F. Once the cloud point is reached, the polymer phase may be removed from the aqueous phase by microfiltration. Since no cloud point was known to exist for the PVP, a solvent / non-solvent system was devised to bring the polymer out of solution. Laboratory tests indicate a 50% v/v mixture of acetone with the aqueous polymer will cause dissolution of the PVP. Once the polymer is out of solution, it may again be removed via microfiltration. Further study into separation technology revealed a method called ultrafiltration. This technology is well developed and may be used to remove dissolved solids much smaller than either polymer under consideration, thus requiring no fractional dissolution prior to separation. Though further pilot plant work is recommended, literature substantiates the use of ultrafiltration to remove PVP from water. Preliminary economic evaluation suggests that ultrafiltration is the best separation technology presented.

Table of Contents

Page

Introduction to the Polymer Recovery and Re-injection Study 1

Feasible Separation Design Systems 1

Types of Membranes 2

Operational Procedure 5

- Acetone Fractional Dissolution for PVP 5
- VC-713 Cloud Point Dissolution Procedure 5
- Ultrafiltration for VC-713 and PVP 5

Economic Summary 10

Conclusions 21

Recommendations 22

List of References 23

List of Figures and Tables

Figures **Page**

Figure 1: Flat Sheet Membrane Module 3

Figure 2: Tubular Membrane Module 4

Figure 3: Spiral Wound Membrane Module 4

Figure 4: Acetone Fractional Dissolution for PVP: Process Flow Schematic 6

Figure 5: VC-713 Cloud Point Dissolution Procedure: Process Flow Schematic 7

Figure 6: Ultra-Filtration for PVP and VC-713: Process Flow Schematic 8

Tables **Page**

Table 1: Design and Cost Calculations for Ultra-filtration 11

Table 2: Economic Summary: Acetone Fractional Dissolution for PVP 12

Table 3: Economic Summary: VC-713 Cloud Point Dissolution Procedure 14

Table 4: Economic Summary: Ultra-Filtration for PVP and VC-713 16

Table 5: Cash Flow Summary: Acetone Fractional Dissolution for PVP 18

Table 6: Cash Flow Summary: VC-713 Cloud Point Dissolution Procedure 19

Table 7: Cash Flow Summary: Ultra-Filtration for PVP and VC-713 20

INTRODUCTION TO THE POLYMER RECOVERY AND REINJECTION STUDY

The purpose of this study was to economically justify replacing the current Amoco hydrate inhibitor with one of two polymers, PVP or VC-713. Daily costs for the current MEG hydrate inhibitor system are roughly $500. To justify switching to the polymer, it must be recycled to minimize make-up costs. The scope of this project is to design a separation / recycle system that economically outperforms the current system.

This paper presents the most viable separation schemes and variations where available. Optional design schemes are given as well as economic evaluations of each. Conclusions are based on the net present value (NPV) of changing from MEG relative to a 12% rate of return (ROR).

FEASIBLE SEPARATION DESIGN SYSTEMS

Literature survey suggests that two of the most promising separations for aqueous polymer systems are fractional dissolution and ultrafiltration. For VC-713, fractional dissolution is accomplished via the cloud point while a water / acetone solvent / non-solvent system can be used to fractionate PVP aqueous solutions. Ultrafiltration, however, shows application to both polymer systems.

Fractional dissolution was the first separation scheme investigated. The PVP polymer can be brought out of solution by adding equal volume amounts of acetone; whereas VC-713 requires raising the temperature above the cloud point (100 °F). Fractional dissolution has drawbacks since an additional microfiltration separation is required to concentrate the polymer after dissolution. In addition, the solvent / non-solvent system requires recovery of the non-solvent.

Separation processes are classified based on particle or molecular size. For the separation of high molecular weight organic polymers from process streams, ultrafiltration as a form of separation is commonly applied. Ultrafiltration is a process by which macromolecules are

separated and concentrated from a process stream using a membrane in a pressure driven system. Ultrafiltration allows for the solvent to filter through the membrane to the collection tube while retaining the macromolecules on the retentate side. Since this separation process is specialized for larger molecules, the osmotic pressure is often low. Also, no phase change occurs, hence, the system energy requirements are much lower than alternative separation processes.

TYPES OF MEMBRANES

Ultrafiltration membranes are sub-divided into two categories: microporous and asymmetric. Microporous membranes are membranes containing various pore sizes. These membranes selectively retain particles with greater diameters than the pore size. In our system, we are interested in retaining all of the polymer, therefore, this membrane will not work for our purposes.

Asymmetric membranes are membranes which retain almost one hundred percent of the macromolecules and allow the solvent to pass through the membrane. This macromolecule rejection takes place on the surface of the membrane which is supported on a frame. Because of this design, the pores do not plug up but they are susceptible to fouling. Fouling is the term used to describe the loss of throughput of a membrane device because it has become changed, chemically or physically, by the process fluid. Fouling results in a net flux loss which is irreversible unless cleaning is applied to the membrane.

Retention, the build-up of fouling products on the membrane, depends strongly on system conditions. Each membrane has its own rejection range. Membranes in different configurations (flat sheet supported on a frame, tubular, and spiral wound) also tend to reject differently from each other. Membrane material may also influence rejection rates. Another retention factor concerns the size and shape of the solute molecules. Large molecules are better rejected than small molecules. Operating conditions also effect the retention rate. For example, if flux increases, retention will decrease, if velocity increases, retention will increase, and if concentration increases, the retention

will also increase. Therefore, no specific characteristics can be made for a particular membrane since retention is dependent upon many important system characteristics.

Flux is defined as the permeate flow per unit membrane per unit time. When build-up occurs on the membrane, a gel layer is formed. This gel layer reduces the penetration of permeate through the membrane. To prevent this build-up, processes are often forced by pressure causing higher fluxes. Flux is also dependent on system temperature. The relationship between temperature and flux strongly depends on the membrane and the feed stock.

There are several choices to make concerning an ultrafiltration system design and operation. As mentioned above, membranes are made in several forms. The most expensive form is the flat sheet membrane which is supported by some sort of frame. The membrane is laid flat on a diagonal support device which is installed into some sort of pressurized compartment. The feed is then forced to flow over the membrane surface area and the permeate filters through membrane. Figure 1 shows an example of a flat sheet membrane

Figure 1

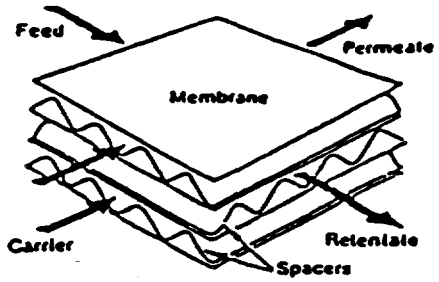

Plate and Frame Module

A second configuration is referred to as a tubular module. This type of pressure driven configuration resembles a shell and tube heat exchanger with baffles. Tubes are thin-walled and porous. Feed enters the tubes at one end and retentate exits the other end while the permeate leaves through the tube walls. Figure 2 shows an example of the tubular module.

Figure 2

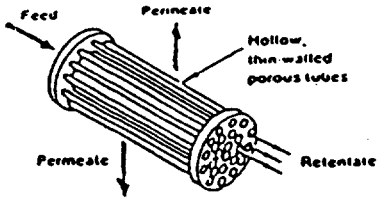

Tubular Module

The third configuration is the spiral wound membrane module. Currently, this is the most inexpensive form of membrane used for ultrafiltration. These spiral wound membranes have proven both effective in separating large organic polymers from solutions and are easily cleaned. Their design also offers a large packing density.

Spiral wound module designs consist of two membrane sheets, separated by a porous support material. This porous material both supports the membrane and provides a pathway for the permeate to flow. Membrane sheets are glued together and attached to a perforated hollow tube. This tube is the removal pathway for the permeate stream. Mesh spacers are placed between the rolls to separate the membrane surfaces. Spacers also assist the permeate flow to the center of the tube. The concentrate stream containing the polymer is removed out the end of the membrane roll. Figure 3 shows the spiral wound membrane as manufactured.

Figure 3

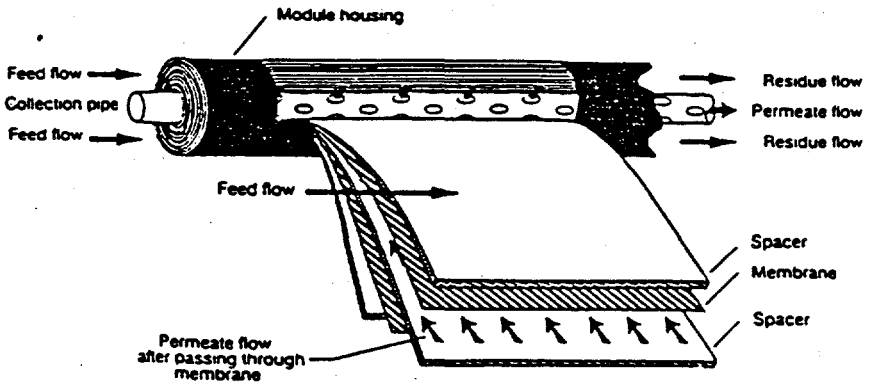

4 Spiral-wound membrane module.

OPERATIONAL PROCEDURE

Acetone Fractional Dissolution for PVP (Figure 4)

The hydrate inhibitor solution from the pipeline is pumped to a mixing chamber where it is diluted 1:1 with acetone to cause dissolution of the polymer. The aqueous / acetone polymer suspension is then pumped through a microfilter where most of the water and acetone are removed. The acetone is removed from the polymer rich phase in a flash chamber. The aqueous polymer effluent from the flash chamber is pumped to the Inde platform. Polymer lost in the separation process is replenished from a make-up tank. The water / acetone permeate from the filter unit is sent to an air stripper where the acetone is removed and mixed with the vapor from the retentate acetone flash chamber. The combined acetone vapor stream is condensed, purged of air, and recycled to the mixing chamber. Acetone reclamation is assumed to be 97% and make-up is provided from a holding tank.

VC-713 Cloud Point Dissolution Procedure (Figure 5)

The gas pipeline aqueous effluent is heated above its cloud point to cause dissolution of the polymer. The aqueous polymer suspension is pumped through a microfilter where one phase is concentrated in polymer and returned to the reinjection system after make-up is added. The permeate is sent to water treatment.

Ultrafiltration for VC-713 and PVP (Figure 6)

The aqueous gas pipeline discharge is pumped directly to a spiral wound ultrafiltration module. The filtration unit allows water to permeate through the membrane to the collection tube

Figure 4

Acetone Fractional Dissolution for PVP
Process Flow Schematic

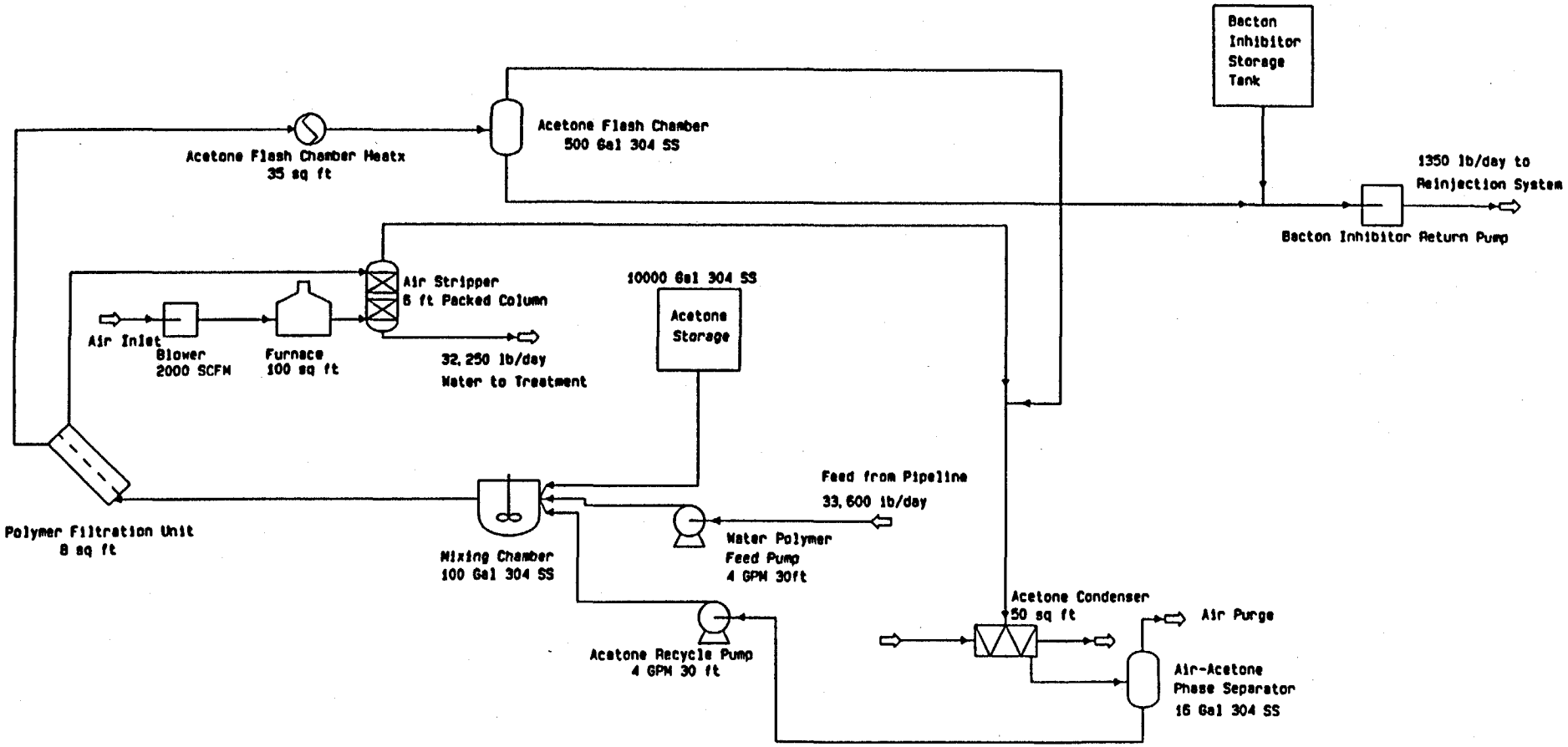

Figure 5

VC-713 Cloud Point Dissolution Procedure Process Flow Schematic

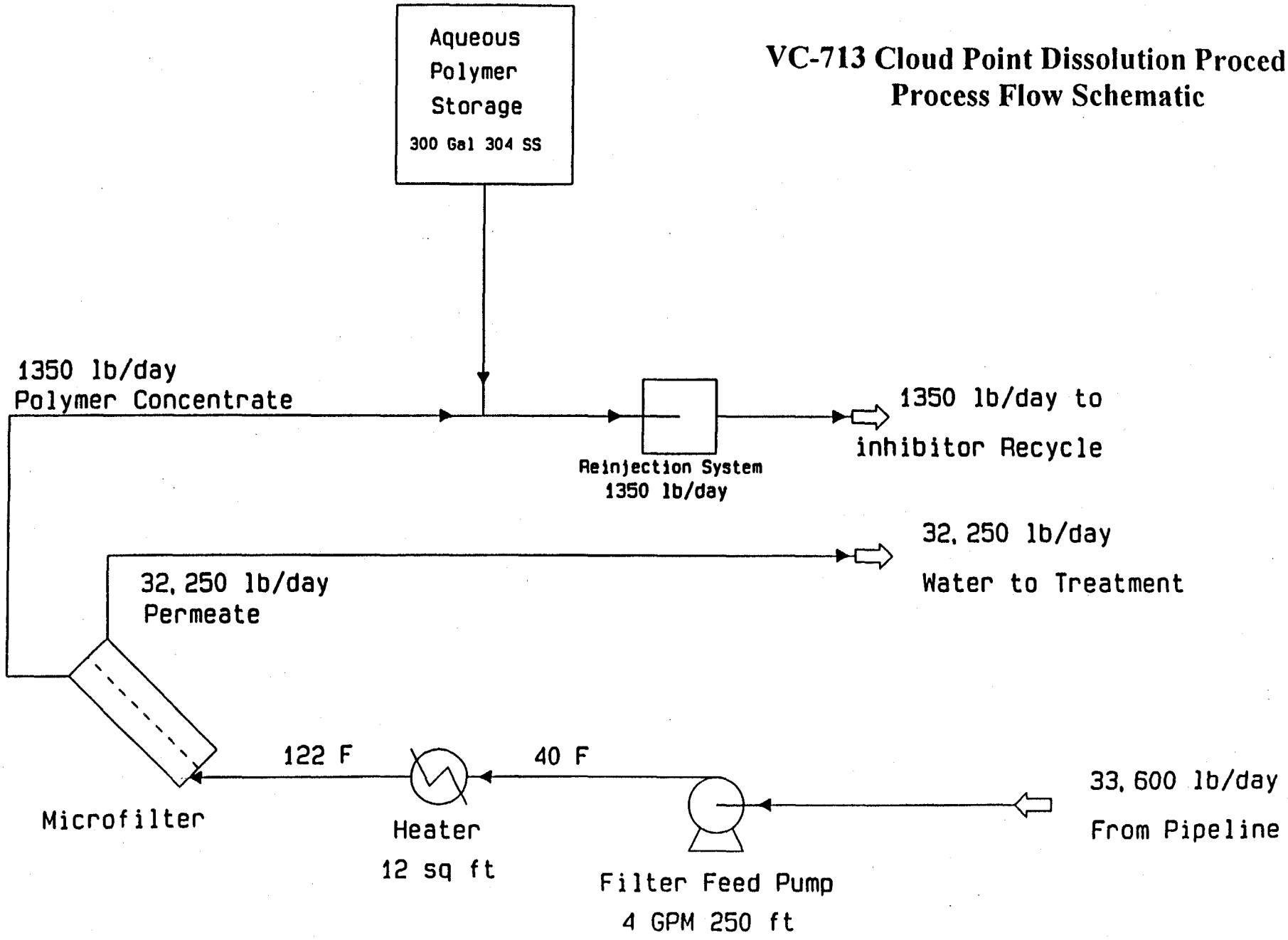

Figure 6

Ultra-Filtration for PVP and VC-713
Process Flow Schematic

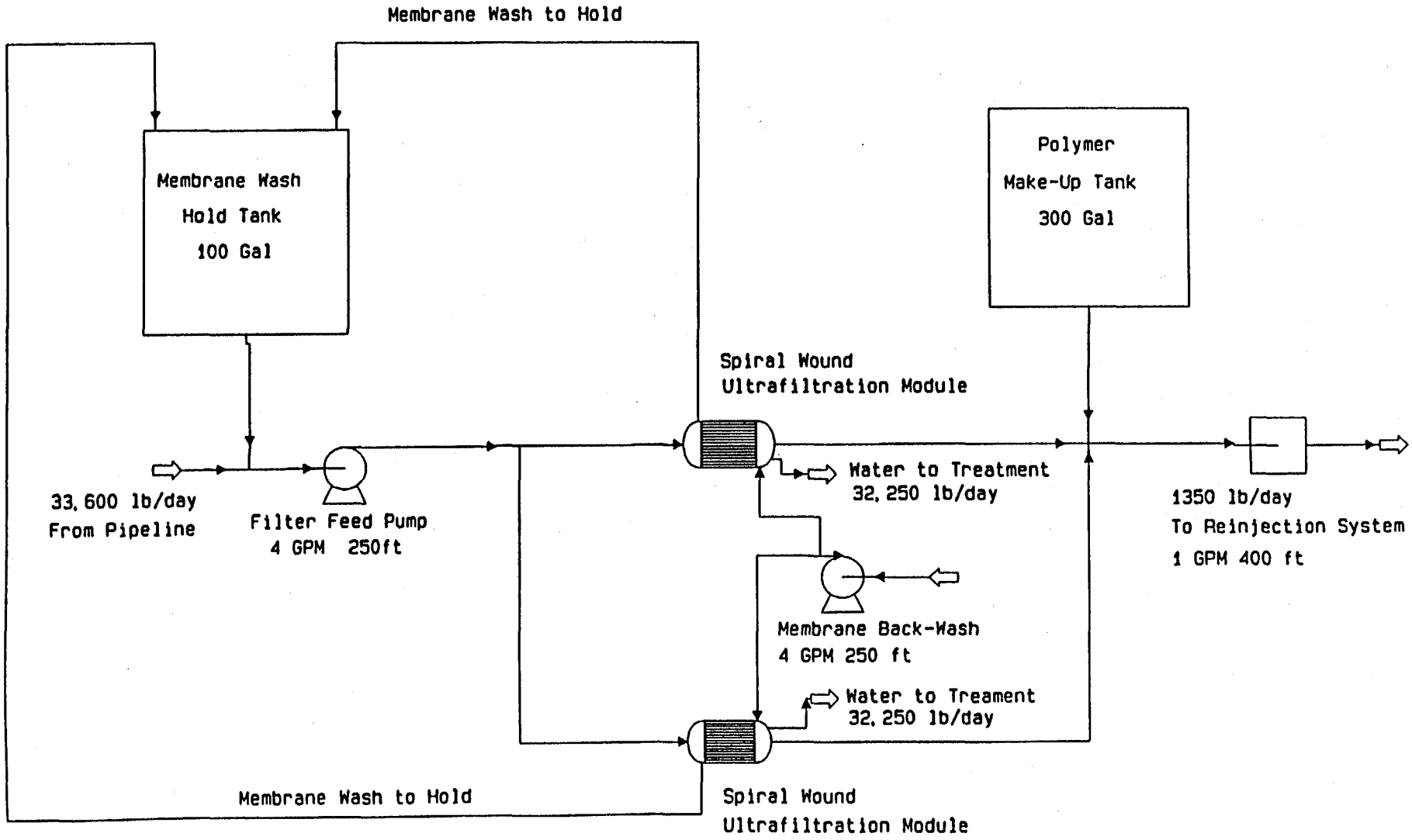

concentrating the retentate in polymer. Vendor data suggest that a retention of 95% can be realized for the PVP polymer. The retentate polymer concentration is controlled by regulating the permeate flowrate. Periodic backflushing of the membrane unit is required to prevent excessive fouling of the membrane. The backflush solution is sent to a holding tank, then re-introduced to the system under normal operating conditions. Two membrane units allow for continuous operation and periodic backflushing. A 10% w/w polymer solution is added to the re-injection line from a holding tank to account for the loss of polymer through the membrane.

ECONOMIC SUMMARY

Ultrafiltration membrane design calculations are shown in Table 1. Spiral wound membrane modules were chosen due to economic favorability. Economic evaluations for all separations schemes are listed in Tables 2 - 4. Specifications and capacities for auxiliary equipment were based on mass and energy balances and design heuristics found in Woods and Timmerhaus. Information pertaining specifically to ultrafiltration units was found in the Membrane Handbook. Installed costs, other indirect costs, and energy consumption costs were estimated using scaling factors from Douglas and Perry's Handbook.

Incremental cash flow calculations based on the current MEG operating costs are presented in Tables 5 - 7. Fixed capital costs, startup costs and initial working capital were not amortized and operating costs were adjusted for a 3% annual inflation rate. Incremental net present value (NPV) based on a 12% rate of return (ROR) indicates that the acetone fractional dissolution procedure for PVP is slightly below break-even (-$26,000). The cloud point procedure for VC-713 realizes an NPV of $1.5 MM while the ultrafiltration scheme shows the highest savings with an NPV of $1.7 MM over the 10 year project lifetime.

This economic evaluation, though preliminary, suggests that ultrafiltration and dissolution of VC-713 using the cloud point warrant further investigation.

Table 1

Design and Cost Calculations for Ultra-Filtration
PVP and VC-713 Hydrate Inhibitors

Basis:						
Water Flow From Well	32234	lbm/day				
Pipeline Polymer Con'c	0.4	w/w%				
Recycle Flow Rate	161.86	GPD	1350	lbm/day	0.11	GPM
Polymer Circulation Rate	134.34	lbm/day				
Recycle Polymer Con'c	9.95	w/w%				
Permeate Flow Rate	32234	lbm/day	609.49	L/hr	2.68	GPM
Polymer Price	6	$/lbm				

Membrane Filtration Scheme	Construction Material	Avg Aqueous Sol'n Flux (L/m^2 hr)	Req'd Membrane Area (m^2)	Avg Membrane Cost ($/m^2)	Total Membrane Cost ($)	Avg % Solute Retention	Polymer Loss (lbm/day)	Polymer Make-Up Cost ($/day)	Installed Membrane Cost ($/m^2)	Membrane Unit Installed Cost ($)	Membrane Replacement Cost ($/yr)	Membrane Cleaning Cost ($/yr)	Total Polymer Makeup Cost ($/yr)	Yearly OP Cost ($)
Tubular	Polysulfone	250	2.44	250	$609	95	6.72	$40	1000	$3,047	$609	$183	$14,710	$15,502
Spiral	Polyamide	200	3.05	150	$457	95	6.72	$40	1000	$3,505	$457	$198	$14,710	$15,365
Plate	Polyamide	200	3.05	300	$914	95	6.72	$40	1000	$3,962	$914	$244	$14,710	$15,868

Table 2

Economic Summary
Acetone Fractional Dissolution for PVP

Page 1

Fixed Capital Investment Direct Costs ISBL Equipment	Specifications & Capacity	Purchased Cost	Total Installed Cost
Agitated Mixing Chamber	100 gal 304 SS	$3,300	$4,455
Polymer Filtration Unit	Area = 8 ft^2	$15,000	$20,250
Acetone Flash Chamber	500 gal 304SS Tank	$8,000	$10,800
Air Stripper	6' Packed Column	$10,000	$13,500
Acetone Condenser	Fixed Tube HX Area = 50 ft^2	$1,000	$1,350
Air-Acetone Phase Separator	16 gal 304SS Tank	$500	$675
Acetone Storage Tank	10000 gal 304SS Tank	$35,000	$47,250
Blower Unit for Air Stripper	2000 SCFM	$2,000	$2,700
Water-Polymer Feed Pump	Cent (316SS): 4 GPM, 30 ft -> 1/2 bhp	$1,800	$2,430
Acetone Recycle Pump	Cent (316SS): 4 GPM, 30 ft -> 1/2 bhp	$1,800	$2,430
Acetone Flash Chamber Heat Exchanger	Double Pipe HX Area = 35 ft^2	$950	$1,283
Feed Air Furnace	100 ft^2 area	$10,000	$13,500
Bacton Inhibitor Storage Tank (1 mo. supply)	300 gal Al Tank for 10% w/w Soln	$2,200	$2,970
Bacton Inhibitor Solution Recycle Pump	Recip (316SS): 1 GPM, 400 ft, Recip -> 1 bhp	$2,500	$3,375
Inde Inhibitor Storage Tank (1 day supply)	150 gal Al Tank	$1,400	$1,890
Pipeline Injection Pump	Recip (316SS): 1 GPM, 1200 psi discharge	$5,000	$6,750
Piping	200 ft / 1" sch 40 steel		$1,600
Total ISBL			$137,208
Total OSBL	20% ISBL		$27,442
Total DC	ISBL + OSBL		$164,649
Indirect Costs			
Engineering & Supervision	5% FCI		$13,496
Construction	12% FCI		$32,390
Contractor Fee	2% FCI		$5,398
Contingency	20% FCI		$53,983
Total IC			$105,267
Total FCI			$269,916

Table 2 (Con't)

Economic Summary
Acetone Fractional Dissolution for PVP

Page 2

Initial Working Capital			
Acetone (initial charge + 3 month make-up)	3850 + 10000 gal @ 98% Recovery	$1.53 / gal	$21,191
Kinetic Inhibitor (initial charge + 3 month make-up)	650 lbm	$6 / lbm	$3,900
Total IWC			$25,091
Start-Up	10% FCI		$26,992
Operational Costs	Requirement	Unit Cost	Total Yearly Cost
Utilities			
Power	100000 kWhr	$0.04 / KW/hr	$4,000
Steam	500000 lbm	$5.20 / 1000 lbm	$2,600
Water	25 MMgal	$0.03 / 1000 gal	$750
Total Utilities			$7,350
Labor & Supervision	10% Yearly OP Cost		$15,672
Depreciation	10% FCI		$26,992
Taxes & Insurance	3% FCI		$8,097
Repairs	8% FCI		$21,593
Misc	5% FCI		$13,496
Total			$85,850
Materials			
Acetone Makeup @ 98% Recovery	31500 gal/ yr	$1.53 / gal	$48,195
Kinetic Inhibitor Makeup	7 lbm / day	$6 / lbm	$15,330
Total Materials			$63,525
Total OC			$156,725

Table 3

Economic Summary
VC-713 Cloud Point Dissolution Procedure

Page 1

Fixed Capital Investment Direct Costs ISBL Equipment	Specifications & Capacity	Purchased Cost	Total Installed Cost
Filter Feed Pump	Cent (316SS): 4GPM, 250 ft -> 1bhp	$2,600	$3,510
Filter Unit	Area = 8 ft^2	$15,000	$20,250
Feed Heat Exchanger	Double Pipe HX (316SS): Area = 12 ft^2	$1,100	$1,485
Bacton Inhibitor Solution Recycle Pump	Recip (316SS): 1 GPM, 400 ft -> 1 bhp	$2,500	$3,375
Bacton Inhibitor Storage Tank (1 mo. supply)	300 gal Al Tank for 10% w/w Soln	$2,200	$2,970
Inde Inhibitor Storage Tank (1 day supply)	150 gal Al Tank	$1,400	$1,890
Pipeline Injection Pump	Recip (316SS): 1 GPM, 1200 psi discharge	$5,000	$6,750
Piping	100 ft / 1" sch 40 steel		$1,600
Total ISBL			$41,830
Total OSBL	20% ISBL		$8,366
Total DC			$50,196
Indirect Costs			
Engineering & Supervision	5% FCI		$3,535
Construction	12% FCI		$8,484
Contractor Fee	2% FCI		$1,414
Contingency	10% FCI		$7,070
Total IC			$20,503
Total FCI			$70,699
Initial Working Capital			
Kinetic Inhibitor (initial charge + 3 month make-up)	650 lbm	$6 / lbm	$3,900
Total IWC			$3,900
Start-Up	10% FCI		$7,070

Table 3 (Con't)

Economic Summary
VC-713 Cloud Point Dissolution Procedure

Page 2

Operational Costs	Requirement	Unit Cost	Total Yearly Cost
Utilities			
Power	35000 kWhr	$0.04 / KW/hr	$1,400
Steam	1.2 MM lbm / yr	$5.20 / 1000 lbm	$6,240
Total Utilities			$7,640
Labor & Supervision	10% Yearly OP Cost		$4,766
Depreciation	10% FCI		$7,070
Taxes & Insurance	3% FCI		$2,121
Repairs	8% FCI		$5,656
Misc	5% FCI		$3,535
Total			$23,148
Materials			
Kinetic Inhibitor Makeup	7 lbm / day	$6 / lbm	$15,330
Total OC			$46,118

Table 4

Economic Summary
Ultra-Filtration for PVP and VC-713

Page 1

Fixed Capital Investment Direct Costs ISBL Equipment	Specifications & Capacity	Purchased Cost	Total Installed Cost
Membrane Units (2)	Polyamide Spiral Wound: Area = 3 m^2		$7,010
Membrane Unit Feed Pump	Cent (316SS): 4 GPM, 250 ft -> 1 bhp	$2,600	$3,510
Flush Water Pump	Cent (316SS): 4 GPM, 250 ft -> 1 bhp	$2,600	$3,510
Membrane Wash Hold Tank	100 gal Al Tank	$1,000	$1,350
Bacton Inhibitor Solution Recycle Pump	Recip (316SS): 1 GPM, 400 ft -> 1 bhp	$2,500	$3,375
Bacton Inhibitor Storage Tank (1 mo. supply)	300 gal Al Tank for 10% w/w Soln	$2,200	$2,970
Inde Inhibitor Storage Tank (1 day supply)	150 gal Al Tank	$1,400	$1,890
Pipeline Injection Pump	Recip (316SS): 1 GPM, 1200 psi discharge	$5,000	$6,750
Piping	100 ft / 1" sch 40 steel		$800
Total ISBL			$31,165
Total OSBL	20% ISBL		$6,233
Total DC	ISBL + OSBL		$37,398
Indirect Costs			
Engineering & Supervision	5% FCI		$2,634
Construction	12% FCI		$6,321
Contractor Fee	2% FCI		$1,053
Contingency	10% FCI		$5,267
Total IC			$15,275
Total FCI			$52,673
Initial Working Capital			
Kinetic Inhibitor (3 month supply for make-up)	650 lbm	$6 / lbm	$3,900
Total IWC			$3,900
Start-Up	10% FCI		$5,267

Table 4 (Con't)

Economic Summary
Ultra-Filtration for PVP and VC-713

Page 2

Operational Costs	Requirement	Unit Cost	Total Yearly Cost
Energy / Power (4 kWhr / hr)	35000 kWhr	$0.04 / kWhr	$1,400
Membrane Replacement	2 Replacements	$600 / Cartridge	$1,200
Membrane Cleaning Solutions	5% Yearly OP Cost	$450	$450
Labor: Membrane Cleaning	10% Yearly OP Cost		$875
Repairs	4% Yearly OP Cost		$350
Depreciation	10% FCI		$5,267
Taxes & Insurance	3% FCI		$1,580
Misc	5% FCI		$2,634
Total			$13,756
Materials			
Kinetic Inhibitor Makeup	6.72 lbm / day	$6 / lbm	$14,710
Total Materials			$14,710
Total OC			$28,466

Table 5

Cash Flow Summary
Acetone Fractional Dissolution for PVP

Economic Component	Year 0	1	2	3	4	5	6	7	8	9
ISBL	$137,208									
OSBL	$27,442									
Total Direct Costs	$164,650									
Total Indirect Costs	$105,267									
Total FCI	$269,917									
Start - Up	$26,992									
Working Capital	$25,091									
Total Non Operational CF	(-$322,000)									
Operating Costs										
Utilities	$7,350	$7,571	$7,798	$8,032	$8,272	$8,521	$8,776	$9,040	$9,311	$9,590
Labor, Depr, Taxes, Repairs, Misc	$85,850	$88,426	$91,078	$93,811	$96,625	$99,524	$102,509	$105,585	$108,752	$112,015
Materials	$63,525	$65,431	$67,394	$69,415	$71,498	$73,643	$75,852	$78,128	$80,472	$82,886
Total OC	$156,725	$161,427	$166,270	$171,258	$176,395	$181,687	$187,138	$192,752	$198,535	$204,491
MEG OC	$182,500	$187,975	$193,614	$199,423	$205,405	$211,568	$217,915	$224,452	$231,186	$238,121
Incremental OC (MEG - Total OC)	$25,775	$26,548	$27,345	$28,165	$29,010	$29,880	$30,777	$31,700	$32,651	$33,631
Total Incremental CF	(-$296,225)	$26,548	$27,345	$28,165	$29,010	$29,880	$30,777	$31,700	$32,651	$33,631
Incremental NPV @ 12%	(-$26,519)									

Table 6

Cash Flow Summary
VC-713 Cloud Point Dissolution Procedure

Economic Component	Year 0	1	2	3	4	5	6	7	8	9
ISBL	$41,830									
OSBL	$8,366									
Total Direct Costs	$50,196									
Total Indirect Costs	$20,503									
Total FCI	$70,699									
Start - Up	$7,070									
Working Capital	$3,900									
Total Non Operational CF	(-$81,669)									
Operating Costs										
Utilities	$7,640	$7,869	$8,105	$8,348	$8,599	$8,857	$9,123	$9,396	$9,678	$9,968
Labor, Depr, Taxes, Repairs, Misc	$23,148	$23,842	$24,558	$25,294	$26,053	$26,835	$27,640	$28,469	$29,323	$30,203
Materials	$15,330	$15,790	$16,264	$16,752	$17,254	$17,772	$18,305	$18,854	$19,420	$20,002
Total OC	$46,118	$47,502	$48,927	$50,394	$51,906	$53,463	$55,067	$56,719	$58,421	$60,174
MEG OC	$182,500	$187,975	$193,614	$199,423	$205,405	$211,568	$217,915	$224,452	$231,186	$238,121
Incremental OC (MEG - Total OC)	$136,382	$140,473	$144,688	$149,028	$153,499	$158,104	$162,847	$167,733	$172,765	$177,948
Total Incremental CF	$54,713	$140,473	$144,688	$149,028	$153,499	$158,104	$162,847	$167,733	$172,765	$177,948
Incremental NPV @ 12%	$1,481,798									

Table 7

Cash Flow Summary
Ultra-Filtration for VC-713 and PVP

Economic Component	Year 0	1	2	3	4	5	6	7	8	9
ISBL	$31,165									
OSBL	$6,233									
Total Direct Costs	$37,398									
Total Indirect Costs	$15,275									
Total FCI	$52,673									
Start - Up	$5,267									
Working Capital	$3,900									
Total Non Operational CF	(-$61,840)									
Operating Costs										
Utilities	$1,400	$1,442	$1,485	$1,530	$1,576	$1,623	$1,672	$1,722	$1,773	$1,827
Labor, Depr, Taxes, Repairs, Misc	$12,356	$12,727	$13,108	$13,502	$13,907	$14,324	$14,754	$15,196	$15,652	$16,122
Materials	$14,710	$15,151	$15,606	$16,074	$16,556	$17,053	$17,565	$18,091	$18,634	$19,193
Total OC	$28,466	$29,320	$30,200	$31,106	$32,039	$33,000	$33,990	$35,010	$36,060	$37,142
MEG OC	$182,500	$187,975	$193,614	$199,423	$205,405	$211,568	$217,915	$224,452	$231,186	$238,121
Incremental OC (MEG - Total OC)	$154,034	$158,655	$163,415	$168,317	$173,367	$178,568	$183,925	$189,442	$195,126	$200,979
Total Incremental CF	$92,194	$158,655	$163,415	$168,317	$173,367	$178,568	$183,925	$189,442	$195,126	$200,979
Incremental NPV @ 12%	$1,703,987									

CONCLUSIONS

The best choice for the separation of inhibitor is the ultrafiltration system. We have shown that the module may be installed with minimal impact on the present gas processing system, requires the least amount of auxiliary equipment, and is the most economically sound choice, giving an incremental NPV of $1.7 MM based on a 12% ROR against current MEG operating costs. Although these calculations are preliminary and should be investigated further, they show a relatively more promising outlook than either of the other systems described. It is recommended that a vendor of ultrafiltration modules be contacted and asked to perform pilot scale experiments with the polymer of choice. Formation of a gel layer on the membrane surface due to agglomeration will certainly change the flux through the membrane. This effect will alter the size parameter and hence the economics, but will not alter the final choice of which apparatus to use since gel formation will affect all separation schemes adversely.

RECOMMENDATIONS

- Experimentally determine the gel point of PVP and VC-713 in water. This will allow for an accurate value of the maximum aqueous polymer concentration in the injection solution recycle stream. Sizing of pumps and piping could be better estimated with known recycle stream flowrates using this concentration.

- Contact vendors of filtration units and have pilot scale experimentation conducted with actual inhibitor injection solutions.

- Determine the mean particle size of suspended polymer solids during the dissoluton process to calculate pore size of membranes.

- Utilize existing inhibitor recycle loop to minimize capital expenditures.

List of References

Baker, et al., *Membrane Separation Systems: Recent Developments and Future Directions*, New Jersey: Noyes Data Corporation, 1991.

Baker, R. W., "Methods of Fractionating Polymers by Ultrafiltration," *Journal of Applied Polymer Science*, (13)369-376:(1969).

Campbell, Kane, Ottewill, "Polyvinylpyrrolidone. I. Distribution of Molecular Weights: Experimental Methods and Applications," *Journal of Polymer Science*, (12)611-620:(1954).

Doulas, James, *Conceptual Design of Chemical Processes*, New York: McGraw-Hill,1988.

Helminiak, Meier, "Osmotic Pressures of Aqueous Polyvinylpyrrolidone Solutions," *Journal of Polymer Science*, (44)539-545:(1960).

Jirgensons, "Solubility and Fractionation of Polyvinylpyrrolidone," *Journal of Polymer Science*, (8)519-527:1951.

Mulder, M., *Basic Principles of Membrane Technology*, Kluwer Academic publishers, 1992, chap. 1,6,8.

Perry's Handbook for Chemical Engineers, 6th ed., New York: McGraw Hill, 1984.

Peters & Timmerhaus, *Plant Design and Economics for Chemical Engineers*, 3rd ed., New York: McGraw Hill, 1969.

Porter, *Handbook of Separation Techniques for Chemical Engineers*, 2nd ed., P.A. Schweitzer editor, New York: McGraw Hill, 1988.

Reinhold, Van Nostrand, *Membrane Handbook, Part VII: Ultrafiltration*, Ho &Sirkar editors,1992.

Woods, Donald, *Selecting Process Equipment*, 6th ed., (1),1990.

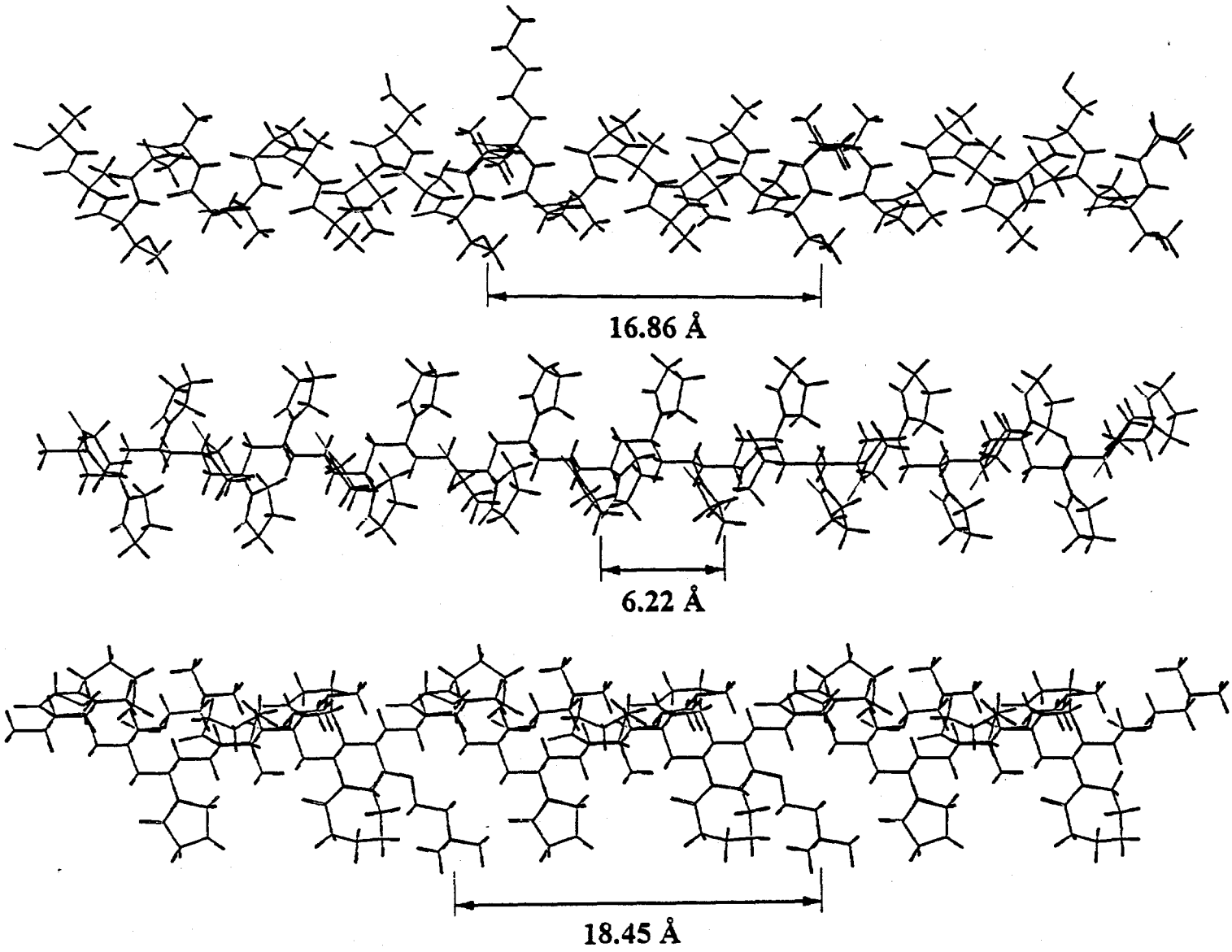

Figure 77. WINTER FLOUNDER POLYPEPTIDE, PVP, AND VC-713 POLYMERS

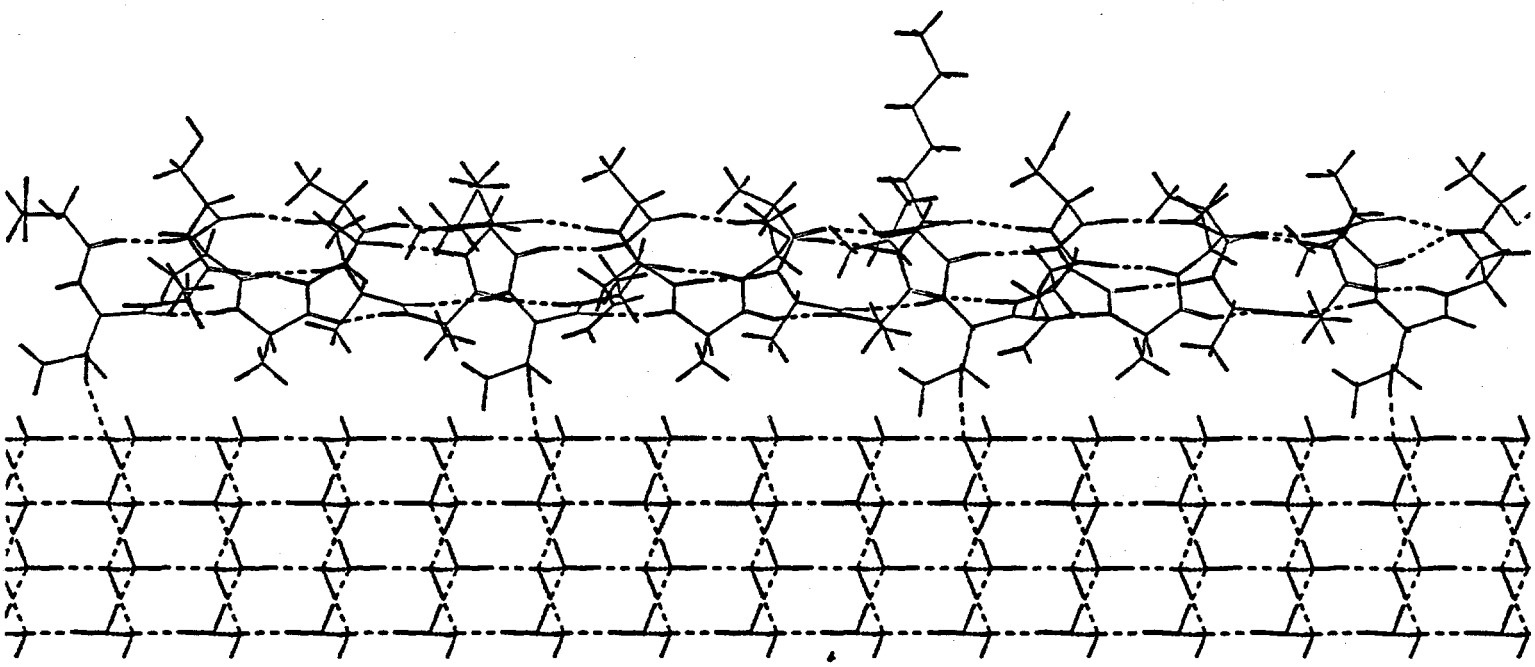

Figure 78. WINTER FLOUNDER POLYPEPTIDE FITTING ON ICE

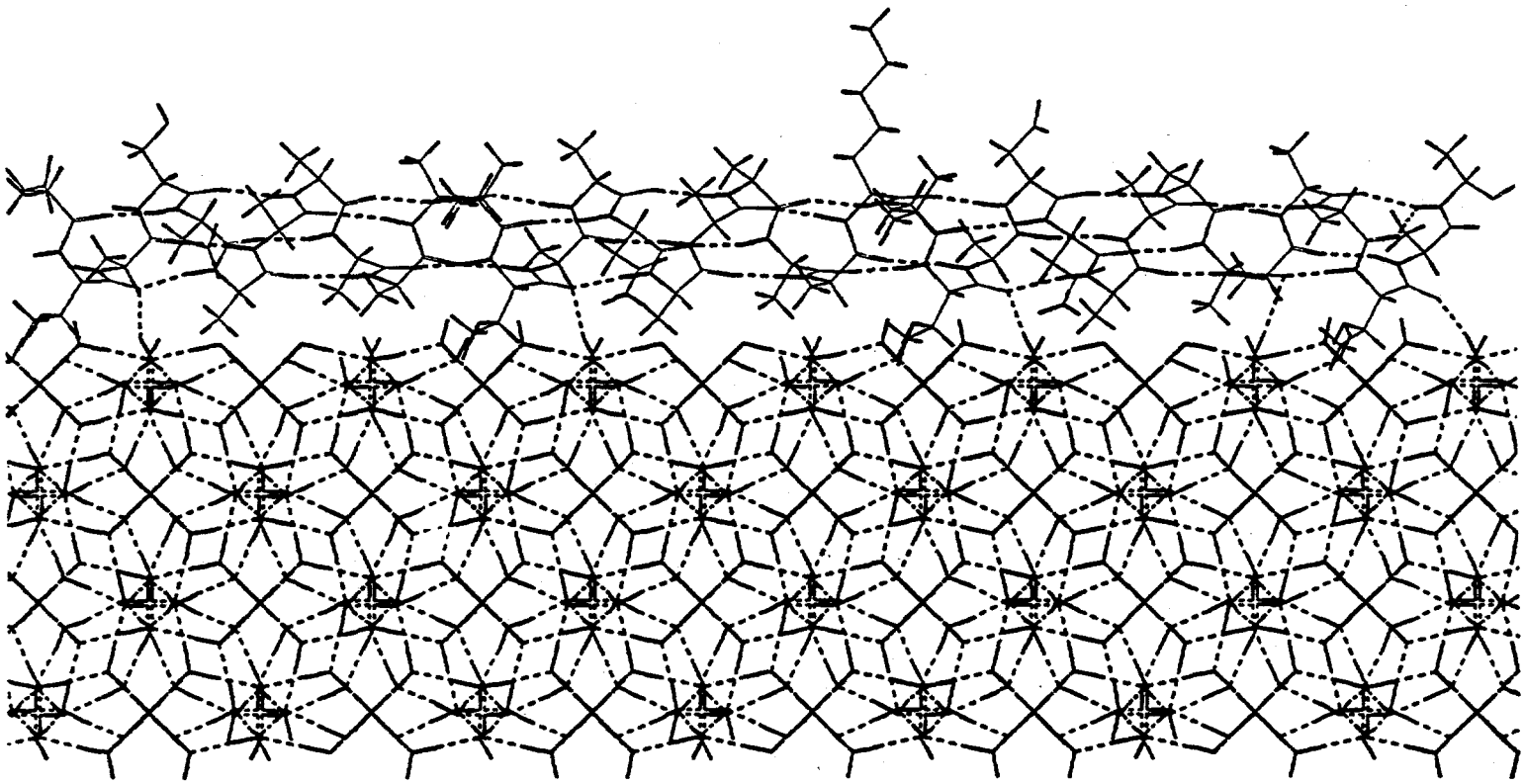

Figure 79. WINTER FLOUNDER POLYPEPTIDE FIT ON STRUCTURE II

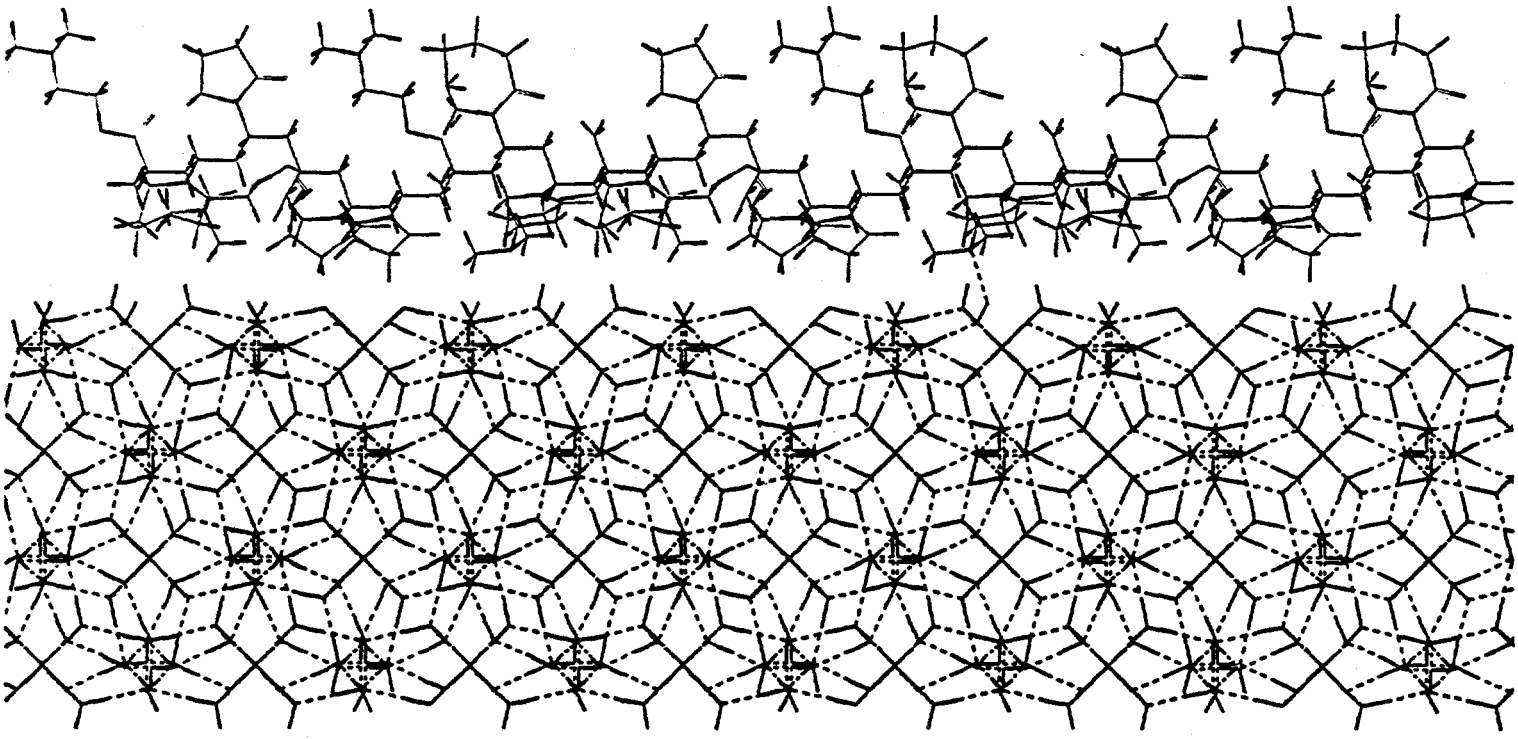

Figure 80. FITTING OF VC-713 POLYMER ON HYDRATE STRUCTURE II